# THE REACTION OF BIS(THIOETHER) COMPLEXES OF (OCTAETHYLPORPHYRINATO)RUTHENIUM(II) WITH DIOXYGEN, AND THE CATALYZED $O_2$-OXIDATION OF THIOETHERS

by

ARSENIO ANDREW PACHECO-OLIVELLA
B.Sc., The University of British Columbia, 1982
M.Sc., The University of British Columbia, 1986

A THESIS SUBMITTED IN PARTIAL FULFILLMENT OF
THE REQUIREMENTS FOR THE DEGREE OF
DOCTOR OF PHILOSOPHY
in
THE FACULTY OF GRADUATE STUDIES
THE DEPARTMENT OF CHEMISTRY

We accept this thesis as conforming
to the required standard

THE UNIVERSITY OF BRITISH COLUMBIA
September 1992

© Arsenio Andrew Pacheco-Olivella, 1992

In presenting this thesis in partial fulfilment of the requirements for an advanced degree at the University of British Columbia, I agree that the Library shall make it freely available for reference and study. I further agree that permission for extensive copying of this thesis for scholarly purposes may be granted by the head of my department or by his or her representatives. It is understood that copying or publication of this thesis for financial gain shall not be allowed without my written permission.

(Signature)

Department of Chemistry

The University of British Columbia
Vancouver, Canada

Date December 8th 1992

## ABSTRACT

This thesis describes a detailed study of the reactivity of Ru(OEP)(RR'S)$_2$ complexes (where OEP ≡ the dianion of 2,3,7,8,12,13,17,18-octaethylporphyrin, R ≡ methyl, ethyl or decyl, and R' ≡ methyl or ethyl) with O$_2$, in various solvents.

Exposure to O$_2$ (or air) of a benzene, toluene or methylene chloride solution containing PhCOOH and Ru(OEP)(RR'S)$_2$ at ambient conditions, results in the selective oxidation of the axial ligand(s) on the metalloporphyrin complex to the corresponding sulfoxide(s). For a CD$_2$Cl$_2$ solution containing ≈ 20 mM of Ru(OEP)(dms)$_2$ (dms ≡ dimethylsulfide) and ≈ 12 mM PhCOOH, exposed to 1 atm of O$_2$ at room temperature, $^1$H-nmr analysis shows that most of the Ru(OEP)(dms)$_2$ has oxidized to Ru(OEP)(dmso)$_2$ over a period of 35h. Three detected intermediates are identified as Ru(OEP)(dms)(dm$\underline{s}$o) (where $\underline{s}$ indicates S-coordination of the sulfoxide), Ru(OEP)(dms)$_2^+$PhCOO$^-$ and Ru(OEP)(dms)(PhCOO).

To identify the products and intermediates of oxidation, the complexes in the series Ru(OEP)(RR'S)$_2$, Ru(OEP)(RR'SO)$_2$ and Ru(OEP)(RR'S)$_2^+$BF$_4^-$, as well as Me$_4$N$^+$ Ru(OEP)(PhCOO)$_2^-$, were synthesized and characterized by use of $^1$H-nmr, ir and uv/vis spectroscopy, cyclic voltammetry, and elemental analysis; the x-ray crystal stucture of Ru(OEP)(decMS)$_2^+$BF$_4^-$ was obtained. The Ru(OEP)(dm$\underline{s}$o)$_2$ complex exists as the bis(S-bound) isomer in the solid state, although variable temperature uv/vis studies suggest that isomerization to O-bound species occurs in solution.

The Ru(OEP)(RR'S)(RR'$\underline{S}$O) complexes could not be isolated pure, but they were characterized in solution by $^1$H-nmr, CV, and uv/vis studies. For solutions containing

$Ru(OEP)(Et_2SO)_2$, $Ru(OEP)(Et_2S)(Et_2\underline{S}O)$, $Ru(OEP)(Et_2S)_2$, and varying concentrations of $Et_2S$ and $Et_2SO$, the equilibrium and rate constants governing the relative solution concentrations of the three species were determined from stopped-flow experiments.

The Ru(OEP)(RR'S)(PhCOO) complexes could not be isolated in pure form either, but solutions containing 1:1 mixtures of $Ru(OEP)(dms)_2{}^+BF_4{}^-$ and $Me_4N^+Ru(OEP)(PhCOO)_2{}^-$ were shown by $^1H$-nmr to generate Ru(OEP)(dms)(PhCOO).

On the basis of detected intermediates and their properties, a "three-stage" mechanism is proposed for the $O_2$-oxidation of the thioether ligands of $Ru(OEP)(RR'S)_2$ in acidic organic media. For example, for the bis(dms) system, in the "first stage", $O_2$ coordinates to $Ru^{II}(OEP)(dms)$ formed by dissociation of a dms ligand. This is followed by electron transfer from the metal to $O_2$; the $O_2{}^-$ formed is protonated by PhCOOH to yield $HO_2$, while $Ru^{III}(OEP)(dms)(PhCOO)$ is also formed. The $HO_2$ disproportionates to $O_2$ and $H_2O_2$, and the latter oxidizes $Et_2S$ to $Et_2SO$. In the "second stage", a $Ru^{III}$ species, probably $Ru^{III}(OEP)(dms)(PhCOO)$, is oxidized to $Ru^{IV}$ by another $Ru^{III}$ species, probably $Ru^{III}(OEP)(dms)_2{}^+PhCOO^-$ (i.e. $2Ru^{III} \rightarrow Ru^{IV} + Ru^{II}$). During the "third stage", the $Ru^{IV}$ species is thought to be converted to $O{=}Ru^{IV}(OEP)(dms)$, which then reacts with dms to produce $Ru^{II}(OEP)(dms)(dm\underline{s}o)$. The overall process results in two moles of dms being oxidized to dmso per mole of $O_2$ consumed. The basic mechanism appears to be the same for the oxidation of dialkylsulfides in $CH_2Cl_2$, benzene or toluene, but with some differences in detail.

In the presence of excess thioether, solutions of $Ru(OEP)(RR'S)_2$ in $CH_2Cl_2$, benzene or toluene, containing PhCOOH, catalyze the $O_2$-oxidation of thioether to sulfoxide, but light above 480 nm is required. It is believed that, under catalytic

conditions, $O_2$-coordination to the metal is inhibited by the presence of excess thioether, and that light is then required to provide energy for the otherwise unfavourable outer-sphere electron transfer from the metal to $O_2$. After the initial electron transfer, the reaction would follow the same course as in the stoichiometric oxidation. The catalytic system was studied for the case in which RR'S = $Et_2S$. The stoichiometry: $2Et_2S + O_2 \rightarrow 2Et_2SO$ was verified by gas chromatography and by oxygen-uptake experiments.

A kinetic analysis of the gas uptake data showed that, under the experimental conditions used, the initial rate approached a maximum value for $[Ru]_o > 2$ mM, $[O_2] > 0.14$ M, and [PhCOOH] > 54 mM, with the limiting rate being imposed by the complete absorption of the incident light by the reaction solution. The results of a kinetic modelling analysis suggest that the photoexcited state that gives rise to the observed photochemistry has a minimum lifetime of $10^{-8}$ s (in the absence of $O_2$), and that Ru(OEP)($Et_2S$)($Et_2\underline{S}O$), which accumulates as the concentration of $Et_2SO$ builds up, is outside of the catalytic cycle.

## TABLE OF CONTENTS

ABSTRACT . . . . . . . . . . . . . . . . . . . . . . . . . . . . . . . . . . . . . . . . . ii

TABLE OF CONTENTS . . . . . . . . . . . . . . . . . . . . . . . . . . . . . . . . . . v

LIST OF TABLES . . . . . . . . . . . . . . . . . . . . . . . . . . . . . . . . . . . . . . x

LIST OF FIGURES . . . . . . . . . . . . . . . . . . . . . . . . . . . . . . . . . . . . . xi

LIST OF ABBREVIATIONS AND SYMBOLS . . . . . . . . . . . . . . . . . . . . . . xviii

ACKNOWLEDGEMENTS . . . . . . . . . . . . . . . . . . . . . . . . . . . . . . . . . xx

CHAPTER 1 INTRODUCTION . . . . . . . . . . . . . . . . . . . . . . . . . . . . . 1
- 1.1 General Introduction . . . . . . . . . . . . . . . . . . . . . . . . . . . . . 1
- 1.2 Reactivity of Ruthenium Porphyrins with Dioxygen . . . . . . . . . . . . . . 5
- 1.3 Reactivity of Dialkylsulfides with Dioxygen . . . . . . . . . . . . . . . . . 14
- 1.4 Outline of this Thesis . . . . . . . . . . . . . . . . . . . . . . . . . . . . 19
- NOTES AND REFERENCES FOR CHAPTER 1 . . . . . . . . . . . . . . . . 20

CHAPTER 2 REACTION OF Ru(OEP)(RR'S)$_2$ COMPLEXES WITH DIOXYGEN IN ACIDIC MEDIA . . . . . . . . . . . . . . . . . . . . . . . . . . 23
- 2.1 Introduction . . . . . . . . . . . . . . . . . . . . . . . . . . . . . . . . . 23
- 2.2 Experimental . . . . . . . . . . . . . . . . . . . . . . . . . . . . . . . . 24
  - 2.2.1 General Reagents, Gases and Solvents . . . . . . . . . . . . . . . 24
  - 2.2.2 Tetramethylammonium Benzoate ($Me_4N^+PhCOO^-$) . . . . . . . . 25
  - 2.2.3 Tetra-n-butylammonium Tetrafluoroborate ($n\text{-}Bu_4N^+BF_4^-$) . . . . 26
  - 2.2.4 Ruthenium Porphyrin Complexes . . . . . . . . . . . . . . . . . . . 26
    - 2.2.4.1 Ru(OEP)(dms)$_2$ . . . . . . . . . . . . . . . . . . . . . . . . 27

2.2.4.2 Ru(OEP)($Et_2S$)$_2$ . . . . . . . . . . . . . . . . . . . . . . . . . 28

2.2.4.3 Ru(OEP)(dm$\underline{s}$o)$_2$ and the dmso-d$_6$ Analogue . . . . . . . 28

2.2.4.4 Ru(OEP)(Et$_2\underline{S}$O)$_2$ . . . . . . . . . . . . . . . . . . . . . . . . 29

2.2.4.5 Ru(OEP)(decM$\underline{S}$O)$_2$ . . . . . . . . . . . . . . . . . . . . . . . 29

2.2.4.6 Ru(OEP)(dms)$_2^+$BF$_4^-$ . . . . . . . . . . . . . . . . . . . . . . . . 30

2.2.4.7 Ru(OEP)(Et$_2$S)$_2^+$BF$_4^-$ . . . . . . . . . . . . . . . . . . . . . . . 31

2.2.4.8 Ru(OEP)(decMS)$_2^+$BF$_4^-$ . . . . . . . . . . . . . . . . . . . . . . 31

2.2.4.9 Me$_4$N$^+$Ru(OEP)(PhCOO)$_2^-$ . . . . . . . . . . . . . . . . . . 32

2.2.5 Instrumentation . . . . . . . . . . . . . . . . . . . . . . . . . . . . . 32

2.2.5.1 Ultraviolet/Visible Absorption Spectroscopy . . . . . . . 32

2.2.5.2 Infrared Spectroscopy . . . . . . . . . . . . . . . . . . . . . 33

2.2.5.3 Proton Nuclear Magnetic Resonance Spectroscopy . . . 33

2.2.5.4 Conductivity . . . . . . . . . . . . . . . . . . . . . . . . . . . 33

2.2.5.5 Cyclic Voltammetry . . . . . . . . . . . . . . . . . . . . . . 33

2.2.5.6 Elemental Analysis . . . . . . . . . . . . . . . . . . . . . . . 36

2.3 Characterization of Ru(OEP)(RR'$\underline{S}$O)$_2$ Complexes . . . . . . . . . . . . . 36

2.4 Characterization of Ru$^{III}$(OEP) Complexes . . . . . . . . . . . . . . . . . 40

2.5 Reaction of Ru(OEP)(dms)$_2$ With Dioxygen and Benzoic Acid in Methylene Chloride . . . . . . . . . . . . . . . . . . . . . . . . . . . . . . . . 49

2.6 Reaction of Ru(OEP)(RR'S)$_2$ Complexes with Dioxygen and Benzoic Acid in Hydrocarbon Solvents . . . . . . . . . . . . . . . . . . . . . . . . . 71

REFERENCES AND NOTES FOR CHAPTER 2 . . . . . . . . . . . . . . . . 81

CHAPTER 3 A MECHANISTIC STUDY OF THE O$_2$-OXIDATION OF DIETHYLSULFIDE CATALYZED BY Ru(OEP)(Et$_2$S)$_2$ . . . . . . . . . . . . 84

3.1 Introduction . . . . . . . . . . . . . . . . . . . . . . . . . . . . . . . . . 84

3.2 Experimental . . . . . . . . . . . . . . . . . . . . . . . . . . . . . . . . 85

3.2.1 Materials . . . . . . . . . . . . . . . . . . . . . . . . . . . . . . . . . 85

3.2.2 Stopped-Flow Experiments . . . . . . . . . . . . . . . . . . . . . . 85

3.2.2.1 Sample Handling . . . . . . . . . . . . . . . . . . . . . . . 85

3.2.2.2 Instrumentation . . . . . . . . . . . . . . . . . . . . . . . . . 86
3.2.3 Gas Chromatography . . . . . . . . . . . . . . . . . . . . . . . . . 86
3.2.3.1 Sample Handling . . . . . . . . . . . . . . . . . . . . . . . . 86
3.2.3.1 Instrumentation . . . . . . . . . . . . . . . . . . . . . . . . . 87
3.2.4 Oxygen Uptake Experiments . . . . . . . . . . . . . . . . . . . . . . 87
3.2.4.1 Sample Handling . . . . . . . . . . . . . . . . . . . . . . . . 87
3.2.4.2 Apparatus Setup . . . . . . . . . . . . . . . . . . . . . . . . . 88
3.2.5 Data Treatment . . . . . . . . . . . . . . . . . . . . . . . . . . . 92
3.3 Ru(OEP)$(Et_2S)_2$-Catalyzed $O_2$-Oxidation of $Et_2S$ in Benzene Solution - General Observations . . . . . . . . . . . . . . . . . . . . . . . . . . 92
3.4 Stopped-Flow Analysis of $Et_2SO$ Substitution by $Et_2S$ in Ru(OEP)$(Et_2SO)_2$ in Benzene Solution . . . . . . . . . . . . . . . . . . . . 113
3.4.1 Data Treatment and Results . . . . . . . . . . . . . . . . . . . . . . 113
3.4.2 Error Analysis . . . . . . . . . . . . . . . . . . . . . . . . . . . . 129
3.4.2.1 Uncertainties in the Solution Concentrations . . . . . . . 129
3.4.2.2 Instrumental Uncertainties . . . . . . . . . . . . . . . . . . 129
3.4.2.2.1 Uncertainties on the Millisecond Timescale . 130
3.4.2.2.2 Uncertainties in the One Hundred Second Timescale . . . . . . . . . . . . . . . . . . . . . . . 134
3.4.3 Discussion of the Parameter Values . . . . . . . . . . . . . . . . . 135
3.5 Catalytic Oxidation of $Et_2S$ - Rate Dependence on $[O_2]$ [PhCOOH] and [Ru(OEP)$(Et_2S)_2$] . . . . . . . . . . . . . . . . . . . . . . . . . . . 138
3.5.1 Data Treatment and Results . . . . . . . . . . . . . . . . . . . . . . 138
3.5.2 Error Analysis and Discussion . . . . . . . . . . . . . . . . . . . . 153
3.5.2.1 Experimental Uncertainties . . . . . . . . . . . . . . . . . 153
3.5.2.2 Evaluation of the Kinetic Model . . . . . . . . . . . . . . 154
NOTES AND REFERENCES FOR CHAPTER 3 . . . . . . . . . . . . . . . . 170

CHAPTER 4 RATE LAW DERIVATION FOR THE $O_2$-OXIDATION OF DIETHYLSULFIDE CATALYZED BY Ru(OEP)$(Et_2S)_2$ . . . . . . . . . . . . 172

4.1 Introduction . . . . . . . . . . . . . . . . . . . . . . . . . . . . . . . . . . . . 172

4.2 The Equilibria between Ru(OEP)($Et_2S$)$_2$, Ru(OEP)($Et_2S$)($Et_2SO$) and Ru(OEP)($Et_2SO$)$_2$ . . . . . . . . . . . . . . . . . . . . . . . . . . . . . 172

4.2.1 Rate Law Derivations . . . . . . . . . . . . . . . . . . . . . . . . . . . . 172

4.2.2 Correlation of Uv/Vis Absorbance Changes to the Derived Rate Laws . . . . . . . . . . . . . . . . . . . . . . . . . . . . . . . . 181

4.2.2.1 First Substitution Reaction . . . . . . . . . . . . . . . . . 181

4.2.2.2 Second Substitution Reaction . . . . . . . . . . . . . . . . 185

4.3 Catalytic $O_2$-Oxidation of $Et_2S$ by Ru(OEP)($Et_2S$)$_2$ . . . . . . . . . . . . . . 189

4.3.1 General Rate Law Derivation . . . . . . . . . . . . . . . . . . . . . . . . 189

4.3.2 An Approximate Expression for $I_a$ . . . . . . . . . . . . . . . . . . 196

4.3.3. Modifications to the Proposed Mechanism . . . . . . . . . . . . 202

4.3.3.1 Internal Rearrangement . . . . . . . . . . . . . . . . . . . . 203

4.3.3.2 Photoactivation Via Metal-to-Porphyrin Charge Transfer . . . . . . . . . . . . . . . . . . . . . . . . . . . 205

CHAPTER 5 GENERAL CONCLUSIONS AND SUGGESTIONS FOR FURTHER STUDIES . . . . . . . . . . . . . . . . . . . . . . . . . . . . . . 209

REFERENCES FOR CHAPTER 5 . . . . . . . . . . . . . . . . . . . . . . . . 213

APPENDIX 1 QUICK BASIC PROGRAMS . . . . . . . . . . . . . . . . . . . . . . . 213

A1.1 LINFIT . . . . . . . . . . . . . . . . . . . . . . . . . . . . . . . . . . . . 213

A1.2 POLFIT . . . . . . . . . . . . . . . . . . . . . . . . . . . . . . . . . . . . 217

A1.3 ONEDMIN . . . . . . . . . . . . . . . . . . . . . . . . . . . . . . . . . . 221

A1.4 TWODMIN . . . . . . . . . . . . . . . . . . . . . . . . . . . . . . . . . . 229

A1.5 ODEGRPH . . . . . . . . . . . . . . . . . . . . . . . . . . . . . . . . . . 237

APPENDIX 2 RESULTS OF STOPPED-FLOW EXPERIMENTS . . . . . . . . . . . 242

A2.1 Experiments Carried Out Using Light of 400.5 nm Wavelength . . . . . 242

A2.1.1 Experiments Carried Out Using a Constant [$Et_2SO$] of

1.18 ± 0.03 mM . . . . . . . . . . . . . . . . . . . . . . . . . . . . . . 243
A2.1.2 Experiments Carried Out Using a Constant [$Et_2SO$] of 17.7 ± 0.2 mM . . . . . . . . . . . . . . . . . . . . . . . . . . . . . . . 249
A2.2 Experiments Carried Out Using Light of 402.8 nm Wavelength . . . . . 254
A2.2.1 Experiments Carried Out Using a Constant [$Et_2SO$] of 1.18 ± 0.03 mM . . . . . . . . . . . . . . . . . . . . . . . . . . . . . . 255
A2.3 Blank Experiments . . . . . . . . . . . . . . . . . . . . . . . . . . . . . . 259

APPENDIX 3 RESULTS OF OXYGEN UPTAKE EXPERIMENTS . . . . . . . . . . 260
A3.1 First Data Set . . . . . . . . . . . . . . . . . . . . . . . . . . . . . . 260
A3.1.1 [Ru]$_o$ Dependence Studies . . . . . . . . . . . . . . . . . . . . . . 261
A3.1.2 [PhCOOH] Dependence Studies . . . . . . . . . . . . . . . . . . . . 266
A3.1.3 [$O_2$] Dependence Studies . . . . . . . . . . . . . . . . . . . . . . 270
A3.2 Second Data Set . . . . . . . . . . . . . . . . . . . . . . . . . . . . . 274
A3.2.1 [Ru]$_o$ Dependence Studies . . . . . . . . . . . . . . . . . . . . . . 274
A3.2.2 [PhCOOH] Dependence Studies . . . . . . . . . . . . . . . . . . . . 278
A3.3 Additional Data Sets . . . . . . . . . . . . . . . . . . . . . . . . . . . 282
A3.3.1 Dependence of the Reaction Rates on the Reaction Vessel Shaking Speed . . . . . . . . . . . . . . . . . . . . . . . . . . . . . . 282
A3.3.2 Dependence of the Reaction Rates on the Volume of the Reaction Mixture . . . . . . . . . . . . . . . . . . . . . . . . . . . . . 284

## LIST OF TABLES

Table 2.1 Summary of the $^1$H-nmr Peak Positions in $CD_2Cl_2$ for the Ru(OEP) Complexes Discussed in Section 2.5 . . . . . . . . . . . . . . . . . . . . . . . . 52
Table 2.2 Positions of the $^1$H-nmr Signals ($\delta_{obs}$), Assigned to $Ru^{II}(OEP)(dms)_2$ + $Ru^{III}(OEP)(dms)_2^+PhCOO^-$ in the Experiment Illustrated in Figure 2.7, and the Calculated Remaining Mole Fraction of $Ru(OEP)(dms)_2$ ($N_{II}$) . . . . . . . . 57
Table 2.3 Selected Bond Distances (Å) and Bond Angles (deg) for $Ru(OEP)(decMS)_2$ and $Ru(OEP)(decMS)_2^+BF_4^-$ . . . . . . . . . . . . . . . . . . . 60
Table 2.4 Summary of the $^1$H-nmr Peak Positions in $C_6D_6$ for the dms- and dmso-Containing Ru(OEP) Complexes Discussed in Section 2.6 . . . . . . . . . . . . 73
Table 2.5 Summary of the $^1$H-nmr Peak Positions in $C_6D_6$ for the $Et_2S$- and $Et_2SO$-Containing Ru(OEP) Complexes Discussed in Section 2.6 . . . . . . . . 76
Table 3.1 Fundamental Parameters Derived from Equations 3.18 and 3.19 . . . . . . 121
Table 3.2 Fundamental Parameters Derived from Equations 3.24 and 3.25 . . . . . . 129
TABLE 3.3 Fundamental Parameters Derived from the Plots of $k_{obs}$ vs. $[Ru]_o$, [PhCOOH] and $[O_2]$ . . . . . . . . . . . . . . . . . . . . . . . . . . . . . . . 152

# LIST OF FIGURES

Figure 1.1. Structure of the porphyrin ring skeleton . . . . . . . . . . . . . . . . . . . . . 2

Figure 1.2. Sample structures of Ru(OEP)$L_2$ and Ru(TMP)$L_2$ complexes. a) Ru(OEP)($Ph_2S$)$_2$ (taken from reference 19); b) Ru(TMP)(THF)($N_2$) (taken from reference 8b). . . . . . . . . . . . . . . . . . . . . . . . . . . . . . . . . . . . . . . . . 9

Figure 1.3. Proposed catalytic cycle for the epoxidation of olefins catalyzed by Ru(TMP)(O)$_2$ (taken from reference 11). . . . . . . . . . . . . . . . . . . . . . . 11

Figure 2.1. Cyclic voltammetry cell: (A) platinum bead working electrode; (B) platinum wire spiral auxilliary electrode; (C) non-aqueous salt bridge; (D) aqueous Ag/AgCl reference electrode; (E) KCl reservoir; (F) sample preparation flask. . . . . . . . . . . . . . . . . . . . . . . . . . . . . . . . . . . 35

Figure 2.2. Changes in the visible spectrum of a $CH_2Cl_2$ solution containing 0.039 mM Ru(OEP)($Et_2SO$)$_2$, and 4.72 mM free $Et_2SO$, as the temperature is increased in 10° intervals, from 20-50° C. . . . . . . . . . . . . . . . . . . . . 38

Figure 2.3. Uv/vis spectra in $CH_2Cl_2$ of (a) Ru(OEP)(dms)$_2$ and Ru(OEP)(dms)$_2^+BF_4^-$, and (b) $Me_4N^+$Ru(OEP)(PhCOO)$_2^-$. . . . . . . . . . . . . 41

Figure 2.4. Cyclic voltammograms in $CH_2Cl_2$/n-$Bu_4N^+BF_4^-$ for (a) Ru(OEP)(dms)$_2$, (b) Ru(OEP)(dmso)$_2$, and (c) $Me_4N^+$Ru(OEP)(PhCOO)$_2^-$. The cyclic voltammograms of the other dialkylsulfide and sulfoxide complexes are virtually indistinguishable from those of the dms and dmso complexes illustrated. Also, a CV identical to (a) was obtained for Ru(OEP)(dms)$_2^+BF_4^-$. . . . . . . . . . . . . . . . . . . . . . . . . . . 43

Figure 2.5. (a) Visible spectrum of a 1:1 mixture of Ru(OEP)($Et_2SO$)$_2$ and $AgBF_4$ in $CH_2Cl_2$; (b) $^1$H-nmr spectrum of a $CD_2Cl_2$ solution initially containing [Ru(OEP)]$_2$($BF_4$)$_2$ and free dmso in approximately 1:8 ratio; S ≡ solvent, T = 20° C. . . . . . . . . . . . . . . . . . . . . . . . . . . . . . . . . . . 44

Figure 2.6. $^1$H-nmr spectrum of Ru(OEP)(decMS)$_2^+BF_4^-$ in $CD_2Cl_2$, taken at 20.0° C; S ≡ solvent. . . . . . . . . . . . . . . . . . . . . . . . . . . . . . . . 48

Figure 2.7. $^1H$-nmr spectral changes over time after an acidic $CD_2Cl_2$ solution of Ru(OEP)(dms)$_2$ is exposed to 1 atm of $O_2$ at room temperature (approximately 20° C). The peak assignments for each species are summarized in table 2.2. . . . . . . . . . . . . . . . . . . . . . . . . . . . . . 50

Figure 2.8. $^1H$-nmr spectrum of a $CD_2Cl_2$ solution of Ru(OEP)(dms)$_2$ (approximately 5 mM) to which an excess of a mixture containing 3:1 dms/dmso (neat) has been added. Under these conditions, the major Ru(OEP) species in solution is Ru(OEP)(dms)(dm$\underline{s}$o). . . . . . . . . . . . . . . 51

Figure 2.9. $^1H$-nmr spectrum of an acidic $CD_2Cl_2$ solution of Ru(OEP)(dms)$_2$ 35 h after exposure to 1 atm of $O_2$ at room temperature (cf. figure 2.7); S ≡ solvent. . . . . . . . . . . . . . . . . . . . . . . . . . . . . . . . . . . . . . . . 54

Figure 2.10. $^1H$-nmr spectrum of Ru(OEP)(dms)$_2{}^+BF_4^-$; 20.0° C in $CD_2Cl_2$; S ≡ solvent. . . . . . . . . . . . . . . . . . . . . . . . . . . . . . . . . . . . . . . . 56

Figure 2.11. Crystal structure of Ru(OEP)(decMS)$_2{}^+BF_4^-$; selected bond lengths and angles are given in table 2.3. . . . . . . . . . . . . . . . . . . . . . . . . . 59

Figure 2.12. $^1H$-nmr spectrum of (a) a mixture (approximately 1:1) of Ru(OEP)(dms)$_2{}^+BF_4^-$ and $Me_4N^+$Ru(OEP)(PhCOO)$_2^-$ about 1 h after mixing; (b) pure $Me_4N^+$Ru(OEP)(PhCOO)$_2^-$. Both spectra in $CD_2Cl_2$ at 20.0° C, and systems sealed under vacuum; S ≡ solvent. . . . . . . . . . . 64

Figure 2.13. Cyclic voltammogram of a solution ($CH_2Cl_2$/n-$Bu_4N^+BF_4^-$) initially containing 0.78 mM Ru(OEP)(decMS)$_2$, 71 mM decMS, and 25 mM decMSO. . . . . . . . . . . . . . . . . . . . . . . . . . . . . . . . . . . . . . . . 69

Figure 2.14. $^1H$-nmr spectrum of a $C_6D_6$ solution, initially containing 8.2 mM Ru(OEP)(dms)$_2$ and 8.2 mM PhCOOH, which was exposed to 1 atm of $O_2$ for about 36 h at room temperature; S ≡ solvent, g ≡ grease, ? ≡ unidentifed signals. . . . . . . . . . . . . . . . . . . . . . . . . . . . . . . . . . 72

Figure 2.15. $^1H$-nmr spectrum of a $C_6D_6$ solution, initially containing 2.3 mM Ru(OEP)(Et$_2$S)$_2$ and 3.3 mM PhCOOH, which was exposed to 1 atm of $O_2$ for about 12 h at 35° C; S ≡ solvent, g ≡ grease, ? ≡ unidentified signals. . . . . . . . . . . . . . . . . . . . . . . . . . . . . . . . . . . . . . . . 75

Figure 2.16. $^1$H-nmr spectrum of a $C_6D_6$ solution, initially a suspension of $Ru^{III}(OEP)(dms)_2{}^+BF_4^-$ and $Me_4N^+Ru^{III}(OEP)(PhCOO)_2$ (approximately $4x10^{-6}$ mol of each), which was allowed to stand overnight under vacuum; S ≡ solvent, ? ≡ unidentified signals. . . . . . . . . . . . . . . . . . . . . . . . 78

Figure 3.1. Apparatus used for gas uptake measurements. (a) Complete setup; (b) Close-up view of the oil bath and housing, showing the orientation of the light source. Key components: (A) Thermostatted and insulated oil bath; (B) Reaction vessel; (C) Oil manometer; (D) Mercury burette and reservoir; (E) Projection lamp; (F) Aluminum foil; (G) Compressed air manifold; (H) Screen. (1)-(12): Various taps and valves; see text for explanations. . . . . . . . . . . . . . . . . . . . . . . . . . . . . . . . . . . . 89

Figure 3.2. Dependence of $Et_2SO$ production rate on reaction vessel illumination. $[Ru(OEP)(Et_2S)_2]$ = 0.34 mM; [PhCOOH] = 5.3 mM; $[Et_2S]$ = 0.74 M; the reaction was carried out in benzene solution at 35° C, in a flask exposed to the air. Reaction progress was followed by gas chromatography. . . . . . . . . . . . . . . . . . . . . . . . . . . . . . . . . 94

Figure 3.3. (a) Uv/visible spectra of $Ru(OEP)(Et_2S)_2$, and of the yellow and blue filters used to test which wavelengths are necessary for $Et_2S$ oxidation to proceed. (b) Effects of the cutoff filters on the rate of $Et_2SO$ production, as measured by $O_2$-absorption at 35° C; in each case, a benzene solution initially containing 0.84 mM $Ru(OEP)(Et_2S)_2$, 24 mM PhCOOH, and 0.74 M $Et_2S$ was exposed to 0.81 atm of $O_2$ (corrected for benzene vapour pressure). . . . . . . . . . . . . . . . . . . . . . . . . . . . . . . . . . . . 95

Figure 3.4. Scheme showing the types of electronic transitions which can occur in $d^6$ six-coordinate ruthenium porphyrins (adapted from reference 8). . . . . . . 97

Figure 3.5. Two possible mechanisms for the photochemical stage of the $O_2$-oxidation of $Et_2S$ catalyzed by $Ru(OEP)(Et_2S)_2$: a) porphyrin $\pi$-$\pi^*$ transition, followed by transfer of the excited electron to $O_2$; b) direct metal-to-porphyrin charge-transfer, followed by transfer of the excited electron to $O_2$. . . . . . . . . . . . . . . . . . . . . . . . . . . . . . . . . . . 98

Figure 3.6. Relationship between the light energy absorbed by $Ru(OEP)(Et_2S)_2$ at 525 nm, and the relative free energy changes associated with various transformations; see text for details. . . . . . . . . . . . . . . . . . . . . . . . . 102

Figure 3.7. Gas chromatographic trace of a benzene solution initially containing 0.42 mM $Ru(OEP)(Et_2S)_2$, 6.5 mM benzoic acid, and 0.74 M $Et_2S$, exposed to 0.81 atm of $O_2$ (corrected for benzene vapour pressure) at 35° C for 2.5 h. 4.89 min: $Et_2S_2$; 6.05 min: $Et_2SO$; 7.11 min: $Et_2SO_2$; 7.90 min: n-undecane; 9.30 min: benzoic acid. The signal at 13.16 min is that of an unidentified product; the rest of the unidentified signals are present at the start of the reaction. . . . . . . . . . . . . . . . . . . . . . . . . . . . . . . . . 104

Figure 3.8. Scheme proposed for the $O_2$-oxidation of $Et_2S$ to $Et_2SO$, catalyzed by $Ru(OEP)(Et_2S)_2$ and PhCOOH (dotted pathways imply that these processes can be neglected under catalytic conditions). . . . . . . . . . . . . . . . . . . . . . 106

Figure 3.9. A typical plot showing the accumulation of $Et_2SO$ with time, determined by monitoring the $O_2$-uptake (see section 3.5 for full details). For this experiment at 35° C, the initial concentrations of the reagents are: $[Ru(OEP)(Et_2S)_2]$ = 0.202 mM; [PhCOOH] = 24.4 mM; $[Et_2S]$ = 0.742 M; $pO_2$ = 0.813 atm (corrected for benzene vapour pressure). . . . . . . . . . 108

Figure 3.10. Relationship between the light energy absorbed by $Ru(OEP)(Et_2S)(Et_2\underline{S}O)$ at 525 nm, and the free energy changes associated with various transformations. ΔG° for the oxidation at the metal of $Ru^{II}(OEP)(Et_2S)(Et_2\underline{S}O)$ was estimated from the CV data for the analogous Ru(OEP)(decMS)(decM$\underline{S}$O) system (see section 2.5 and figure 2.13); for the one-electron ring oxidation, ΔG° is assumed to be the same as in the $Ru(OEP)(Et_2S)_2$ system (see figure 3.6). . . . . . . . . . . . . . . . . . . . . . . . 110

Figure 3.11 Uv/vis spectra of a benzene solution initially containing 0.202 mM $Ru(OEP)(Et_2S)_2$, 0.742 M $Et_2S$, and no benzoic acid, at various times after exposure to a light source, and 0.813 atm of $O_2$ (corrected for benzene vapour pressure). The same results were obtained . . . . . . . . . . . . . . . . 111

Figure 3.12. Scheme showing the proposed mechanisms for the sequential substitution of two $Et_2SO$ ligands by $Et_2S$ in $Ru(OEP)(Et_2SO)_2$. In solution, the bis-sulfoxide species is believed to exist as a mixture of the S- and O-bound linkage isomers (see section 2.3). . . . . . . . . . . . . . . . . . . . . . . . 114

Figure 3.13. Uv/vis spectral changes observed as: (a) a benzene solution initially containing $3.4x10^{-6}$ M $Ru(OEP)(Et_2SO)_2$ and 0.19 M free $Et_2SO$ is titrated with neat $Et_2S$; (b) a benzene solution initially containing $1.7x10^{-5}$ M $Ru(OEP)(Et_2S)_2$ and 0.74 M free $Et_2S$ is titrated with neat $Et_2SO$. T = 35° C for both experiments. . . . . . . . . . . . . . . . . . . . . . . . . . . . . . . . . 115

Figure 3.14. A typical, fitted stopped-flow trace of the change in absorbance over 100 ms, at $\lambda$ = 400.5 nm, when $Et_2S$ is substituted for $Et_2SO$ in $Ru(OEP)(Et_2SO)_2$. $[Et_2S] = 9.27\pm0.09$ mM; $[Et_2SO] = 1.18\pm0.03$ mM; $[Ru]_o = (3.44\pm0.07)x10^{-6}$ M. The first four points likely are in the dead time of the instrument, and are neglected in the fit. . . . . . . . . . . . . . . . . 122

Figure 3.15. Portions of the plots of $[Et_2S]/\beta_1$ vs $[Et_2S]$ for data collected at $\lambda$ = 400.5 nm over 100-ms time-frames. a) $[Et_2SO] = 1.18\pm0.03$ mM; b) $[Et_2SO] = 17.7\pm0.2$ mM. In each case $[Ru]_o = (3.44\pm0.07)x10^{-6}$ M. The residual plots show the full range of data collected; the main plots show only the region in which $\beta_1$ increases (Q is the goodness of fit given the obtained $\chi^2$ value). . . . . . . . . . . . . . . . . . . . . . . . . . . . . . . . . 123

Figure 3.16. Portions of the plots of $[Et_2S]/v_{o1}$ vs. $[Et_2S]$ for data collected at $\lambda$ = 400.5 nm over 100-ms time-frames. a) $[Et_2SO] = 1.18\pm0.03$ mM; b) $[Et_2SO] = 17.7\pm0.2$ mM. In each case, $[Ru]_o = (3.44\pm0.07)x10^{-6}$ M. The residual plots show the full range of data collected; the main plots show only the region in which $v_{o1}$ increases. . . . . . . . . . . . . . . . . . . . . 124

Figure 3.17. A typical, fitted stopped-flow trace of the change in absorbance over 100 s, at $\lambda$ = 402.8 nm, when $Et_2S$ is substituted for $Et_2SO$ in $Ru(OEP)(Et_2S)(Et_2\underline{S}O)$.
$[Et_2S] = 18.6\pm0.2$ mM; $[Et_2SO] = 1.18\pm0.03$ mM; $[Ru]_o = (3.44\pm0.07)x10^{-6}$ M. 127

Figure 3.18. Portions of the plots of: a) $[Et_2S]^2/\beta_2$ vs $[Et_2S]$, and b) $[Et_2S]^2/v_{o2}$ vs $[Et_2S]$, for data collected at $\lambda$ = 402.8 nm over 100-s time-frames. $[Et_2SO]$

= 1.18±0.03 mM; $[Ru]_o$ = $(3.44\pm0.07)x10^{-6}$ M. There is one off-scale point at $[Et_2S]$ = 0.232±0.002 M for each plot; all of the data are tabulated in appendix 2. . . . . . . . . . . . . . . . . . . . . . . . . . . . . . . 128

Figure 3.19. Variation of the parameters $\beta_1$ and $\gamma_1$ from experiment to experiment, when all reagent concentrations are held constant. The error bars represent the uncertainties estimated from fitting the raw stopped-flow data. . . . . . . . . . . . . . . . . . . . . . . . . . . . . . . . . . . . . . 131

Figure 3.20. Weakening of $\pi$-bonds *trans* to a sulfoxide; $\sigma$ bonds *trans* to the sulfoxide will also be weakened, since the sulfoxide can transfer more $\sigma$-electron density to the Ru $d_z$2 orbital than a comparable ligand incapable of $\pi$-bonding (see text). . . . . . . . . . . . . . . . . . . . . . . . . . . . . . 137

Figure 3.21. Visible spectra of pure $Ru(OEP)(Et_2S)_2$ (**3**), a solution containing mostly $Ru(OEP)(Et_2S)(Et_2\underline{S}O)$ (**2**, see text), and pure $Ru(OEP)(Et_2SO)_2$ (**1** and **1'**). The dashed lines indicate the region of all three spectra over which the integrated extinction coefficients were calculated (see text for details). . . . . . . . . . . . . . . . . . . . . . . . . . . . . . . . . . . . . 144

Figure 3.22. A plot of $[Et_2SO]$ vs. time, fitted using the least squares procedure described in the text. For this experiment, the initial concentrations of the reagents are: $[Ru(OEP)(Et_2S)_2]$ = 0.202 mM; [PhCOOH] = 2.31 mM; $[Et_2S]$ = 0.742 M; $pO_2$ = 0.813 atm (corrected for benzene vapour pressure). . . . . . . . . . . . . . . . . . . . . . . . . . . . . . . . . . . . . 147

Figure 3.23. Plots of $k_{obs}$ vs.: (a) $[Ru]_o$, with [PhCOOH] and $[O_2]$ held constant at 24.4 and 7.63 mM, respectively; (b) [PhCOOH], with $[Ru]_o$ and $[O_2]$ held constant at 0.408 and 7.63 mM, respectively; (c) $[O_2]$ with $[Ru]_o$ and [PhCOOH] held constant at 0.408 and 24.4 mM, respectively. The error bar magnitude in each case is given by $\sigma$. . . . . . . . . . . . . . . . . . . . . . . 149

Figure 3.24. Plots of $k_{obs}$ vs.: (a) $[Ru]_o$, with [PhCOOH] and $[O_2]$ held constant at 24.4 and 7.63 mM, respectively; (b) [PhCOOH], with $[Ru]_o$ and $[O_2]$ held constant at 0.202 and 7.63 mM, respectively. The error bar magnitude in each case is given by $\sigma$. . . . . . . . . . . . . . . . . . . . . . . . . . . . . . 151

Figure 3.25. Plots of the goodness of fit parameter (Q) vs.: (a) $[Ru]_o$; (b) [PhCOOH]; (c) $[O_2]$ for the fitting procedures illustrated in figures 3.23 and 3.24, and assuming that $\psi$ = 0.85 (see text for details). . . . . . . . . . . 155

Figure 3.26. Plots of the goodness of fit parameter (Q) vs.: (a) $[Ru]_o$; (b) [PhCOOH]; (c) $[O_2]$ for the fitting procedures illustrated in figures 3.21 and 3.22, and assuming that $\psi$ = 0.6 (see text for details). . . . . . . . . . . 160

Figure 3.27. A plot of $[Et_2SO]$ vs. time, fitted using: (a) the least squares procedure described in the text; (b) the function $[Et_2SO] = 2k_3[Ru]_ot$. For this experiment, the initial concentrations of the reagents are: $[Ru(OEP)(Et_2S)_2]$ = 0.0253 mM; [PhCOOH] = 24.4 mM; $[O_2]$ = 7.63 mM; $[Et_2S]$ = 0.742 M. . . . . . . . . . . . . . . . . . . . . . . . . . . . . . 164

Figure 4.1. Mechanism proposed for the sequential substitution of two $Et_2SO$ ligands by $Et_2S$, assuming that in solution the bis(sulfoxide) species exists as a mixture of the S- and O-bound linkage isomers. . . . . . . . . . . . . . . 174

Figure 4.2. Mechanism proposed for the $O_2$-oxidation of $Et_2S$ to $Et_2SO$, catalyzed by $Ru(OEP)(Et_2S)_2$ and PhCOOH (dotted pathways imply that these processes can be neglected, or do not occur, under catalytic conditions; see the assumptions on pp. 140-141). . . . . . . . . . . . . . . . . . . . . . . . . 190

Figure 4.3. Alternative mechanism for the photochemical stage of the $O_2$-oxidation of $Et_2S$ catalyzed by $Ru(OEP)(Et_2S)_2$; see text for details. . . . . . . . . . . . 206

## LIST OF ABBREVIATIONS AND SYMBOLS

Where possible, all abbreviations used are those recommended in: "Handbook for Authors". *Amer. Chem. Soc. Publications*, Washington, D. C., 1978; pp. 29-47. The following is a list of specialized abbreviations and symbols used in this thesis.

| Symbol or Abbreviation | Meaning |
|---|---|
| AZBN | azoisobutyronitrile |
| Cp | cyclopentadienyl anion |
| CT | charge transfer |
| CV | cyclic voltammetry |
| d | doublet |
| decMS | n-decylmethylsulfide |
| decMSO | n-decylmethylsulfoxide |
| DMA | N,N′-dimethylacetamide |
| dms | dimethylsulfide |
| dmso | dimethylsulfoxide |
| m | multiplet |
| NHE | normal hydrogen electrode |
| OCP | meso-tetra(2,6-dichlorophenyl)porphyrinato dianion |
| OEP | 2,3,7,8,12,13,17,18-octaethylporphyrinato dianion |
| Porp | any general porphyrinato dianion |

| | |
|---|---|
| ppm | parts per million |
| py | pyridine |
| q | quartet |
| qn | quintet |
| s | singlet |
| SCE | saturated calomel electrode |
| sx | sextet |
| t | triplet |
| TMP | meso-tetramesitylporphyrinato dianion |
| TPP | meso-tetraphenylporphyrinato dianion |

# ACKNOWLEDGEMENTS

I wish to thank all of those who helped me, directly or indirectly, to complete this work. First, I wish to express my deepest gratitude to Professor B. R. James, for his expert guidance and support during the course of my studies; it has been a pleasure to work for him. I also owe special thanks to my wife Muriel, not only for her unfailing moral support, but also for doing the illustrating for the thesis. My thanks to colleagues in both the B. R. James and D. Dolphin research groups, for their friendship and helpful discussions; many an idea crystallized while sharing theories over coffee! In the same vein I wish to thank my good friends K. Barnard and S. Habib, for enduring innumerable questions about numerical analysis, and coming up with helpful answers. I am also grateful to Dr. E. Burnell of this department for his helpful comments and suggestions. The prompt and courteous services provided by the crystallographer Dr. S. Rettig, and by the nmr, Elemental Analysis, Electronic, Glassblowing and Mechanical shop personnel are deeply appreciated. Finally, I would like to thank my family, especially my parents and my brother, for their unfailing love and support.

# CHAPTER 1

# INTRODUCTION

## 1.1 General Introduction

The porphyrin macrocycle (figure 1.1) is a planar 18-electron aromatic system, containing a total of 11 conjugated double bonds. The four pyrrolic nitrogen atoms define an equatorial plane, and the porphyrin dianion, formed by removing the two internal protons, is a planar tetradentate chelating agent capable of forming coordination compounds with all the transition and lanthanide metals, as well as many of the main group metals and semimetals, and a number of actinides.[1]

Iron porphyrins are ubiquitous in natural protein and enzyme systems, and have been identified as vital components in the active sites of such diverse molecules as hemoglobin which is an oxygen transport protein, the cytochromes which perform an assortment of oxidation-reduction tasks, and oxygenases which catalyze selective oxidations using $O_2$.[2] Because of their importance in natural systems, iron porphyrins have been the subject of intense investigation over the last 30 years, and several model (i.e. "protein-free") systems, using a variety of synthetic porphyrins, have been devised.[3] In addition to their use within model systems for naturally occurring iron porphyrins, studies are now under way to use robust synthetic iron porphyrin catalysts in industrial oxidation processes.[4]

As mentioned, porphyrin systems containing almost every metal in the periodic table have now been synthesized and characterized.[1] In large part the interest in metalloporphyrins other than Fe(Porp) has also been fuelled by a desire to better

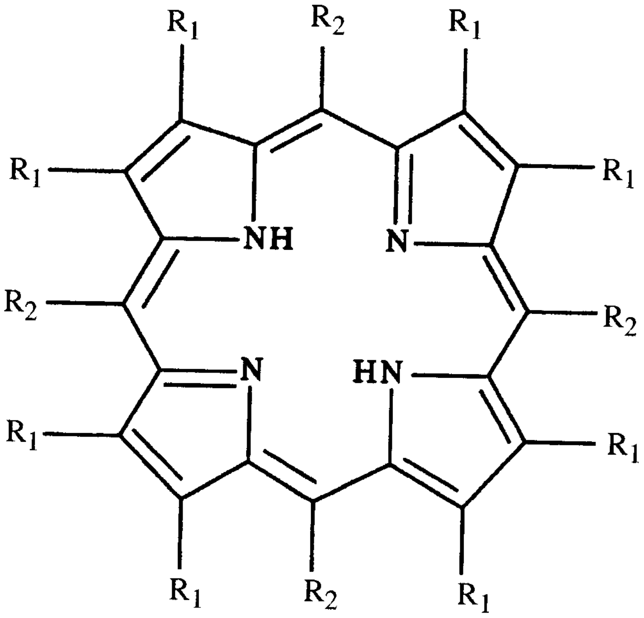

| | **$R_1$** | **$R_2$** |
|---|---|---|
| OEP | $C_2H_5$ | H |
| TPP | H | $C_6H_5$ |
| TMP | H | 2, 4, 6-$Me_3C_6H_2$ |
| OCP | H | 2, 6-$Cl_2C_6H_3$ |

Figure 1.1. Structure of the porphyrin ring skeleton

understand the natural porphyrin systems;[1] much can be learned about one element by comparing and contrasting its behaviour with that of other elements. Because ruthenium is immediately below iron in the periodic table, the possibility of comparing and contrasting ruthenium porphyrins with iron porphyrins is especially intriguing, and since 1969 various ruthenium porphyrins have been synthesized and characterized.[1,5]

Despite the fact that it has been over twenty years since the first ruthenium porphyrin complex was prepared, it still appears too early to assess the full impact of the ruthenium porphyrin studies on the understanding of the naturally occurring iron porphyrin systems; what can be said for sure is that the study of ruthenium porphyrins has developed into a mature and interesting field in its own right.

Much of the work done to date has focused on the synthesis of novel ruthenium porphyrins and, in this respect, the dimeric complexes such as $[Ru(OEP)]_2$[6] and $[Ru(OEP)BF_4]_2$[7] (OEP ≡ dianion of octaethylporphyrin), and the four-coordinate Ru(TMP)[8] (TMP ≡ dianion of tetramesitylporphyrin) deserve special mention (see figure 1.1 for porphyrin systems). These complexes are coordinatively unsaturated, and exhibit many remarkable physical and chemical properties.[6-8] The lack of axial ligands also makes these complexes excellent starting materials for the preparation of other Ru(Porp) complexes (Porp = dianion of a porphyrin in general); indeed, using the dimeric and four-coordinate complexes as starting materials, a wide variety of $Ru^0$, $Ru^{II}$, $Ru^{III}$, $Ru^{IV}$ and $Ru^{VI}$ materials has now been synthesized.[6-9]

Investigations into the reactivity of various ruthenium porphyrins have also yielded interesting catalytic properties in reactions as diverse as the decarbonylation of aldehydes,[10] and the $O_2$-oxidation of various organic compounds, including olefins to epoxides.[11] One problem with some of the catalysis studies carried out to date is that often the reactivity patterns of the ruthenium porphyrins are complex; consequently, many of these studies provided only a rough outline of the possible mechanisms involved; this was the case, for example, in the decarbonylation process,[10] and in the $O_2$-oxidation of phosphines (see below).[12] However, the advances in synthetic methods of recent years, and the isolation and concomitant characterization of higher-valent Ru(Porp) complexes (notably of $Ru^{III}$, $Ru^{IV}$ and $Ru^{VI}$ species)[9] now makes it possible to identify intermediates in complex reaction pathways, which in turn means that detailed mechanistic studies are now feasible. This thesis describes just such a study, on the autoxidation of thioethers to sulfoxides catalyzed by $Ru(OEP)(RR'S)_2$ complexes (R and R′ are alkyl groups).

Interest in the possible autoxidation of thioethers to sulfoxides, using Ru(Porp) complexes as catalysts, was sparked by earlier studies in our laboratories which showed that $Ru(OEP)(PPh_3)_2$ catalyzes the autoxidation of free $PPh_3$ to $OPPh_3$ (see section 1.2).[12] As the subject of a detailed study, the selective oxidation of sulfides to sulfoxides was more attractive than the oxidation of $PPh_3$ to $OPPh_3$, because of the potential commercial value of the former process;[13,14] this consideration played a part in the initial decision of which system to investigate further. As will be seen in the following two sections of this chapter, many advances have been made in the field of catalytic $O_2$-oxidation of thioethers since this project was first conceived, and at present two other processes[9b,15] appear more effective than the process described in this thesis (this topic is discussed in more detail in chapter 5). Nevertheless, this thesis project has revealed some interesting properties of ruthenium porphyrins, some of which may have bearing on the results of earlier investigations on catalyzed $O_2$-oxidation of $PPh_3$[12], and the catalyzed decarbonylation of aldehydes,[10] for which mechanistic details were lacking.

## 1.2 Reactivity of Ruthenium Porphyrins with Dioxygen

Early studies on the reactivity of Ru(Porp) complexes with dioxygen focused on $Ru^{II}$ species, and commented on the high stability of the $Ru^{II}$ species to oxidation by air when compared to the then known $Fe^{II}$ analogues.[16,17] The stability was rationalized in terms of the larger ruthenium d-orbitals leading to greater ligand field stabilization by the porphyrin, as well as to more efficient metal-to-porphyrin $\pi$-backbonding.[16,17] While $Ru^{II}$(Porp) complexes are more thermodynamically stable to oxidation than $Fe^{II}$(Porp) complexes, those prepared in the early studies were exceptionally stable, and many air-sensitive Ru(Porp) complexes have been prepared since that time,[18,19] including species that bind $O_2$ reversibly.[20] The first $Ru^{II}$(Porp) complexes isolated contained CO as an axial ligand, and it was proposed that efficient $\pi$-backbonding from the ruthenium d-orbitals to the carbonyl $\pi^*$ orbitals was decreasing the electron density around the metal, and thus stabilizing the lower oxidation state (a well-known property of the CO ligand).[21] The next Ru(Porp) complexes to be prepared were of the form $Ru^{II}(Porp)L_2$, where L = py or another nitrogenous base; although these complexes exhibited ($Ru^{III} + e^- \rightleftharpoons Ru^{II}$) reduction potentials as much as 0.6 V lower than those of the Ru(Porp)CO complexes, they also appeared to be rather stable to air-oxidation.[17] Proceeding from the hypothesis that $O_2$-oxidation required initial coordination of $O_2$ to the metal center, the apparent stability of the $Ru(Porp)L_2$ complexes was attributed to the fact that all of these compounds were substitutionally relatively inert; Ru(TPP)$py_2$ (TPP ≡ dianion of tetraphenylporphyrin, see figure 1.1), for instance, took a week under 1 atm CO at room temperature to give the thermodynamically favoured (carbonyl)pyridine product.[16] In recent years many Ru(Porp) complexes have been prepared with labile axial ligands such as MeCN, THF, $N_2$ and $Ph_2S$[8,19,20] and a series of monomeric and dimeric complexes exemplified by Ru(TMP)[8], $[Ru(OEP)]_2$ and $[Ru(TPP)]_2$,[6] which contain no extraneous axial ligands have been isolated; all such complexes are invariably extremely air- sensitive.

If a $Ru^{II}(Porp)L_2$ complex is substitutionally inert, one could still envision an "outer sphere" electron transfer from $Ru^{II}$ to $O_2$. In fact, such a mechanism has been invoked in several instances; for example, in the $O_2$-oxidation of $PPh_3$ to $OPPh_3$ catalyzed by $Ru(OEP)(PPh_3)_2$, mentioned at the end of the last section, the initial step in the cycle was proposed to be[12]

$$Ru^{II}(OEP)(PPh_3)_2 + O_2 \rightleftharpoons Ru^{III}(OEP)(PPh_3)_2^+ + O_2^- \qquad 1.1$$

However, this reaction is highly unfavourable thermodynamically,[12] and a proton source is required to promote the subsequent reactions:

$$O_2^- + H^+ \rightleftharpoons HO_2 \qquad 1.2$$

$$2HO_2 \rightarrow H_2O_2 + O_2 \qquad 1.3$$

The disproportionation reaction 1.3 is irreversible,[22] and it was hypothesized that this step makes possible the otherwise unfavourable outer sphere oxidation of $Ru(OEP)(PPh_3)_2$ complexes by $O_2$. The following steps were proposed to account for the phosphine oxidation, and to regenerate the $Ru^{II}$ species and complete the catalytic cycle:[12]

$$H_2O_2 + PPh_3 \rightleftharpoons OPPh_3 + H_2O \qquad 1.4$$

$$2Ru^{III}(OEP)(PPh_3)_2^+ + H_2O + PPh_3 \rightleftharpoons 2Ru^{II}(OEP)(PPh_3)_2 + 2H^+ + OPPh_3 \qquad 1.5$$

Equations 1.1-1.5 constitute a net catalytic pathway by which two moles of $PPh_3$ are oxidized by one mole of $O_2$:

$$2PPh_3 + O_2 \rightleftharpoons 2OPPh_3 \qquad 1.6$$

Outer sphere electron transfer is a major topic of this thesis, and it will be seen in chapter 3 that, for some systems at least, the presence of a proton source is not thermodynamically sufficient to permit a process such as equation 1.1 to occur; the reaction also requires a light source to provide the necessary energy. The study referred to above[12] mentions difficulty in obtaining reproducible kinetic data, and it is possible that this difficulty arose from an unrecognized light dependence.

In the absence of an oxygen atom acceptor such as $PPh_3$, $O_2$-oxidation of $Ru(OEP)L_2$ and $Ru(TPP)L_2$ complexes (where L ≡ a neutral ligand such as THF) often leads, in the presence of an anion source $X^-$, ultimately to the formation of the thermodynamically stable $[Ru^{IV}(Porp)X]_2O$.[9c,23,24] For example, if the complex $Ru(OEP)(Ph_2S)_2$ is exposed to air, it is rapidly oxidized to $[Ru(OEP)OH]_2O$, and the freed thioether axial ligands are recovered intact (trace water is believed to provide the $OH^-$).[19] Complexes such as this one, referred to commonly but incorrectly as "$\mu$-oxo dimers", were first prepared in 1981 by Masuda et al.,[24] and have been characterized extensively since that time.[9c,23,24] The $\mu$-oxo dimers appear to be quite resistant to reduction, and so their formation is a problem if one wants to establish a system for catalytic $O_2$-oxidation using Ru(Porp) complexes. Of note, although resistant to reduction, there is evidence that $\mu$-oxo dimers can be slowly demetallated in benzene solution, according to the following reaction:[12]

$$[Ru(OEP)(OH)]_2O + H_2O \rightarrow 2RuO_2 + 2H_2(OEP) \qquad 1.7$$

If the ortho (and para) protons on the phenyls of TPP are replaced by methyl groups, the resultant TMP system, when metallated, has sterically crowded axial sites; figure 1.2 shows an OEP system (which is less sterically hindered at the axial sites than TPP systems) and a TMP system. The phenyl rings of TMP are perpendicular to the porphyrin plane, and space filling molecular models show that the o-methyls crowd the

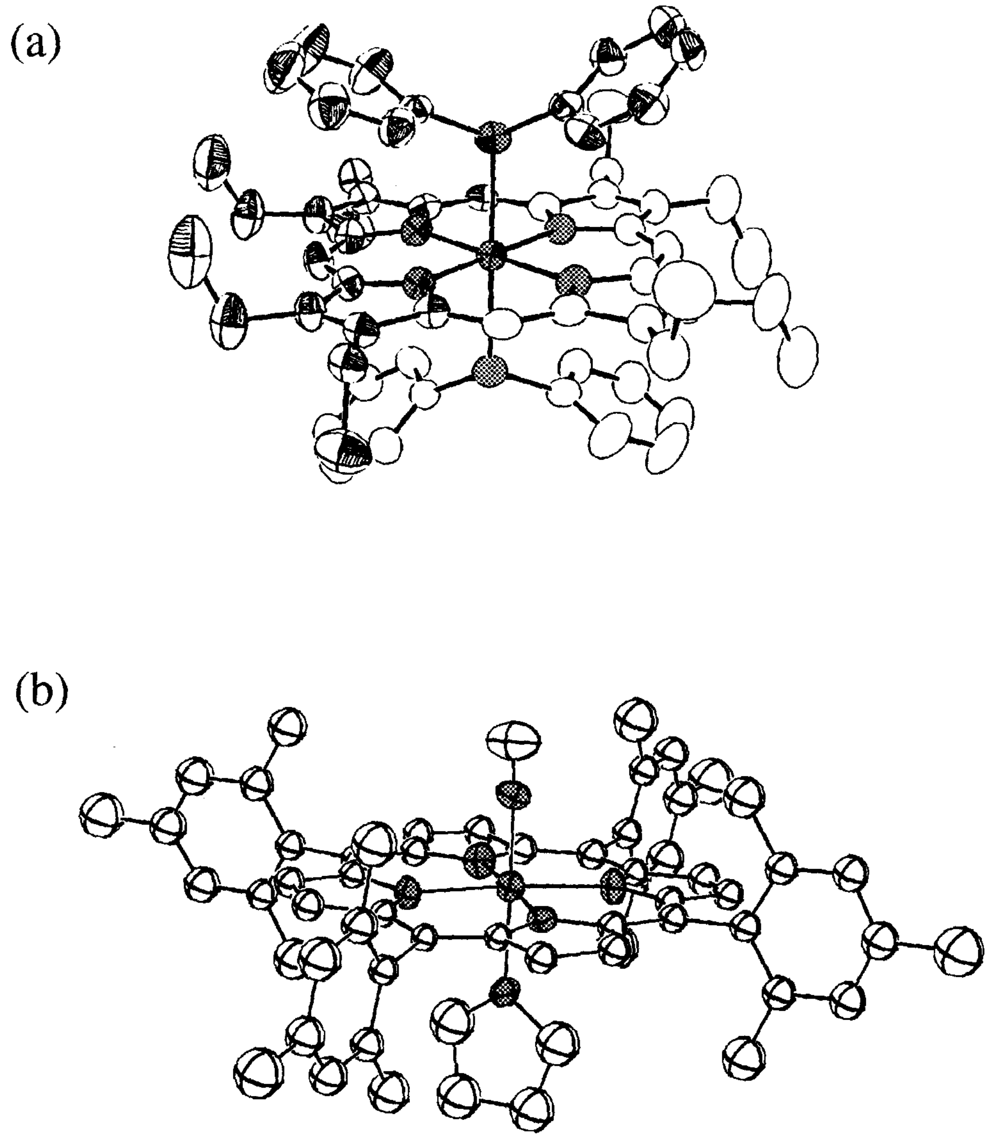

Figure 1.2. Sample structures of Ru(OEP)$L_2$ and Ru(TMP)$L_2$ complexes.
a) Ru(OEP)($Ph_2S$)$_2$ (taken from reference 19); b) Ru(TMP)(THF)($N_2$) (taken from reference 8b).

axial sites. Of importance, Ru(TMP) is sterically prevented from forming $\mu$-oxo dimers, and the end-product of Ru(TMP) oxidation, and of Ru(TMP)$L_2$ oxidation when L is a labile axial ligand such as MeCN or THF, has been shown to be the *trans*-dioxo species $Ru^{VI}(TMP)(O)_2$.[8,9b,11] Unlike the $\mu$-oxo dimers, which do not act as O-atom donors, $Ru^{VI}(TMP)(O)_2$ reacts readily with oxygen atom acceptors such as olefins[11] and organic sulfides,[9b,25] to give the corresponding epoxides and sulfoxides. This type of reaction (O-atom transfer from metal-oxo species generated via $O_2$) has generated considerable interest in recent years, and several studies have been published on the subject;[4,9b,11,25,26] two examples will be considered in detail.

In their 1985 paper, Groves and Quinn reported that Ru(TMP)$(O)_2$ will catalyze the $O_2$-oxidation of various alkenes to their corresponding epoxides, with two moles of epoxide being produced for every mole of $O_2$ consumed.[11] The *trans*-dioxo species was also found to oxidize alkenes stoichiometrically in the absence of $O_2$, if pyridine was added to the reaction mixture. Thus the products of the stoichiometric oxidation of norbornene were about 1.6 equivalents of norbornene oxide and $Ru^{II}(TMP)py_2$.[11] The mechanism proposed for the catalytic oxidation is shown in figure 1.3. The *trans*-$Ru^{VI}$dioxo species transfers an O-atom to an alkene, leaving an epoxide and $O{=}Ru^{IV}(TMP)$; this species disproportionates to $Ru^{VI}(TMP)(O)_2$ and Ru(TMP), which is immediately oxidized back to $O{=}Ru^{IV}(TMP)$ by $O_2$. The intermediacy of the $O{=}Ru^{IV}(TMP)$ species has since been verified by independent spectroscopic studies, as has its sensitivity to disproportionation.[27] Structures of *trans*-Ru(OCP)$(O_2)$[28] and Ru(OCP(CO)(Styrene Oxide)[29] have been reported also, where OCP

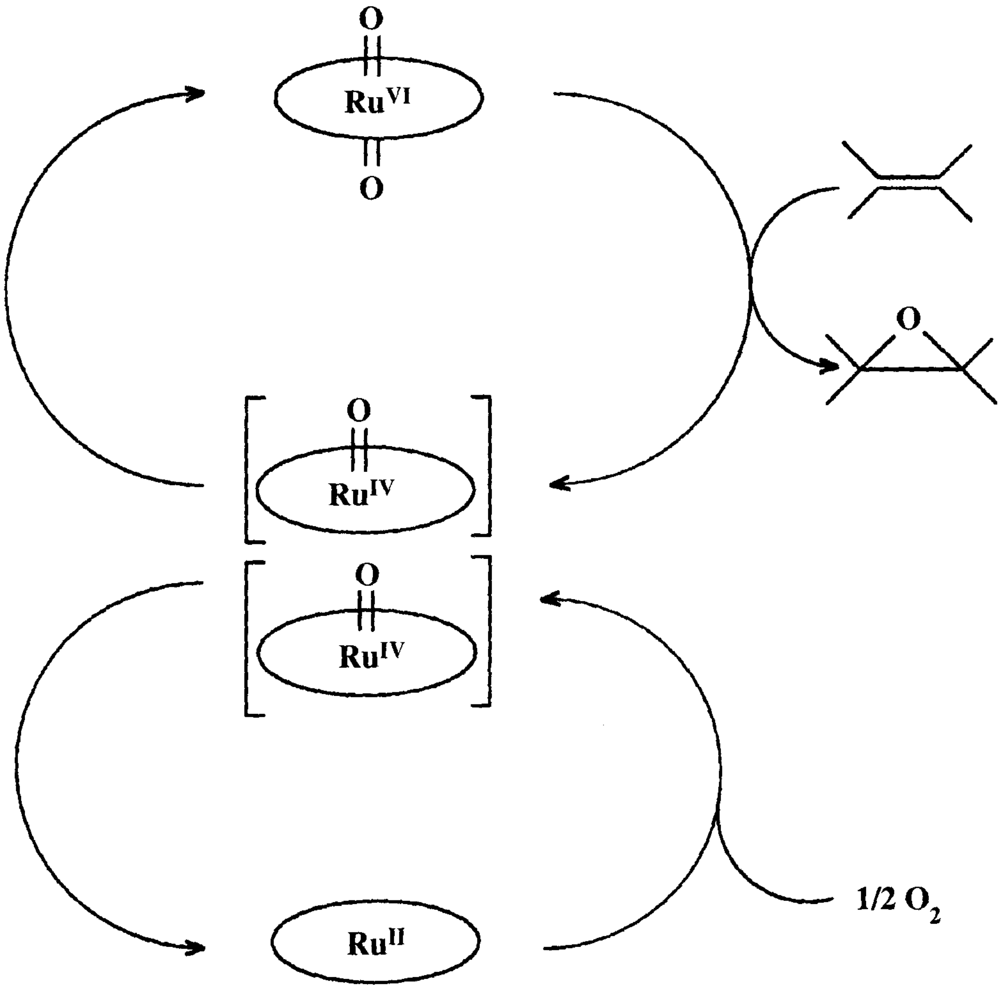
O
Ru$^{VI}$
O
O
O
Ru$^{IV}$
O
Ru$^{IV}$
Ru$^{II}$
1/2 $O_2$

Figure 1.3. Proposed catalytic cycle for the epoxidation of olefins catalyzed by Ru(TMP)$(O)_2$ (taken from reference 11).

("octachloroporphyrin") is the dianion of meso-tetra(2,6-dichlorophenyl)porphyrin (see below).

Studies carried out in our laboratories have focused in detail on the reactions of $Ru(TMP)(O)_2$ with phenol and with dialkylsulfides;[9b,9h,25] the latter reactions are directly related to the subject of this thesis, and will be discussed in some detail. Uv/vis and $^1H$-nmr experiments showed that if excess of a dialkylsulfide such as $Et_2S$ was added to a benzene solution of $Ru(TMP)(O)_2$ under argon (or dioxygen), $Ru^{II}(TMP)(\underline{O}SR_2)_2$, $Ru^{II}(TMP)(\underline{O}SR_2)(O\underline{S}R_2)$, and $Ru^{II}(TMP)(O\underline{S}R_2)_2$ were produced consecutively ($\underline{O}$ and $\underline{S}$ signify oxygen- and sulfur-bound sulfoxides, respectively). The mechanism (supported by kinetic data) proposed for these transformations was:

$$Ru(TMP)(O)_2 + SR_2 \rightarrow [O{=}Ru(TMP)\underline{O}SR_2] \tag{1.8}$$

$$[O{=}Ru(TMP)\underline{O}SR_2] + SR_2 \rightarrow Ru(TMP)(\underline{O}SR_2)_2 \tag{1.9}$$

$$Ru(TMP)(\underline{O}SR_2)_2 \rightarrow Ru(TMP)(\underline{O}SR_2)(O\underline{S}R_2) \tag{1.10}$$

$$Ru(TMP)(\underline{O}SR_2)(O\underline{S}R_2) \rightarrow Ru(TMP)(O\underline{S}R_2)_2 \tag{1.11}$$

The $O{=}Ru(TMP)\underline{O}SR_2$ intermediate was not observed experimentally, and kinetic data implied that reaction 1.9 was much faster than 1.8. Interestingly, this situation is different from that implied by the results obtained for the epoxidation of olefins; in this latter case, the major species present during catalysis was considered to be $O{=}Ru(TMP)$;[11,27] it appears that the substrate being oxidized plays an important role in determining the preferred oxidation state of the detected ruthenium species. The data imply that $Ru^{VI}(TMP)(O)_2$ is more effective than $Ru^{IV}(TMP)O$ for olefin epoxidation, while $Ru^{IV}(TMP)(O)(\underline{O}SR_2)$ is more effective than $Ru^{VI}(TMP)(O)_2$ for O-atom transfer to thioethers. Both reactions 1.8 and 1.9 are much faster than the subsequent axial ligand isomerization reactions 1.10 and 1.11; once formed, $Ru(TMP)(O\underline{S}R_2)_2$ is substitutionally inert under the ambient reaction conditions.[9b,9h,25]

The $Ru(TMP)/O_2$ system will catalytically oxidize dialkylsulfides selectively to the corresponding sulfoxides; however, the catalysis stops after about 8 turnovers at ambient conditions.[9b,9h,25] The catalysis was considered to occur via the loss of the O-bonded sulfoxides from $Ru(TMP)(\underline{O}SR_2)_2$ to regenerate under $O_2$ the *trans*-dioxo species, while formation of the substitutionally inert $Ru(TMP)(O\underline{S}R_2)_2$ inhibited the catalytic cycle. At higher temperatures (e.g. 65° C), up to 15 turnovers were recorded; however, under these conditions rapid catalyst degradation occurred.

More efficient catalytic oxidation of dialkylsulfides was obtained by using *trans*-$Ru(OCP)(O)_2$ as a catalyst instead of the TMP system.[9b,9h] The axial sites of Ru(OCP) are sterically hindered as in Ru(TMP), so that again $\mu$-oxo dimer formation is prevented. In addition, the electron-withdrawing chloro groups on the phenyls make the porphyrin more resistant to self-oxidation, a well established phenomenon.[4] The greater robustness of $Ru(OCP)(O)_2$, compared to the TMP system, allowed its use at temperatures as high as 100° C, and, under these conditions, more than 30 equivalents of dialkylsulfide could be oxidized to sulfoxide, with no observable decomposition of the catalyst.[9b,9h] Of note, in addition to making the catalyst more resistant to self-oxidation, the Cl substituents also make the O=Ru=O moiety more electrophilic,[4] which has two beneficial effects: first, the reactivity toward the thioether substrate is increased, as evidenced by increased reaction rates even at room temperatures, and second, Ru(OCP)($\underline{O}SR_2$)$_2$ is stabilized relative to the S-bound isomers.[9b,9d] Previous reports in the 1970s (on non-porphyrin systems) have suggested that S-bonded dimethylsulfoxide (dmso) complexes of ruthenium are favoured in cases where the metal center is electron-rich (in which case Ru→S $\pi$-backbonding can reduce the electron density on the metal), whereas O-bonding is favoured when the metal center is more electron-deficient;[30,31] however, more recent findings on both dmso and tetramethylenesulfoxide derivatives of $Ru^{II}$ suggest that steric factors dominate the choice of oxygen- versus sulfur-bonding.[32]

## 1.3 Reactivity of Dialkylsulfides with Dioxygen

Under ambient conditions and in the absence of a catalyst or radical initiator, dialkylsulfides do not react with $O_2$.[33] In the presence of a free-radical initiator such as azoisobutyronitrile (AZBN), autoxidation of the dialkylsulfides proceeds via hydrogen atom abstraction; the observed product distribution has been rationalized by the following mechanistic scheme:[33]

*Stage 1*

$$R'CH_2SR'' + R\cdot \rightarrow R'(CH\cdot)SR'' \qquad \text{(Chain Initiation)} \qquad 1.12$$

$$R'(CH\cdot)SR'' + O_2 \rightarrow R'CH(O_2\cdot)SR'' \qquad 1.13$$

$$R'CH(O_2\cdot)SR'' + R'CH_2SR'' \rightarrow R'CH(O_2H)SR'' + R'(CH\cdot)SR'' \qquad 1.14$$

*Stage 2*

$$R'CH(O_2H)SR'' + R'CH_2SR'' \rightarrow R'CH(OH)SR'' + R'CH_2(SO)R'' \qquad 1.15$$

*Stage 3*

$$R'CH(OH)SR'' \rightarrow R'CHO + R''SH \qquad 1.16$$

$$R'CH(OH)SR'' + R''SH \rightarrow H_2O + \text{Complex sulfides} \qquad 1.17$$

As can be seen, the free-radical process yields a fairly complex product distribution, which is generally undesirable. The aim of our investigations, as well as those of other researchers in the field, has been to try to find catalysts which result in the selective (preferably exclusive) production of dialkylsulfoxides,[13] or sometimes dialkylsulfones.[13b]

In 1985 Riley and Correa reported that, in polar solvents, and under conditions of high temperature ($>100°$ C) and $O_2$ pressure ($\sim 40$ atm), dialkylsulfides were slowly but selectively oxidized to the corresponding sulfoxides.[34] The mechanism suggested for this reaction was[34,35]

$$R_2S + O_2 \rightarrow R_2S^{+\cdot} + O_2^{-\cdot} \qquad 1.18$$

$$R_2S^{+\cdot} + O_2 \rightarrow R_2S^{+}OO^{\cdot} \qquad 1.19$$

$$R_2S^{+}OO^{\cdot} + O_2^{-\cdot} \rightarrow R_2S^{+}OO^{-} + O_2 \qquad 1.20$$

$$R_2S^{+}OO^{-} + R_2S \rightarrow 2R_2SO \qquad 1.21$$

Two later papers[15,36] reported that cerium(IV) ammonium nitrate is a very efficient catalyst for the process just described; it was proposed that cerium(IV), being a better oxidant than $O_2$, was now responsible for the initial one-electron oxidation of the $R_2S$ (reaction 1.18).[15,36] Thus

$$R_2S + Ce^{IV} \rightarrow R_2S^{+\cdot} + Ce^{III} \qquad 1.22$$

The thioether radical cation could then undergo reaction 1.19, after which the $Ce^{IV}$ would be regenerated according to the process

$$R_2S^{+}OO^{\cdot} + Ce^{III} \rightarrow R_2S^{+}OO^{-} + Ce^{IV} \qquad 1.23$$

Finally, two sulfoxides would be regenerated according to equation 1.21. This system is reportedly very efficient; thus, for example, in a 9:1 $CH_3CN/H_2O$ solution, containing about 0.017 M ceric ammonium nitrate and 1.0 M tetrahydrothiophene under 125 psi $O_2$

pressure, the thioether was completely oxidized with a half-life of 7 min at 75° C.

The $Ce^{IV}$ systems from Riley's group,[15,36] and those reported from this laboratory and discussed in section 1.2,[9b,9h,25] appear to be the only ones, apart from a system to be described in this thesis, in which the selective catalytic $O_2$-oxidation of dialkylsulfides to the corresponding sulfoxides is accomplished with potentially useful turnovers. Other systems for the metal-complex catalyzed $O_2$-oxidation of thioethers to sulfoxides have been described,[37-42] but in every case a stoichiometric reagent other than $O_2$ was also required. Two such systems are given as examples.

In 1984 Riley and Shumate reported that *cis*-$RuCl_2(dmso)_4$ and *trans*-$RuBr_2(dmso)_4$ catalyzed selective oxidation of various dialkylsulfides to their corresponding sulfoxides, under 100 psi of $O_2$ at 100° C.[37] This reaction proceeded only in alcoholic solvents. From kinetic studies and product analysis, the following mechanistic scheme was proposed:

$$\text{"Ru}^{II}\text{"} + 2H^+ + O_2 \rightarrow \text{"Ru}^{IV}\text{"} + H_2O_2 \qquad 1.24$$

$$R_2S + H_2O_2 \rightarrow R_2SO + H_2O \qquad 1.25$$

$$\text{"Ru}^{IV}\text{"} + Me_2CHOH \rightarrow \text{"Ru}^{II}\text{"} + Me_2C{=}O + 2H^+ \qquad 1.26$$

The 1984 article gave no conclusions as to the nature of the actual catalytic species, but later studies provided evidence which suggested that the *trans,trans,trans*-$RuX_2(SR_2)_2(dmso)_2$ species are the starting catalysts.[38] No further details were given on the possible nature of the $Ru^{IV}$ intermediate. The original paper cited the lack of free radical products of alcohol oxidation, and separate studies with various discrete $Ru^{III}$ species supported the hypothesis that $Ru^{II}$ is oxidized directly to $Ru^{IV}$ via reaction 1.24.[37]

Another system in which catalytic oxidation of thioethers was observed involved the autoxidation of diphenylsulfide catalyzed by $RhCl_3(dmso)_3$, in N,N'-dimethylformamide (DMA) solvent.[39] In this case, $H_2$ was used as the coreductant, following earlier work on the use of $H_2$ with $Rh^{III}$ to reduce dmso catalytically to the sulfide.[40] The following mechanism was proposed for the sulfide oxidation:

$$Rh^{III}dmso + DMA \rightleftharpoons Rh^{III}DMA + dmso \qquad 1.27$$

$$Rh^{III}DMA + H_2 \rightarrow [Rh^{I}DMA] + 2H^+ \qquad 1.28$$

$$[Rh^{I}DMA] + O_2 \rightarrow Rh^{III}(O_2^{2-})(DMA) \qquad 1.29$$

$$Rh^{III}(O_2^{2-})(DMA) + H_2 \rightarrow [Rh^{I}DMA] + H_2O_2 \qquad 1.30$$

$$H_2O_2 + Ph_2S \rightarrow H_2O + Ph_2SO \qquad 1.31$$

Steps 1.27 and 1.28 generate the $O_2$-sensitive catalyst; the catalysis operates via steps 1.29-1.31. Attempts at carrying out these reactions in other solvents, such as 1,2-dichloroethane, were not successful. Interestingly, more basic dialkylsulfides were not oxidized by the $RhCl_3(dmso)_3$ system. This suggested that, in this case, coordination by sulfides inactivated a potentially catalytic system.[39]

## 1.4 Outline of this Thesis

Earlier work from these laboratories had noted briefly that $Ru(OEP)(decMS)_2$ (decMS = decylmethylsulfide) could catalyze the air-oxidation of free decMS in benzene;[19,43] this catalysis was very slow, but could be accelerated if the solutions were made acidic. The product distributions observed for the catalytic reaction varied unpredictably, and decMSO was not generally the only product; however, in the absence of excess thioether, exposure of $Ru(OEP)(decMS)_2$ to air resulted in its slow but clean stoichiometric oxidation to Ru(OEP)(decMS)(decMSO). Furthermore, addition of an excess of decMS to the Ru(OEP)(decMS)(decMSO) solution regenerated the starting $Ru(OEP)(decMS)_2$ complex, thus constituting one turn of a catalytic cycle.[43]

The first part of the investigation described in this thesis focussed on elucidating the mechanism of the stoichiometric $O_2$-oxidation of $Ru(OEP)(decMS)_2$ and other $Ru(OEP)(RR'S)_2$ complexes. This part of the investigation is related in chapter 2. Attention then turned to the problem of using $Ru(OEP)(RR'S)_2$ complexes to catalyze the selective $O_2$-oxidation of free thioethers to the corresponding sulfoxides. The conditions under which such catalysis can take place, along with a detailed kinetic analysis of the catalytic system, are all included in chapter 3. The derivations of rate laws, used in the kinetic analysis described in chapter 3, are given in chapter 4.

## NOTES AND REFERENCES FOR CHAPTER 1

1. Buchler, J. W. In *The Porphyrins*, Dolphin, D., Ed., Academic Press, New York, N. Y., 1978; vol. I, p. 389.

2. a) *Iron Porphyrins*, Lever, A. B. P. and Gray, H. B., Eds.; Addison-Wesley, Massachusetts, Parts 1 and 2, 1981. b) *Oxygen Complexes and Oxygen Activation by Transition Metals*, Martell, A. E. and Sawyer, D. T., Eds.; Plenum, New York, N. Y., 1988.

3. See for example: a) Collman, J. P. *Acc. Chem. Res.* **1977**, *10*, 265. b) Perutz, M. F. *Scientific Am.* **1978**, *239*, 256. c) Mansuy, D. *Pure and Appl. Chem.* **1987**, *59*, 759. d) Collman, J. P.; Kodadak, T.; Brauman, J. I. *J. Am. Chem. Soc.* **1986**, *108*, 2588.

4. See for example: a) Ellis, P. E., Jr.; Lyons, J. E. *J. Chem. Soc., Chem. Commun.* **1989**, 1189. b) Ellis, Jr. P. E.; Lyons, J. E. *Coord. Chem. Rev.* **1990**, *105*, 181.

5. Fleischer, E. B.; Thorp, R.; Venerable, D. *J. Chem. Soc., Chem. Commun.* **1969**, 475.

6. Collman, J. P.; Barnes, C. E.; Swepston, P. N.; Ibers, J. A. *J. Am. Chem. Soc.* **1984**, *106*, 3500.

7. Collman, J. P.; Prodolliet, J. W.; Leidner, C. R. *J. Am. Chem. Soc.* **1986**, *108*, 2916.

8. a) Camenzind, M. J.; James, B. R.; Dolphin, D. *J. Chem. Soc., Chem. Commun.* **1986**, 1137. b) Camenzind, M. J.; James, B. R.; Dolphin, D.; Sparapany, J. W.; Ibers, J. A. *Inorg. Chem.* **1988**, *27*, 3054.

9. Several more recent publications on various aspects of ruthenium porphyrin chemistry include: a) Mashiko, T.; Dolphin, D.; In *Comprehensive Coordination Chemistry*, Wilkinson, G., Gillard, R. D. and McCleverty, J. A., Eds.; Pergamon Press, Oxford, 1987; Vol. 2, p. 813. b) James, B. R.; *Chem. Ind.* **1992**, *47*, 245, and references therein. c) Ke, M.; Sishta, C.; James, B. R.; Dolphin, D.; Sparapany, J. W.; Ibers, J. A. *Inorg. Chem.* **1991**, *30*, 4766, and references therein. d) Rajapakse, N.; James, B. R.; Dolphin, D. *Can. J. Chem.* **1990**, *68*, 2274. e) Huang, J.; Che, C.; Li, Z.; Poon, C. *Inorg. Chem.* **1992**, *31*, 1313. f) Seyler, J. W.; Safford, L. K.; Fanwick, P. E.; Leidner, C. E. *Inorg. Chem.* **1992**, *31*, 1545. g) Sishta, P. C. Ph.D. Dissertation, The University of British Columbia, Vancouver, B. C., 1990. h) Rajapakse, N. Ph.D. Dissertation, The University of British Columbia, Vancouver, B. C., 1990.

10. a) Domazetis, G.; Tarpey, B.; Dolphin, D.; James, B. R. *J. Chem. Soc., Chem. Commun.* **1980**, 939. b) Domazetis, G.; James, B. R.; Tarpey, B.; Dolphin, D. *ACS Symp. Ser.* **1981**, *152*, 243.

11. Groves, J. T.; Quinn, R. *J. Am. Chem. Soc.* **1985**, *107*, 5790.

12. James, B. R.; Mikkelsen, S. R.; Leung, T. W.; Williams, G. M.; Wong, R. *Inorg. Chim. Acta* **1984**, *85*, 209.

13. a) Ranky, W. O.; Nelson, D. C. In *Organic Sulfur Compounds*, Karasch N., Ed., Pergamon Press, New York, N. Y., 1961; Vol I, Chapter 17. b) Ledlie, M. A.; Alum, K. G.; Howell, J. V.; Pitkethly, G. *J. Chem. Soc., Perkin Trans. 1* **1976**, 1734.

14. Riley, D. P.; Correa, P. E. *J. Chem. Soc., Chem. Commun.* **1986**, 1097.

15. Riley, D. P.; Smith, M. R.; Correa, P. E. *J. Am. Chem. Soc.* **1988**, *110*, 177.

16. Chow, B. C.; Cohen, I. A. *Bioinorg. Chem.* **1971**, *1*, 57.

17. a) Brown, G. M.; Hopf, F. R.; Ferguson, J. A.; Meyer, T. J.; Whitten, D. G. *J. Am. Chem. Soc.* **1973**, *95*, 5939. b) Brown, G. M.; Hopf, F. R.; Meyer, T. J.; Whitten, D. G. *J. Am. Chem. Soc.* **1975**, *97*, 5385.

18. See for example, references 6 or 8.

19. James, B. R.; Pacheco, A. A.; Rettig, S. J.; Ibers, J. A. *Inorg. Chem.* **1988**, *27*, 2414.

20. a) Farrell, N. P.; Dolphin, D.; James, B. R. *J. Am. Chem. Soc.* **1978**, *100*, 324. b) Barringer, L. F.; Rillema, D. P.; Ham, J. H. *J. Inorg. Biochem.* **1984**, *21*, 195.

21. See for example: Collman, J. P.; Hegedus, L. S. *Principles and Applications of Organotransition Metal Chemistry*, University Science Books, Mill Valley, CA, 1980; p. 27.

22. Sawyer, D. T.; Valentine, J. S. *Acc. Chem. Res.* **1981**, *14*, 393.

23. Collman, J. P.; Barnes, C. E.; Brothers, P. J.; Collins, T. J.; Ozawa, T.; Gallucci, J. C.; Ibers, J. A. *J. Am. Chem. Soc.* **1984**, *106*, 5151.

24. a) Masuda, H.; Taga, T.; Osaki, K.; Sugimoto, H.; Mori, M.; Ogoshi, H. *J. Am. Chem. Soc.* **1981**, *103*, 2199. b) Masuda, H.; Taga, T.; Osaki, K.; Sugimoto, H.; Mori, M.; Ogoshi, H. *Bull. Chem. Soc. Jap.* **1982**, *55*, 3887.

25. a) Rajapakse, N.; James, B. R.; Dolphin, D. *Catal. Lett.* **1989**, *2*, 219. b) Rajapakse, N.; James, B. R.; Dolphin, D. *Stud. Surf. Sci. Catal.* **1990**, *66*, 109.

26. Tavares, M.; Ramasseul, R.; Marchon, J. C. *Catal. Lett.* **1990**, *4*, 163.

27. Groves, J. T.; Ahn, K. H. *Inorg. Chem.* **1987**, *26*, 3833.

28. Groves, J. T. Lecture K6 presented at the 8th International Symposium on Homogeneous Catalysis, Amsterdam, August, 1992.

29. Groves, J. T.; Han, Y; Engen, D. V. *J. Chem. Soc., Chem. Commun.* **1990**, 436.

30. a) McMillan, R. S.; Mercer, A.; James, B. R.; Trotter, J. *J. Chem. Soc., Dalton Trans.* **1975**, 1006. b) Mercer, A.; Trotter, J. *J. Chem. Soc., Dalton Trans.* **1975**, 2480.

31. Davies, A. R.; Einstein, F. W. B.; Farrell, N. P.; James, B. R.; McMillan, R. S. *Inorg. Chem.* **1978**, *17*, 1965.

32. a) Yapp, D. T. T.; Jaswal, J.; Rettig, S. J.; James, B. R.; Skov, K. A. *Inorg. Chim. Acta* **1990**, *177*, 199. b) Alessio, E.; Milani, B.; Mestroni, G.; Calligaris, M.; Faleschini, P.; Attia, W. M. *Inorg. Chim. Acta* **1990**, *177*, 255.

33. Barnard, D.; Bateman, L.; Cuneen, J. I. In *Organic Sulfur Compounds*, Karasch N., Ed., Pergamon Press, New York, N. Y., 1961; Vol. I, Chapter 21.

34. Correa, P. E.; Riley, D. P. *J. Org. Chem.* **1985**, *50*, 1787.

35. Correa, P. E.; Hardy, G.; Riley, D. P. *J. Org. Chem.* **1988**, *53*, 1695.

36. Riley, D. P.; Correa, P. E. *J. Chem. Soc., Chem. Commun.* **1986**, 1097.

37. Riley, D. P.; Shumate, R. S. *J. Am. Chem. Soc.* **1984**, *106*, 3179.

38. Riley, D. P.; Oliver, J. D. *Inorg. Chem.* **1986**, *25*, 1814.

39. a) Gamage, S. N. Ph.D. Dissertation, The University of British Columbia, Vancouver, B. C., 1985. b) Gamage, S. N.; James, B. R.; *J. Chem. Soc., Chem. Commun.* **1989**, 1624.

40. James, B. R.; Ng, F. T. T.; Rempel, G. L. *Can. J. Chem.* **1969**, *47*, 4521.

41. Srivastava, R. S.; Milani, B.; Alessio, E.; Mestroni, G. *Inorg. Chim. Acta* **1992**, *191*, 15, and references therein.

42. Taqui-Khan, M. M.; Bajaj, H. C.; Chatterjee, D. *J. Mol. Catal.* **1992**, *71*, 177, and references therein.

43. James, B. R.; Pacheco, A.; Rettig, S. J.; Thorburn, I. S.; Ball, R. G.; Ibers, J. A. *J. Mol. Catal.* **1987**, *41*, 147.

# CHAPTER 2

# REACTION OF Ru(OEP)(RR'S)$_2$ COMPLEXES WITH DIOXYGEN IN ACIDIC MEDIA

## 2.1 Introduction

Previous studies carried out in our laboratories showed that if a benzene solution of Ru(OEP)(decMS)$_2$ (decMS ≡ n-decylmethylsulfide) was exposed to air for an extended period of time (from a week to a few months), the complex underwent ligand oxidation to give Ru(OEP)(decMS)(decMSO) and Ru(OEP)(decMSO)$_2$ (decMSO ≡ n-decylmethylsulfoxide) as the major products, along with other minor products.[1a] Later studies have shown that Ru(OEP)(dms)$_2$ (dms ≡ dimethylsulfide) and Ru(OEP)(Et$_2$S)$_2$ have similar reactivity, both in benzene and other solvent systems.[1b] The degree of reactivity of the complex, as well as the exact product distribution observed, depend not only on the dialkylsulfide and solvent used, but also on the dryness of the solvent and other variables which are difficult to quantify. Because of this it is difficult to get reproducible results when studying such systems. On the other hand, if an *acidic* solution of Ru(OEP)(RR'S)$_2$ (where R ≡ methyl, ethyl or decyl and R' ≡ methyl or ethyl) is exposed to air, the axial ligands are oxidized to the corresponding sulfoxides in a highly reproducible manner, both in benzene (or toluene) and in methylene chloride. Furthermore, several intermediates are observable over the course of the oxidation process. In this chapter these intermediates are identified and characterized, and a mechanism for the oxidation of the Ru(OEP)(RR'S)$_2$ complexes is proposed based on the presence of the intermediates and other observations.

## 2.2 Experimental

### 2.2.1 General Reagents, Gases and Solvents

All non-deuterated solvents were obtained from BDH. Hydrocarbon solvents were reagent grade, and were stored in-vacuo over sodium benzophenone ketyl; all other solvents were glass-distilled spectroscopic grade, and were stored in-vacuo over 3 Å molecular sieves. Deuterated solvents were obtained from MSD Isotopes or from CIL, and were stored in the same way as the non-deuterated solvents.

Gases were supplied by Union Carbide of Canada Ltd. Dinitrogen for the glove-box was prepurified grade, all others were USP grade. Unless otherwise specified, all gases were used without further purification. A gas could be dried by passing it through a drying tower containing 3 Å molecular sieves; for especially air-sensitive solutions, argon was passed down a Ridox deoxygenation column prior to use.

Air- or moisture-sensitive solids were stored in a glove-box, the $N_2$ atmosphere of which was continuously recirculated through a Dri-Train HE-439 purification tower packed with 2.4 kg of 3 Å molecular sieves, 1.5 kg of 7 Å molecular sieves, and 2 kg of Ridox deoxygenation catalyst. This treatment kept the concentration of $O_2$ and $H_2O$ below 1 ppm, as evidenced by the long lifetime of an exposed 25-W light bulb filament within the box.[2]

The thioethers dms and $Et_2S$ were obtained from Aldrich, while decMS was obtained from Fairfield chemicals; all three were distilled prior to use,and their purity checked by gas chromatography and $^1$H-nmr spectroscopy. Dimethylsulfoxide (dmso) was spectrograde from BDH, while dmso-$d_6$ was from MSD isotopes. Diethylsulfoxide and decMSO were synthesized according to standard procedures.[1a,3] Both dmso and $Et_2SO$

were stored under argon over 3 Å molecular sieves; decMSO is a solid and not particularly hygroscopic, so no special storage precautions were employed.

Benzoic acid (PhCOOH) was of uncertain origin, but its purity was verified by $^1$H-nmr spectroscopy, melting point comparison with literature values, and titration with NaOH. Tetrafluoroboric acid ($HBF_4$) was obtained as a 48% aqueous solution from MCB, and used without further purification.

Tetramethylammonium hydroxide ($Me_4N^+OH^-$) was obtained from Anachemia chemicals as a nominally 25% aqueous solution; tetra-n-butylammonium hydroxide was nominally a 40% aqueous solution from BDH. Both were used without further purification.

Silver tetrafluoroborate ($AgBF_4$) was obtained from Aldrich chemicals, and was opened and stored in the glove-box.

### 2.2.2 Tetramethylammonium Benzoate ($Me_4N^+PhCOO^-$)

A 0.9 M solution of PhCOOH in ethanol was added dropwise to about 4 g of 25% aqueous $Me_4N^+OH^-$ until the resultant mixture was slightly acidic to litmus (approximately 14 mL of acid solution were required). The water and ethanol were removed using a rotary evaporator, and the resultant solid was redissolved in ethanol (125 mL); the mixture was refluxed for about 10-15 min, and then filtered to remove a greyish-white flaky precipitate. The volume of the filtered solution was reduced to approximately 2 mL using a rotary evaporator, at which point 40 mL of diethyl ether were added. The desired product was obtained as a white precipitate, which was filtered and dried overnight at 80° C. $Me_4N^+PhCOO^-$ is extremely hygroscopic, and had to be stored and handled in a glove-box; in solution, the salt was handled exclusively in-vacuo. It is stable indefinitely in acetonitrile solution, but slowly degrades in methylene chloride. Yield: 2.13 g (95% relative to $Me_4N^+OH^-$ used) Anal. Calcd. for $C_{11}H_{17}NO_2$: C, 67.66; H, 8.78; N, 7.17. Found: C, 67.76; H, 8.60; N, 6.99. NMR ($\delta$; $CD_3CN$ or $CD_2Cl_2$, 20° C): 7.29 m ($H_{m,p}$), 7.96 m ($H_o$), 3.48 s ($NCH_3$).

### 2.2.3 Tetra-n-butylammonium Tetrafluoroborate (n-$Bu_4N^+BF_4^-$)

To about 95 g (0.146 mol) of n-$Bu_4N^+OH^-$ solution was added enough $HBF_4$ solution to produce a pH-neutral mixture (checked by litmus test). The resulting white precipitate was filtered off, washed with three 50-mL aliquots of ice-cold water, and then dried in-vacuo for 24 h. The dry powder was dissolved in 45 mL of ethyl acetate, passed through a filter paper to remove cloudiness, and then recrystallized by adding approximately 0.6 equivalents of n-pentane, and cooling at -5° C for 1h. After a second recrystallization procedure, the product was dried in-vacuo at room temperature for 48 h. Prepared in this way, n-$Bu_4N^+BF_4^-$ showed no electrochemical activity in cyclic voltammetric scans from -1.6 to +1.6 V.

### 2.2.4 Ruthenium Porphyrin Complexes

Ruthenium was obtained on loan from Johnson, Matthey Ltd, in the form of $RuCl_3.3H_2O$ (approximately 40% by weight). $H_2OEP$ was kindly provided by Dr. D. Dolphin of this department.

$Ru_3CO_{12}$,[4] Ru(OEP)(CO)py,[5] and Ru(OEP)$py_2$,[5] the necessary precursors to make $[Ru(OEP)]_2$[6] and $[Ru(OEP)]_2(BF_4)_2$,[7] were made by the literature procedures cited; for all these compounds the spectroscopic data (nmr, uv/vis, ir) were in excellent agreement with those reported previously, and elemental analysis for C, H, and N was within 0.3% of the theoretical values. A detailed description of the specialized high pressure and photolysis equipment used in our laboratories for the syntheses of $Ru_3CO_{12}$ and $Ru(OEP)py_2$ can be found in reference 1a.

The dimer $[Ru(OEP)]_2$ was prepared by high-vacuum pyrolysis of $Ru(OEP)py_2$,[6] while the oxidized dimer $[Ru(OEP)]_2(BF_4)_2$ was prepared by adding 2 equivalents of $AgBF_4$ to a benzene solution of $[Ru(OEP)]_2$.[7] Removal of metallic silver from the oxidized dimer required that a $CH_2Cl_2$ solution of the complex be filtered through a Celite pad; the fine frits available in our laboratories were not fine enough to prevent the passage of finely divided metallic silver. Both dimers are extremely air-sensitive, both in solution and in the solid state. The solids were stored in the glove-box. In solution the dimers were handled using vacuum-transfer techniques where possible; when this was impractical, manipulations were carried out as fast as possible under dry, deoxygenated argon, using a combination of Schlenk and syringe techniques.[8]

The synthesis and characterization of $Ru(OEP)(decMS)_2$ has been previously described.[9]

### 2.2.4.1 $Ru(OEP)(dms)_2$

Approximately 25 $\mu$L (0.34 mmol) of dms and 5 mL of methylene chloride were vacuum-transferred onto 0.1083 g (0.085 mmol) of $[Ru(OEP)]_2$, which immediately gave a red solution. The volume was increased to about 15 mL with n-hexane, and then slowly reduced until traces of precipitate appeared. The solution was filtered, and the volume further decreased until considerable precipitation occurred. This concentrate was now heated to redissolve the complex, and then allowed to cool slowly, first to room temperature and then to 0° C. The dark purple crystalline Ru(OEP)(dms)$_2$ was filtered off and dried in vacuo at 70° C overnight. Yield: 0.104 g (0.137 mmol, 81%). Anal. calcd. for $C_{40}H_{56}N_4S_2Ru$: C, 63.37; H, 7.45; N, 7.39. Found: C, 63.47; H, 7.48; N, 7.20. NMR ($\delta$; $CD_2Cl_2$, 20.0° C): OEP, 1.81 t ($CH_3$), 3.85 q ($CH_2$), 9.32 s ($H_{meso}$); dms, -2.66 s. Uv/vis (0.0445 mM soln. in $C_6H_6$ containing 68 mM dms) $\lambda_{max}$ (log $\epsilon$): 407.5 (5.34)(Soret), 498 (4.17), 525 (4.42) nm.

### 2.2.4.2 Ru(OEP)(Et$_2$S)$_2$

The procedure for the synthesis of Ru(OEP)(Et$_2$S)$_2$ was analogous to that of Ru(OEP)(dms)$_2$. Yield: 0.257 g (0.315 mmol, 85%). Anal. calcd. for $C_{44}H_{64}N_4S_2Ru$: C, 64.91; H, 7.92, N, 6.88. Found: C,64.73; H,7.87; N,6.68. NMR ($\delta$; $CD_2Cl_2$, 20.0° C): OEP, 1.78 t ($CH_3$), 3.96 q ($CH_2$), 9.25 s ($H_{meso}$); Et$_2$S, -1.32 t ($CH_3$), -2.47 q ($CH_2$). Uv/vis (0.0340 mM soln. in $C_6H_6$ containing 74 mM Et$_2$S) $\lambda_{max}$ (log $\epsilon$): 409 (5.23) (Soret), 499 (4.13), 525 (4.39) nm.

### 2.2.4.3 Ru(OEP)(dm$\underline{s}$o)$_2$ and the dmso-d$_6$ Analogue

Ru(OEP)(dm$\underline{s}$o)$_2$ (where $\underline{s}$ implies s-bonded) was prepared by adding 16 $\mu$L (0.23 mmol) of dry, degassed dmso, and 8 mL of methylene chloride to 0.072 g (.057 mmol) of [Ru(OEP)]$_2$. To the deep red solution product were added 10 mL of n-hexane, and then the solvents were slowly removed until solid just appeared. The solution was filtered, and the volume further reduced until considerable precipitation occurred. The microcrystalline product was filtered, and then dried in-vacuo overnight at 70° C. The dmso-perdeuterated analogue was prepared in an identical manner, using dmso-$d_6$ as the sulfoxide source. Yields: approximately 80% in each case.[10] Anal. Calcd. for $C_{40}H_{56}N_4O_2S_2Ru$: C, 60.81; H, 7.14; N, 7.09. Found: C, 60.39; H, 7.40; N, 6.78. NMR ($\delta$; $CD_2Cl_2$, 20.0° C): OEP, 1.87 t ($CH_3$), 3.98 q ($CH_2$), 9.78 s ($H_{meso}$); dmso, -2.18 s. IR ($cm^{-1}$, in Nujol): $\nu_{\underline{S}O}$, 1105. Uv/vis (0.0169 mM soln. in $C_6H_6$ containing 22.6 mM dmso) $\lambda_{max}$ (log $\epsilon$): 397.5 (5.44) (Soret), 533 (4.04) nm.

### 2.2.4.4 Ru(OEP)(Et$_2\underline{S}$O)$_2$

Ru(OEP)(Et$_2\underline{S}$O)$_2$ was prepared in a manner analogous to that for Ru(OEP)(dm$\underline{s}$o)$_2$. Yield: approximately 80%.[10] Anal. calcd. for $C_{44}H_{64}N_4O_2S_2Ru$: C, 62.45; H, 7.62; N, 6.62. Found: C, 62.32; H, 7.58; N, 6.68. NMR ($\delta$; $CD_2Cl_2$, 20.0° C): OEP, 1.84 t ($CH_3$), 3.96 q ($CH_2$), 9.70 s ($H_{meso}$); $Et_2SO$, -1.55 br ($CH_3$), -2.12 br $(CH_2)_a$, -2.74 br $(CH_2)_b$. Uv/vis (0.0390 mM soln. in $C_6H_6$ containing 4.7 mM $Et_2SO$) $\lambda_{max}$ (log $\epsilon$): 399.5 (5.49) (Soret), 527 (4.10) nm.

### 2.2.4.5 Ru(OEP)(decM$\underline{S}$O)$_2$

To 0.0692 g (0.0545 mmol) of [Ru(OEP)]$_2$ were added 0.0501 g (0.245 mmol) of decMSO, and about 5 mL of benzene. The solution immediately became a bright, ruby red. After about 10 minutes the solvent was removed, the solid redissolved in about 6 mL of n-pentane, and the resulting solution filtered to remove small amounts of a brown solid. The filtrate was then cooled to -100° C for 15 min to effect precipitation of the desired product. Ru(OEP)(decM$\underline{S}$O)$_2$ was filtered off at - 100° C as a scarlet powder, and dried in-vacuo overnight. Note- the complex is extremely lipophilic, and great care had to be taken to avoid contamination with stopcock grease. Yield: approximately 80%.[10] Anal. Calcd. for $C_{58}H_{92}N_4O_2S_2Ru$: C, 66.82; H, 8.89; N, 5.37; S, 6.15. Found: C, 66.89; H, 8.89; N, 5.18; S, 5.95. NMR ($\delta$; $C_7D_8$ 20.0° C): OEP, 1.86 t ($CH_3$), 3.96 q ($CH_2$), 9.72 s ($H_{meso}$); decMSO, -2.34 s ($SCH_3$), -2.78 m ($^1CH_2$), -1.11 m ($^2CH_2$), -0.02 m ($^3CH_2$), 0.37 qn ($^4CH_2$), 0.73 qn ($^5CH_2$), 0.95 qn ($^6CH_2$), 1.0-1.25 m ($^{7-9}CH_2$), 0.839 t ($^{10}CH_3$). Uv/vis (0.0101 mM soln. in $C_6D_6$ containing 0.20 mM decMSO) $\lambda_{max}$ (log $\epsilon$): 399 (5.59) (Soret), 530 (4.15) nm.

### 2.2.4.6 $Ru(OEP)(dms)_2{}^+BF_4^-$

To 0.0529 g (0.0368 mmol) of $[Ru(OEP)]_2(BF_4)_2$ were added about 10.7 $\mu$L (0.147 mmol) and 5 mL of methylene chloride. The solution was stirred for 30 min, during which time it became a dark orange colour. At this point about 5 mL of n-hexane were added, and the total volume reduced until precipitation just occurred. The solution was filtered, and the volume further reduced until most of the desired complex had precipitated, and the supernatant was a very pale orange. The brownish-purple needles were filtered off, washed with n-pentane, and then dried in vacuo at 70° C overnight. Yield: approximately 80%.[10] Anal. calcd. for $C_{40}H_{56}N_4S_2RuBF_4$: C, 56.86; H, 6.68; N, 6.63. Found: C, 56.67; H, 6.70; N, 6.44. NMR ($\delta$; $CD_2Cl_2$, 20.0° C): OEP, 1.52 br ($CH_3$), 23.85 br ($CH_2$), 1.73 br ($H_{meso}$); dms, -0.174 br. Uv/vis (0.111 mM soln. in $CH_2Cl_2$) $\lambda_{max}$ (log $\epsilon$): 394 (5.05) (Soret), 505 (4.05), 533 (4.03) nm.

### 2.2.4.7 Ru(OEP)(Et$_2$S)$_2$$^+$BF$_4^-$

The preparation of this complex was analogous to that described for Ru(OEP)(dms)$_2$$^+$BF$_4^-$. Yield: approximately 80%.[10] Anal. calcd. for $C_{44}H_{64}N_4S_2RuBF_4$: C, 58.66; H, 7.16; N, 6.22. Found: C, 58.39; H, 7.17; N, 6.15. NMR ($\delta$; $CD_2Cl_2$, 20.0° C): OEP, 1.31 br ($CH_3$), 23.09 br ($CH_2$), 1.61 br ($H_{meso}$); Et$_2$S, 3.57 br ($CH_2$), 7.82 br ($CH_3$). Uv/vis (0.0838 mM soln. in $CH_2Cl_2$) $\lambda_{max}$ (log $\epsilon$): 394 (4.98) (Soret), 505 (4.01), 533 (3.98) nm.

### 2.2.4.8 Ru(OEP)(decMS)$_2$$^+$BF$_4^-$

To 0.171 g (0.119 mmol) of [Ru(OEP)]$_2$(BF$_4$)$_2$ were added 110 $\mu$L (0.474 mmol) of decMS, and benzene. The purple, insoluble [Ru(OEP)]$_2$(BF$_4$)$_2$ was slowly converted to the orange soluble Ru(OEP)(decMS)$_2$$^+$BF$_4^-$. This product was recrystallized from benzene/n-heptane, in a manner analogous to that described for Ru(OEP)(dms)$_2$$^+$BF$_4^-$. Crystals suitable for an x-ray structure determination were obtained by reducing the volume of a benzene/heptane solution until precipitation just occurred, heating to redissolve the precipitate, then allowing the solution to cool slowly. Approximate yield: 80%.[10] Anal. calcd. for $C_{68}H_{92}N_4S_2RuBF_4$: C, 63.48; H, 8.45; N, 5.11; S, 5.84. Found: C, 63.69; H, 8.62; N, 5.19; S, 5.66. NMR ($\delta$; $CD_2Cl_2$, 20.0° C): OEP, 1.44 br ($CH_3$), 23.13 br ($CH_2$), 1.83 br ($H_{meso}$); decMS, 0.50 br ($SCH_3$), 0.92 t ($^{10}CH_3$); {Tentative: 9.06 br ($^1CH_2$), 4.39 br ($^2CH_2$), 2.22 br ($^3CH_2$), 1.96 br ($^4CH_2$), 1.60 br ($^5CH_2$); signals are progressively sharper, with the last two beginning to show fine structure; 1.44 br ($^{6\text{-}9}CH_2$)}. Uv/vis (0.0921 mM soln. in $CH_2Cl_2$) $\lambda_{max}$ (log $\epsilon$): 394 (5.10) (Soret), 505 (4.11), 533 (4.09) nm. Molar conductivity (1 mM soln. in $CH_2Cl_2$) $\Lambda$ = 52 $\Omega^{-1}cm^2mol^{-1}$.

### 2.2.4.9 $Me_4N^+Ru(OEP)(PhCOO)_2^-$

To 0.104 g (0.0725 mmol) of $[Ru(OEP)]_2^+(BF_4)_2^-$ were added 0.0629 g (0.322 mmol) of $Me_4N^+PhCOO^-$, and about 10 mL of methylene chloride. The colour changed immediately from purple to a greenish-yellow colour, then after about 1 h to a bright red. The solution was cooled to 0° C, filtered to remove solid $Me_4N^+BF_4^-$, then further cooled to -100° C to precipitate the desired, crimson product. This was filtered off, washed with n-pentane, and then dried in-vacuo overnight at room temperature.

$Me_4N^+Ru(OEP)(PhCOO)_2^-$ is highly air-sensitive in solution, and the solid was stored in the glove-box as a precautionary measure. Yield: 0.102g (0.108 mmol, 74%). Anal. calcd. for $C_{54}H_{66}N_5O_4Ru$: C, 68.26; H, 7.00; N, 7.37. Found: C, 68.57; H, 7.16; N, 7.29. NMR ($\delta$; $CD_2Cl_2$, 20° C): OEP, -0.72 br ($CH_3$), 8.08 br ($CH_2$), 2.72 br ($H_{meso}$); $PhCOO^-$, 17.86 br ($H_o$), 10.74 br ($H_m$), 9.35 br ($H_p$); 5.64 br $N(CH)_3$. Uv/vis ($CH_2Cl_2$) $\lambda_{max}$ (log $\epsilon_{approx}$): 401 (5.0) (Soret), 520 (3.9) nm.

### 2.2.5 Instrumentation

Where uv/vis or nmr spectra of air- or moisture-sensitive materials were required, special apparatus, described generally in reference 9, or more specifically in reference 1a was used.

### 2.2.5.1 Ultraviolet/Visible Absorption Spectroscopy

Uv/vis spectra were recorded at 20.0° C on a Perkin-Elmer 552A spectrophotometer with the slit width adjusted to allow 2 nm resolution. To obtain extinction coefficients, the absorbance maximum was scanned manually to avoid errors due to delays in recorder response. Typically the Soret bands were obtained using a 0.1 cm cell, while for the visible bands, which are about 10 times weaker, a 1.0 cm cell was used.

### 2.2.5.2 Infrared Spectroscopy

The ir spectra of Ru(OEP)(dms)$_2$, Ru(OEP)(dm$\underline{s}$o)$_2$ and its dmso-perdeuterated analogue were obtained on a Nicolet 5DX single beam ir spectrometer, operating in Fourier transform mode. Samples were mulled in Nujol, and sandwiched between KBr plates.

### 2.2.5.3 Proton Nuclear Magnetic Resonance Spectroscopy

$^1$H nmr spectra were collected at 20.0° C, using a Varian XL-300 FT instrument.

### 2.2.5.4 Conductivity

The conductivity measurement was performed using a model RCM 15B1 conductivity bridge from the Arthur H. Thomas company; the conductivity cell was of a commercial design (Yellow Springs instrument company), with a cell constant of 1.00 cm$^{-1}$.

### 2.2.5.5 Cyclic Voltammetry

Cyclic voltammetric measurements were carried out using an EG and G PAR Model 175 Universal programmer to control the potential sweep; this unit was linked to a Model 173 PAR potentiostat equipped with a model 176 current-to-voltage converter and a model 178 electrometer probe. Voltammetric traces were recorded on a Hewlett-

Packard Model 7005B X-Y recorder. Scan speed was 100 mV/s unless otherwise indicated.

All electrochemical experiments were carried out in methylene chloride solution, with approximately 0.12 M $n\text{-}Bu_4N^+BF_4^-$ acting as the supporting electrolyte.

The electrochemical cell, based on a design described by Van Duyne and Reilley,[11] was made by S. Rak of this department, and was devised for use with minimal volumes of solution (cyclic voltammograms could be obtained with as little as 2 mL), and to allow manipulation of highly air-sensitive samples where necessary. Figure 2.1 illustrates the cell. The Ag/AgCl reference electrode was a commercial design by Metrohm, and was filled with aqueous saturated KCl. Under the experimental conditions employed throughout this work, the $Cp_2Fe/Cp_2Fe^+$ and $Ru(OEP)py_2^+/Ru(OEP)py_2$[12] couples occurred at $E°' = 0.58 \pm 0.02$ and $0.10 \pm 0.02$ V, respectively, relative to the reference. In a typical experiment involving air-sensitive compounds, a solution containing the material to be analyzed and the supporting electrolyte was first prepared in flask (F), using vacuum transfer techniques. The flask was then filled with dry, deoxygenated argon, and connected to the electrochemical cell at joint 4. Joint 5 was stoppered, the cell was connected to a vacuum pump at joint 3, and evacuated. At this point tap 7 was opened to introduce the electroactive solution into the cell, and then argon was introduced via (3). Finally, under an argon purge, the salt bridge/reference electrode combination and the working/auxiliary electrode housing were installed at joints 4 and 5 as shown in the illustration. Tap 1 was closed, the assembled cell was connected to the instruments, and the cv was obtained. In all experiments carried out in this work, tap 2 was always left open. One could envision, however, that if a solvent

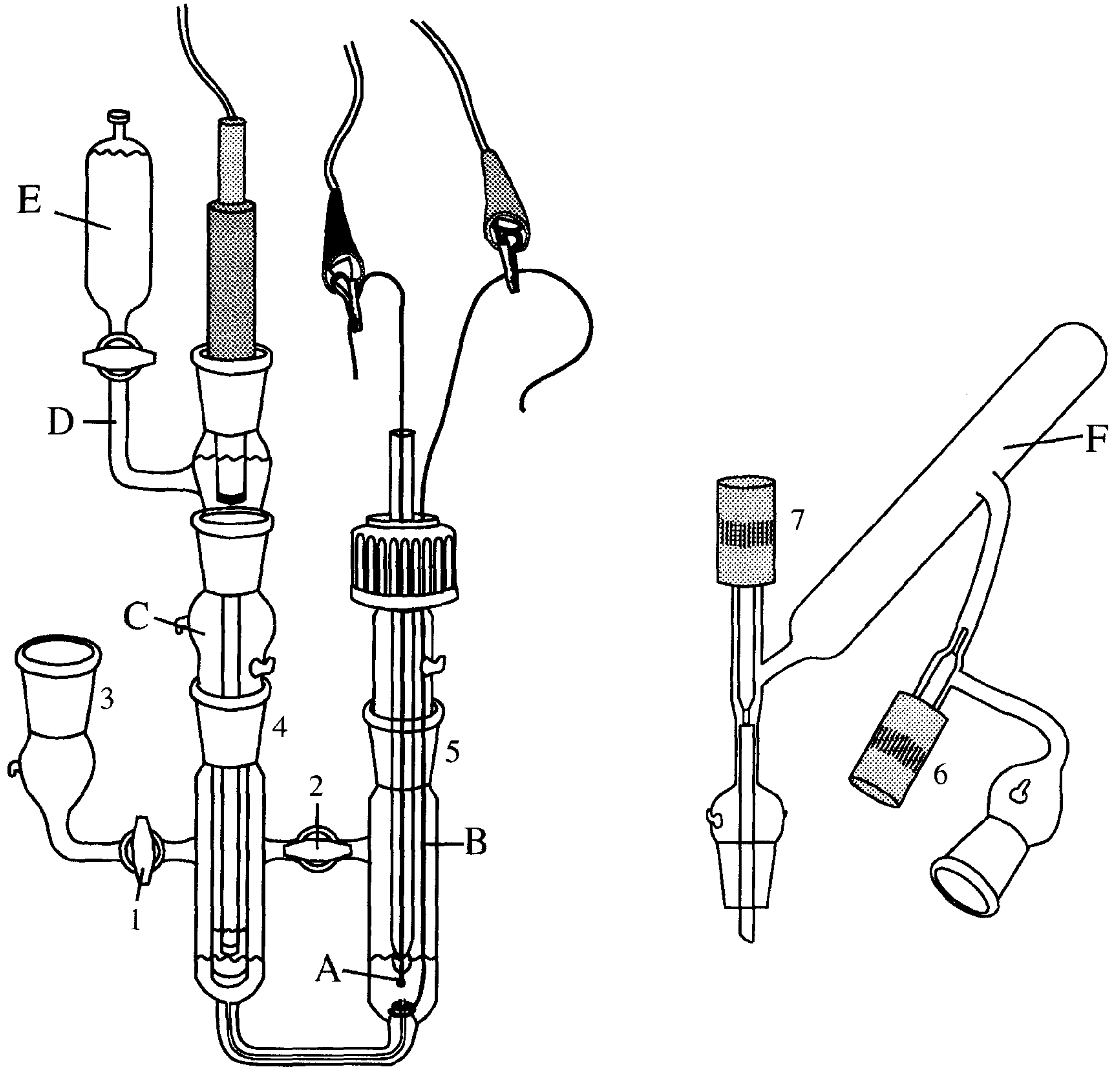

Figure 2.1. Cyclic voltammetry cell: (A) platinum bead working electrode; (B) platinum wire spiral auxilliary electrode; (C) non-aqueous salt bridge; (D) aqueous Ag/AgCl reference electrode; (E) KCl reservoir; (F) sample preparation flask.

with more viscosity than methylene chloride were used, it might not flow easily through the Luggin capillary. In that case, closing tap 2 and pressurizing the reference electrode compartment might succeed in driving the solution through.

### 2.2.5.6 Elemental Analysis

Elemental analyses were carried out by P. Borda of this department.

## 2.3 Characterization of Ru(OEP)(RR'$\underline{S}$O)$_2$ Complexes

A sulfoxide ligand can conceivably bind to a metal center via either its sulfur or oxygen atom; experimentally, both types of complex have been observed, and theories have been proposed to explain the bonding in each case.[13] The bonding between sulfur and oxygen in a free sulfoxide is represented by the following canonical structures:

$$\underset{\text{I}}{\text{RR'S=O}} \longleftrightarrow \underset{\text{II}}{\text{RR'S}^{+}\text{-O}^{-}}$$

In the molecular orbital picture, the bonding is seen to consist of a $\sigma$ interaction and a d$\pi$-p$\pi$ interaction, and the S-O bond order is somewhere between one and two. Coordination of a sulfoxide to a metal via the oxygen atom would tend to stabilize canonical structure II, and thus decrease the S-O bond order relative to that of the free sulfoxide. On the other hand, coordination via sulfur would tend to intensify the positive charge on the sulfur atom, thus destabilizing canonical structure II, and consequently increasing the S-O bond order relative to that of the free sulfoxide. As might be expected then, S-bound and O-bound metal sulfoxide complexes can be readily distinguished by ir spectroscopy:[14] in the S-bound case the S-O stretching frequency is higher than in the free sulfoxide, whereas in the O-bound case it is lower.

The ir spectrum of Ru(OEP)(dm$\underline{s}$o)$_2$ shows a strong band, assigned to $\nu_{SO}$, at 1105 cm$^{-1}$, as compared with 1055 cm$^{-1}$ in free dmso; hence it is characterized as an S-bound complex, at least in the solid state. The ir spectra of the other two Ru(OEP)(RR'$\underline{S}$O)$_2$ complexes were not obtained; however, all three complexes had similar nmr and uv/vis spectra, as well as electrochemical properties (see the next section), which suggests that they share the same bonding patterns. In solution, there is evidence that some isomerization may be taking place. Kinetic studies of substitution of the bis(sulfoxide) systems by dialkylsulfides show that one of the sulfoxides is strongly bound, but the other is extremely labile and can easily be replaced by other ligands. These studies will be dealt with in considerable detail in section 3.4, but of more immediate interest is possible evidence that an S-bound sulfoxide can revert to, or be replaced by, an O-bound sulfoxide in solution. The uv/vis spectra of each of the three bis(sulfoxide) complexes prepared vary somewhat with temperature, even in the presence of a large excess of free sulfoxide ligand; to give an example, figure 2.2 shows the temperature dependence of the Ru(OEP)(Et$_2\underline{S}$O)$_2$ uv/vis spectrum. These variations are reversible, and are not due simply to ligand dissociation, although evidence for the latter process is also observed for dilute solutions containing no added free ligand (see section 3.4). The best explanation for the temperature dependence of the uv/vis spectra is that in solution one of the sulfoxides can be either S-bound or O-bound, and that the ratio of isomeric forms depends on the temperature. Despite these observations, it will be shown

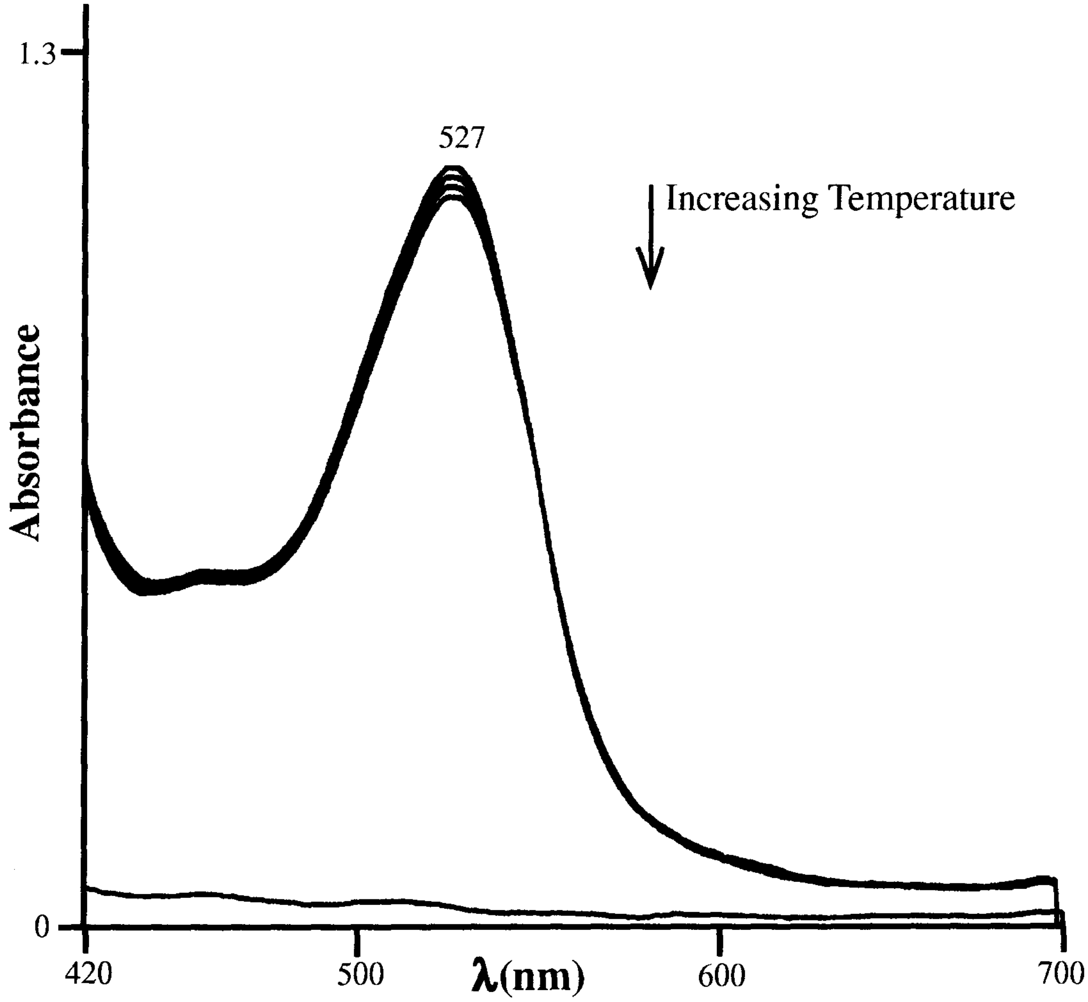

Figure 2.2. Changes in the visible spectrum of a $CH_2Cl_2$ solution containing 0.039 mM $Ru(OEP)(Et_2SO)_2$, and 4.72 mM free $Et_2SO$, as the temperature is increased in 10° intervals, from 20-50° C.

in section 3.4 that, for the purposes of the present study, Ru(OEP)(RR′SO)$_2$ complexes in solution can be thought of as containing only S-bound sulfoxides without changing any conclusions.

It should be added that the $^1$H-nmr spectra of Ru(OEP)(Et$_2$SO)$_2$ and Ru(OEP)(decMSO)$_2$ (see sections 2.2.4.4 and 2.2.4.5) are also somewhat temperature dependent, and also solvent dependent. As an example of solvent dependence, at room temperature in CD$_2$Cl$_2$, the sulfoxide methyl and methylene $^1$H-nmr signals of Ru(OEP)(Et$_2$SO)$_2$ are broad and lacking in fine structure; on the other hand, at the same temperature but in C$_6$D$_6$, the same signals are resolved multiplets. This topic will not be discussed further, as no systematic studies were done; however, it is an interesting subject which deserves more study in the future.

The assignment of the $\nu_{SO}$ ir band requires some comment. Previous studies have mentioned the potential difficulty in distinguishing $\nu_{SO}$ from the $\rho_{CH_3}$ signals of the sulfoxide, and reported that this difficulty could be overcome by comparing data for the dmso complex with those for its dmso-perdeuterated analogue.[13,14] The $\rho_{CH_3}$ modes are isotopically shifted when the perdeuterated analogue is used, whereas the $\nu_{SO}$ signals remain unchanged. In the case of Ru(OEP)(dm$\underline{s}$o)$_2$ and Ru(OEP)(dm$\underline{s}$o-d$_6$)$_2$, the spectra obtained are essentially identical in the region from 500-1500 cm$^{-1}$. Presumably the C-H and C-D rocking modes in these complexes are buried under signals attributable to Ru(OEP). When the ir spectra of Ru(OEP)(dm$\underline{s}$o)$_2$ and the perdeuterated analogue are compared with that of Ru(OEP)(dms)$_2$, the only difference in the region mentioned is that the spectrum of Ru(OEP)(dms)$_2$ lacks the strong 1105 cm$^{-1}$ band; the rest of the spectrum is virtually identical for Ru(OEP)(dms)$_2$, Ru(OEP)(dm$\underline{s}$o)$_2$, and Ru(OEP)(dm$\underline{s}$o-d$_6$)$_2$. This confirms the assignment of this band as $\nu_{SO}$.

The peak positions of all the Ru(OEP)(RR'SO)$_2$ $^1$H-nmr signals are typical of those observed for other related Ru$^{II}$(OEP) species; in fact, the most complex spectrum collected, that of Ru(OEP)(decMSO)$_2$, was assigned by direct analogy with the previously reported spectrum of Ru(OEP)(decMS)$_2$.[9] The predominant factor which determines the peak positions of any diamagnetic porphyrin species is the ring current generated by the porphyrin $\pi$ electrons,[15,16] and the ring current effect as it relates specifically to Ru(OEP)(decMS)$_2$ is discussed in detail in reference 9. This effect will not be discussed further at this time, but it has been extensively investigated, and several semi-quantitative models have been published.[15,16]

## 2.4 Characterization of Ru$^{III}$(OEP) Complexes

Oxidation of metalloporphyrins can occur either at the metal center or at the porphyrin ring, and again there is precedent for both possibilities.[17] Fuhrhop et al. first observed in 1973 that a uv/vis spectrum consisting of 2-3 broad bands covering the visible range from 500 to 700 nm seemed to be characteristic of an organic $\pi$ radical, while one with reasonably localized bands in the region between 500 and 580 nm, which looked very much like those of an unoxidized precursor, indicated that oxidation had occurred at the metal.[18] This qualitative test for oxidation site location is now widely recognized as one of the primary methods of distinguishing the two possibilities.[7] Figure 2.3a shows that the uv/vis spectra of Ru(OEP)(dms)$_2$ and Ru(OEP)(dms)$_2$$^+$BF$_4$$^-$ are quite similar, suggesting that oxidation in synthesis of the latter has occurred at the metal. The spectra of the other Ru(OEP)(RR'S)$_2$$^+$BF$_4$$^-$ complexes were essentially identical to that of

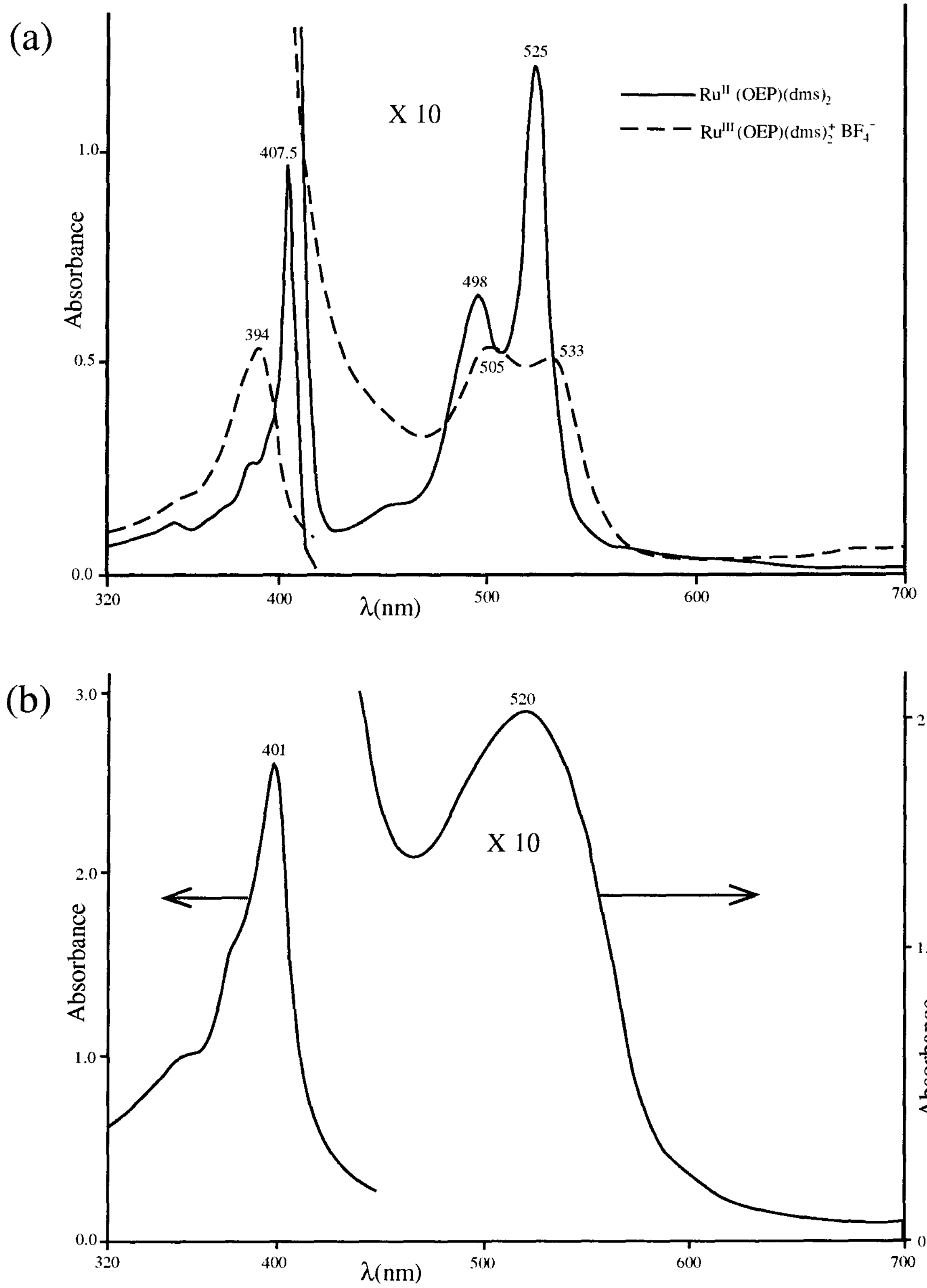

Figure 2.3. Uv/vis spectra in $CH_2Cl_2$ of (a) $Ru(OEP)(dms)_2$ and $Ru(OEP)(dms)_2{}^+BF_4^-$, and (b) $Me_4N^+Ru(OEP)(PhCOO)_2^-$.

the dms one; the spectrum of $Me_4N^+Ru(OEP)(PhCOO)_2^-$ (figure 2.3b) could not be compared to that of the reduced analogue, but also exhibits a fairly localized absorption maximum at 520 nm, and no significant absorption above 600 nm. Again this is suggestive of oxidation at the metal.

To the author's knowledge, all $Ru^{II}(Porp)$ $\pi$-cation radical complexes observed to date contain CO as a $\pi$-accepting axial ligand. It is believed that metal to carbonyl back-bonding in these complexes stabilizes the metal d orbitals of $\pi$ symmetry to the point where they are at lower energy than the highest occupied $\pi$ orbital of the porphyrin ring, and that this is why the ring is preferentially oxidized.[19,20] Previous studies in our laboratories and elsewhere have shown that dialkylsulfide ligands do not partake in significant metal to ligand $\pi$-$\pi^*$ back-bonding,[9] and the cyclic voltammetric (CV) studies show (figure 2.4a) that the standard reduction potentials of all three $Ru(OEP)(RR'S)_2{}^+BF_4^-$ complexes prepared occur at around 0.22 ± 0.02 V relative to Ag/AgCl;[21] such values are comparable to those obtained for systems such as $Ru(OEP)py_2{}^+/Ru(OEP)py_2$, which are known to undergo oxidation at the metal,[19,22] but are well below the reduction potentials of the $Ru(OEP)^{+\cdot}(CO)L/Ru(OEP)(CO)L$ systems ($L \equiv$ a general ligand or a vacant site), which have typically been recorded at around 0.65-0.70V.[19,23a]

A further interesting question arises from the above discussion. Although dialkylsulfides do not partake in significant metal-ligand $\pi$-$\pi^*$ backbonding, there is quite a body of evidence that sulfoxides do.[24a] Would this cause sulfoxide complexes to undergo ring oxidation? An in situ redox titration of $Ru(OEP)(Et_2\underline{S}O)_2$ with $AgBF_4$, gave a uv/vis spectrum (figure 2.5a) very similar to those of the $Ru(OEP)(RR'S)_2{}^+BF_4^-$

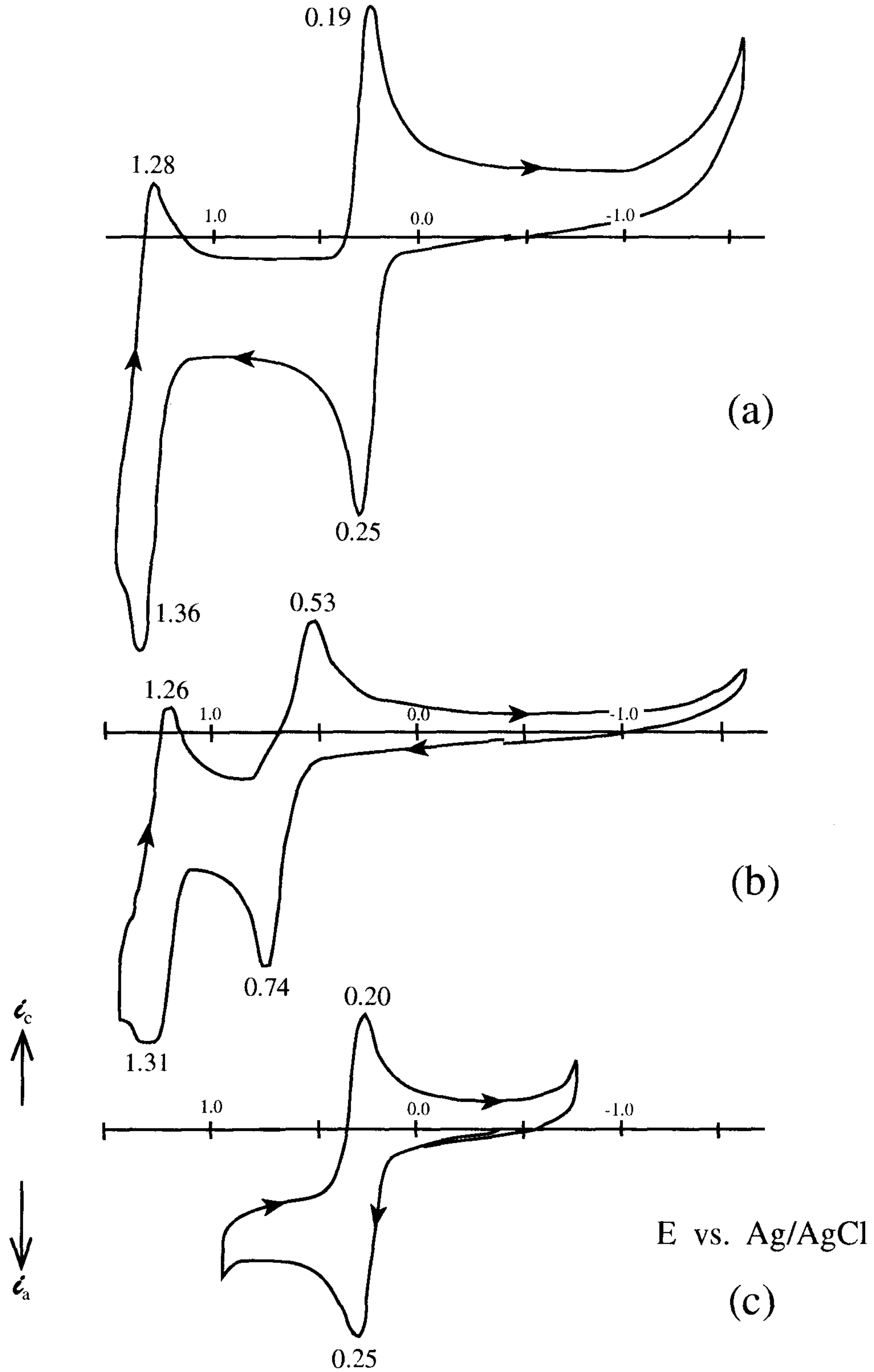

Figure 2.4. Cyclic voltammograms in $CH_2Cl_2$/n-$Bu_4N^+BF_4^-$ for (a) $Ru(OEP)(dms)_2$, (b) $Ru(OEP)(dmso)_2$, and (c) $Me_4N^+Ru(OEP)(PhCOO)_2^-$. The cyclic voltammograms of the other dialkylsulfide and sulfoxide complexes are virtually indistinguishable from those of the dms and dmso complexes illustrated. Also, a CV identical to (a) was obtained for $Ru(OEP)(dms)_2^+BF_4^-$.

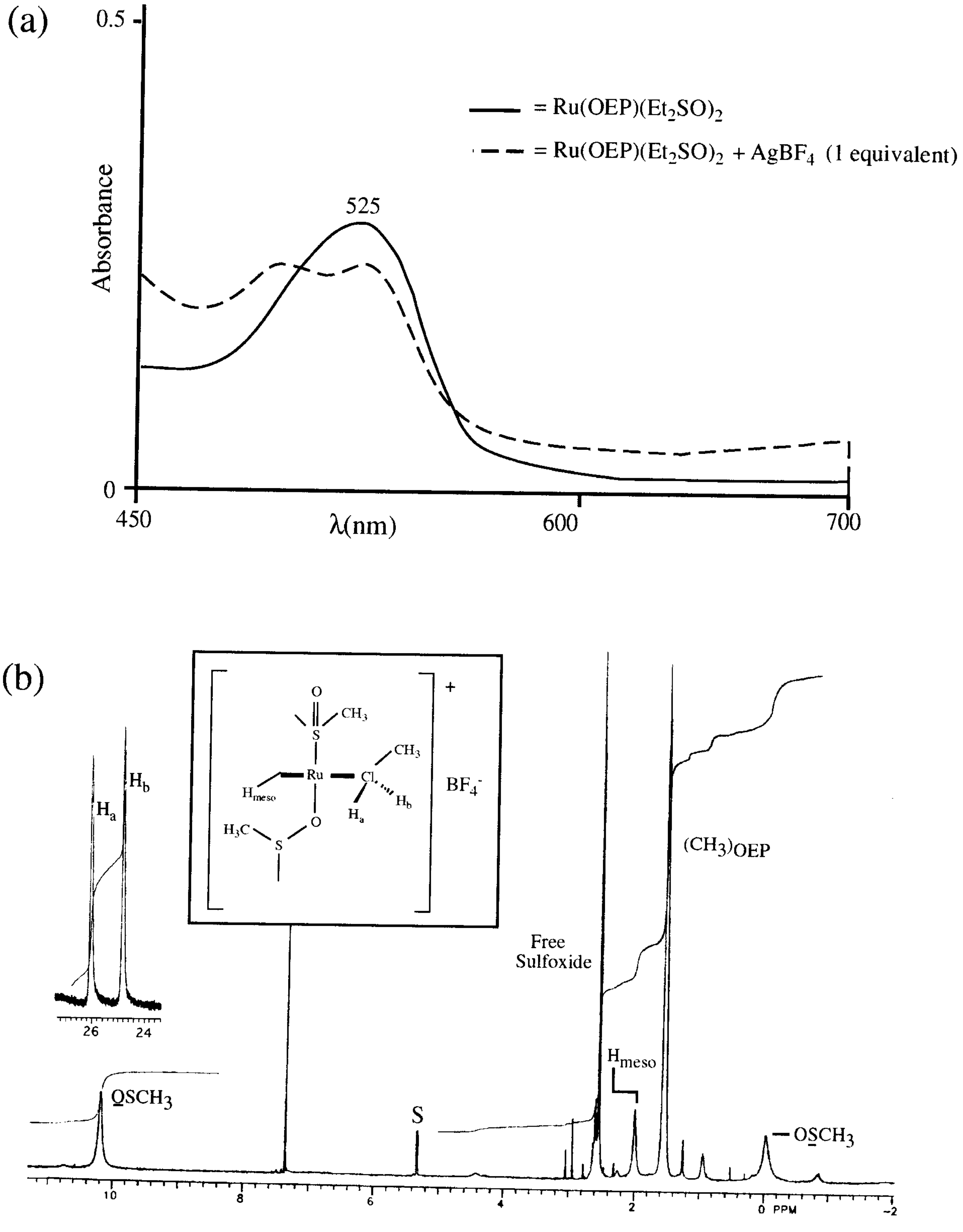

Figure 2.5. (a) Visible spectrum of a 1:1 mixture of Ru(OEP)($Et_2SO$)$_2$ and $AgBF_4$ in $CH_2Cl_2$; (b) $^1$H-nmr spectrum of a $CD_2Cl_2$ solution initially containing [Ru(OEP)]$_2$($BF_4$)$_2$ and free dmso in approximately 1:8 ratio; S ≡ solvent, T = 20° C.

complexes (see figure 2.3a), suggesting that oxidation of the sulfoxide complexes also results in $Ru^{III}$ derivatives. Figure 2.5b shows the $^1$H-nmr spectrum of an in situ mixture of $[Ru(OEP)]_2(BF_4)_2$ and dmso, in $CD_2Cl_2$ at 20° C; this spectrum has several features quite similar to those seen in the corresponding $Ru(OEP)(dms)_2{}^+BF_4{}^-$ spectrum (see figure 2.10, and the discussion later in this section). However, the presence of two signals for the OEP methylenes indicates that the two faces of the porphyrin are inequivalent (ie: the porphyrin plane is not a plane of symmetry in this complex). There are also several small signals, some of which can probably be assigned to another minor Ru(OEP) paramagnetic product. The presence of these extra signals complicates the assignment of any signals due to coordinated dmso; however, the signals at 0.02 and 10.20 ppm each have the correct integration for one sulfoxide. Furthermore, if the whole experiment is repeated using dmso-$d_6$, both these signals are absent from the resulting spectrum. Based on this uv/vis and $^1$H-nmr evidence, the major product of $Ru(OEP)(RR'\underline{S}O)_2$ oxidation is tentatively assigned as $Ru^{III}(OEP)(RR'\underline{S}O)(RR'S\underline{O})^+BF_4{}^-$; the nmr signal at 0.02 ppm is assigned to the S-bound sulfoxide by comparison with the $Ru(OEP)(dms)_2{}^+BF_4{}^-$ system (see figure 2.10 in the next section), while the signal at 10.2 ppm is assigned to the O-bound sulfoxide. The cyclic voltammograms for the $Ru(OEP)(RR'\underline{S}O)_2$ complexes (figure 2.4b) also show evidence of a change in coordination on changing the oxidation state; the oxidation wave has a maximum current at 0.74 V vs. Ag/AgCl, while the reduction maximum occurs at 0.53 V vs. Ag/AgCl. The large peak to peak separation indicates that the complex being reduced is not the same one that was oxidized, but the shape of the CV does not change regardless of how many times the scan is repeated, which suggests that upon reduction the original complex is recovered intact. This is consistent with the postulated mechanism:[24b]

$$\mathrm{Ru^{II}(OEP)(RR'\underline{S}O)_2} \rightleftharpoons \mathrm{Ru^{III}(OEP)(RR'\underline{S}O)_2^+} + e^- \qquad E^{\circ\prime} \approx 0.74\ \mathrm{V} \tag{2.1}$$

$$\mathrm{Ru^{III}(OEP)(RR'\underline{S}O)_2^+} \rightleftharpoons \mathrm{Ru^{III}(OEP)(RR'\underline{S}O)(RR'S\underline{O})^+} \tag{2.2}$$

$$\mathrm{Ru^{III}(OEP)(RR'\underline{S}O)(RR'S\underline{O})^+} + e^- \rightleftharpoons$$

$$\mathrm{Ru^{II}(OEP)(RR'\underline{S}O)(RR'S\underline{O})} \qquad E^{\circ\prime} \approx 0.53\ \mathrm{V} \tag{2.3}$$

$$\mathrm{Ru^{II}(OEP)(RR'\underline{S}O)(RR'S\underline{O})} \rightleftharpoons \mathrm{Ru(OEP)(RR'\underline{S}O)_2} \tag{2.4}$$

Note that 0.74 V is actually higher than the $E^{\circ\prime}$ values reported for Ru(OEP)(CO),[19,23a] and so if both sulfoxides were to remain S-bound, ring oxidation might be predicted. It is possible that ring oxidation does occur initially, and that internal electron transfer takes place after one of the sulfoxides rearranges to yield the O-bound isomer. Internal electron transfer upon modification of the coordination sphere has been previously documented for ruthenium porphyrins.[23a,23b]

Both the $\mathrm{Ru(OEP)(RR'S)_2}$ and $\mathrm{Ru(OEP)(RR'\underline{S}O)_2}$ complexes exhibit a second redox couple at around 1.3 V (figures 2.4a,b). No further investigation of this couple was carried out in this work, but previous studies in our laboratories have yielded evidence that the second oxidation of similar complexes containing two neutral axial ligands occurred at the ring at around 1.3 V, to yield the $Ru^{III}$ $\pi$-cation radical.[23a] Figure 2.3c shows the corresponding redox couple (0.23 V) for $Me_4N^+Ru(OEP)(PhCOO)_2^-$. Notice that the coordination of two anionic ligands on the metal center renders the complex much more easily oxidizable; in fact, oxidation of the bis(benzoate) ruthenium(III) species is as easy as the one-electron oxidation of the $Ru^{II}(OEP)(RR'S)_2$ complexes. This point will be very important in the following section. Presumably, given the ease of oxidation, electron abstraction from $Me_4N^+Ru(OEP)(PhCOO)_2^-$ takes place at the metal to generate Ru(IV) species. Corresponding potentials for the related $Ru(OEP)X_2$ species (X $\equiv$ Cl, Br) occur at 0.40 and 0.42 V, respectively;[22] the 0.2 V difference relative to $Ru(OEP)(PhCOO)_2$ can be attributed to the stronger basicity of $PhCOO^-$ relative to $Cl^-$ and $Br^-$.

The signals in the paramagnetic $^1$H-nmr spectra of $Ru(OEP)(dms)_2{}^+BF_4^-$, $Ru(OEP)(Et_2S)_2{}^+BF_4^-$, $Ru(OEP)(decMS)_2{}^+BF_4^-$ and $Me_4N^+Ru(OEP)(PhCOO)_2^-$ are shifted considerably from their characteristic diamagnetic positions, which is typical for paramagnetic complexes.[25a] The magnitudes and directions of the observed paramagnetic shifts (from 0-20 ppm, with the methylene proton signals shifting downfield, and the meso proton signals shifting upfield) are fairly representative of those seen for $Ru^{III}$(OEP) low spin complexes (no $Ru^{III}$(Porp) high spin complexes have ever been observed);[26] $Ru^{IV}$(OEP) complexes generally (but not always) show much greater shifts (as high as 100 ppm).[27] The spectra of $Ru(OEP)(dms)_2{}^+BF_4^-$, $Ru(OEP)(Et_2S)_2{}^+BF_4^-$ and $Me_4N^+Ru(OEP)(PhCOO)_2^-$ are assigned primarily based on the relative intensities of all the signals. The spectrum for $Ru(OEP)(decMS)_2{}^+BF_4^-$ (figure 2.6) was more difficult to interpret. The porphyrin signals and the $SCH_3$ signals are assigned by analogy to the

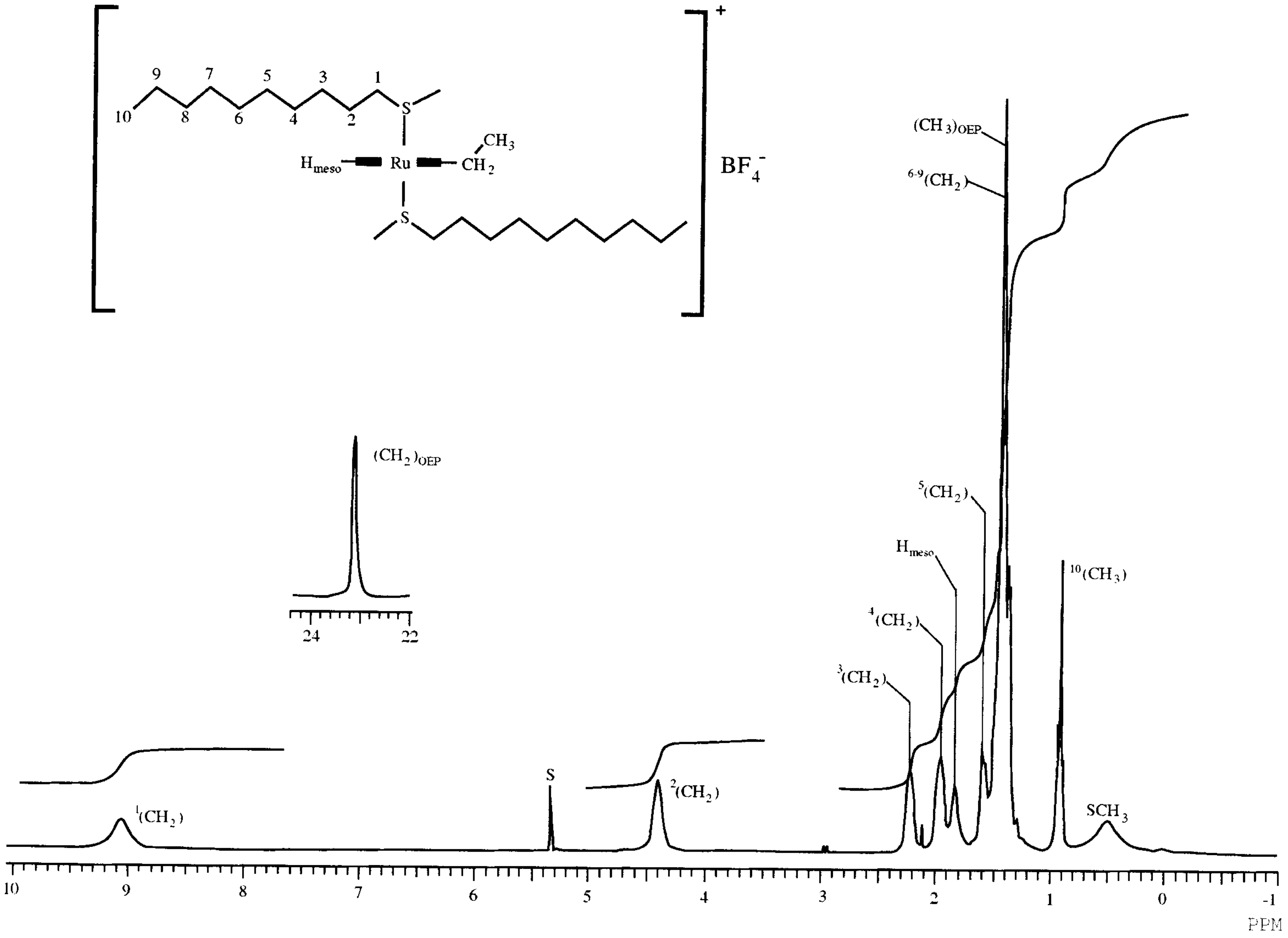

Figure 2.6. $^1$H-nmr spectrum of $Ru(OEP)(decMS)_2{}^+BF_4^-$ in $CD_2Cl_2$, taken at 20.0° C; S ≡ solvent.

simpler systems, while the signal due to the thioether $^{10}CH_3$ is unshifted relative to either that of the free ligand or the $Ru^{II}$-coordinated analogue.[9] A peak at 9.06 ppm is tentatively assigned to ($^1CH_2$), based on its integration and the fact that it is the broadest of the unassigned signals. A series of progressively sharper signals at 4.39, 2.22, 1.96, and 1.60 ppm are assigned to ($^2CH_2$)-($^5CH_2$); the last two actually show some fine structure. Finally, the signals for ($^{6-9}CH_2$) are buried beneath the porphyrin methyl signal, although a broad multiplet is just discernible at 1.38 ppm.

## 2.5 Reaction of Ru(OEP)(dms)$_2$ With Dioxygen and Benzoic Acid in Methylene Chloride

Figure 2.7 shows the $^1H$-nmr spectral changes over time as a solution containing about 20 mM Ru(OEP)(dms)$_2$ and 12 mM benzoic acid in $CD_2Cl_2$ is exposed to 1 atm of $O_2$ at room temperature. For simplicity only part of the spectrum is shown, but comparable changes are seen throughout the spectrum, from -3 to 25 ppm (see table 2.1). When the other dialkylsulfide complexes are exposed to the same conditions, spectral changes analogous to those illustrated in figure 2.5 are observed, at least in the 5-25 ppm region; below this, the spectra of the reaction mixtures are too complicated to interpret readily.

The two sharp singlets seen between 9.5 and 10 ppm are assigned to the OEP meso protons of Ru(OEP)(dms)(dm$\underline{s}$o) and Ru(OEP)(dm$\underline{s}$o)$_2$, respectively. Ru(OEP)(dms)(dm$\underline{s}$o) could not be obtained pure, but in titrations of Ru(OEP)(dms)$_2$ with dmso, or of Ru(OEP)(dm$\underline{s}$o)$_2$ with dms, the mixed species could be unequivocally identified by uv/vis or $^1H$-nmr data (see for example figure 2.8). In fact, for the

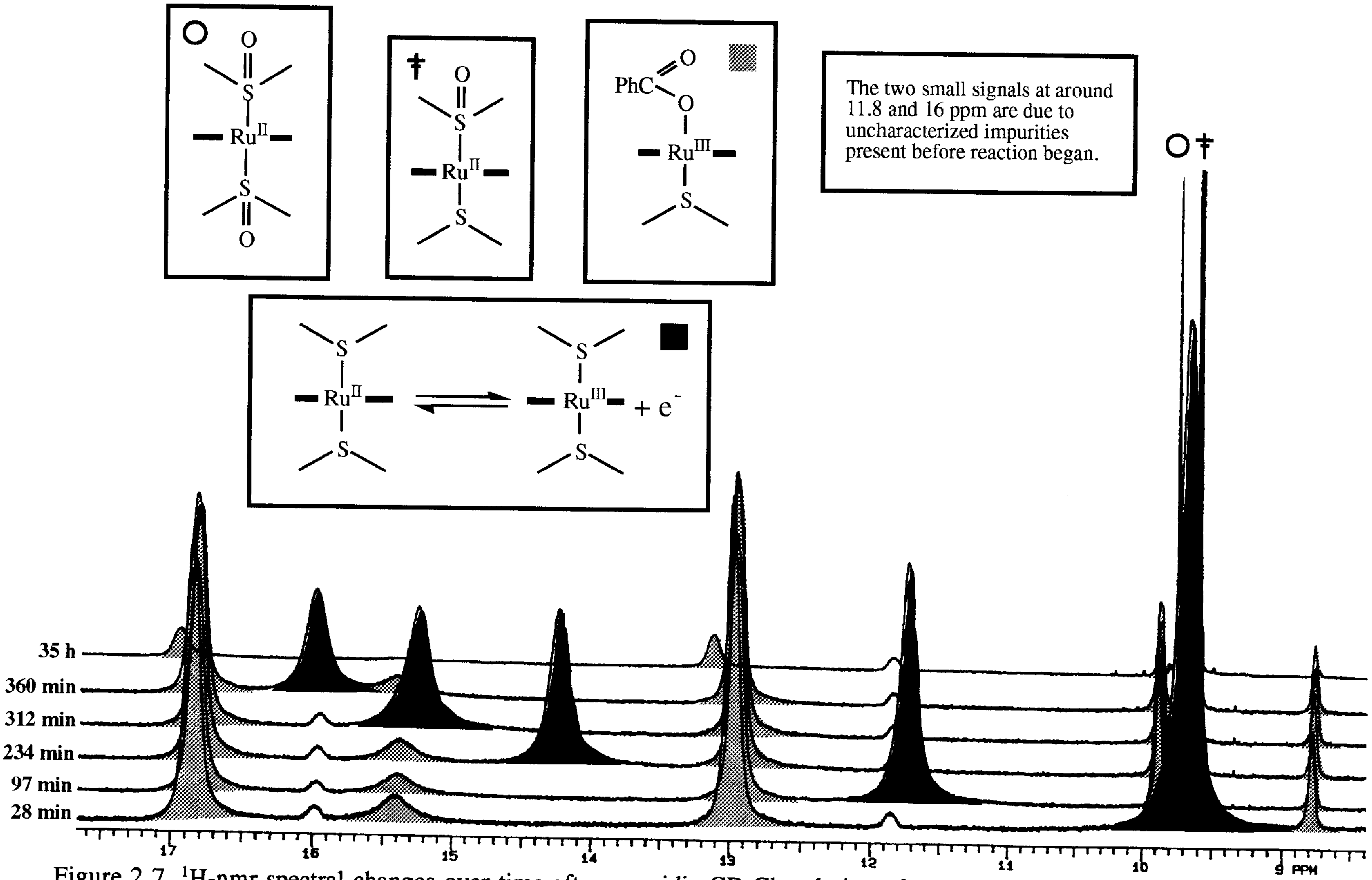

The two small signals at around 11.8 and 16 ppm are due to uncharacterized impurities present before reaction began.

Figure 2.7. $^1$H-nmr spectral changes over time after an acidic $CD_2Cl_2$ solution of Ru(OEP)(dms)$_2$ is exposed to 1 atm of $O_2$ at room temperature (approximately 20° C). The peak assignments for each species are summarized in table 2.2.

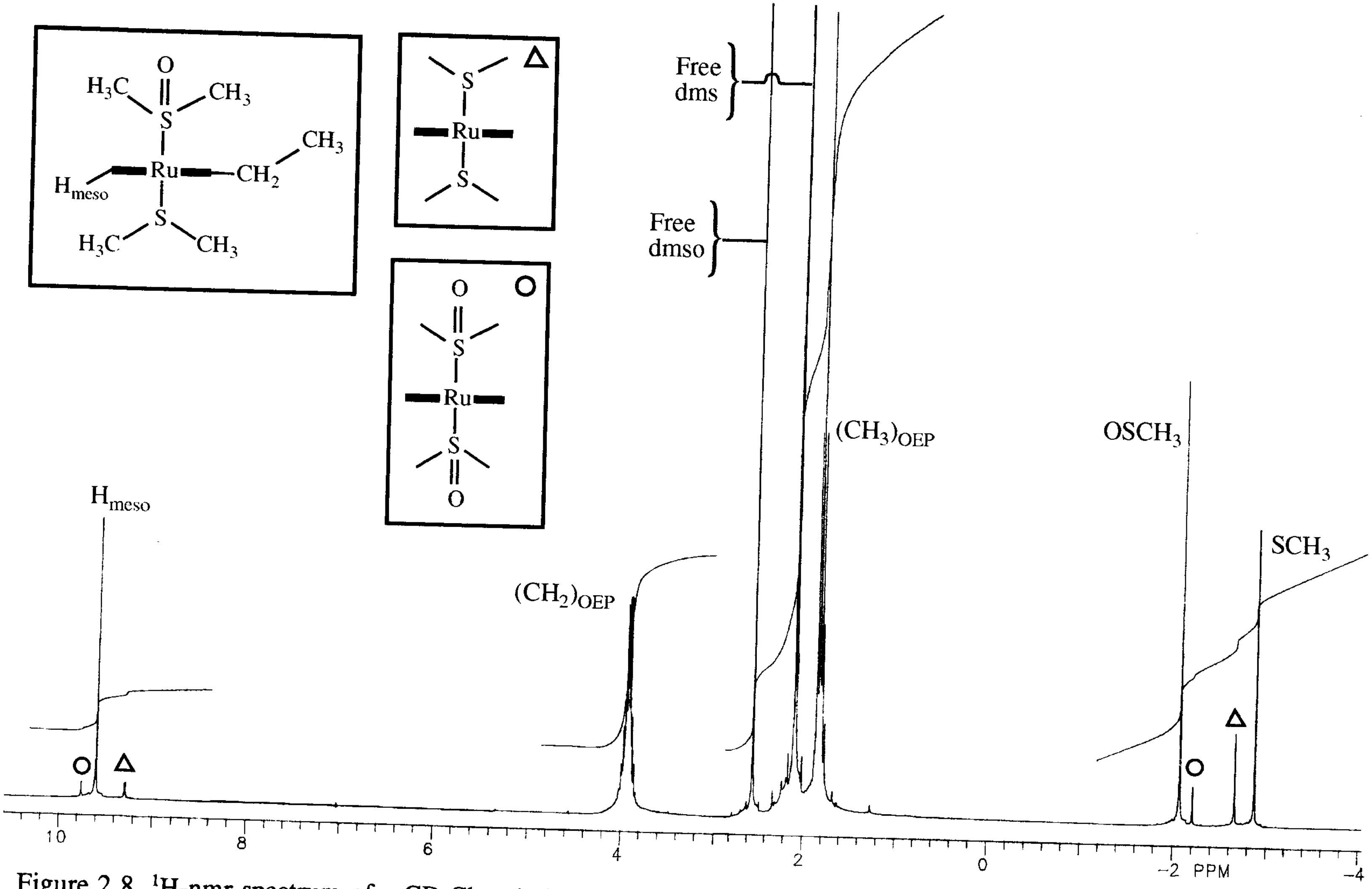

Figure 2.8. $^1$H-nmr spectrum of a $CD_2Cl_2$ solution of Ru(OEP)(dms)$_2$ (approximately 5 mM) to which an excess of a mixture containing 3:1 dms/dmso (neat) has been added. Under these conditions, the major Ru(OEP) species in solution is Ru(OEP)(dms)(dm$\underline{s}$o).

## Table 2.1
## Summary of the $^1$H-nmr Peak Positions in $CD_2Cl_2$ for the Ru(OEP) Complexes Discussed in Section 2.5

| | OEP Signals (ppm) | | | Axial Ligand Signals (ppm) | | | | |
|---|---|---|---|---|---|---|---|---|
| | $CH_3$ | $CH_2$ | $H_{meso}$ | dms | dmso | PhCOO | | |
| | | | | | | $H_o$ | $H_m$ | $H_p$ |
| Ru(OEP)$(dms)_2$ | 1.81,t | 3.85,q | 9.32,s | -2.66,s | - | - | - | - |
| Ru(OEP)(dms)(dm$\underline{\text{s}}$o) | 1.83,t | 3.92,m | 9.60,s | -2.87,s | -2.07,s | - | - | - |
| Ru(OEP)$(\text{dm}\underline{\text{s}}\text{o})_2$ | 1.87,t | 3.98,q | 9.78,s | - | -2.18,s | - | - | - |
| Ru(OEP)$(dms)_2{}^+BF_4^-$ [a] | 1.52[b] | 23.85 | 1.73 | -0.17 | - | - | - | - |
| Ru(OEP)(dms)(PhCOO) | 0.46 | 16.75,12.87 | 4.07 | -0.49 | - | 15.34 | 9.84 | 8.75 |
| $Me_4N^+$Ru(OEP)$(PhCOO)_2^-$ [c] | -0.72 | 8.08 | 2.72 | - | - | 17.86 | 10.74 | 9.35 |

(a) The signal positions are assumed to be essentially unchanged regardless of the counterion.
(b) All of the signals attributed to $Ru^{III}$ complexes are broad, and lacking in fine structure.
(c) The signal for the $Me_4N^+$ counterion is seen at 5.64 ppm.

analogous system involving $Et_2S$ and $Et_2SO$, the equilibrium constants as well as the rate constants for the substitution processes were determined by stopped-flow spectrophotometry; this will be fully discussed in section 3.4.

Initially, very little of the bis sulfoxide complex is seen. In fact, in all of the spectra collected up to 360 min the Ru(OEP)(dm$\underline{s}$o)$_2$ signals are barely discernible; however, figure 2.9 shows that in the final spectrum taken, after 35 h, the bis-sulfoxide is the major Ru(OEP) product. Another important point seen in figure 2.9 is that after 35 h the phenyl signals for the benzoate/benzoic acid are at the same position as at the start; that is, the benzoic acid is recovered intact. The only difference is that the COOH proton, clearly identifiable at 11.4 ppm before the reaction was initiated, is no longer visible. A broad, underlying hump is visible around 5 ppm in figure 2.9 (most clearly seen in the integral scan), which suggests that water is now present, and the COOH proton is rapidly exchanging with it. In the spectra collected from 28 to 360 min, the benzoate phenyl proton signals are shifted significantly from their positions in benzoic acid; this is likely due to interaction of $PhCOO^-$ anions with paramagnetic $Ru^{III}$(OEP) (and possibly $Ru^{IV}$) species (see below). Presumably $PhCOO^-$ counter-ions would exchange rapidly with PhCOOH, and only time-averaged $^1$H-nmr phenyl signals would be observed. In all of the spectra collected between 28 min and 35 h, a broad signal, presumably due to the acid proton of PhCOOH exchanging with $H_2O$, is observed in the region between 5 and 7 ppm.

The broad signal in figure 2.7 that shifts over time (black shading) is one of four, attributable to a time-averaged spectrum of rapidly exchanging Ru(OEP)(dms)$_2^+$$PhCOO^-$ and Ru(OEP)(dms)$_2$ (all of the peak positions, for all of the spectra collected, are listed in

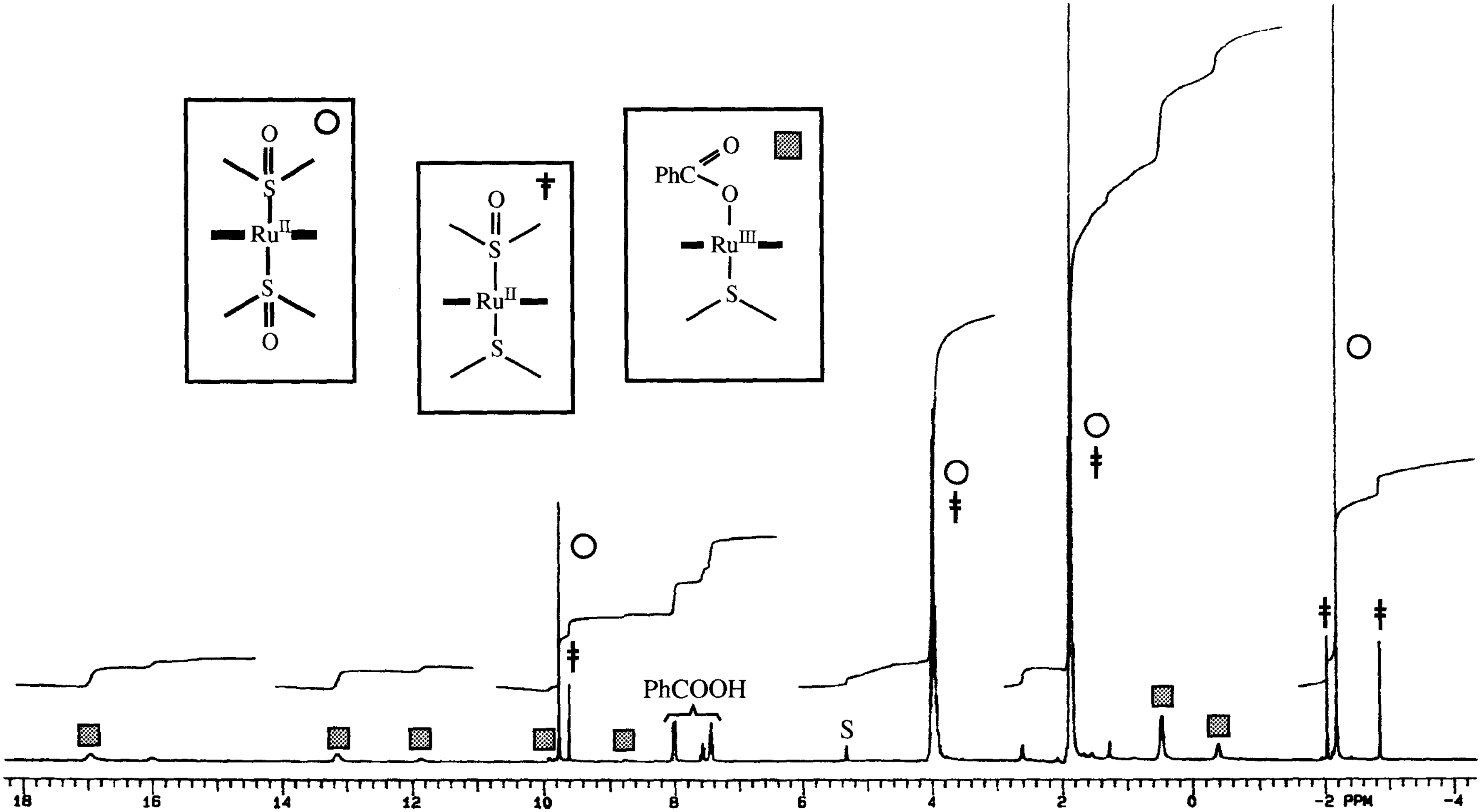

Figure 2.9. $^1$H-nmr spectrum of an acidic $CD_2Cl_2$ solution of Ru(OEP)(dms)$_2$ 35 h after exposure to 1 atm of $O_2$ at room temperature (cf. figure 2.7); S ≡ solvent.

table 2.2). Figure 2.10 shows the spectrum of pure $Ru(OEP)(dms)_2{}^+BF_4{}^-$. When this complex was mixed with $Ru(OEP)(dms)_2$, only time-averaged signals could be seen in the $^1$H-nmr spectrum, and the location of all four signals depended exclusively on the concentration ratio of $Ru^{III}/Ru^{II}$. This shows that electron transfer between $Ru(OEP)(dms)_2$ and $Ru(OEP)(dms)_2{}^+X^-$ ($X \equiv PhCOO, BF_4$) at 20° C is very rapid. The following analysis provides an idea of just how fast the electron transfer is. For the case in which a proton can be at one of two sites (in this case either in a $Ru^{III}$ environment or a $Ru^{II}$ environment), the necessary condition for detecting separate resonances for the proton in each environment is given by $\tau' > 2^{0.5}/(2\pi\Delta\nu)$, where $\tau'$ is the lifetime of the proton at each site, and $\Delta\nu$ is the separation of the peaks (in Hz) when no exchange is taking place.[25b] For the OEP methylene protons, the peak separation between the $Ru^{II}$ and the $Ru^{III}$ positions is 20 ppm (see table 2.1), or 6000 Hz when a 300 MHz machine is used. Since separate resonances are not observed for the OEP methylenes of $Ru(OEP)(dms)_2$ and $Ru(OEP)(dms)_2{}^+BF_4{}^-$ in a mixture of the two species, $\tau'$ cannot be larger than $3.8\times10^{-5}$ s at 20° C.

In figure 2.7, the OEP methylene signal shifts over time towards the $Ru^{III}$ position, at the same time decreasing in overall intensity. This shows that the overall concentration of the two species is decreasing, while the ratio of $Ru^{III}/Ru^{II}$ is increasing with time; table 2.2 lists the calculated value of the fraction $N_{II}$ (where $N_{II}$ = $[Ru(OEP)(dms)_2]/([Ru(OEP)(dms)_2] + [Ru(OEP)(dms)_2{}^+PhCOO^-])$) for each spectrum collected. Based on the oxidation mechanism proposed later in this section, we hypothesize that the concentration of $Ru(OEP)(dms)_2{}^+PhCOO^-$ is in a steady state for most of the reaction, while that of $Ru(OEP)(dms)_2$ decreases steadily.

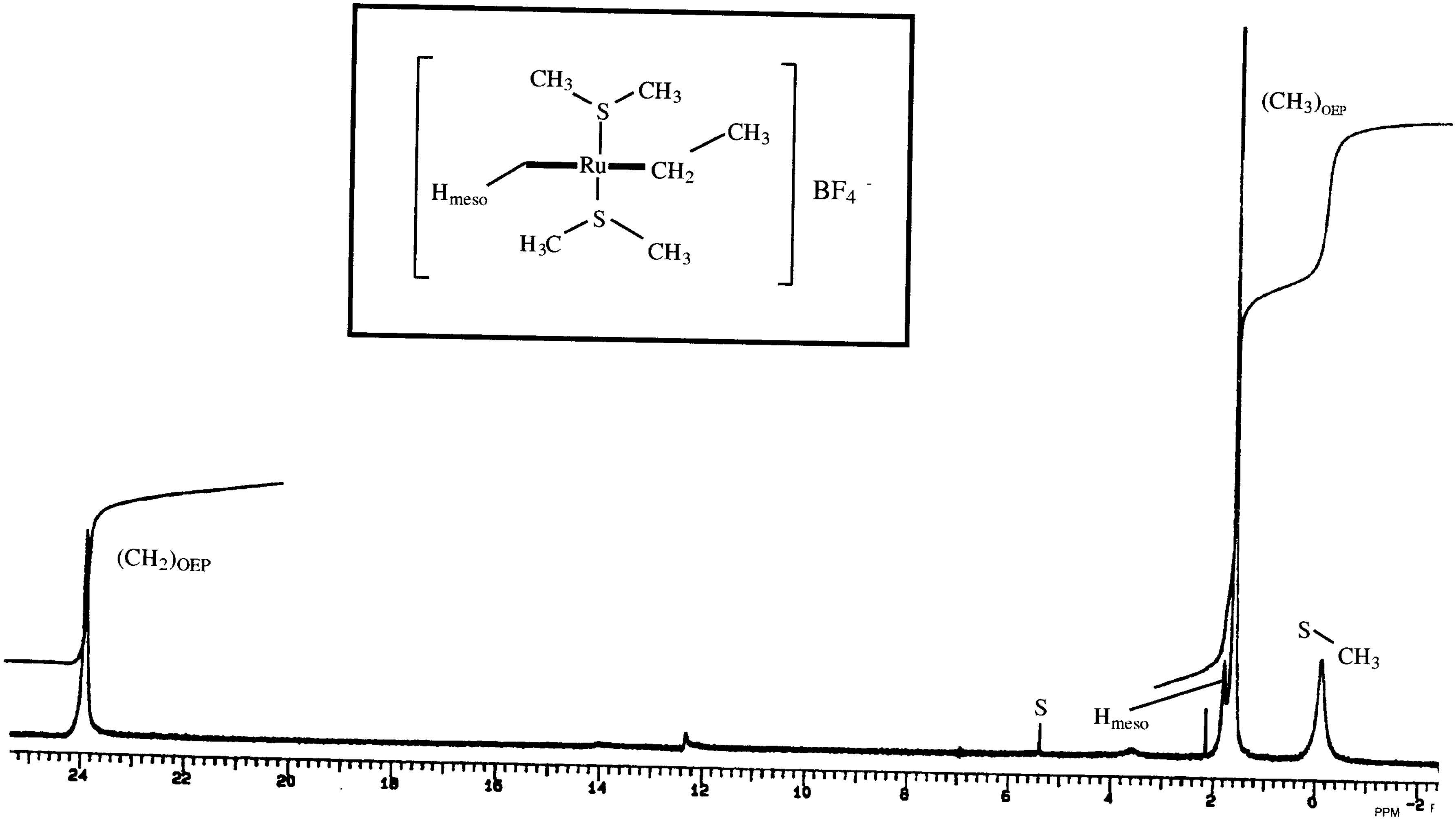

Figure 2.10. $^{1}$H-nmr spectrum of Ru(OEP)(dms)$_2{}^+$BF$_4{}^-$; 20.0° C in CD$_2$Cl$_2$; S ≡ solvent.

### Table 2.2
### Positions of the $^1$H-nmr Signals ($\delta_{obs}$), Assigned to $Ru^{II}(OEP)(dms)_2$ + $Ru^{III}(OEP)(dms)_2{}^+PhCOO^-$ in the Experiment Illustrated in Figure 2.7, and the Calculated Remaining Mole Fraction of $Ru(OEP)(dms)_2$ ($N_{II}$)[a]

| Time | $\delta_{obs}$, ($N_{II}$) | | | |
|---|---|---|---|---|
| (min) | $CH_3$ | $CH_2$ | $H_{meso}$ | $SCH_3$ |
| 28 | 1.73, (0.72) | 9.67, (0.71) | 7.10, (0.71) | -1.92, (0.70) |
| 97 | 1.68, (0.55) | 11.76, (0.61) | 6.33, (0.61) | -1.62, (0.58) |
| 234 | 1.67, (0.51) | 14.26, (0.48) | 5.39, (0.48) | -1.31, (0.46) |
| 312 | 1.66, (0.48) | 15.29, (0.43) | 5.00, (0.43) | -1.19, (0.41) |
| 360 | 1.64, (0.41) | 16.02, (0.39) | 4.71, (0.39) | -1.10, (0.37) |

(a) The mole fraction is calculated by the formula: $N_{II} = (\delta_{obs} - \delta_{III})/(\delta_{III} - \delta_{II})$, where $\delta_{II}$ and $\delta_{III}$ are the values of $\delta$ (in ppm) for $Ru^{II}(OEP)(dms)_2$ and $Ru^{III}(OEP)(dms)_2{}^+BF_4{}^-$, respectively ($\delta$ for $Ru(OEP)(dms)_2{}^+$ is assumed to be the same whether the counter-ion is $PhCOO^-$ or $BF_4{}^-$.

The rapid electron transfer giving rise to the observed time-averaged nmr spectrum almost certainly occurs via an outer-sphere process. Such processes have been extensively documented in porphyrin systems, and the porphyrin ring is thought to mediate facile electron transfer from a donor to the metal center or vice-versa.[28] We have obtained the crystal structure of $Ru(OEP)(decMS)_2{}^+BF_4{}^-$ (figure 2.11), which is expected to be closely analogous to that of $Ru(OEP)(dms)_2{}^+BF_4{}^-$.[29] Table 2.3 compares selected bond lengths and angles of the $Ru^{III}$ complex with those of $Ru(OEP)(decMS)_2$, whose crystal structure we previously obtained.[9] The differences in corresponding bond length between the two species are within about 0.020 Å, while the corresponding bond angles are within 5° of each other. In our report on the structure of $Ru(OEP)(decMS)_2$, we included a fairly extensive survey of crystal structures of $Ru^{II}(OEP)$ complexes, as well as other complexes containing Ru-S bonds.[9] The geometrical differences between $Ru(OEP)(decMS)_2$ and $Ru(OEP)(decMS)_2{}^+BF_4{}^-$ are not significant when compared to the variations found in this survey. It is clear that the change in oxidation state does not significantly affect the geometry of the complex. Thus electron transfer between the two Ru species requires minimal bond reorganization, and this leads to fast and efficient electron exchange.[30] Note that in a 1971 article,[31] Stynes and Ibers point out that a change in spin state upon oxidation or reduction will reduce the electron exchange rate to a much greater extent than even a relatively large change in bond lengths. As mentioned previously, no $Ru^{III}(OEP)$ high spin complex has ever been detected, and all of the available spectroscopic data for $Ru(OEP)(dms)_2{}^+BF_4{}^-$ are similar to those of previously reported $Ru^{III}(OEP)$ low spin $d^5$ complexes; the fast electron exchange between $Ru^{II}$ and $Ru^{III}$ provides further evidence that both complexes are low spin.

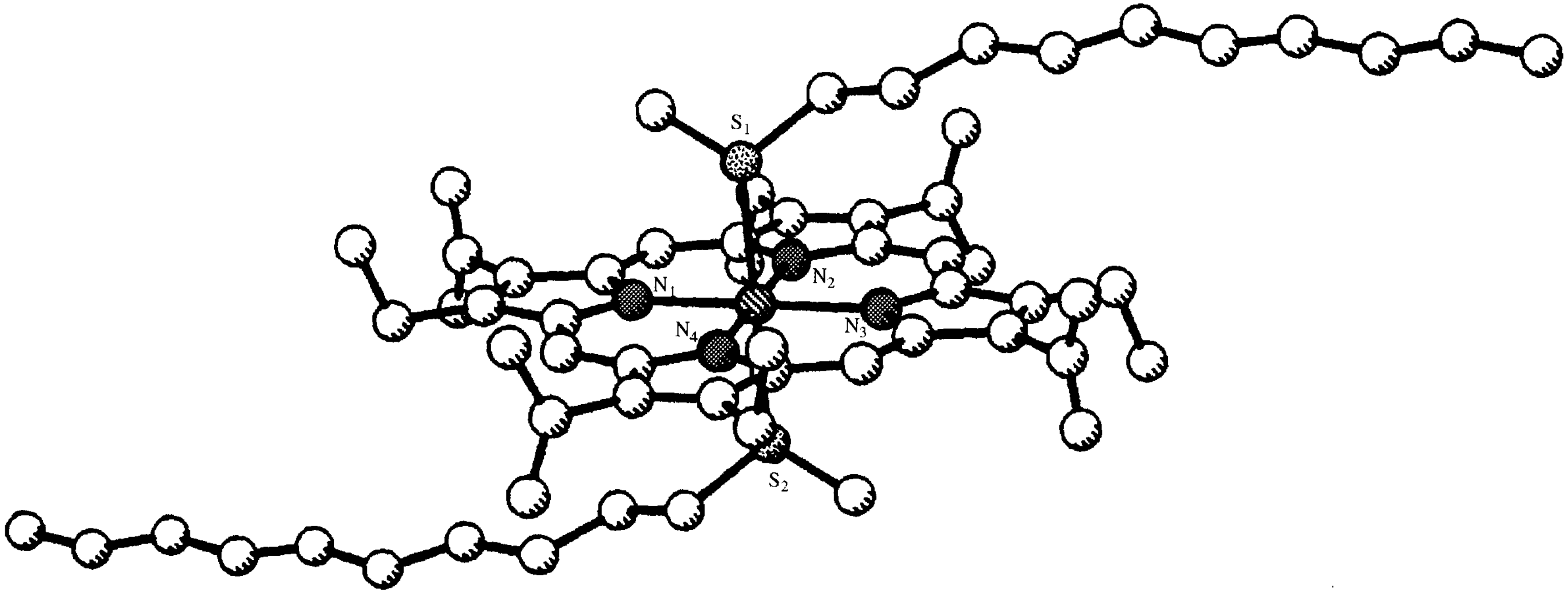
S1
N1
N2
N3
N4
S2

Figure 2.11. Crystal structure of Ru(OEP)(decMS)$_2{}^+$BF$_4{}^-$; selected bond lengths and angles are given in table 2.3.

## Table 2.3
## Selected Bond Distances (Å) and Bond Angles (deg) for Ru(OEP)(decMS)$_2$ and Ru(OEP)(decMS)$_2^+$BF$_4^-$ [a]

| | Ru(OEP)(decMS)$_2$ | Ru(OEP)(decMS)$_2^+$BF$_4^-$ |
|---|---|---|
| Distances | | |
| Ru-S(1) | 2.376 (1) | 2.383 (6) |
| Ru-S(2) | 2.361 (1) | (b) |
| Ru-N(1) | 2.044 (3) | 2.029 (6) |
| Ru-N(2) | 2.044 (3) | 2.045 (5) |
| Ru-N(3) | 2.056 (3) | (b) |
| Ru-N(4) | 2.041 (3) | (b) |
| Angles | | |
| N(1)-Ru-S(1) | 90.2 (1) | 85.6 (2) |
| N(2)-Ru-S(1) | 86.9 (1) | 90.1 (2) |
| N(3)-Ru-S(1) | 90.9 (1) | (b) |
| N(4)-Ru-S(1) | 94.0 (1) | (b) |
| N(1)-Ru-S(2) | 90.7 (1) | 94.4 (2) |
| N(2)-Ru-S(2) | 94.7 (1) | 89.9 (2) |
| N(3)-Ru-S(2) | 88.3 (1) | (b) |
| N(4)-Ru-S(2) | 84.5 (1) | (b) |
| S(1)-Ru-S(2) | 178.27 (3) | 180.00 |

---

(a) Standard deviations in parentheses. (b) Ru(OEP)(decMS)$_2^+$BF$_4^-$ has a crystallographic inversion center.

The two major signals in figure 2.7 which are shaded grey are attributable to the OEP methylene protons of a paramagnetic complex of formulation Ru(OEP)(dms)(PhCOO) (see below); two signals are observed since in this case the two axial ligands are different, which makes the methylene protons magnetically inequivalent. The other signals which are shaded grey are also attributed to the same complex; the complete assignment is listed in table 2.1, and is discussed below. The signals due to Ru(OEP)(dms)(PhCOO) maintain approximately the same intensity (e.g. relative to the impurity at 16 ppm) until the last (35 h) spectrum, in which their intensity is greatly diminished (figure 2.9). At this point the signals are also slightly but significantly shifted relative to their position in earlier spectra. No immediate explanation is available for this observation; all of the signals initially assigned to the Ru(OEP)(dms)(PhCOO) complex are still present in the final spectrum, but shifted to varying degrees. It is possible that in the first five spectra the signals are actually time-averages due to exchange between Ru(OEP)(dms)(PhCOO) and some other complex, and that by the time of the final collected spectrum the concentration of this exchanging complex is negligible.

The presence of Ru(OEP)(dms)(PhCOO) and $\mathrm{Ru(OEP)(dms)_2{}^+PhCOO^-}$ is best explained by the following reaction sequence:

$$\mathrm{2Ru^{II}(OEP)(dms)_2 + O_2 + 2PhCOOH \rightarrow 2Ru^{III}(OEP)(dms)_2{}^+PhCOO^- + H_2O_2} \qquad 2.5$$

$$\mathrm{Ru^{III}(OEP)(dms)_2{}^+PhCOO^- \rightleftharpoons Ru^{III}(OEP)(dms)(PhCOO) + dms} \qquad 2.6$$

Step one would involve initial electron transfer from $Ru^{II}$ to $O_2$ to form $Ru^{III}$ and the superoxide anion, followed by superoxide protonation and subsequent disproportionation to give hydrogen peroxide and dioxygen. The latter process is known to be very fast, and irreversible,[32] so it would drive the process to completion. Note that in equations 2.5, 2.6 and throughout this thesis, ionic species are always written with the cation and associated anion. This is convenient for book-keeping purposes, but it is also meant to suggest a physical picture: given the low dielectric constant of the $CH_2Cl_2$ solvent (8.93),[33] all of the ionic species are probably best described as ion pairs.[33]

The initial electron transfer in equation 2.5 could occur either following initial coordination of $O_2$ to the metal center (inner-sphere), or by direct outer-sphere electron transfer; there is precedence for both mechanisms.[34] For the stoichiometric process being discussed here, the inner sphere mechanism is almost certainly the only significant pathway, as evidenced by the fact that the reaction can be stopped completely if an excess of dms is added (at least in the absence of an intense light source; see below). Presumably, the excess thiother ligand is competing with the dioxygen for the axial binding site. Thermodynamically, the direct formation of superoxide via an outer-sphere electron transfer is extremely unfavourable; the ($O_2 + e^- \rightleftharpoons O_2^-$) standard reduction potential in dry, non-aqueous media has been measured at -0.8 V vs. Ag/AgCl[32] which, when combined with the $Ru^{III}(OEP)(RR'S)_2/Ru^{II}(OEP)(RR'S)_2$ couple of about 0.22 V reported in section 2.4, gives a cell potential of about -1 V. This translates to an equilibrium constant value of about $10^{-17}$ (for $Ru^{II} + O_2 \rightleftharpoons Ru^{III} + O_2^-$). Theoretically, even a highly unfavourable equilibrium can be overcome if the product removal in a subsequent step (e.g. in this case, by protonation of superoxide) is faster than the reverse reaction; however, product removal cannot overcome the effect of an initial, slow forward reaction. In this case it appears that outer sphere electron transfer from $Ru^{II}$ to $O_2$ is not only thermodynamically unfavourable, but also kinetically slow, at least under normal laboratory conditions. In chapter 3 it will be seen that $Ru(OEP)(RR'S)_2$ complexes *can* react with $O_2$ and PhCOOH in the presence of excess dialkylsulfide, *if the solution is irradiated with a reasonably intense source of visible light*; in this case, the reaction is hypothesized to take place via an outer sphere process, but light is required to supply the extra energy.

Hydrogen peroxide is known to react rapidly with dialkylsulfides, especially in non-hydroxylic solvents.[35] Thus the $H_2O_2$ produced in reaction 2.5 is expected to react rapidly with free dms (produced in reaction 2.6) to give water and dmso:

$$H_2O_2 + \text{dms} \rightarrow H_2O + \text{dmso} \qquad 2.7$$

Hydrogen peroxide could also react with coordinated dms, but free dms is a stronger nucleophile.

Numerous unsuccessful attempts were made to prepare Ru(OEP)(dms)(PhCOO) pure; figure 2.12a, which shows the $^1$H-nmr spectrum obtained for an approximately 1:1 mixture of $Ru(OEP)(dms)_2{}^+BF_4{}^-$ and $Me_4N^+Ru(OEP)(PhCOO)_2{}^-$, illustrates the basic problem (figure 2.12b shows the spectrum of pure $Me_4N^+Ru(OEP)(PhCOO)_2{}^-$ for comparison). The major signals in the spectrum are attributable to the desired complex Ru(OEP)(dms)(PhCOO). Signals due to residual $Me_4N^+Ru(OEP)(PhCOO)_2{}^-$ are also

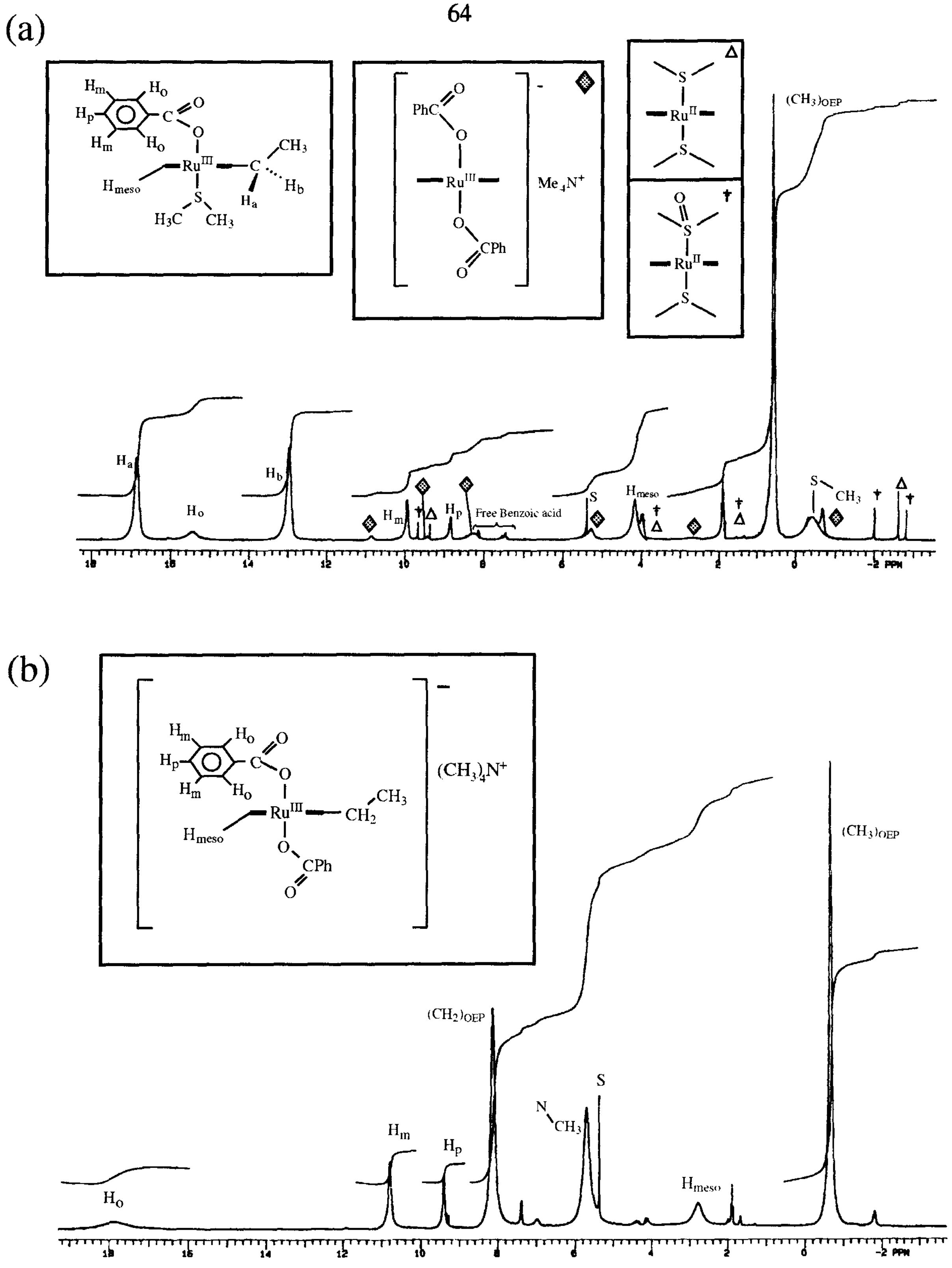

Figure 2.12. $^1$H-nmr spectrum of (a) a mixture (approximately 1:1) of $Ru(OEP)(dms)_2{}^+BF_4{}^-$ and $Me_4N^+Ru(OEP)(PhCOO)_2{}^-$ about 1 h after mixing; (b) pure $Me_4N^+Ru(OEP)(PhCOO)_2{}^-$. Both spectra in $CD_2Cl_2$ at 20.0° C, and systems sealed under vacuum; S ≡ solvent.

present because the original mixture was not exactly 1:1, but this is not a factor when the reaction is scaled up, as the starting materials can then be weighed out more accurately. The problem is that figure 2.12a shows small amounts of $\mathrm{Ru(OEP)(dms)_2}$ and Ru(OEP)(dms)(dm$\underline{\mathrm{s}}$o) to be present as well, in essentially a 1:1 proportion. Attempts to crystallize out the desired product using hydrocarbon solvents resulted in a dramatic increase in the concentrations of $\mathrm{Ru^{II}}$ species, this time with a predominance of $\mathrm{Ru(OEP)(dms)_2}$. In every attempt to prepare Ru(OEP)(dms)(PhCOO), $\mathrm{Ru(OEP)(dms)_2}$ and Ru(OEP)(dms)(dm$\underline{\mathrm{s}}$o) were obtained as co-products; in $\mathrm{CH_2Cl_2}$ the species were in trace amounts and 1:1 proportion, but as soon as hydrocarbons were added, large amounts of $\mathrm{Ru(OEP)(dms)_2}$ were recovered (this will be discussed further in section 2.6).

Although the desired Ru(OEP)(dms)(PhCOO) could not be prepared pure, experiments such as that illustrated in figure 2.12a, which certainly demonstrate its existence, also provide a valuable clue as to the nature of the overall reaction of interest (i.e. the stoichiometric oxidation of $\mathrm{Ru(OEP)(dms)_2}$). We speculate that a disproportionation such as the following can take place:

$$\begin{aligned}&\mathrm{Ru^{III}(OEP)(dms)_2{}^{+}PhCOO^{-}} + \mathrm{Ru^{III}(OEP)(dms)(PhCOO)} \rightleftharpoons \\ &\qquad \mathrm{Ru^{II}(OEP)(dms)_2} + \mathrm{Ru^{IV}(OEP)(dms)(PhCOO)^{+}PhCOO^{-}}\end{aligned} \tag{2.8}$$

In this scenario, coordination of the benzoate to the $\mathrm{Ru^{III}}$ metal center brings the $\mathrm{Ru^{III}/Ru^{IV}}$ redox couple into the range of the $\mathrm{Ru(OEP)(dms)_2{}^{+}/Ru(OEP)(dms)_2}$ couple; the CV studies discussed in section 2.4 already show how coordination of two benzoates to

$Ru^{III}$ can decrease its oxidation potential from about 1.3 to 0.22 V, making it almost as easy to oxidize to $Ru^{IV}$ as it is to oxidize $Ru^{II}(OEP)(Et_2S)_2$ to the corresponding $Ru^{III}$ species. The presence of $Ru^{IV}$ could well explain the slight shifts observed in the Ru(OEP)(dms)(PhCOO) $^1$H-nmr signals while the stoichiometric oxidation reaction is under way (see figures 2.7 and 2.9), if the equilibrium 2.8 is very fast.

After reaction 2.8, the $Ru^{IV}$ species could be converted to one equivalent of Ru(OEP)(dms)(dm$\underline{s}$o) by the following sequence of reactions:

$$Ru^{IV}(OEP)(dms)(PhCOO)^{+}PhCOO^{-} + H_2O \rightleftharpoons$$

$$O{=}Ru^{IV}(OEP)(dms) + 2PhCOOH \qquad 2.9$$

$$O{=}Ru^{IV}(OEP)(dms) + dms \rightarrow Ru^{II}(OEP)(dms)(dms\underline{o}) \qquad 2.10$$

$$Ru^{II}(OEP)(dms)(dms\underline{o}) \rightleftharpoons Ru^{II}(OEP)(dms) + dmso \qquad 2.11$$

$$Ru^{II}(OEP)(dms) + dmso \rightleftharpoons Ru^{II}(OEP)(dms)(dm\underline{s}o) \qquad 2.12$$

The conversion of coordinated dms$\underline{o}$ to dm$\underline{s}$o could alternatively involve an intramolecular process and a π-bonded S=O moiety in the transition state,[24b] although some kinetic findings imply otherwise; this will be discussed in section 3.5.2.2. Finally, as free dmso accumulates, the bis sulfoxide complex would be formed via

$$\mathrm{Ru(OEP)(dms)(dm\underline{s}o) + dmso \rightleftharpoons Ru(OEP)(dm\underline{s}o)_2 + dms} \qquad 2.13$$

Equation 2.8 can be thought of as an acid-base reaction leaving a hydroxide as counter-ion to the $\mathrm{Ru^{IV}}$ cationic species, followed by nucleophilic addition of the hydroxide to the coordinated benzoate, and subsequent displacement of the $\mathrm{Ru^{IV}}$-oxo. Alternatively, the acid-base reaction could be followed by a simple displacement of the coordinated benzoate by the hydroxide, followed by deprotonation of the coordinated ligand. Water in the required stoichiometric amount of reaction 2.9 would be produced in reaction 2.7. The reactivity suggested in equations 2.10-2.12 has precedent in Ru(porphyrin) chemistry (see section 1.2).[36] Notice that the overall stoichiometry for equations 2.5-2.13 is

$$\mathrm{Ru^{II}(OEP)(dms)_2 + O_2 \rightleftharpoons Ru^{II}(OEP)(dm\underline{s}o)_2} \qquad 2.14$$

As previously mentioned, the benzoic acid is not consumed in the reaction, and acts merely as a catalyst.

It should be emphasized that although equations 2.8 and 2.9 fit well into the scheme for the observed reactivity of $\mathrm{Ru(OEP)(dms)_2}$, they are meant to suggest a general "$\mathrm{Ru^{IV}{=}O}$" mechanism whereby the reaction takes place, and not necessarily the exact mechanism. There are a considerable number of variations which could be proposed for equations 2.8 and 2.9; a particularly plausible example might be:

$$\mathrm{Ru^{III}(OEP)(dms)(PhCOO) + H_2O \rightleftharpoons Ru^{III}(OEP)(dms)(OH) + PhCOOH} \qquad 2.8'$$

$$\mathrm{Ru^{III}(OEP)(dms)(OH) + Ru^{III}(OEP)(dms)_2{}^{+}PhCOO^{-}} \rightleftharpoons$$

$$\mathrm{Ru^{II}(OEP)(dms)_2 + O{=}Ru^{IV}(OEP)(dms) + PhCOOH} \qquad 2.9'$$

In this scenario, reaction 2.6 is viewed, in effect, as a side equilibrium, and not really as part of the reaction pathway.

Further equilibria might arise as free dmso accumulates from reaction 2.7. Some of the sulfoxide might tend to coordinate to $\mathrm{Ru^{III}}$:

$$\mathrm{Ru^{III}(OEP)(dms)_2{}^{+}PhCOO^{-} + dmso \rightleftharpoons Ru^{III}(OEP)(dms)(dm\underline{s}o)^{+}PhCOO^{-} + dms} \qquad 2.15$$

The cyclic voltammetry experiments show (figure 2.4b) that coordination of a sulfoxide to $\mathrm{Ru^{III}}$ makes the metal much more reducible than its dialkylsulfide counterpart; thus if a species such as $\mathrm{Ru(OEP)(dms)(dm\underline{s}o)^{+}PhCOO^{-}}$ is formed during the $\mathrm{Ru(OEP)(dms)_2}$ oxidation sequence, it will be rapidly and preferentially reduced to the $\mathrm{Ru^{II}}$ form, either in a step analogous to step 2.8, or via electron transfer from a $\mathrm{Ru^{II}(OEP)(dms)_2}$ molecule. Figure 2.13 shows the cyclic voltammogram of a solution containing primarily $\mathrm{Ru(OEP)(decMS)(decM\underline{S}O)}$ prepared by mixing 0.78 mM $\mathrm{Ru(OEP)(decMS)_2}$, 71 mM decMS, and 25 mM decMSO (all three $\mathrm{Ru(OEP)(RR'S)(RR'\underline{S}O)}$ complexes have a distinctive band at 404 nm in their uv/vis spectra, and this can be used to investigate the composition of the above mixture). Initially, as the potential is scanned in the positive direction, the major signal, attributed to the oxidation of $\mathrm{Ru(OEP)(decMS)(DecM\underline{S}O)}$, is found at 0.59 V; the signal at 0.28, attributed to $\mathrm{Ru(OEP)(decMS)_2}$ oxidation, is minor

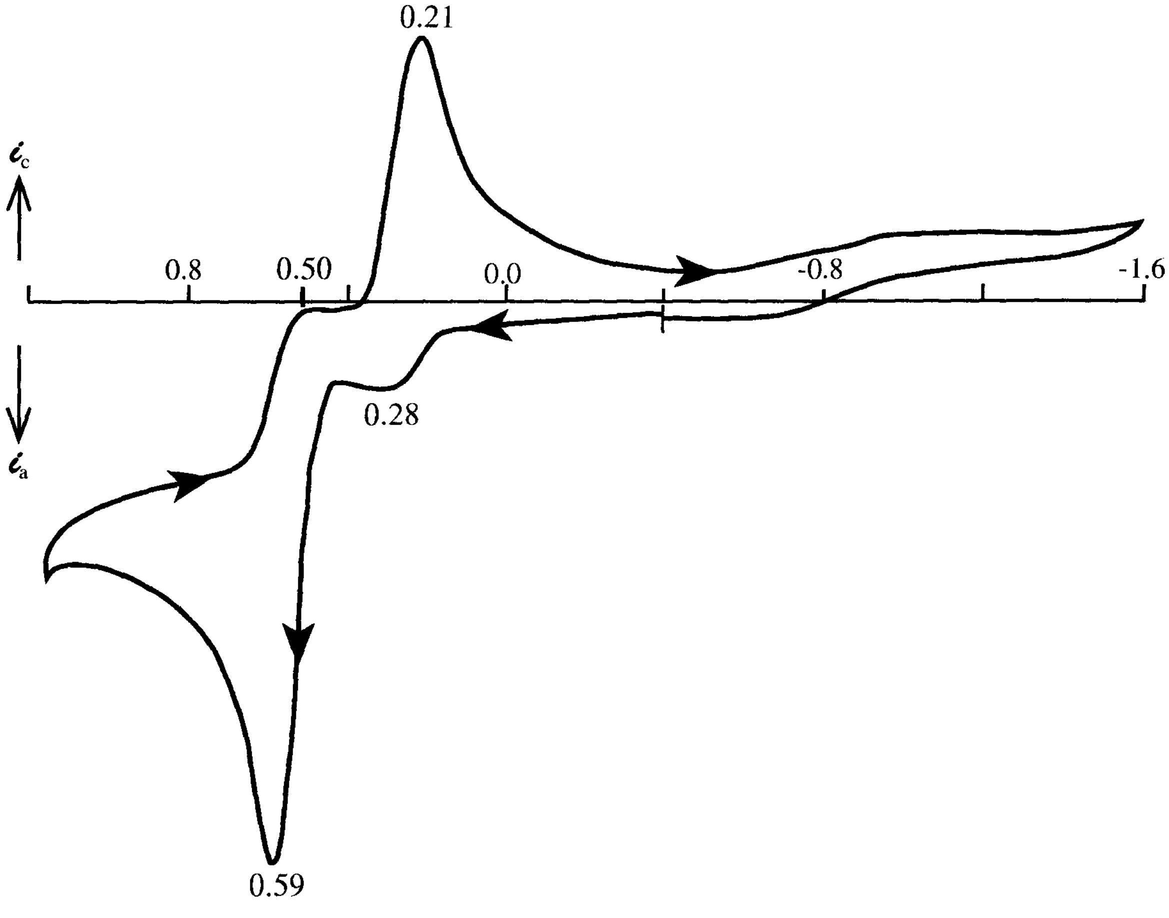

Figure 2.13. Cyclic voltammogram of a solution ($CH_2Cl_2$/n-$Bu_4N^+BF_4^-$) initially containing 0.78 mM Ru(OEP)(decMS)$_2$, 71 mM decMS, and 25 mM decMSO.

by comparison. As the potential is scanned back in the negative direction, the peak due to $Ru^{III}(OEP)(decMS)_2^+$ reduction (at 0.21 V) is now the major one, while that due to $Ru^{III}(OEP)(decMS)(decM\underline{S}O)^+$ reduction (at 0.50 V) is comparatively minor. The observation is explained by the following reaction sequence:

$$Ru^{II}(OEP)(decMS)(decM\underline{S}O) \rightleftharpoons Ru^{III}(OEP)(decMS)(decM\underline{S}O)^+ + e^- \qquad 2.16$$

$$Ru^{III}(OEP)(decMS)(decM\underline{S}O)^+ + decMS \rightleftharpoons Ru^{III}(OEP)(decMS)_2^+ + decMSO \quad 2.17$$

$$Ru^{III}(OEP)(decMS)_2^+ + e^- \rightleftharpoons Ru^{II}(OEP)(decMS)_2 \qquad 2.18$$

This experiment shows that sulfide coordination to $Ru^{III}$ is preferred over sulfoxide coordination; thus equation 2.15 should not play an important role in the stoichiometric oxidation, except possibly at the point when most of the sulfide has been converted to sulfoxide.

All of the alternate reaction pathways proposed, though different in detail to equations 2.8-2.9, nevertheless share the essential feature: $Ru^{III}(OEP)(dms)(L)^+PhCOO^-$ ($L \equiv$ dms, dmso) is reduced to $Ru^{II}$ by a $Ru^{III}$ species which has had its oxidation potential lowered upon replacement of one coordinated thioether by an anionic ligand, and the resulting $Ru^{IV}$ species is converted to $O{=}Ru^{IV}(OEP)(dms)$.

## 2.6 Reaction of Ru(OEP)(RR'S)$_2$ Complexes with Dioxygen and Benzoic Acid in Hydrocarbon Solvents

In benzene or toluene containing benzoic acid, exposure of Ru(OEP)(dms)$_2$, Ru(OEP)(Et$_2$S)$_2$ or Ru(OEP)(decMS)$_2$ to O$_2$, under conditions analogous to those described for the reactions in methylene chloride, also ultimately results in the production of the Ru(OEP) mono- and bis- sulfoxide complexes. In a general sense, the mechanism suggested in equations 2.5-2.13 is consistent with the reactivity observed in benzene or toluene; however, the lower polarity of these solvents (dielectric constant $\approx$ 2) does result in some minor, but interesting, differences between what is observed in methylene chloride, and what is observed in, say, benzene.

Figure 2.14 shows the $^1$H-nmr spectrum of a C$_6$D$_6$ solution containing 8.2 mM Ru(OEP)(dms)$_2$ and 8.2 mM PhCOOH, which was exposed to 1 atm of O$_2$ for about 36 h at room temperature (table 2.4 summarizes the peak assignments). Several points are noteworthy about this reaction. First, it is much slower than the analogous reaction in methylene chloride; figure 2.9 shows that, after 35 h, a substantial proportion of the Ru(OEP) has been converted to Ru(OEP)(dm$\underline{s}$o)$_2$, and no Ru(OEP)(dms)$_2$ can be detected. In the reaction illustrated in figure 2.14, only about 66% of the original complex has reacted to give Ru(OEP)(dms)(dm$\underline{s}$o), and the bis(sulfoxide) is present in trace amounts. A second point is that no significant amounts of Ru$^{III}$ complexes are visible in the reaction mixture (actually, trace amounts of Ru(OEP)(dms)(PhCOO) are detectable, if the spectrum is expanded sufficiently). In a separate experiment, in which [PhCOOH] was 20 times that of Ru(OEP)(dms)$_2$, the characteristic signals of Ru$^{III}$(OEP)(dms)(PhCOO) (table 2.4) could be detected in significant quantities, but even

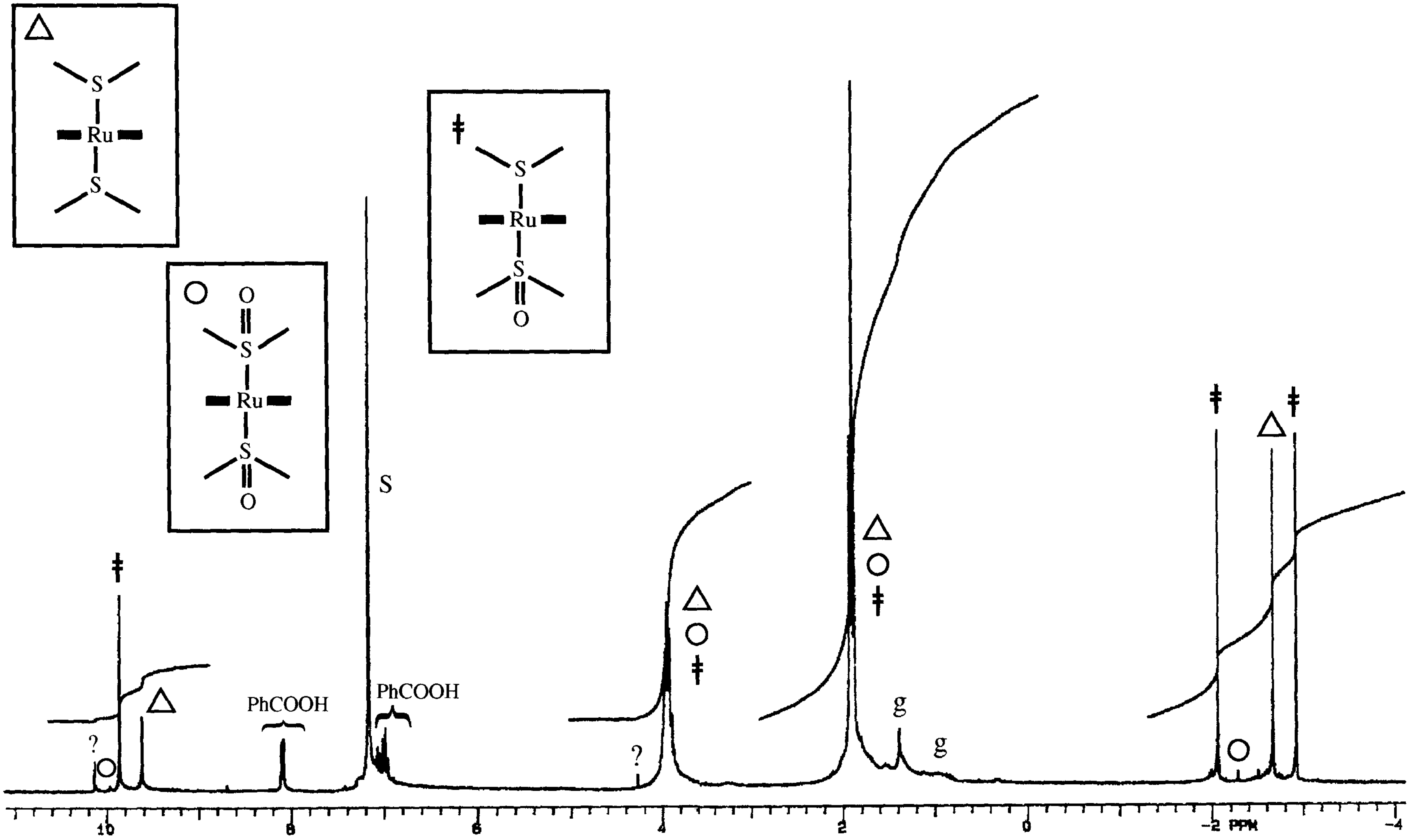

Figure 2.14. $^1$H-nmr spectrum of a $C_6D_6$ solution, initially containing 8.2 mM Ru(OEP)(dms)$_2$ and 8.2 mM PhCOOH, which was exposed to 1 atm of $O_2$ for about 36 h at room temperature; S ≡ solvent, g ≡ grease, ? ≡ unidentifed signals.

## Table 2.4
## Summary of the $^1$H-nmr Peak Positions in $C_6D_6$ for the dms- and dmso-Containing Ru(OEP) Complexes Discussed in Section 2.6

| | OEP Signals (ppm) | | | Axial Ligand Signals (ppm) | | | | |
|---|---|---|---|---|---|---|---|---|
| | $CH_3$ | $CH_2$ | $H_{meso}$ | dms | dmso | PhCOO | | |
| | | | | | | $H_o$ | $H_m$ | $H_p$ |
| Ru(OEP)(dms)$_2$ | 1.90,t | 3.90,q | 9.62,s | -2.68,s | - | - | - | - |
| Ru(OEP)(dms)(dmso) | 1.88,t | 3.93,m | 9.85,s | -2.94,s | -2.08,s | - | - | - |
| Ru(OEP)(dmso)$_2$ [a] | 1.93,t | 3.99,q | 9.94,s | - | -2.32,s | - | - | - |
| Ru(OEP)(dms)(PhCOO) [b] | 0.30 | 15.73, 12.33 | 4.12 | 0.20 | - | 16.88 | 9.77 | ~8.45[c] |

(a) This spectrum was obtained in $C_7D_8$; note that Ru(OEP)(dmso)$_2$ is sparingly soluble in all hydrocarbon solvents.
(b) All of the signals for this paramagnetic complex are broad, and lacking in fine structure.
(c) This signal overlaps another set of signals attributed to unidentified diamagnetic species, which makes it difficult to establish the exact peak position.

under these conditions there was no evidence for the presence of $Ru^{III}(OEP)(dms)_2{}^+$ $PhCOO^-$. Clearly the $Ru^{III}$ species are much more difficult to generate in the non-polar benzene solvent, and also equation 2.6, in which $Ru(OEP)(dms)_2{}^+PhCOO^-$ is considered to dissociate dms and form Ru(OEP)(dms)(PhCOO) must lie far to the right. Both of these factors would contribute to making the overall reaction slower in hydrocarbon solvents (cf. equation 2.8). A third feature of figure 2.14 worth pointing out is the presence of the trace signals at 4.3 and 10.1 ppm. The presence of both these signals was noted in our earlier studies on the oxidation of $Ru(OEP)(decMS)_2$,[1a] although the signals were much more prominent.[1a] There is no immediately apparent assignment for the signal at 4.3 ppm, but that at 10.1 ppm is almost certainly attributable to the meso proton of a $Ru^{II}(OEP)$ complex.[37] It is impossible to be sure which complex is giving rise to this signal, but it may be a Ru(OEP)(CO)L species (L $\equiv$ a neutral ligand, possibly dms or dmso), as such species exhibit an $H_{meso}$ signal at around 10.1 ppm in benzene.[1a] It is well known that the CO-containing complexes are thermodynamic sinks in Ru(Porp) chemistry, and the appearance of Ru(OEP)(CO)L under conditions where there is no obvious source of CO has been documented, although often without explanation (but see below).[1a,22,38,39]

The presence of end-products other than the sulfoxide complexes (which are desired within the catalytic $O_2$-oxidation of thioethers to sulfoxide; see chapter 3) seems to be characteristic of the reactions carried out in hydrocarbon solvents. Figure 2.15 shows the result of exposing a solution containing 2.3 mM $Ru(OEP)(Et_2S)_2$ and 3.3 mM

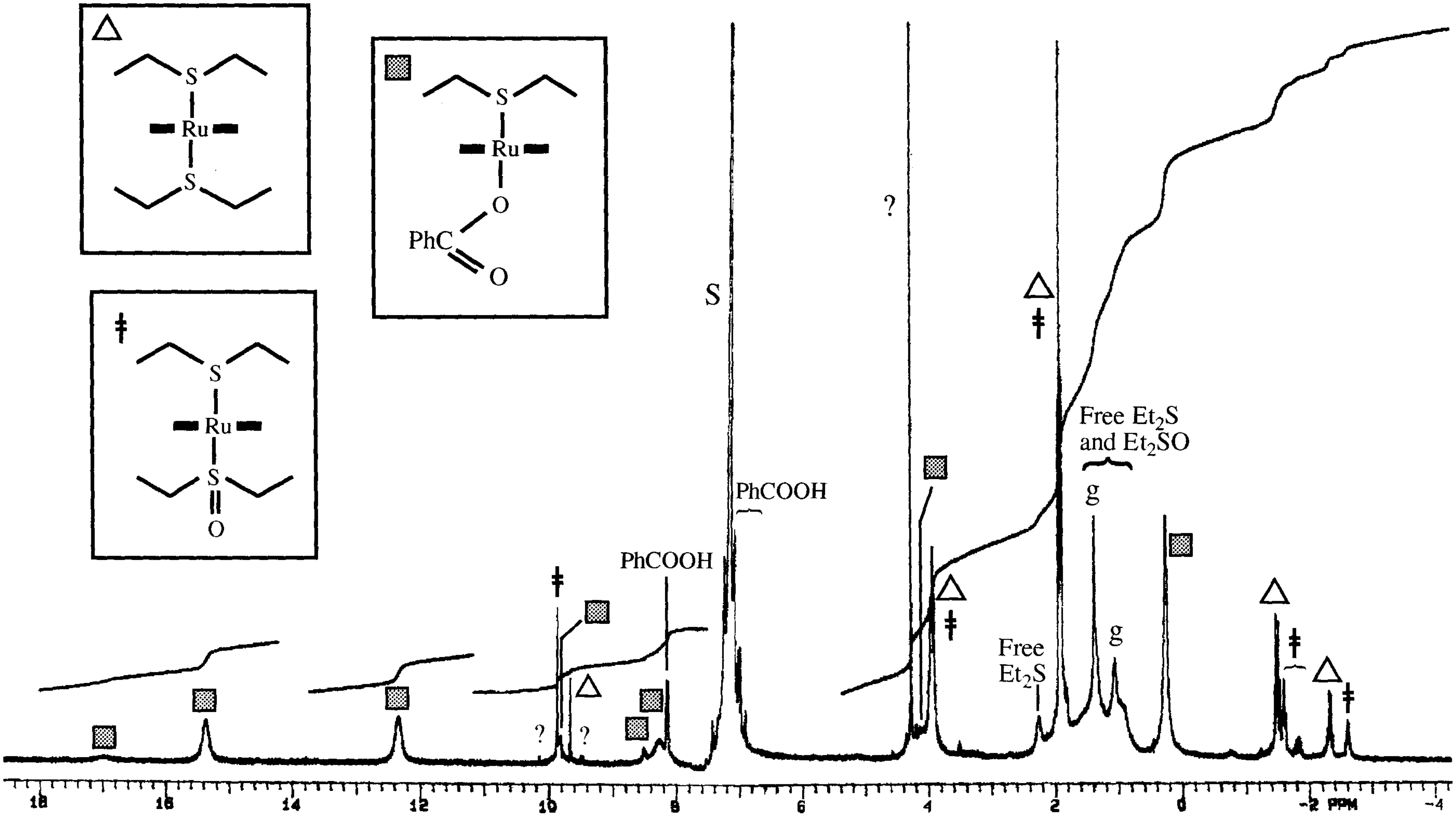

Figure 2.15. $^1$H-nmr spectrum of a $C_6D_6$ solution, initially containing 2.3 mM Ru(OEP)$(Et_2S)_2$ and 3.3 mM PhCOOH, which was exposed to 1 atm of $O_2$ for about 12 h at 35° C; S ≡ solvent, g ≡ grease, ? ≡ unidentified signals.

## Table 2.5
## Summary of the $^1$H-nmr Peak Positions in $C_6D_6$ for the $Et_2S$- and $Et_2SO$-Containing Ru(OEP) Complexes Discussed in Section 2.6

| | OEP Signals (ppm) | | | Axial Ligand Signals (ppm) | | | | | | |
|---|---|---|---|---|---|---|---|---|---|---|
| | $CH_3$ | $CH_2$ | $H_{meso}$ | $Et_2S$ | | $Et_2SO$ | | PhCOO | | |
| | | | | $CH_2$ | $CH_3$ | $CH_2$ | $CH_3$ | $H_o$ | $H_m$ | $H_p$ |
| $Ru(OEP)(Et_2S)_2$ | 1.91,t | 3.91,q | 9.65,s | -2.34,q | -1.49,t | - | | - | - | - |
| $Ru(OEP)(Et_2S)(Et_2\underline{S}O)$ | 1.91,t | 3.96,m | 9.85,s | -1.4 to -2.7[a] | | -1.4 to -2.7[a] | | - | - | - |
| $Ru(OEP)(Et_2\underline{S}O)_2$ [b] | 1.90,t | 3.94,q | 9.90,s | - | | -(2.11,2.68)[c] | -1.65,t | - | - | - |
| $Ru(OEP)(Et_2S)(PhCOO)$ | 0.24 | 15.40, 12.36 | ~4.1[d] | 8.22 | ~4.1[d] | - | | 17.00 | 9.80 | 8.55[d] |

(a) These signals have not yet been unequivocably assigned.

(b) This spectrum was obtained in $C_7D_8$.

(c) For $Ru(OEP)(Et_2\underline{S}O)_2$ the sulfoxide methylene protons are magnetically inequivalent, and give rise to two separate multiplets.

(d) Tentative positions; overlap of signals makes it difficult to determine the exact positions of these signals.

PhCOOH, to 1 atm of $O_2$ for 12 h at 35° C (these are the conditions under which the experiments described in the next chapter were run, except that in the latter an excess of thioether was added). The peak assignments for figure 2.15 are given in table 2.5. For the $Et_2S$ system, $Ru^{III}(OEP)(Et_2S)(PhCOO)$ does accumulate significantly (in fact the signals attributable to this complex were present within 20 min of starting the reaction). It appears that $Ru^{III}(OEP)(Et_2S)(PhCOO)$ is significantly more "stable" than its dms counterpart under the reaction conditions. Still, there is no evidence in figure 2.15 for the presence of $Ru^{III}(OEP)(Et_2S)_2{}^+PhCOO^-$; thus even for the $Et_2S$ complex, the ionic species is not stable in the less polar solvent, so that the $Et_2S$ equivalent of equation 2.6 lies far to the right. What little $Ru(OEP)(Et_2S)_2{}^+PhCOO^-$ is produced perhaps rapidly undergoes the disproportionation reaction 2.8 and subsequent reactions, to give neutral species such as $O{=}Ru(OEP)(Et_2S)$, and eventually $Ru(OEP)(Et_2S)(Et_2\underline{S}O)$. Figure 2.15 also shows the signals at about 4.3 and 10.1 ppm (note that here the 4.3 signal is quite intense), and also two other signals of about equal intensity near 9.5 ppm. Again, one can only speculate as to the identity of the complexes which give rise to these signals, but previous studies have shown that the meso protons of complexes having the form $[Ru^{IV}(OEP)L]_2O$ ($L \equiv$ an anionic ligand) have signals around 9.5 ppm in benzene solution.[40] These so-called $\mu$-oxo dimers are well known thermodynamic sinks in ruthenium porphyrin chemistry when $O_2$ and $H_2O$ are present, and so it is likely that the two signals at around 9.5 ppm in figure 2.15 are due to two complexes of this type (perhaps with $L \equiv$ PhCOO and/or OH).[40]

There are other studies which shed some light on the observations made about the $^1$H-nmr data of figures 2.14 and 2.15. Figure 2.16 shows the $^1$H-nmr spectrum of a

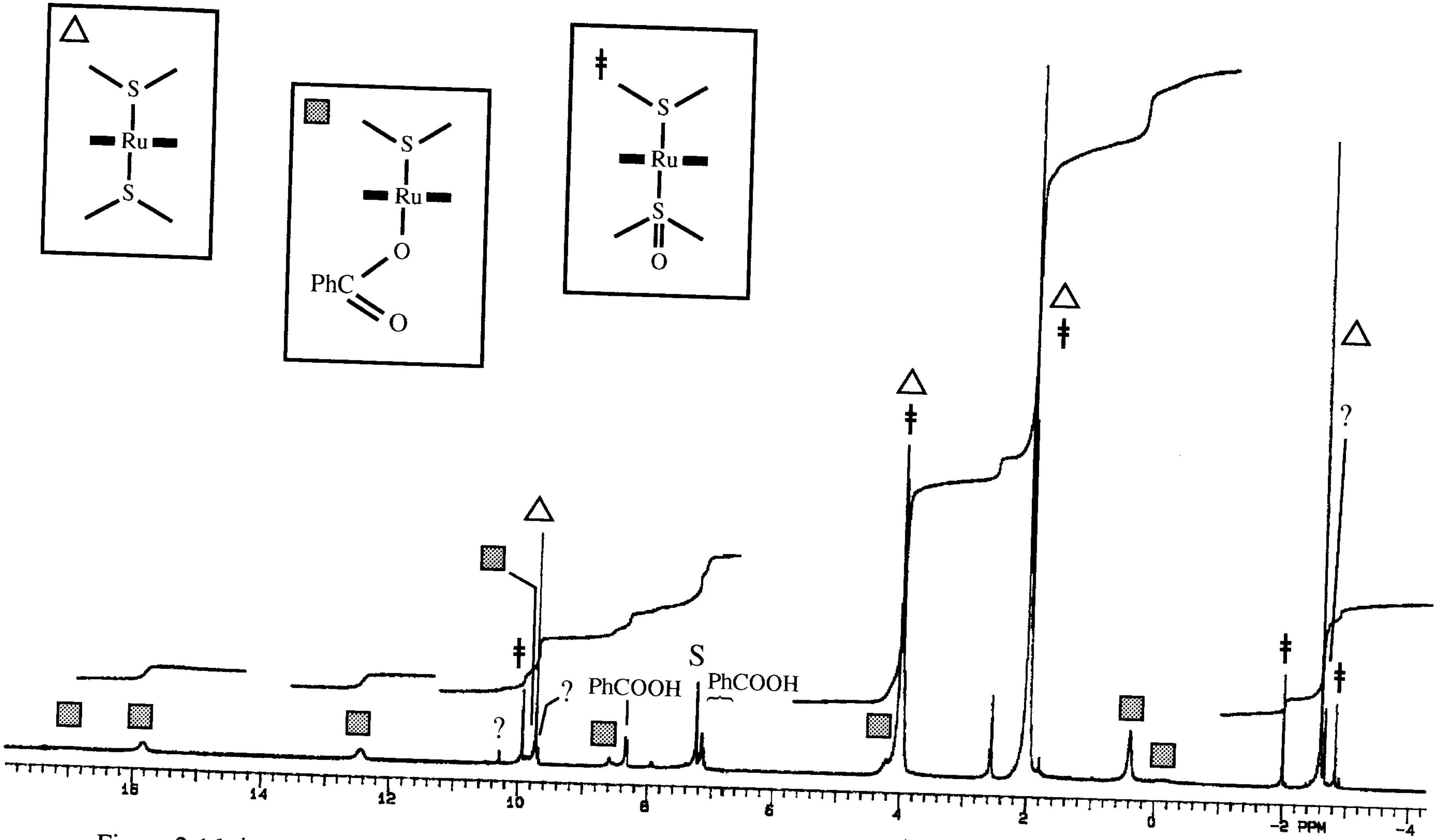

Figure 2.16. $^1$H-nmr spectrum of a $C_6D_6$ solution, initially a suspension of Ru$^{III}$(OEP)(dms)$_2{}^+$BF$_4^-$ and Me$_4$N$^+$Ru$^{III}$(OEP)(PhCOO)$_2$ (approximately 4x10$^{-6}$ mol of each), which was allowed to stand overnight under vacuum; S ≡ solvent, ? ≡ unidentified signals.

solution obtained by allowing a suspension of $Ru(OEP)(dms)_2{}^+BF_4{}^-$ and $Me_4N^+Ru(OEP)(PhCOO)_2{}^-$ (approximately $4x10^{-6}$ mol of each in about 0.6 mL of solvent) to stand overnight under vacuum in thoroughly dried $C_6D_6$. At the time the spectrum was taken, all of the solid had dissolved, and the resulting solution was dark red-orange. The spectrum shows that $Ru(OEP)(dms)_2$ and Ru(OEP)(dms)(dm$\underline{s}$o) are formed in an approximately 3:1 ratio, along with comparatively small amounts of Ru(OEP)(dms)(PhCOO), and other unidentified $Ru^{II}$ products. This is a very different product distribution from that obtained when $Ru(OEP)(dms)_2{}^+BF_4{}^-$ and $Me_4N^+Ru(OEP)(PhCOO)_2{}^-$ are mixed under vacuum in $CD_2Cl_2$ (see figure 2.12a in the previous section); in this solvent, the major product is Ru(OEP)(dms)(PhCOO), and the small quantities of $Ru(OEP)(dms)_2$ and Ru(OEP)(dms)(dm$\underline{s}$o) observed can be attributed to the presence of a trace amount of water, which presumably allows reactions 2.8-2.13 to take place to a limited extent. It appears that in benzene, the $Ru^{III}$ species are sufficiently unstable in solution that, even in the absence of $H_2O$, an alternative reduction pathway is being used to generate substantial amounts of Ru(II). One plausible route is via a process formally described by:

$$Ru^{III}(OEP)(dms)_2{}^+BF_4{}^- + Me_4N^+Ru(OEP)(PhCOO)_2{}^- \rightarrow$$
$$Ru^{II}(OEP)(dms)_2 + \text{"}(PhCOO)_2\text{"} + Me_4N^+BF_4{}^- + \text{Unidentified } Ru^{II} \text{ Products} \quad 2.19$$

In practice, benzoyl peroxide is not observed; however, this could be because the benzoyl radicals react further with other compounds in solution, which would explain the presence of the other unidentified products, and also of coordinated dmso. In hydrocarbon solvent, such free-radical processes might take place to a limited extent under even under $O_2$ atmospheres, when $H_2O$ is available (from the reaction of dms with $H_2O_2$, equation 2.7), which could also help explain the formation of unidentified Ru(OEP) products obtained in the aerobic oxidations of Ru(OEP)(dms)$_2$ and Ru(OEP)(Et$_2$S)$_2$ in hydrocarbon solutions. For example, the presence of the PhCOO radical in aerobic conditions could initiate auto-oxidation of the thioethers. This is known to produce, among other products, aldehydes,[35] and it has been shown that Ru(OEP) complexes can catalyze the decarbonylation of aldehydes.[41] Thus Ru(OEP)(CO)L could indeed be giving rise to the signal at 10.1 ppm, with the CO resulting from free-radical autoxidation of the thioethers, and subsequent decarbonylation of the primary auto-oxidation products.

Despite the minor side products which are observed when Ru(OEP)(RR′S)$_2$ complexes react with $O_2$ and PhCOOH, it does appear that the major oxidation pathway can be described by equations 2.5-2.13, whether the oxidation is carried out in methylene chloride or benzene. This conclusion becomes a key assumption in the experiments described in the following chapter.

# REFERENCES AND NOTES

# FOR CHAPTER 2

1. a)Pacheco, A. A. M.Sc. Dissertation, The University of British Columbia, Vancouver, B. C., 1986. b) Pacheco, A. A. Unpublished data.

2. Sekutowski, D. G.; Stucky, G. D. *J. Chem. Educ.* **1976**, *53*, 110.

3. Fieser, L. F. and Fieser, M. *Reagents for Organic Synthesis*, J. Wiley and Sons, Inc, New York, 1967; vol I, pp 471 and 472.

4.Bruce, M. I.; Matisons, J. G.; Wallis, R. C.; Patrick, J. M.; Skelton, B. W.; White, A. M. *J. Chem. Soc., Dalton Trans.* **1983**, 2365.

5. Antipas, A.; Buchler, J. W.; Gouterman, M.; Smith, P. D. *J. Am. Chem. Soc.* **1978**, *100*, 3015.

6. Collman, J. P.; Barnes, C. E.; Sweptson, P. N.; Ibers, J. A. *J. Am. Chem. Soc.* **1984**, *106*, 3500.

7. Collman, J. P.; Prodolliet, J. W.; Leidner, C. R. *J. Am. Chem. Soc.* **1986**, *108*, 2916.

8. A good reference on the subject of handling air-sensitive compounds is:
Shriver, D. F. *The Manipulation of Air Sensitive Compounds*, McGraw-Hill, New York, N.Y., 1969.

9. James, B. R.; Pacheco, A. A.; Rettig, S. J.; Ibers, J. A. *Inorg. Chem.* **1988**, *27*, 2414.

10. The yields for these complexes were not explicitly determined; however, the supernatants after recrystallization showed only negligible color, which suggests that any losses in yield were due primarily to incomplete transfer of the precipitate from the filter to the weighing vial. For approximately 100 mg quantities of a precipitate, 80-90% transfer was commonly obtained.

11.Van Duyne, R. P.; Reilley, C. N. *Anal. Chem.* **1972**, *44*, 142.

12. This couple was previously recorded at 0.08 V vs. SCE (see references 19 and 20 below), which is the same within experimental error; the SCE is 0.04V higher than that of Ag/AgCl (relative to NHE) in aqueous solution (Brady, J. E.; Humiston, G. E. *General Chemistry, Principles and Structure*, 2nd ed., John Wiley and Sons, New York, N. Y., 1978; p. 463).

13. J. A. Davies, *Adv. in Inorg. Chem. Radiochem.* **1981**, *24*, 115 and references therein.

14. See for example: James, B. R.; Morris, R. H.; Reimer, K. J. *Can. J. Chem.* **1977**, *55*, 2352, and references therein.

15. Janson, T.R.; Katz, J. In *The Porphyrins*, Dolphin, D., Ed, Academic Press, New York, N. Y., 1978; vol. VI, chapter 1.

16. Scheer, H.; Katz, J. In *Porphyrins and Metalloporphyrins*, Smith, K. M., Ed., Elsevier Scientific, Amsterdam, The Netherlands, 1975; Chapter 10.

17. Davis, D. G. In *The Porphyrins*, Dolphin, D., Ed., Academic Press, New York, N. Y., 1978; vol. V, chapter 4.

18. Fuhrhop, J. H.; Kadish, K. M.; Davis, D. G. *J. Am. Chem. Soc.* **1973**, *95*, 5140.

19. Brown, G. M.; Hopf, F. R.; Ferguson, J. A.; Meyer, T. J.; Whitten, D. G. *J. Am. Chem. Soc.* **1973**, *95*, 5939.

20. Brown, G. M., Hopf, F. R., Meyer, T. J., Whitten, D. G. *J. Am Chem. Soc.*, **1975**, *97*, 5385.

21. The X-Y recorder used for the CV studies was not ideal for obtaining precise data, and the experimental uncertainty in the obtained $E^{\circ\prime}$ values is estimated at $\pm 0.02$ V. Therefore the $E^{\circ\prime}$ values for all three complexes are the same within experimental error.

22. Sishta, P. C. Ph.D. Dissertation, The University of British Columbia, Vancouver B. C., 1990.

23. a) Barley, M.; Becker, J. Y.; Domazetis, G.; Dolphin, D.; James, B. R. *Can. J. Chem.* **1983**, *61*, 2389. b) Barley, M.; Dolphin, D.; James, B. R. *J. Chem. Soc., Chem. Commun.* **1984**, 1499.

24. a) See reference 9 and references therein. b) Rearrangement of S-bound sulfoxide to the O-bound isomer in Ru(dmso) complexes after metal-centered oxidation was previously observed for $Ru^{II}(NH_3)_5(dm\underline{s}o)$ in aqueous solution: Scott, A. Y. N.; Taube, H. *Inorg. Chem.* **1982**, *21*, 2542. A 7-coordinate transition state was postulated for the isomerization process.

25. Drago, R. S. *Physical Methods in Chemistry*, W. B. Saunders, Philadelphia, PA, 1977; a) Chapter 12; b) Chapter 8.

26. Ke, M.; Rettig, S. J.; James, B. R.; Dolphin, D. *J. Chem. Soc., Chem. Commun.* **1987**, 1110.

27. Sishta, C.; Ke, M.; James, B. R.; Dolphin, D. *J. Chem. Soc., Chem. Commun.* **1986**, 787.

28. Castro, C. E. In *The Porphyrins*, Dolphin, D., Ed., Academic Press, New York, N. Y., 1978; Vol. V, Chapter 1.

29. A complete analysis of the crystal structure is described elsewhere; Pacheco, A. A.; Rettig, S. J.; James, B. R. To be Published.

30. Wilkins, R. G. *Kinetics and Mechanisms of Reactions of Transition Metal Complexes*, VCH, Weinheim, 1991; Chapter 5.

31. Stynes, H. C.; Ibers, J. A. *Inorg. Chem.* **1971**, *10*, 2304.

32. Sawyer, D. T.; Valentine, J. S. *Acc. Chem. Res.* **1981**, *14*, 393.

33. Sawyer, D. T.; Roberts, Jr. J. L. *Experimental Electrochemistry for Chemists*, John Wiley and Sons, New York, N. Y., 1974; Chapter 4.

34. A good review of this subject is provided in reference 28; another useful review is found in: Chu, M. M. L.; Castro, C. E.; Hathaway, G. M. *Biochem.* **1978**, *17*, 481.

35. Barnard, D.; Bateman, L.; Cuneen, J. I. In *Organic Sulfur Compounds*, Kharasch N., Ed., Pergamon Press, New York, N. Y., 1961; Vol. I, Chapter 21.

36. Rajapakse, N.; James, B. R.; Dolphin, D. *Catal. Lett.* **1989**, *2*, 219.

37. A singlet between 9.0 and 10.5 ppm in the $^1$H-nmr of Ru(OEP) complexes is characteristic of the meso protons; see reference 9 and references therein.

38. Ke, M. Ph.D. Dissertation, The University of British Columbia, Vancouver B. C., 1988.

39. In one study, it was even shown that Ru(Porp) complexes can react with CO present in the walls of the reaction vessel: Corsini, A.; Mehdi, H.; Chan, A. *Can. J. Chem.* **1980**, *58*, 527.

40. Collman, J. P.; Barnes, C. E.; Brothers, P. J.; Collins, T. J.; Ozawa, T.; Gallucci, J. C.; Ibers, J. A. *J. Am. Chem. Soc.* **1984**, *106*, 5151.

41. Domazetis, G.; Tarpey, B.; Dolphin, D.; James, B. R. *J. Chem. Soc., Chem. Commun.* **1980**, 939.

# CHAPTER 3

# A MECHANISTIC STUDY OF THE $O_2$-OXIDATION OF DIETHYLSULFIDE CATALYZED BY Ru(OEP)($Et_2S$)$_2$

## 3.1 Introduction

In the previous chapter a mechanism was proposed for the stoichiometric oxidation of Ru(OEP)(RR'S)$_2$ complexes to Ru(OEP)(RR'S)(RR'$\underline{S}$O) and Ru(OEP)($Et_2\underline{S}O$)$_2$ by dioxygen in acidic organic media. It is clear that, in the presence of a large excess of dialkylsulfide, the starting bis(thioether) complex could be regenerated from Ru(OEP)(RR'S)(RR'$\underline{S}$O), thus making the process catalytic. This assumption was confirmed experimentally, and in the process new insights were obtained. In particular, a completely new and interesting feature of the catalytic reaction became apparent, namely its rate dependence on visible light. This chapter begins by summarizing qualitative features peculiar to the catalytic process. Based on these, and on the conclusions drawn in chapter 2 about the stoichiometric oxidations, a mechanism for the catalytic oxidation of dialkylsulfides is proposed. The second part of the chapter deals with the kinetic analysis of quantitative stopped-flow and oxygen-uptake experiments, which were used to monitor the catalytic process. The data are fitted to a rate law derived from the proposed mechanism; the actual derivation of the rate law is deferred to chapter 4.

All of the studies discussed in this chapter refer specifically to $Et_2S$ oxidation catalyzed by Ru(OEP)($Et_2S$)$_2$, in benzene. Qualitatively, excess dms in the presence of Ru(OEP)(dms)$_2$ and decMS in the presence of Ru(OEP)(decMS)$_2$ were found be oxidized in the same way as $Et_2S$ in the presence of Ru(OEP)($Et_2S$)$_2$, and the systems exhibited qualitative dependences on the same variables. Furthermore, all the reactions proceeded in either methylene chloride or toluene; in fact, it was already shown in chapter 2 that the stoichiometric reaction proceeds more cleanly in methylene chloride than in benzene, and this is probably true of the catalytic system as well; unfortunately the high vapour pressure of methylene chloride was a problem when quantitative studies were attempted. Dimethylsulfide also had the problem of high vapour pressure.

## 3.2 Experimental

### 3.2.1 Materials

n-Undecane, used as an internal standard for the GC measurements, was from Aldrich. The origins or methods of preparation of all other materials used in the experiments described in this chapter were previously described in chapter 2.

### 3.2.2 Stopped-Flow Experiments

#### 3.2.2.1 Sample Handling

All experiments were carried out under aerobic conditions; no special precautions were taken to exclude air or water. It is assumed that side-reactions with these potential reagents are slow enough to be ignored under the conditions of high sulfide and sulfoxide concentrations used, and indeed the excellent reproducibility of the results verifies this assumption (see section 3.4). For any given experiment, one of the drive syringes was filled with a benzene solution of $Et_2S$, and the other with a benzene solution of $Ru(OEP)(Et_2SO)_2$ and $Et_2SO$. One experiment was taken to be the average of five stopped-flow runs done at constant concentration of all reagents. In any given series of experiments, the concentration of $Et_2S$ was varied, while the concentrations of the reagents in the other syringe were held constant. A blank run in which the $Et_2S$ syringe contained only benzene was carried out for each series. The free ligand concentrations ($Et_2S$ and $Et_2SO$) were always held high enough so that they would remain effectively constant for the duration of an experiment.

#### 3.2.2.2 Instrumentation

All stopped-flow experiments were carried out on an Applied Photophysics model SF.17MV stopped-flow spectrophotometer, equipped with 2.5 mL drive syringes. A pressure of 650 kPa was used to drive the syringes.[1] A constant temperature of $35.0\pm0.1°$ C was achieved using a Grant LTD 6 constant-temperature bath connected to the stopped-flow sample handling unit via Tygon tubing.

Changes in the reaction mixture were monitored by following the absorbance change at one of two wavelengths: 400.5, or 402.8 nm (see section 3.4.1). The absorbance change with time was monitored across a 1.00 cm path-length cell. The monochromator entrance and exit slits were both set at 0.2 mm. A high brightness 150-W Xenon arc lamp was used as the light source.

### 3.2.3 Gas Chromatography

#### 3.2.3.1 Sample Handling

Sample preparation and handling for gas chromatographic experiments was essentially identical to that described below for the gas uptake experiments. The only significant difference was that samples to be analyzed by gas chromatography had 23.7

mM n-undecane added to them as an internal standard.

### 3.2.3.1 Instrumentation

Gas chromatography was carried out on a Hewlett-Packard HP 5890A gas chromatograph, equipped with a 15 m x 0.20 mm HP-1 capillary column (0.33 $\mu$m film thickness), a split capillary inlet (insert packed with 3% OV-1 on 100/120 chromosorb W-HP), and a flame ionization detector. Helium was used as the carrier and makeup gas. Other chromatographic conditions were as follows: sample volume, 2 $\mu$L; column flow, 0.33 mL/min; split ratio, 45:1; injector temperature, 220° C; detector temperature, 325° C; oven temperature program, 80° C for 5 min then increased at a rate of 20° C per min to 170° C, and held for 15 min.

## 3.2.4 Oxygen Uptake Experiments

### 3.2.4.1 Sample Handling

Unless otherwise stated, all the gas uptake experiments were carried out in 10.0 mL aliquots of a benzene solution, containing an initial $Et_2S$ concentration of 0.742 M. For experiments in which $Ru(OEP)(Et_2S)_2$ concentrations of less than 0.5 mM were required, a stock solution containing about 5 mM $Ru(OEP)(Et_2S)_2$ and 0.742 M $Et_2S$ was first made up. The appropriate amount of this solution was then added to the reaction vessel using a Unimetrics microliter syringe, and the total volume made up to 10.0 ml with a 0.742 M solution of $Et_2S$ in benzene. Between experiments, the stock $Ru(OEP)(Et_2S)_2$ solutions were kept in the dark, and all stock was used up in a maximum of three days. For experiments requiring $Ru(OEP)(Et_2S)_2$ concentrations greater than 0.5

mM, the appropriate amount of crystalline complex was weighed out and added directly to the reaction vessel.

Crystalline benzoic acid was weighed out into a small glass bucket, which was suspended above the reaction mixture by means of a dropping sidearm (see fig.3.1a), until the moment when the reaction was to be initiated. Prior to reaction, the solution was subjected to two freeze/pump/thaw degassing cycles in order to remove dissolved nitrogen.

### 3.2.4.2 Apparatus Setup

The gas uptake apparatus used for this series of experiments was simply a modified version of a design which has seen extensive use in our laboratories,[2] so that a full written description of all the parts and basic operation is omitted here. Nevertheless, there are a sufficient number of procedural differences in the way the modified apparatus was used to warrant some discussion.

The complete apparatus is illustrated in figure 3.1. The principal design difference between this apparatus and its predecessors is in the use of high-vacuum Teflon valves at positions 3 and 4, in place of standard greased stopcocks (figure 3.1a). When Teflon valve 3 is closed to seal off the small volume of gas in the right arm of the oil manometer, a significant pressure is exerted, causing a very noticeable change in the oil levels. Thus the oil manometer must be re-levelled before proceeding (see below). In addition, when valve 4 is closed, a much smaller but still measurable pressure change takes place. This too must be compensated for (see below).

Additional modifications to the apparatus were peculiar to this series of

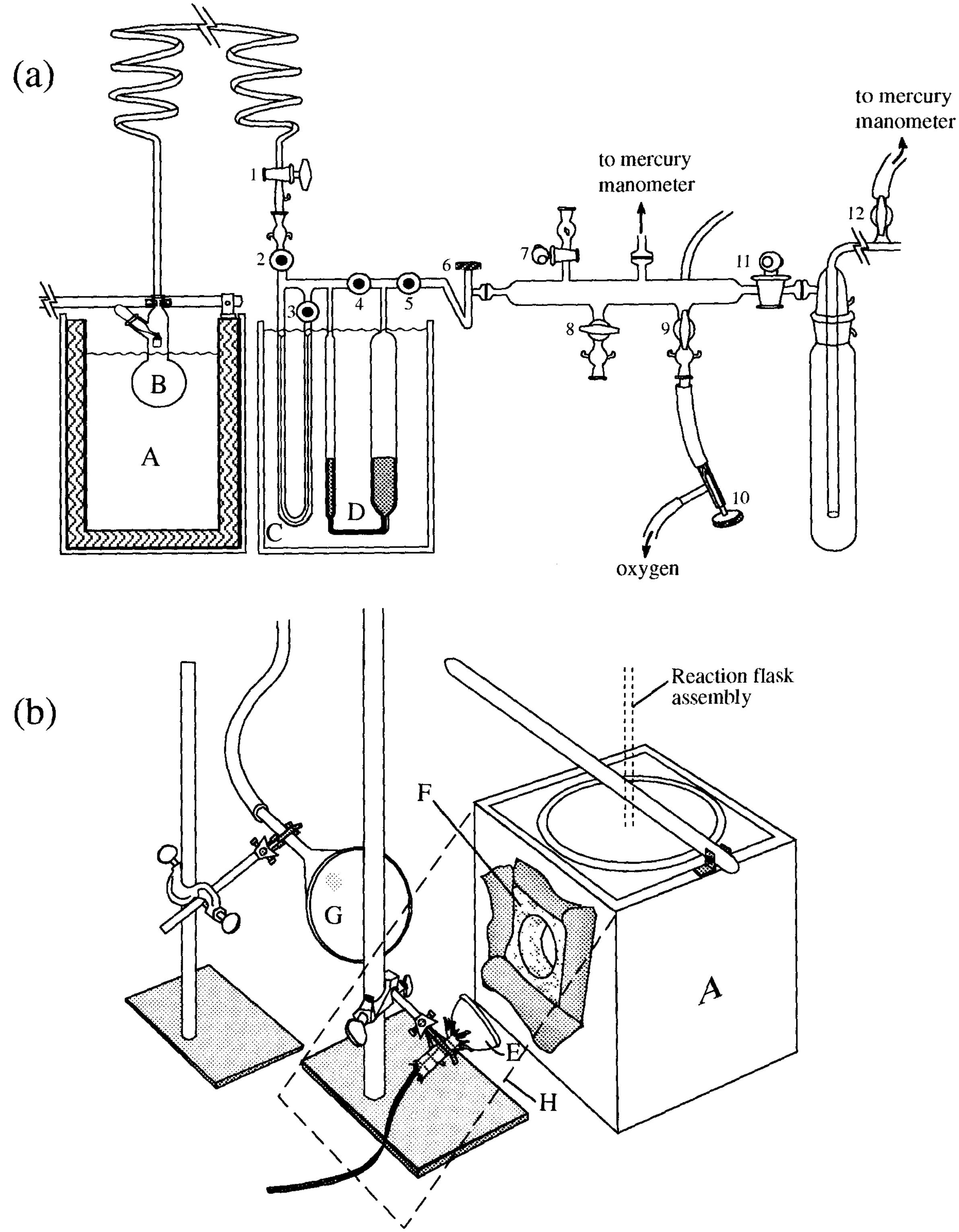
(a)
to mercury manometer
to mercury manometer
1
2
3
4
5
6
7
8
9
10
11
12
B
A
C
D
oxygen
(b)
Reaction flask assembly
F
G
A
E
H

Figure 3.1. Apparatus used for gas uptake measurements. (a) Complete setup; (b) Close-up view of the oil bath and housing, showing the orientation of the light source. Key components: (A) Thermostatted and insulated oil bath; (B) Reaction vessel; (C) Oil manometer; (D) Mercury burette and reservoir; (E) Projection lamp; (F) Aluminum foil; (G) Compressed air manifold; (H) Screen. (1)-(12): Various taps and valves; see text for explanations.

experiments, and were required to keep the reaction solution intensely and constantly illuminated. These modifications are illustrated in figure 3.1b. A GTE/Sylvania ENX 360 Watt projection lamp (E), of the type commonly used in Kodak carousel slide projectors, was used as a source of light. The solution was illuminated via a hole in the oil bath housing insulation, normally used to inspect visually the reaction mixture. A Powerstat variable transformer was used to supply 30 V AC to the lamp. The insulation and the outside walls of the oil bath housing had to be covered in foil (F) to protect them from excessive heating by the projection lamp. In addition, the lamp and exterior of the oil bath housing were constantly cooled by blowing compressed air over them via the funnel G, which was a common laboratory glass funnel. During operation, the operator was protected from the intense light by the screen (H), which was simply a sheet of cardboard covered in aluminum foil. Normally a thermostatted heat source is required to keep the oil bath temperature constant. In this case a cooling source also had to be supplied to counteract the uncontrolled heat provided by the projection lamp. The oil bath was cooled by water, supplied from a separate constant-temperature bath, and fed through a copper coil immersed in the oil. With this setup, the temperature could be kept constant at $34.85 \pm 0.15°$ C (but see sections 3.5.2.1 and 3.5.2.2). Finally, because the average surface of reaction solution exposed to the light would tend to vary with the shaking rate, special care was taken to keep this constant at 164 ± 10 cycles/min, unless otherwise stated. The same flask and bucket were used in all of the experiments for the same reason.

As benzene and $Et_2S$ both have a significant vapour pressure at the reaction temperature, a measurable pressure change occurs as the temperature cycles between

34.70 and 35.00° C. This change is visible as an oscillatory motion of the levels in the oil manometer, in the absence of any gas uptake or evolution due to chemical reactions. This phenomenon would incorporate an additional uncertainty in the uptake readings if these were taken at random times. To prevent this, all gas burette readings were taken when the temperature was at the minimum of 34.70° C.

A typical experimental run proceeded as follows. The initial sample preparation was identical to that used with prior versions of the apparatus.[2] Once the reaction vessel (B) was immersed in the oil bath (A), the solution was allowed to equilibrate for about 10 minutes with the projection lamp off (30 minutes for gas pressures of 0.6 atm or less) at a pressure about 10 torr below that desired for the reaction. During this time, valves 7, 8, 10 and 11 were closed, while all others were open. After this time, valve 3 was closed. Oxygen was introduced through needle valve 10, until the oil manometer (C) was nearly levelled (to within 3mm). The total pressure reading at the mercury manometer was recorded; this reading was taken to be the total pressure under which the reaction was carried out, and $pO_2$ was calculated by subtracting the benzene vapour pressure (147.66 mm Hg)[3a] from this value (the solubility of $O_2$ in benzene, at 35° C, is 9.279 mM/atm[3b]). Valves 4 and 6 were now closed, and from this point onward valve 6 was used to introduce or remove oxygen from the part of the apparatus to its left, as required to keep the oil manometer level. The projection lamp was now turned on. This sometimes altered the temperature cycle slightly, and so at the next temperature minimum the oil manometer was checked and re-levelled if necessary. The initial reading was taken on the mercury burette (D), the shaker stopped momentarily, and the reaction started by dropping the bucket containing the benzoic acid into the solution. After the shaker was re-started, the experiment proceeded in the same way as it would with other versions of the gas uptake apparatus, with uptake readings taken each time a temperature minimum was passed (approximately every 6-10 minutes). In experiments for which very little uptake occurred over this time period, the oil level difference was first artificially enhanced by drawing a very slight vacuum via valve 6. Subsequent re-levelling was much easier than via a direct attempt to adjust for a very small level difference. This technique could also be used if too much $O_2$ was introduced via valve 6, so that the level in the right hand side of the oil manometer was higher than that of the left.

### 3.2.5 Data Treatment

Raw data from the stopped-flow experiments were analyzed on an Archimedes workstation using a non-linear least squares fitting program, supplied with the stopped-flow instrumentation, which implements the Levenberg-Marquardt algorithm.[4,5a] All other data analyses, including least-squares methods and numerical solution of differential equations, were carried out on a PC using customized implementations of the programs found in "Numerical Recipes, the Art of Scientific Computing (Quick Basic versions)".[6] The complete customized programs are listed in appendix 1.

## 3.3 $Ru(OEP)(Et_2S)_2$-Catalyzed $O_2$-Oxidation of $Et_2S$ in Benzene Solution - General Observations

Gas chromatographic studies show that in oxygenated solutions containing $Ru(OEP)(Et_2S)_2$, benzoic acid, and an excess of free $Et_2S$ at room temperature or at 35° C, the thioether is catalytically oxidized to $Et_2SO$. However, early attempts to study the kinetics of this catalytic oxidation yielded erratic and generally irreproducible results. Eventually it was found that if the reaction mixture was irradiated by intense visible light at all times, $Et_2SO$ was produced selectively and reproducibly. Figure 3.2 dramatically illustrates the effect light has on the reaction rate. For a benzene solution exposed to the air at 35° C, initially containing 0.34 mM $Ru(OEP)(Et_2S)_2$, 5.3 mM PhCOOH, and 0.74 M $Et_2S$, sulfoxide production (followed by GC) stops completely whenever the irradiating lamp is turned off, and starts again at the same rate whenever the lamp is turned on again. This phenomenon is only observed in the case of catalytic oxidation, where a large excess of dialkylsulfide is present; the stoichiometric oxidation of $Ru(OEP)(RR'S)_2$ complexes, described in detail in the previous chapter, proceeds equally readily in the presence or absence of light.

Assuming that the fate of the metalloporphyrin during the catalytic oxidation of $Et_2S$ is similar to that observed in the absence of excess thioether (see sections 2.5 and 2.6), a likely candidate for the light-dependent step is the initial one-electron transfer from $Ru(OEP)(Et_2S)_2$ with $O_2$. In the presence of a large excess of sulfide, this step probably cannot proceed at any appreciable rate via the inner sphere mechanism proposed for the stoichiometric oxidation, because of competition for the axial sites of the complex by the sulfide. On the other hand, light could provide the extra energy required to proceed via an outer-sphere process, previously shown to be highly unfavourable (see section 2.5).

To establish which of the Ru(Porp) bands are responsible for the observed photochemistry, two gas uptake experiments were carried out using different cut-off filters (figure 3.3a). Of interest, light above about 480 nm is found to be essential for

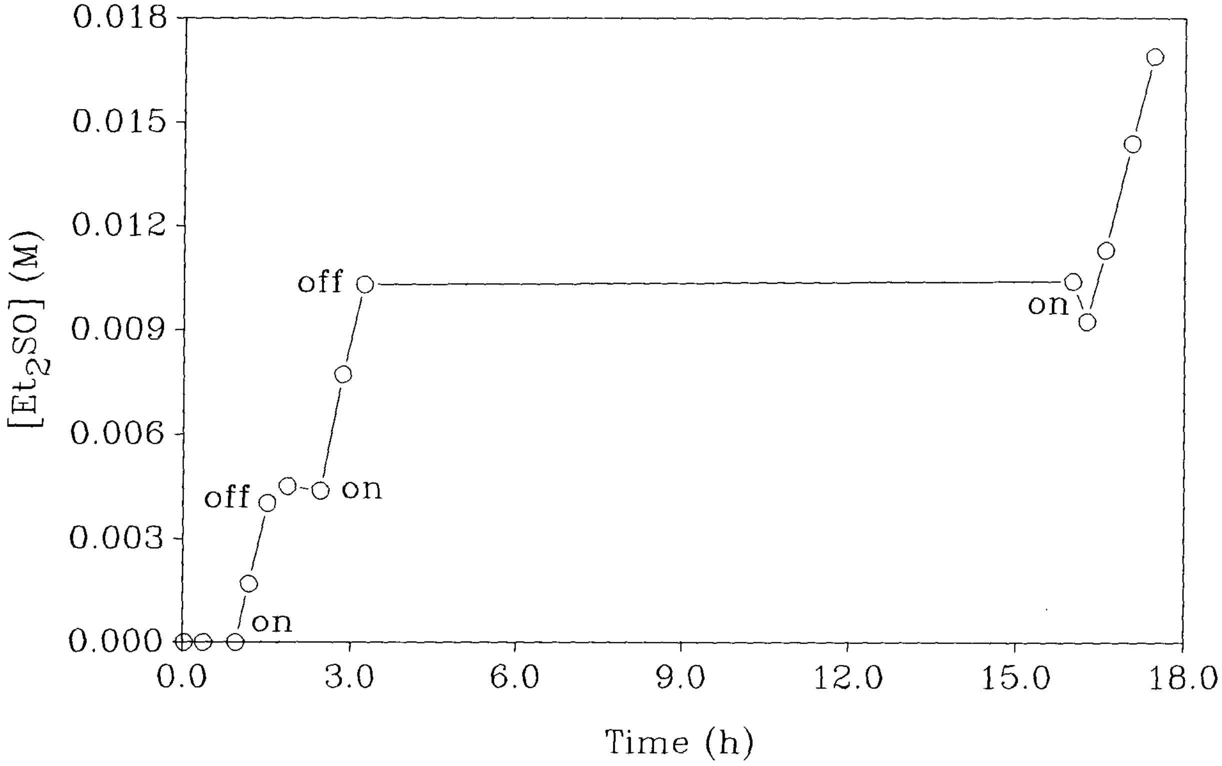

Figure 3.2. Dependence of $Et_2SO$ production rate on reaction vessel illumination. $[Ru(OEP)(Et_2S)_2]$ = 0.34 mM; [PhCOOH] = 5.3 mM; $[Et_2S]$ = 0.74 M; the reaction was carried out in benzene solution at 35° C, in a flask exposed to the air. Reaction progress was followed by gas chromatography.

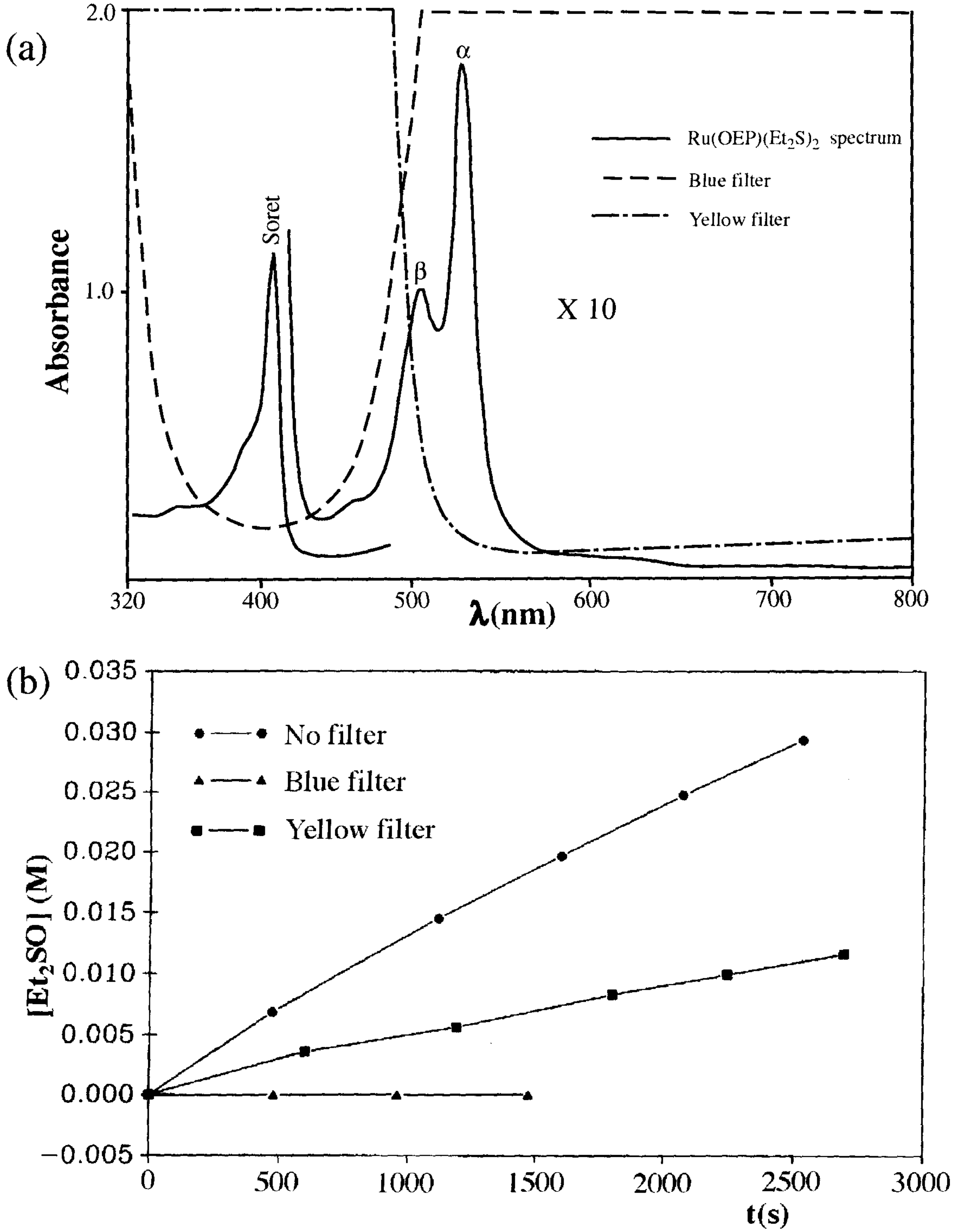

Figure 3.3. (a) Uv/visible spectra of $Ru(OEP)(Et_2S)_2$, and of the yellow and blue filters used to test which wavelengths are necessary for $Et_2S$ oxidation to proceed. (b) Effects of the cutoff filters on the rate of $Et_2SO$ production, as measured by $O_2$-absorption at 35° C; in each case, a benzene solution initially containing 0.84 mM $Ru(OEP)(Et_2S)_2$, 24 mM PhCOOH, and 0.74 M $Et_2S$ was exposed to 0.81 atm of $O_2$ (corrected for benzene vapour pressure).

reaction; when the blue filter absorbing all light above about 480 nm is used, no catalysis at all takes place. Cutting off irradiation of the Soret band (the most intense and energetic in the Ru(OEP) spectrum) with a yellow filter slows (by about 60%), but does not stop, reactivity (figure 3.3b). The slow-down is probably due to the fact that the yellow filter is not completely transparent above 480 nm. Moreover, because of the experimental setup, the light hits the filter at an estimated angle of 30°, so that considerable loss of light intensity due to reflectance is expected.

Figure 3.4 is a qualitative molecular orbital diagram showing the types of transitions which give rise to the uv/vis spectrum of $d^6$ six-coordinate ruthenium porphyrins.[7,8] Both the Soret and the $\alpha$ bands are assigned to $\pi$-$\pi^*$ transitions in the porphyrin ring ($a_{1u},a_{2u} \rightarrow e_g^*$), and are common to all porphyrins and metalloporphyrins; the $\beta$ band is attributed to the addition of one mode of vibrational excitation to the transition which gives rise to the $\alpha$ band.[7] In addition to the $\pi$-$\pi^*$ transitions, many metalloporphyrin spectra,[7] including those of ruthenium porphyrins,[8] have low intensity "extra" bands; in the case of ruthenium porphyrins, these bands are attributed to metal(d)-to-porphyrin($\pi^*$) charge transfer bands (see figure 3.4).[8] Theoretical studies suggest that the $d_{z^2}$ and $d_{x^2-y^2}$ orbitals in Ru(Porp) complexes are too high in energy to play any role in low energy light absorption.[8]

Based on the available electronic transitions (figure 3.4), figure 3.5 illustrates two possible mechanisms for the photochemical effect observed in the catalytic $O_2$-oxidation (the reason for the choice of subscripts for the rate constants will become apparent when the full catalytic cycle is considered, later in this section). In figure 3.5a, the first step ($k_5$) represents a $\pi$-$\pi^*$ transition on the porphyrin ring. The excited electron is more easily

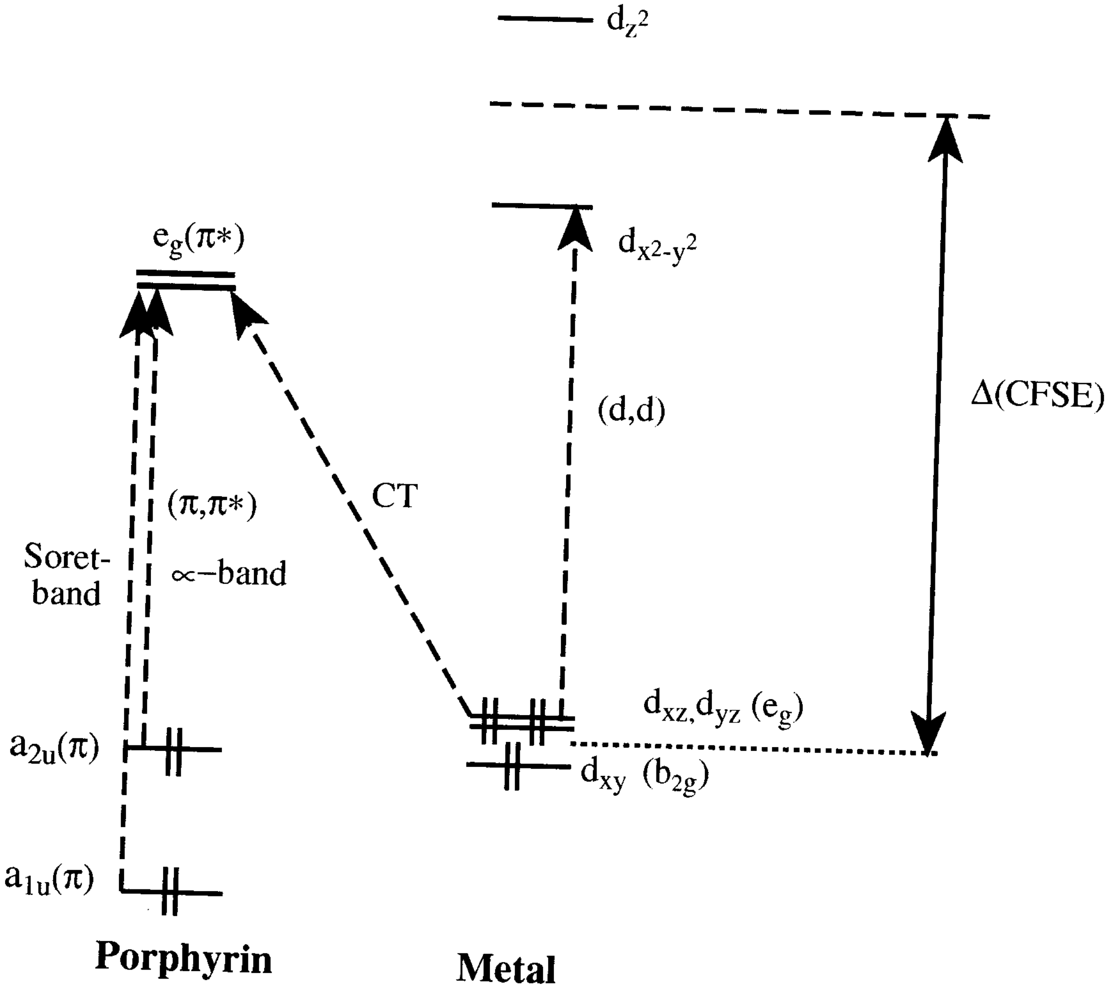
$d_{z^2}$
$d_{x^2-y^2}$
$e_g(\pi^*)$
(d,d)
$\Delta$(CFSE)
CT
$(\pi,\pi^*)$
Soret-band
∝–band
$d_{xz},d_{yz}$ ($e_g$)
$a_{2u}(\pi)$
$d_{xy}$ ($b_{2g}$)
$a_{1u}(\pi)$
Porphyrin
Metal

Figure 3.4. Scheme showing the types of electronic transitions which can occur in $d^6$ six-coordinate ruthenium porphyrins (adapted from reference 8).

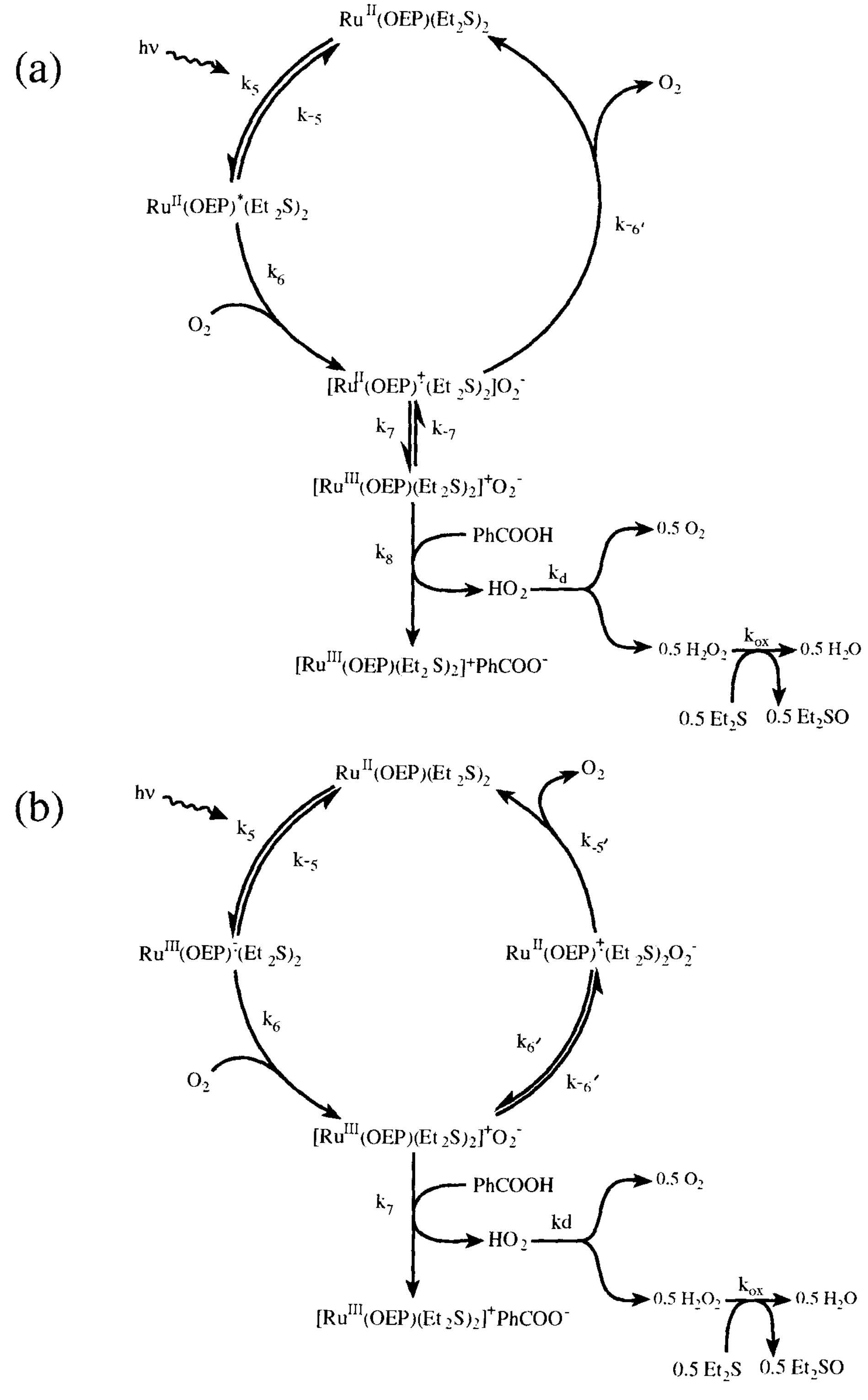
(a)
hν
$Ru^{II}(OEP)(Et_2S)_2$
$k_5$
$k_{-5}$
$O_2$
$Ru^{II}(OEP)^*(Et_2S)_2$
$k_6$
$k_{-6'}$
$O_2$
$[Ru^{II}(OEP)^+(Et_2S)_2]O_2^-$
$k_7$
$k_{-7}$
$[Ru^{III}(OEP)(Et_2S)_2]^+O_2^-$
$k_8$
PhCOOH
$HO_2$
$k_d$
$0.5\ O_2$
$[Ru^{III}(OEP)(Et_2S)_2]^+PhCOO^-$
$0.5\ H_2O_2$
$k_{ox}$
$0.5\ H_2O$
$0.5\ Et_2S$
$0.5\ Et_2SO$
(b)
hν
$Ru^{II}(OEP)(Et_2S)_2$
$O_2$
$k_5$
$k_{-5}$
$k_{-5'}$
$Ru^{III}(OEP)^-(Et_2S)_2$
$Ru^{II}(OEP)^+(Et_2S)_2O_2^-$
$k_6$
$k_{6'}$
$k_{-6'}$
$O_2$
$[Ru^{III}(OEP)(Et_2S)_2]^+O_2^-$
$k_7$
PhCOOH
$HO_2$
kd
$0.5\ O_2$
$[Ru^{III}(OEP)(Et_2S)_2]^+PhCOO^-$
$0.5\ H_2O_2$
$k_{ox}$
$0.5\ H_2O$
$0.5\ Et_2S$
$0.5\ Et_2SO$

Figure 3.5. Two possible mechanisms for the photochemical stage of the $O_2$-oxidation of $Et_2S$ catalyzed by $Ru(OEP)(Et_2S)_2$: a) porphyrin $\pi$-$\pi^*$ transition, followed by transfer of the excited electron to $O_2$; b) direct metal-to-porphyrin charge-transfer, followed by transfer of the excited electron to $O_2$.

abstracted by $O_2$ in the second step ($k_6$), leaving a $\pi$-cation radical. As mentioned in section 2.4, the metal d orbitals lie at higher energy than the porphyrin $\pi$ orbitals under most conditions, and so the cation radical soon rearranges to the more stable $Ru^{III}$ species ($k_7$). Finally, protonation ($k_8$) and subsequent irreversible disproportionation ($k_d$) of the superoxide drive the reaction forward. The reaction $k_{-6'}$ represents a pathway by which $Ru(OEP)(Et_2S)_2{}^+O_2{}^-$ can revert back to $Ru(OEP)(Et_2S)_2$; the prime emphasizes the fact that this is not the reverse of $k_6$. Figure 3.5b illustrates an alternative mechanism, in which the initial light absorption gives rise to a metal-to-porphyrin charge transfer ($k_5$). The resultant zwitterion then reacts with $O_2$ to produce the $Ru(OEP)(Et_2S)_2{}^+O_2$ species directly ($k_6$), which reacts with PhCOOH as before ($k_7$). Apart from the $\alpha,\beta$ bands, the only other band resolved in the visible spectrum of $Ru(OEP)(Et_2S)_2$ (figure 3.3a) is at approximately 450 nm; this band cannot be responsible for the observed photochemistry, because it is completely cut off by the yellow filter, but not by the blue one (figure 3.3a). Nevertheless, there might be a charge-transfer band somewhere in the 480-540 nm region, and this band might be hidden by the more intense $\alpha,\beta$ bands. Metal(d)-to-porphyrin($\pi^*$) charge-transfer is symmetry forbidden, so the bands arising from this process would be weak and easily masked.

If a $\pi$-$\pi^*$ transition is giving rise to the photochemical effect, then on the basis of figure 3.4, it is difficult to rationalize why light absorption in the Soret region does not lead to reaction; nevertheless, this would not be the first instance in which the Soret and the $\alpha,\beta$ bands behave differently, even when the simple molecular orbital picture predicts that they should behave in the same way. For example, it is well established that for many metalloporphyrins,[7] including $Ru^{II}$ porphyrins,[8] the $\alpha,\beta$ bands are hypsochromically shifted (i.e. to shorter wavelength) relative to those of the free-base porphyrins. Based on the simple molecular orbital rationale portrayed in figure 3.4, this phenomenon has been attributed to back-donation of electron density from the metal $e_g$ d-orbitals to the porphyrin $e_g$ $\pi^*$-orbitals, which would raise the energy of the latter. This simple model is quite useful, and has been used to rationalize, for example, the fact that the $\alpha,\beta$ bands shift progressively closer to their free-base positions as axial ligands with stronger $\pi$-accepting properties, such as CO or NO, are used. The explanation put forth is that as the axial ligand accepts more electron density from the metal, less density will be transferred to the porphyrin $\pi^*$ orbitals, and their energy will drop.[7,8] Despite its usefulness, the simple model has one serious flaw: a review of the electronic spectra of several $Ru^{II}(OEP)$ complexes[9] shows that their *Soret* bands are *not* hypsochromically shifted from the free-base position, and there is no obvious correlation between Soret peak position and the $\pi$-acidity of the axial ligands. The simple model predicts that metal-to-porphyrin $\pi$-$\pi^*$ backbonding should cause the Soret to shift hypsochromically by the same amount (in energy units) as the $\alpha,\beta$ bands. The fact that this is not the observed behaviour suggests that there is some kind of interaction between the metal and the porphyrin, which is unique to the excited species generated by irradiating the $\alpha,\beta$ bands. This same unique interaction could be a requirement for the photochemical process. The question of which band is responsible for the observed photochemistry is discussed again in section 3.5.2.2, at which point kinetic evidence is presented which tends to rule out the $\pi$-$\pi^*$ transition mediated mechanism shown in figure 3.5a.

At this point it is worth looking at the predicted thermodynamics of some of the reactions shown in figures 3.5. Recall that in section 2.5 the cell potential for a one-electron transfer from $Ru(OEP)(Et_2S)_2$ to $O_2$ was estimated at about -1 V, which translates to a free energy barrier of about 95 kJ/mol. Assuming for the moment that $Ru(OEP)(Et_2S)_2$ absorbs only at $\lambda = 525$ nm, this will supply the porphyrin complex with 228 kJ/mole. Combining these two relationships allows us to write

$$Ru^{II}(OEP)^{*}(Et_2S)_2 + O_2 \rightleftharpoons Ru^{III}(OEP)(Et_2S)_2{}^{+}O_2^{-} \quad \Delta G^\circ = -133 \text{ kJ/mol} \tag{3.1}$$

Hence light of wavelength around 525 nm provides more than enough energy to allow the overall process of interest to proceed. Moreover, the standard reduction potential for the process $Ru^{II}(OEP)^{+\cdot}(Et_2S)_2/Ru^{II}(OEP)(Et_2S)_2$ is expected to have a value around 0.64 V, which is the standard reduction potential for the $Ru^{II}(OEP)^{+\cdot}(CO)/Ru^{II}(OEP)(CO)$ system (recall section 2.4).[10] At the very most, the ring reduction potential might be as high as that of the free base ($OEPH_2{}^{+\cdot}/OEPH_2$), which was previously recorded as 0.83 V.[10] The latter value (using a value of -0.8 V for the $O_2/O_2^-$ couple, see section 2.5) gives a cell potential of about -1.6 V for the one-electron transfer from the porphyrin ring to $O_2$, which translates to an energy barrier of 154 kJ/mol. Light of 525 nm provides enough energy to overcome even this high barrier:

$$Ru^{II}(OEP)^{*}(Et_2S)_2 + O_2 \rightleftharpoons Ru^{II}(OEP)^{+\cdot}(Et_2S)_2O_2^{-} \quad \Delta G^\circ = -74 \text{ kJ/mol} \tag{3.2}$$

Figure 3.6 summarizes the suggested free energy relationships, which relate directly to the mechanism shown in figure 3.5a. The same general relationships will hold if the

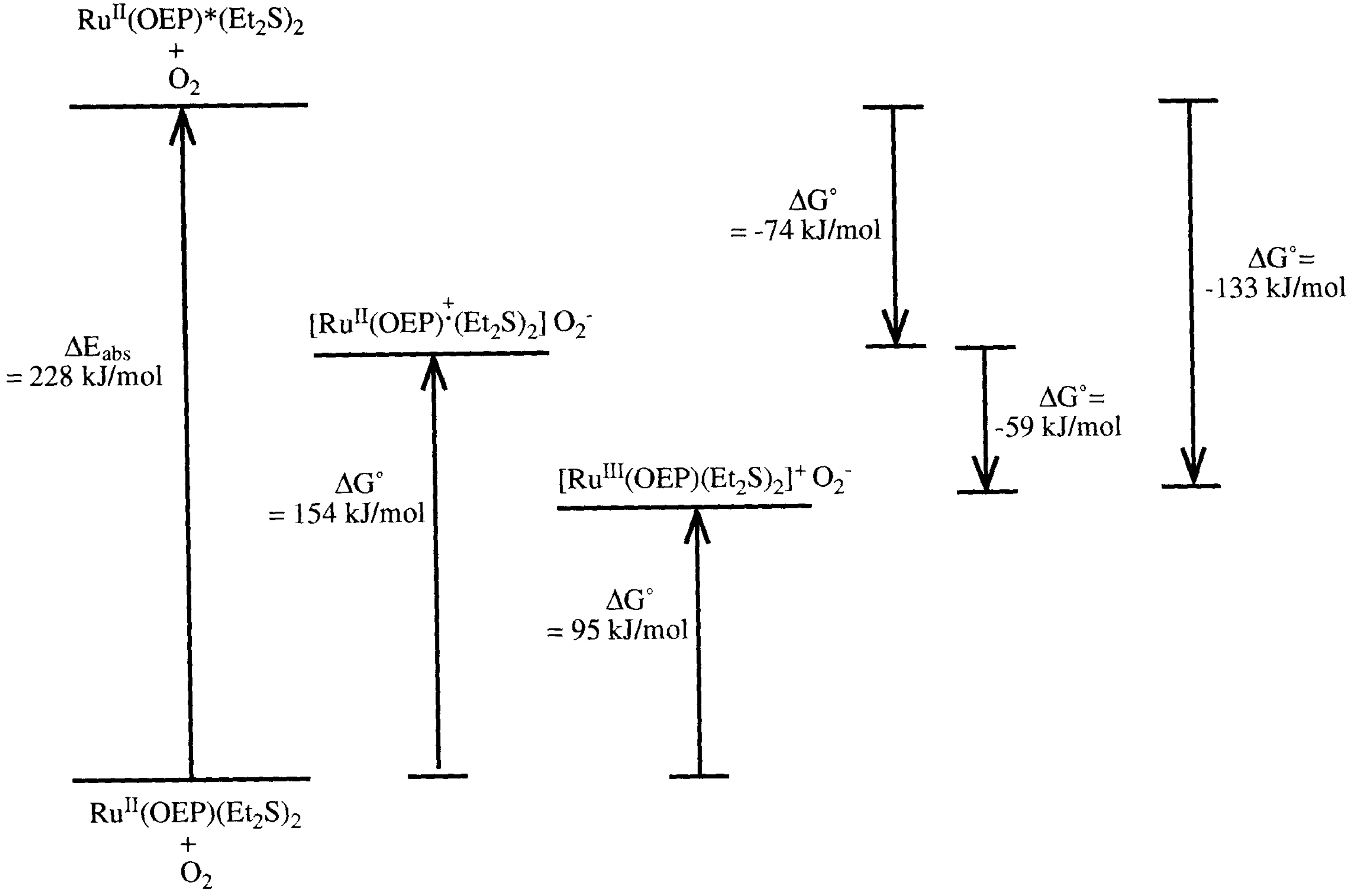
$Ru^{II}(OEP)^{*}(Et_2S)_2$ + $O_2$
$\Delta E_{abs}$ = 228 kJ/mol
$[Ru^{II}(OEP)^{\overset{+}{\cdot}}(Et_2S)_2]\ O_2^{\cdot}$
$\Delta G°$ = 154 kJ/mol
$[Ru^{III}(OEP)(Et_2S)_2]^+\ O_2^{\cdot}$
$\Delta G°$ = 95 kJ/mol
$\Delta G°$ = -74 kJ/mol
$\Delta G°$= -59 kJ/mol
$\Delta G°$= -133 kJ/mol
$Ru^{II}(OEP)(Et_2S)_2$ + $O_2$

Figure 3.6. Relationship between the light energy absorbed by $Ru(OEP)(Et_2S)_2$ at 525 nm, and the relative free energy changes associated with various transformations; see text for details.

photochemical reaction is proceeding via an initial metal-to-ligand charge transfer (figure 3.5b), assuming that the charge transfer absorption band is hidden under the $\alpha,\beta$ bands, somewhere in the region of 525 nm.

Figure 3.7 shows a gas chromatographic trace of a benzene solution initially containing 0.42 mM Ru(OEP)($Et_2S$)$_2$, 6.5 mM benzoic acid, and 0.74 M $Et_2S$, which was exposed to 0.81 atm of oxygen (corrected for benzene vapour pressure) at 35° C for 2.5 h under irradiation. The major oxidation product is $Et_2SO$, with minor amounts of $Et_2SO_2$, $Et_2S_2$, and one other unidentified side product. Initially, the way in which $Et_2SO$ was selectively produced came as a surprise. Earlier studies carried out in our laboratories, which looked at $O_2$-oxidation of decMS catalyzed by Ru(OEP)(decMS)$_2$, revealed sulfur product distributions which were akin to those of dialkylsulfide free-radical autoxidation[11] (for example, didecyldisulfide was a major product); sulfoxide was not obtained as a single product.[12] In the present case, an autoxidation type of reaction would be expected to initially produce EtSH in concentrations comparable to those of $Et_2SO$; the thiol would then further react to produce $Et_2S_2$ (see section 1.3).[11,12] Therefore, the lack of a significant $Et_2S_2$ signal in figure 3.7 also suggests that thiol was never a major product of reaction. In a series of experiments in which total oxygen uptake for a reaction was compared to $Et_2SO$ produced (as determined by gas chromatography) over 1.8-2.5 h periods, the stoichiometry of 2 moles of $Et_2SO$ produced for every mole of $O_2$ consumed, which is implicitly suggested by the type of mechanism being proposed, was confirmed. As an example, when a solution containing 0.420 mM Ru(OEP)($Et_2S$)$_2$, 9.86 mM PhCOOH, and 0.742 M $Et_2S$ was irradiated under 0.812 atm of oxygen (corrected for benzene vapour pressure) at 34.85° C for 1.9 h,

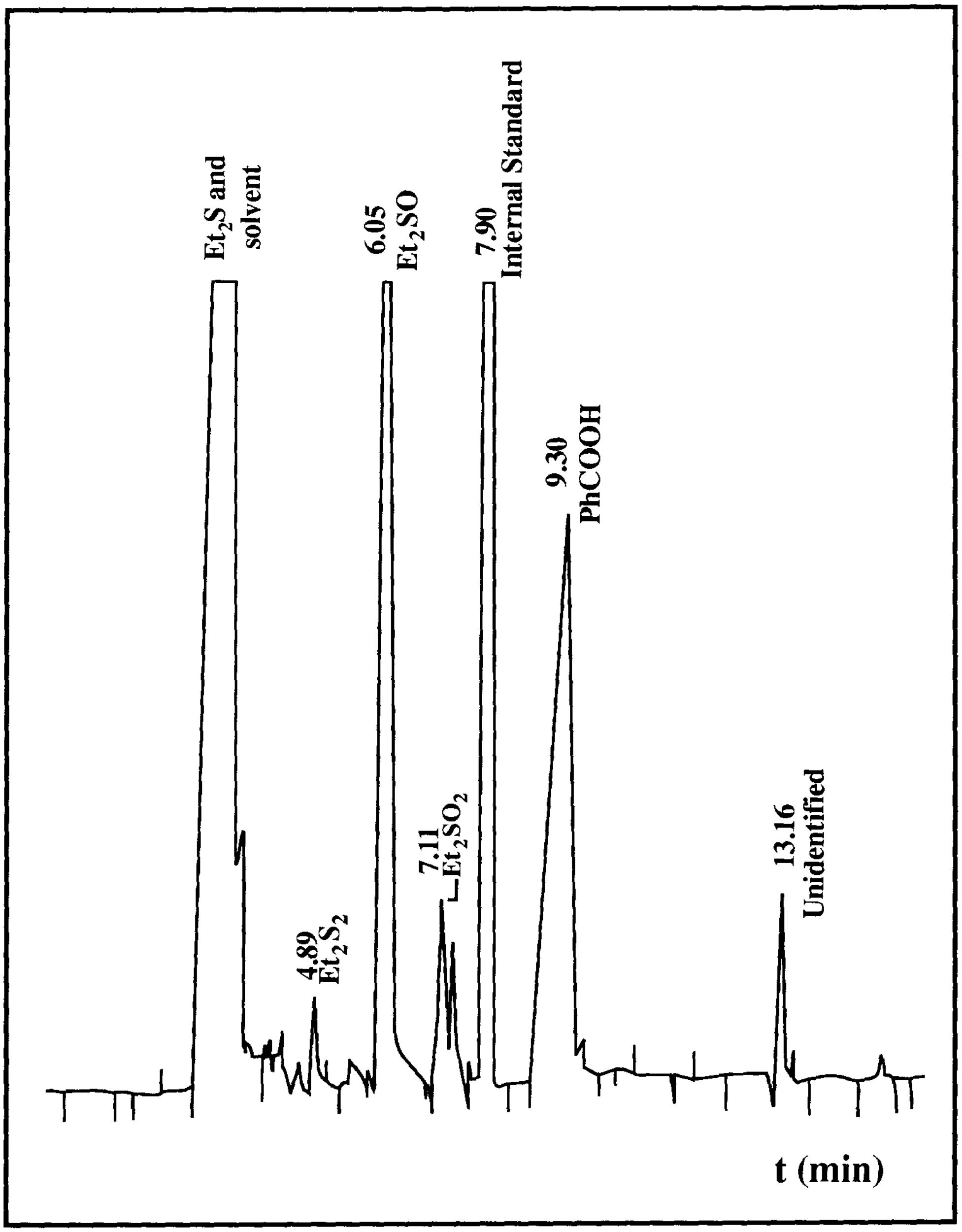

Figure 3.7. Gas chromatographic trace of a benzene solution initially containing 0.42 mM Ru(OEP)(Et$_2$S)$_2$, 6.5 mM benzoic acid, and 0.74 M Et$_2$S, exposed to 0.81 atm of O$_2$ (corrected for benzene vapour pressure) at 35° C for 2.5 h. 4.89 min: Et$_2$S$_2$; 6.05 min: Et$_2$SO; 7.11 min: Et$_2$SO$_2$; 7.90 min: n-undecane; 9.30 min: benzoic acid. The signal at 13.16 min is that of an unidentified product; the rest of the unidentified signals are present at the start of the reaction.

32.9 ± 0.4 mM $Et_2SO$ were produced, and 16.8 ± 0.2 mM of $O_2$ were consumed.

In light of the results discussed in the previous paragraph, the decMS used in the early experiments was carefully re-examined by GC, and found to contain some decanethiol and other impurities; this almost certainly explains the presence of didecyldisulfide as a reaction product in those experiments.

Figure 3.8 provides a scheme for the overall catalytic cycle, which takes into account the conclusions of chapter 2, and the observed light dependence when excess sulfide is present. The reaction path flows counterclockwise, starting at $Ru(OEP)(Et_2S)_2$, which is just left of the top of the circle. The first four steps ($k_5$ to $k_8$) correspond to the photochemical mechanism portrayed in figure 3.5a, and result in the production of one mole of $Et_2SO$, one of $H_2O$, and two moles of $Ru(OEP)(Et_2S)_2{}^+PhCOO^-$ for every two moles of $Ru(OEP)(Et_2S)_2$ oxidized. At this stage, no evidence has been given to favour either mechanism 3.5a or 3.5b; figure 3.8 incorporates mechanism 3.5a because, as will be seen in sections 3.5 and 4.3.2, this mechanism can be tested directly.

The next two steps in the catalytic cycle ($k_9$ and $k_{10}$) represent one of the possible disproportionation processes suggested in the previous chapter (section 2.5). Whichever process (or combination of processes) is actually going on, disproportionation will give rise to one mole of a $Ru^{IV}$ species for every two moles of $Ru(OEP)(Et_2S)_2$ originally oxidized (with regeneration of one mole of $Ru(OEP)(Et_2S)_2$). Note that all of the steps beyond superoxide protonation are portrayed as irreversible; it is assumed that, in the presence of high concentrations of $Et_2S$, all of the $Ru^{III}$ and $Ru^{IV}$ species will be consumed as rapidly as they are produced.

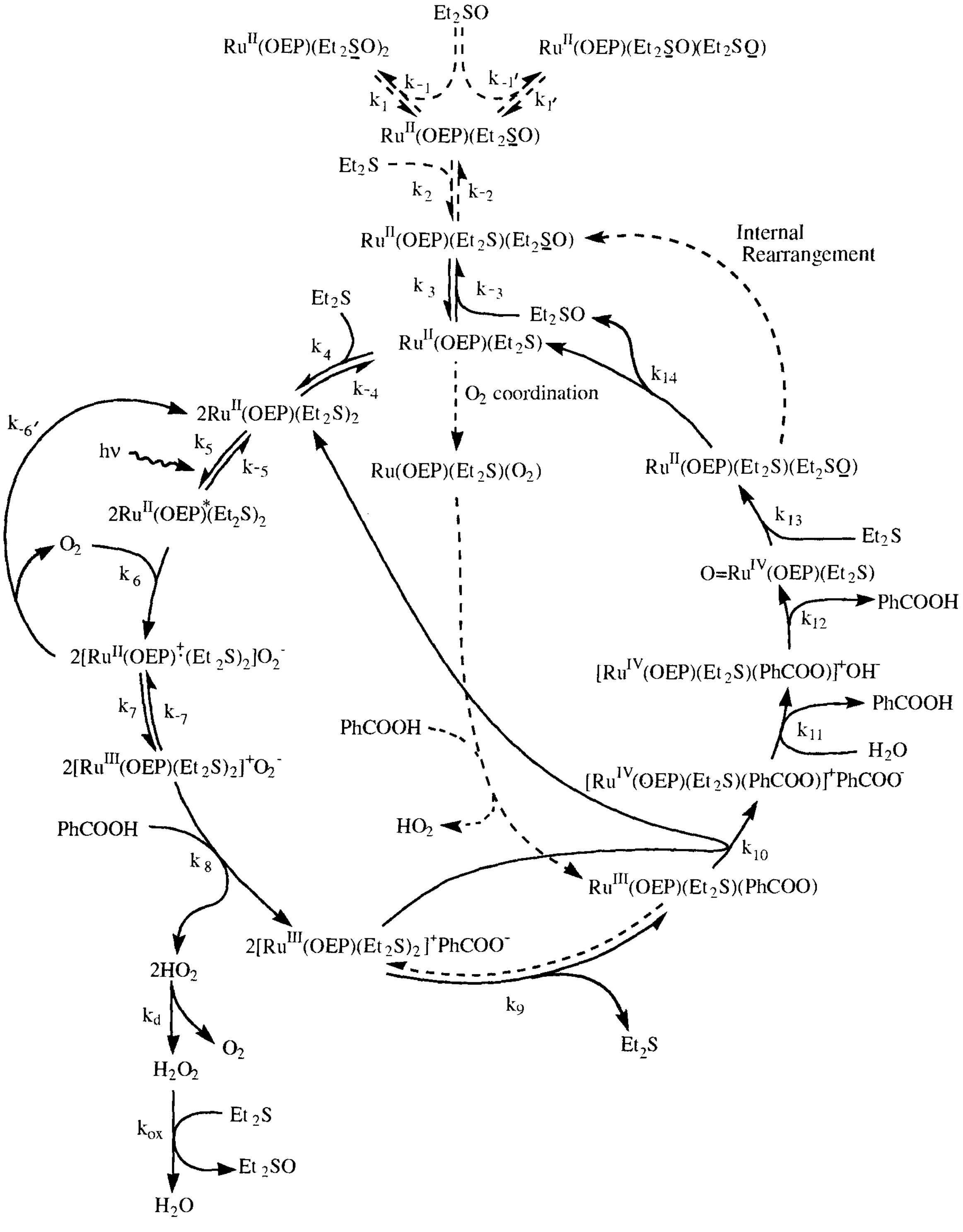
Et2SO
RuII(OEP)(Et2SO)2
RuII(OEP)(Et2SO)(Et2SO)
k-1
k1
k-1'
k1'
RuII(OEP)(Et2SO)
Et2S
k2
k-2
RuII(OEP)(Et2S)(Et2SO)
Internal Rearrangement
Et2S
k3
k-3
Et2SO
RuII(OEP)(Et2S)
k4
k-4
k14
O2 coordination
k-6'
2RuII(OEP)(Et2S)2
hν
k5
k-5
Ru(OEP)(Et2S)(O2)
RuII(OEP)(Et2S)(Et2SO)
2RuII(OEP)*(Et2S)2
k13
Et2S
O2
k6
O=RuIV(OEP)(Et2S)
PhCOOH
k12
2[RuII(OEP)+·(Et2S)2]O2-
[RuIV(OEP)(Et2S)(PhCOO)]+OH-
k7
k-7
PhCOOH
k11
H2O
PhCOOH
2[RuIII(OEP)(Et2S)2]+O2-
[RuIV(OEP)(Et2S)(PhCOO)]+PhCOO-
PhCOOH
HO2
k8
k10
RuIII(OEP)(Et2S)(PhCOO)
2[RuIII(OEP)(Et2S)2]+PhCOO-
2HO2
k9
kd
O2
Et2S
H2O2
kox
Et2S
Et2SO
H2O

Figure 3.8. Scheme proposed for the $O_2$-oxidation of $Et_2S$ to $Et_2SO$, catalyzed by $Ru(OEP)(Et_2S)_2$ and PhCOOH (dotted pathways imply that these processes can be neglected, or do not occur, under catalytic conditions).

Reaction of the $Ru^{IV}$ species with water and free $Et_2S$ produces $Ru(OEP)(Et_2S)(Et_2S\underline{O})$ ($k_{11}$ to $k_{13}$), which can either isomerize to give $Ru(OEP)(Et_2S)(Et_2\underline{S}O)$, or react with $Et_2S$ to regenerate $Ru(OEP)(Et_2S)_2$. In the latter case, another mole of free sulfoxide is liberated, to give a total of two moles of free $Et_2SO$ produced for every turn of the catalytic cycle. In either case, the two moles of PhCOOH used to "trap" the high valent Ru species are regenerated at the end of the cycle, and the net result of the process is to produce 2 moles of $Et_2SO$ for every mole of $O_2$ consumed. The production of two of the possible isomers of $Ru(OEP)(Et_2SO)_2$ (at the top of the scheme), and direct $O_2$ coordination to $Ru^{II}$ (vertical pathway), are both portrayed using dashed arrows. This emphasizes that although both processes are known to occur when the concentration of free $Et_2S$ is low, they are probably not important under catalytic conditions. The equilibria between $Ru(OEP)(Et_2S)_2$, $Ru(OEP)(Et_2S)(Et_2\underline{S}O)$ and $Ru(OEP)(Et_2SO)_2$, and the possibility of internal rearrangement of $Ru(OEP)(Et_2S)(Et_2S\underline{O})$ to the S-bound isomer, also portrayed with a dashed arrow in the figure, will be further discussed in the next two sections.

In the scheme portrayed in figure 3.8, any possible reaction of $Ru(OEP)(Et_2S)(Et_2\underline{S}O)$ (or indeed $Ru(OEP)(Et_2SO)_2$) with dioxygen is neglected; these complexes are outside of the catalytic cycle. This means that, according to the model, as $Et_2SO$ is produced, it should have an inhibitory effect on the reaction rate, depending on the equilibria governing formation of the sulfoxide-containing complexes. Figure 3.9 shows a plot of $[Et_2SO]$ vs. time, obtained from an oxygen uptake experiment, and the reaction rate is indeed found to decrease with time (this decrease is not accounted for by the drop in $[Et_2S]$ with time, which is less than 5% over the whole measured interval).

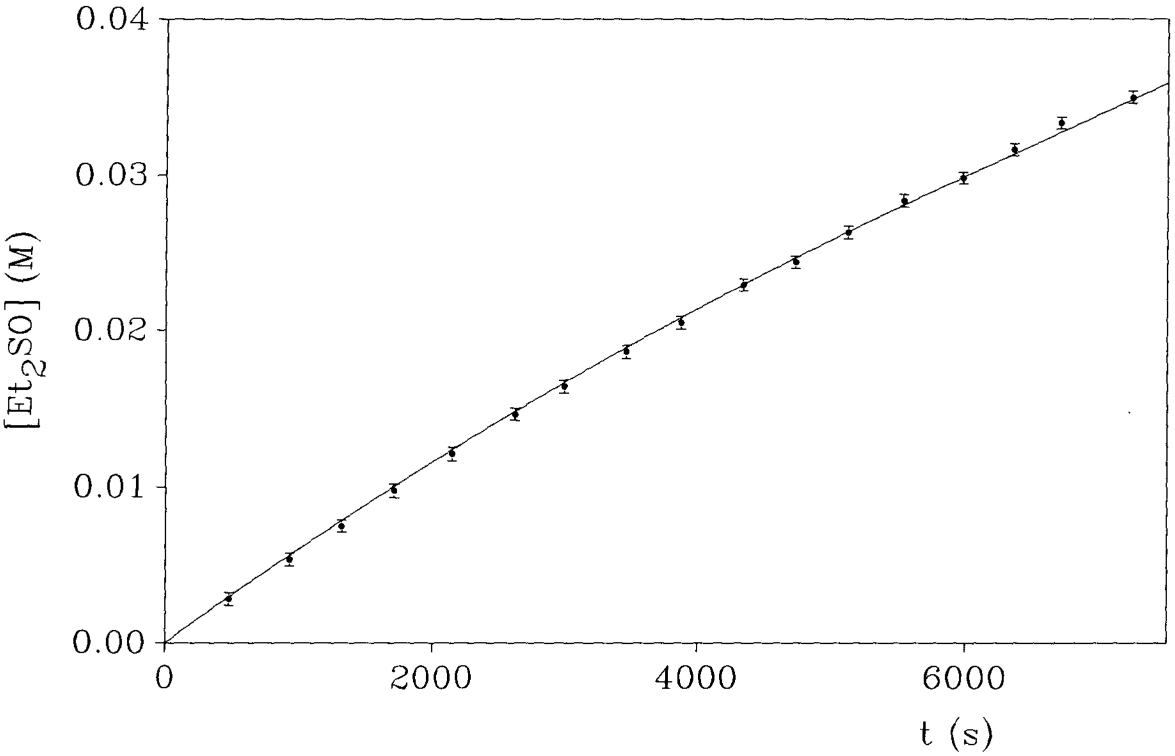

Figure 3.9. A typical plot showing the accumulation of $Et_2SO$ with time, determined by monitoring the $O_2$-uptake (see section 3.5 for full details). For this experiment at 35° C, the initial concentrations of the reagents are: $[Ru(OEP)(Et_2S)_2]$ = 0.202 mM; [PhCOOH] = 24.4 mM; $[Et_2S]$ = 0.742 M; $pO_2$ = 0.813 atm (corrected for benzene vapour pressure).

Section 3.5 describes how the data in figure 3.9, and about 50 other sets of similar data, can be fitted to a rate law derived from the mechanism shown in figure 3.8. As will be seen, the derived rate law fits the experimental data remarkably well; however, the same reasoning used earlier to show that electron transfer from $Ru(OEP)(Et_2S)_2$ to $O_2$ is energetically quite feasible in solutions irradiated by visible light, shows that the less favourable electron transfer from $Ru(OEP)(Et_2S)(Et_2\underline{S}O)$ to $O_2$ is also possible under these conditions. Figure 3.10 summarizes the relevant energy relationships; a full discussion on the possible role of electron transfer from $Ru(OEP)(Et_2S)(Et_2\underline{S}O)$ directly to oxygen is deferred to section 3.5.2.2.

A second omission in figure 3.8 is any mention of catalyst degradation (this is a common weakness of nearly all postulated catalytic cycles). In chapter 2 it was pointed out that the stoichiometric reaction of $O_2$ with $Ru(OEP)(RR'S)_2$ complexes in acidic benzene solutions was not as clean as in methylene chloride, and that small amounts of unidentified Ru(OEP) side products were produced along with $Ru(OEP)(RR'S)(RR'\underline{S}O)$ and $Ru(OEP)(RR'SO)_2$. One might expect such side reactions to occur also to some extent in the catalytic system and, indeed, monitoring the reaction mixtures for extended periods (20 h) by uv/vis, clearly showed that catalyst degradation occurred, but at a slow rate compared to the catalytic rate. Of interest, this catalyst degradation is not acid dependent, and proceeds at about the same rate with or without added acid, provided that the reaction solution is illuminated (see below). The uv/vis spectrum of a reaction mixture, initially containing 0.202 mM $Ru(OEP)(Et_2S)_2$ and 0.742 M $Et_2S$ (but no benzoic acid), after a 24 h exposure to $O_2$ and light at 34.85° C, is shown in figure 3.11; this spectrum is similar to those seen in earlier studies of corresponding

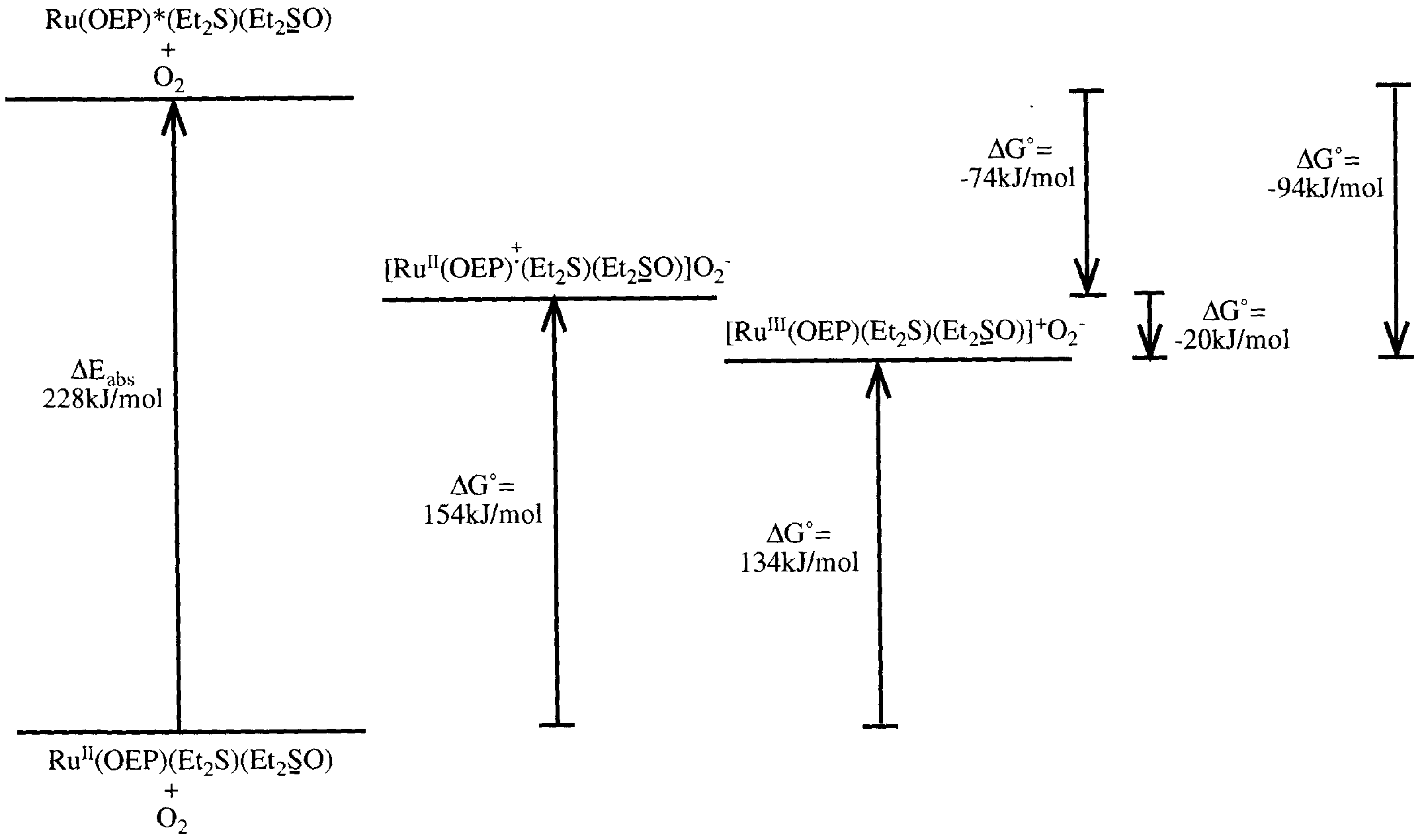
Ru(OEP)*(Et2S)(Et2SO)
+
O2
ΔEabs
228kJ/mol
RuII(OEP)(Et2S)(Et2SO)
+
O2
[RuII(OEP)+·(Et2S)(Et2SO)]O2-
ΔG°=
154kJ/mol
[RuIII(OEP)(Et2S)(Et2SO)]+O2-
ΔG°=
134kJ/mol
ΔG°=
-74kJ/mol
ΔG°=
-20kJ/mol
ΔG°=
-94kJ/mol

Figure 3.10. Relationship between the light energy absorbed by Ru(OEP)($Et_2S$)($Et_2\underline{S}O$) at 525 nm, and the free energy changes associated with various transformations. ΔG° for the oxidation at the metal of $Ru^{II}$(OEP)($Et_2S$)($Et_2\underline{S}O$) was estimated from the CV data for the analogous Ru(OEP)(decMS)(decM$\underline{S}$O) system (see section 2.5 and figure 2.13); for the one-electron ring oxidation, ΔG° is assumed to be the same as in the Ru(OEP)($Et_2S$)$_2$ system (see figure 3.6).

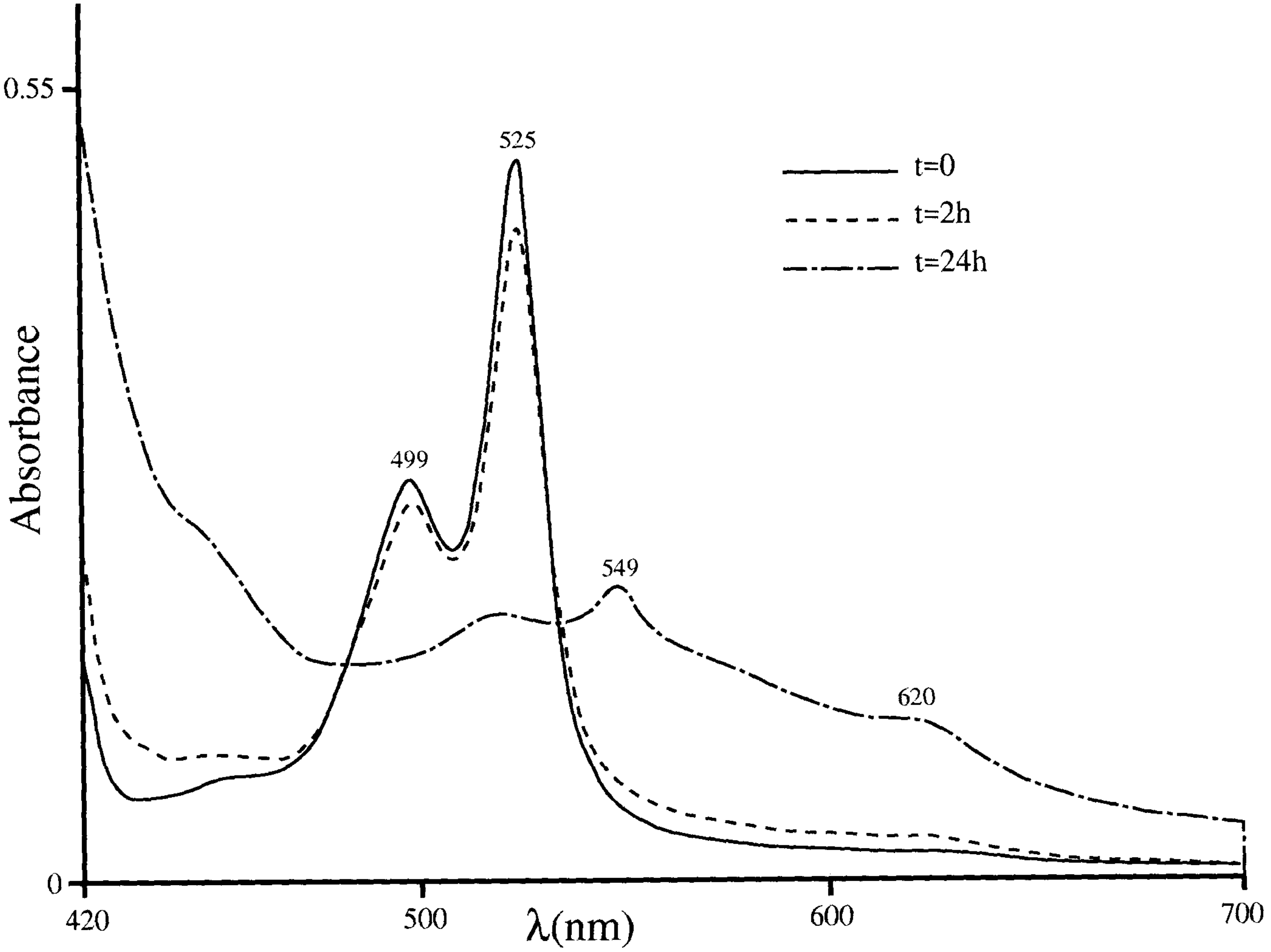

Figure 3.11 Uv/vis spectra of a benzene solution initially containing 0.202 mM $Ru(OEP)(Et_2S)_2$, 0.742 M $Et_2S$, and no benzoic acid, at various times after exposure to a light source, and 0.813 atm of $O_2$ (corrected for benzene vapour pressure). The same results were obtained in the presence of up to 48 mM of PhCOOH.

$Ru(OEP)(decMS)_2/decMS$ systems.[12] The spectrum shows broad bands extending to 700 nm, and no major band at 525 nm, which suggests that very little or none of $Ru(OEP)(Et_2S)_2$, $Ru(OEP)(Et_2S)(Et_2\underline{S}O)$ or $Ru(OEP)(Et_2SO)_2$ remain in solution (the visible spectra of the three $Ru^{II}$ species are illustrated later in figure 3.21, p.144). The relatively sharp band at 549 nm is notable, since this is the position (551 ± 4 nm) at which all known Ru(OEP)(CO)L (L = a neutral ligand) have their $\alpha$ bands;[9a] recall from section 2.6 that there is evidence of a Ru(OEP)(CO)L complex being a minor product in the stoichiometric oxidation of $Ru(OEP)(RR'S)_2$ in benzene and toluene solutions. Since none of $Ru(OEP)(Et_2S)_2$, $Ru(OEP)(Et_2S)(Et_2\underline{S}O)$ or $Ru(OEP)(Et_2SO)_2$ absorb significantly above 600 nm, the absorbance in this region by a reaction mixture at any given time can be used as a crude estimate of catalyst degradation, with the absorbance after 24 h representing maximum degradation. Such an analysis was carried out on the spectrum in figure 3.11, and on several catalytic reaction mixtures containing benzoic acid, and catalyst degradation was estimated to be 7-12% over a 2.5 h period. Note that the error incurred in neglecting catalyst degradation (i.e. ignoring the decrease in reaction that catalyst degradation will produce) will tend to compensate for any error incurred by assuming non-reactivity of $Ru(OEP)(Et_2S)(Et_2\underline{S}O)$ toward $O_2$; this will be discussed further in section 3.5.2.2.

As mentioned, all of the assumptions inherent in figure 3.8 will be discussed again in section 3.5, after a rate law for the reaction has been derived. The next section deals with a quantitative study of the equilibria between $Ru(OEP)(Et_2S)_2$, $Ru(OEP)(Et_2S)(Et_2\underline{S}O)$ and $Ru(OEP)(Et_2SO)_2$, which were studied independently from the rest of the catalytic cycle using stopped-flow experiments.

## 3.4 Stopped-Flow Analysis of $Et_2SO$ Substitution by $Et_2S$ in $Ru(OEP)(Et_2SO)_2$ in Benzene Solution

### 3.4.1 Data Treatment and Results

The equilibria between $Ru(OEP)(Et_2S)_2$, $Ru(OEP)(Et_2S)(Et_2\underline{S}O)$, and $Ru(OEP)(Et_2SO)_2$ were studied in isolation from the rest of the cycle outlined in figure 3.8, using stopped-flow techniques. The details of deriving the rate laws will be discussed fully in chapter 4,[†] but the likely probability that in solution $Ru(OEP)(Et_2SO)_2$ exists as an equilibrium mixture of $Ru(OEP)(Et_2\underline{S}O)_2$ and $Ru(OEP)(Et_2\underline{S}O)(Et_2S\underline{O})$ (see section 2.3) is accounted for in the derivation. In practice, the system was studied by starting with a solution of $Ru(OEP)(Et_2SO)_2$ and excess $Et_2SO$, and adding an excess of $Et_2S$ to it, which is the reverse of the processes which take place during catalysis; for clarity, figure 3.12 shows the substitution steps in isolation. It turns out that substitution of the first sulfoxide in $Ru(OEP)(Et_2SO)_2$ takes place on the 100 ms timescale, which is about 1000 times faster than that of the second. Thus the first equilibrium between $Ru(OEP)(Et_2SO)_2$ and $Ru(OEP)(Et_2S)(Et_2\underline{S}O)$ is established before the second reaction has begun, which simplifies the rate laws considerably, since the two steps can be studied independently.

In addition to occurring on very different timescales, the two substitution equilibria occur in sufficiently different $Et_2S/Et_2SO$ concentration regimes to allow some useful observations to be made by time-independent uv/vis spectroscopy. Thus figure 3.13a shows successive uv/vis spectra obtained for a solution, initially containing $3.4 \times 10^{-6}$ M $Ru(OEP)(Et_2SO)_2$ and 0.19 M $Et_2SO$, as it was titrated with neat $Et_2S$. The band which

---

[†] It is possible to understand sections 3.4 and 3.5 in a qualitative way without going through the theory given in chapter 4; however, many readers will find it helpful to read chapter 4 concurrently with the next two sections of this chapter.

## First Substitution Equilibrium

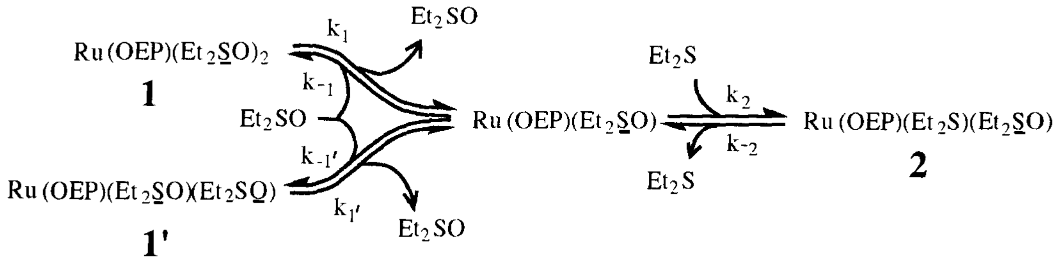
Ru(OEP)(Et$_2$S̲O)$_2$
1
Ru(OEP)(Et$_2$S̲O)(Et$_2$SO̲)
1'
k$_1$
k$_{-1}$
k$_{-1'}$
k$_{1'}$
Et$_2$SO
Et$_2$SO
Et$_2$SO
Ru(OEP)(Et$_2$S̲O)
Et$_2$S
k$_2$
k$_{-2}$
Et$_2$S
Ru(OEP)(Et$_2$S)(Et$_2$S̲O)
2

## Second Substitution Equilibrium

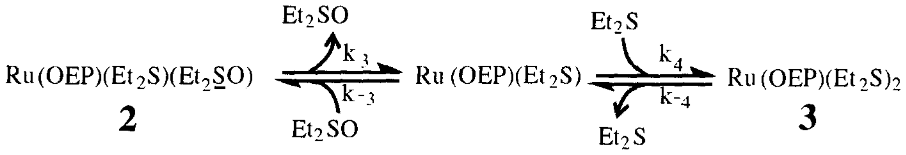
Ru(OEP)(Et$_2$S)(Et$_2$S̲O)
2
Et$_2$SO
k$_3$
k$_{-3}$
Et$_2$SO
Ru(OEP)(Et$_2$S)
Et$_2$S
k$_4$
k$_{-4}$
Et$_2$S
Ru(OEP)(Et$_2$S)$_2$
3

Figure 3.12. Scheme showing the proposed mechanisms for the sequential substitution of two $Et_2SO$ ligands by $Et_2S$ in $Ru(OEP)(Et_2SO)_2$. In solution, the bis-sulfoxide species is believed to exist as a mixture of the S- and O-bound linkage isomers (see section 2.3).

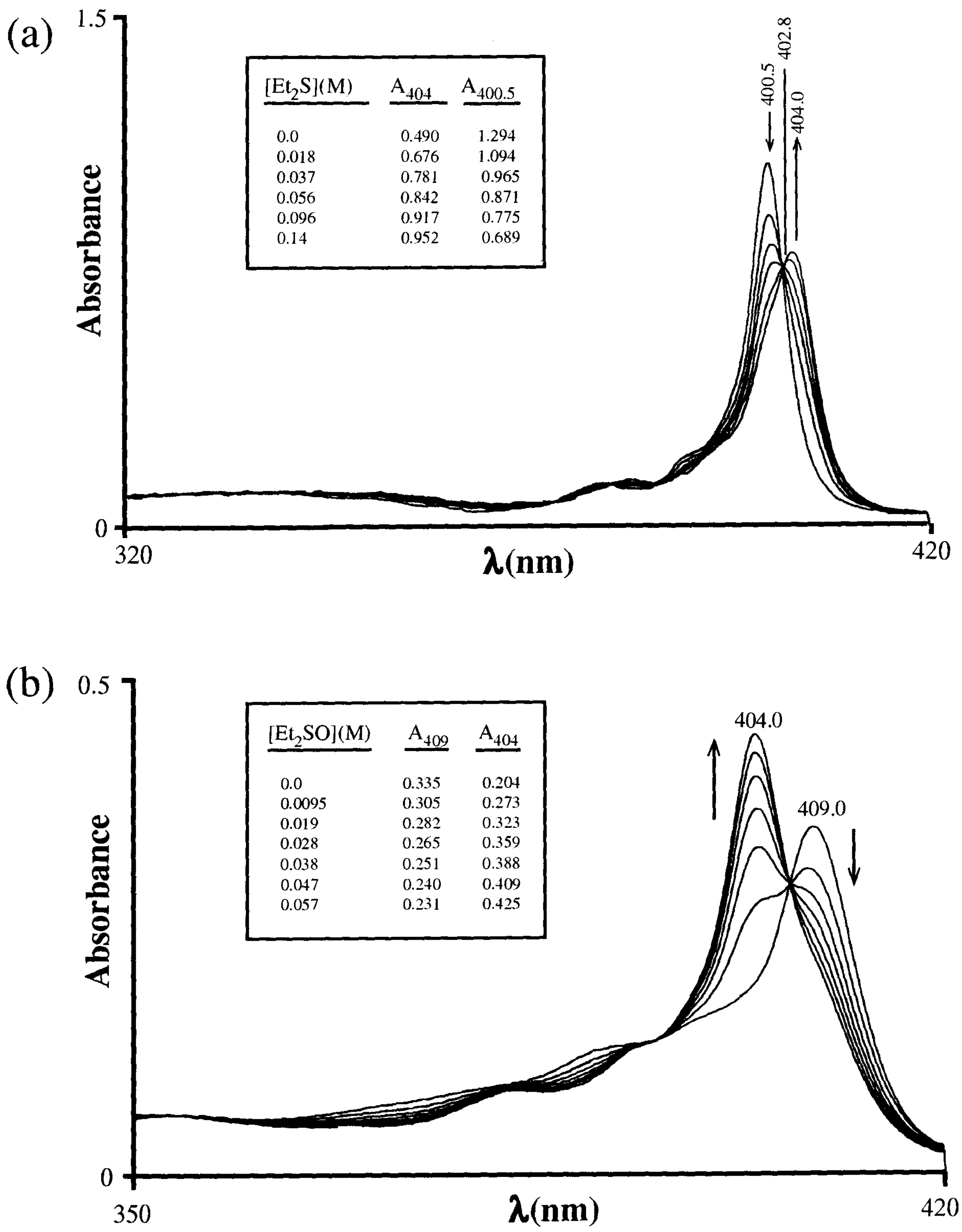

| $[Et_2S](M)$ | $A_{404}$ | $A_{400.5}$ |
|---|---|---|
| 0.0 | 0.490 | 1.294 |
| 0.018 | 0.676 | 1.094 |
| 0.037 | 0.781 | 0.965 |
| 0.056 | 0.842 | 0.871 |
| 0.096 | 0.917 | 0.775 |
| 0.14 | 0.952 | 0.689 |

| $[Et_2SO](M)$ | $A_{409}$ | $A_{404}$ |
|---|---|---|
| 0.0 | 0.335 | 0.204 |
| 0.0095 | 0.305 | 0.273 |
| 0.019 | 0.282 | 0.323 |
| 0.028 | 0.265 | 0.359 |
| 0.038 | 0.251 | 0.388 |
| 0.047 | 0.240 | 0.409 |
| 0.057 | 0.231 | 0.425 |

Figure 3.13. Uv/vis spectral changes observed as: (a) a benzene solution initially containing $3.4 \times 10^{-6}$ M $Ru(OEP)(Et_2SO)_2$ and 0.19 M free $Et_2SO$ is titrated with neat $Et_2S$; (b) a benzene solution initially containing $1.7 \times 10^{-5}$ M $Ru(OEP)(Et_2S)_2$ and 0.74 M free $Et_2S$ is titrated with neat $Et_2SO$. T = 35° C for both experiments.

grows in at 404.0 nm is attributed to $\mathrm{Ru(OEP)(Et_2S)(Et_2\underline{S}O)}$. Similarly, figure 3.13b shows successive uv/vis spectra obtained for a solution, initially containing $1.7\times10^{-5}$ M $\mathrm{Ru(OEP)(Et_2S)_2}$ and 0.74 M $\mathrm{Et_2S}$, as it was titrated with neat $\mathrm{Et_2SO}$; again, the band appearing at 404 nm is attributed to $\mathrm{Ru(OEP)(Et_2S)(Et_2\underline{S}O)}$. The spectra in figures 3.13a and 3.13b both show at least three isosbestic points; isosbestics can result from a) a simple equilibrium between two absorbing species, or b) formation of a third absorbing species from a fixed ratio of two other species. The latter case applies to the first equilibrium in figure 3.12, where $\mathrm{Ru(OEP)(Et_2S)(Et_2\underline{S}O)}$ is formed from a fixed ratio of $\mathrm{Ru(OEP)(Et_2\underline{S}O)_2}$ and $\mathrm{Ru(OEP)(Et_2\underline{S}O)(Et_2S\underline{O})}$, during the titration with $\mathrm{Et_2S}$ (in both substitution equilibria, the 5-coordinate intermediates are assumed to be present in negligible amounts). The equilibrium between $\mathrm{Ru(OEP)(Et_2\underline{S}O)_2}$ and $\mathrm{Ru(OEP)(Et_2\underline{S}O)(Et_2S\underline{O})}$ is independent of either $\mathrm{Et_2SO}$ or $\mathrm{Et_2S}$ concentrations:

$$K' = [\mathbf{1'}]/[\mathbf{1}] \qquad 3.3$$

where $\mathbf{1} \equiv \mathrm{Ru(OEP)(Et_2\underline{S}O)_2}$; $\mathbf{1'} \equiv \mathrm{Ru(OEP)(Et_2\underline{S}O)(Et_2S\underline{O})}$; and

$$K' \equiv k_1k_{-1'}/k_{1'}k_{-1} \qquad 3.4$$

The equilibrium ratio of $\mathrm{Ru(OEP)(Et_2\underline{S}O)_2}$ to $\mathrm{Ru(OEP)(Et_2\underline{S}O)(Et_2S\underline{O})}$ remains constant regardless of the free $[\mathrm{Et_2SO}]$ (or $[\mathrm{Et_2S}]$) ligand concentrations, and thus the Beer-Lambert expression for a solution containing $\mathrm{Ru(OEP)(Et_2\underline{S}O)_2}$, $\mathrm{Ru(OEP)(Et_2\underline{S}O)(Et_2S\underline{O})}$ and $\mathrm{Ru(OEP)(Et_2S)(Et_2\underline{S}O)}$, can be written as

$$A = (\epsilon_1 + \epsilon_{1'}K')\ell[1] + \epsilon_2\ell[2] \qquad 3.5$$

where

$$\mathbf{2} \equiv Ru(OEP)(Et_2S)(Et_2\underline{S}O)$$

and A is the experimentally observed absorbance, $\epsilon_1$, $\epsilon_{1'}$ and $\epsilon_2$ are the extinction coefficients for $Ru(OEP)(Et_2\underline{S}O)_2$, $Ru(OEP)(Et_2\underline{S}O)(Et_2S\underline{O})$ and $Ru(OEP)(Et_2S)(Et_2\underline{S}O)$, respectively, and $\ell$ is the absorbance path length. An isosbestic point will occur wherever $(\epsilon_1 + \epsilon_{1'}K')$ is equal to $\epsilon_2$.

When the approach to the first equilibrium is followed by stopped-flow analysis at the isosbestic wavelength $\lambda = 402.8$ nm, no change is detected in the absorbance at any time, showing that the equilibrium between $Ru(OEP)(Et_2\underline{S}O)_2$ and $Ru(OEP)(Et_2\underline{S}O)(Et_2S\underline{O})$ is not even transiently disturbed. The importance of this observation will become apparent below, and in section 4.2.

In the stopped-flow experiments discussed in the remainder of this section, the two substitution equilibria were monitored at different wavelengths. The first was followed at $\lambda = 400.5$ nm, which is the absorption maximum for $Ru(OEP)(Et_2SO)_2$ solutions at 35° C (see figure 3.13a). During the second substitution, the equilibrium between the mono- and bis-sulfoxide species must be considered and, as will be seen in section 4.2, it is simpler to follow the second substitution reaction at an isosbestic wavelength for a mixture of $Ru(OEP)(Et_2SO)_2$ and $Ru(OEP)(Et_2S)(Et_2\underline{S}O)$ species. The isosbestic wavelength chosen was $\lambda = 402.8$ nm (see figure 3.13a).

Now, with the assumption that the changes in free [$Et_2S$] and [$Et_2SO$] are negligible over the whole reaction, and given that the equilibrium ratio between Ru(OEP)($Et_2\underline{S}O$)$_2$ and Ru(OEP)($Et_2\underline{S}O$)($Et_2S\underline{O}$) is not disturbed at any time, the absorbance changes as a function of time for $\lambda$ = 400.5nm over the first 100 ms, and for $\lambda$ = 402.8nm over 100 s, will both be described by a simple exponential decay equation (see section 4.2):

$$A = \alpha + \beta \, e^{-(\gamma t)} \qquad 3.6$$

where

$$A \equiv \text{The absorbance at time t} \qquad 3.7$$

$$\alpha = A_o - \beta \qquad 3.8$$

($A_o \equiv$ The absorbance at $t = 0$)

The parameter $\beta$ represents the total absorbance change observed for a given reaction, while $\gamma$ is the observed rate constant. All three parameters are themselves functions of the concentrations of the various reagents in solution; of course, the form of these functions is different for the first and second substitution reactions. Before discussing the functions, one other term should be defined, namely

$$v_o \equiv (dA/dt)_{t=0} = -\gamma\beta \tag{3.9}$$

where $v_o$ is the rate of change of the absorbance at the start of the reaction. For both the substitution steps, $\beta$ and $v_o$ are the two most informative parameters. For the first substitution reaction, $\beta$ and $v_o$ are given by (see section 4.2)

$$\beta_1 = -[Ru]_o\Delta\epsilon_1'[Et_2S]/(K_{1App}^{-1}[Et_2SO] + [Et_2S]) \tag{3.10}$$

$$v_{o1} = k_{1App}[Ru]_o\Delta\epsilon_1'[Et_2S]/(K_{m1}[Et_2SO] + [Et_2S]) \tag{3.11}$$

where

$$[Ru]_o \equiv [1] + [1'] + [2] \tag{3.12}$$

$$\Delta\epsilon_1' \equiv (\epsilon_2 - (\epsilon_1 + \epsilon_{1'}K')/(1 + K'))l \quad \text{at } \lambda = 400.5 \text{ nm} \tag{3.13}$$

$$K_{1App} \equiv K_1/(1 + K') \tag{3.14}$$

$$k_{1App} \equiv k_1/(1 + K') + k_{1'}/(1 + (K')^{-1}) \tag{3.15}$$

$$K_{m1} \equiv (k_{-1} + k_{-1'})/k_2 \tag{3.16}$$

$$K_1 \equiv k_1k_2/k_{-1}k_{-2} \tag{3.17}$$

K′ was previously defined (equation 3.4), as were the three extinction coefficients $\epsilon_1$, $\epsilon_{1'}$ and $\epsilon_2$, and the path length $l$ of the absorbing species.

Equations 3.10 and 3.11 (for variation of $\beta_1$ and $v_{o1}$ with $[Et_2S]$ at a fixed $[Et_2SO]$) are the typical rectangular hyperbolas with zero intercept so commonly seen in kinetic analyses,[13] and can be rearranged into linear form:

$$[Et_2S]/\beta_1 = c_1 + c_2[Et_2S] \tag{3.18}$$

$$[Et_2S]/v_{o1} = c_3 + c_4[Et_2S] \tag{3.19}$$

where

$$c_1 \equiv [Et_2SO]c_2/K_{1App} \tag{3.20}$$

$$c_2 \equiv -1/[Ru]_o\Delta\epsilon_1' \tag{3.21}$$

$$c_3 \equiv [Et_2SO]c_4K_{m1} \tag{3.22}$$

$$c_4 \equiv -c_2/k_{1App} \tag{3.23}$$

Two sets of experiments were carried out, one with $[Et_2SO] = 1.18\pm0.03$ mM, the other with $[Et_2SO] = 17.7\pm0.2$ mM. In each case, $[Et_2S]$ was varied from 0.119 mM to 0.464 M over several runs, and $\alpha_1,\beta_1,\gamma_1$ were evaluated using the Levenberg-

Marquardt algorithm.[4,5a,6] These values were then used to generate the variables $[Et_2S]/\beta_1$ and $[Et_2S]/v_{o1}$, which were plotted against $[Et_2S]$. Equations 3.18 and 3.19 could then be fitted to these plots using linear regression, ultimately yielding the desired equilibrium and rate constants. Figure 3.14 gives one typical fitted absorbance vs. time plot for $\lambda$ = 400.5 nm; the rest are all collected in appendix 2 (section A2.1), along with the tabulated values of $\alpha_1,\beta_1,\gamma_1$. Figures 3.15 and 3.16 show the fitted plots of equations 3.18 and 3.19 for the two sets of experiments. Finally, table 3.1 summarizes the obtained values of all the relevant parameters; their significance is discussed in section 3.4.3.

For the second substitution reaction, the concentration functions of the parameters are somewhat more complicated in that linear functions of $[Et_2S]$ at constant $[Et_2SO]$ and

**Table 3.1**
**Fundamental Parameters Derived from Equations 3.18 and 3.19**

| $[Et_2SO]\times10^3$ (M) | $\Delta\epsilon_{400.5}'\times10^{-5}$ ($M^{-1}cm^{-1}$) | $K_{1App}$ | $k_{1App}$ ($s^{-1}$) | $K_{m1}$ | $k_{-2}$ ($s^{-1}$) |
|---|---|---|---|---|---|
| 1.18±0.03 | -(1.92±0.04) | 2.8±0.1 | 135±2 | 0.85±0.03 | 41±2 |
| 17.7±0.2 | -(2.03±0.05) | 2.58±0.06 | 131±3 | 0.74±0.02 | 37±2 |
| Average parameter values | -(1.97±0.05) | 2.7±0.1 | 133±2 | 0.79±0.06 | 39±2 |

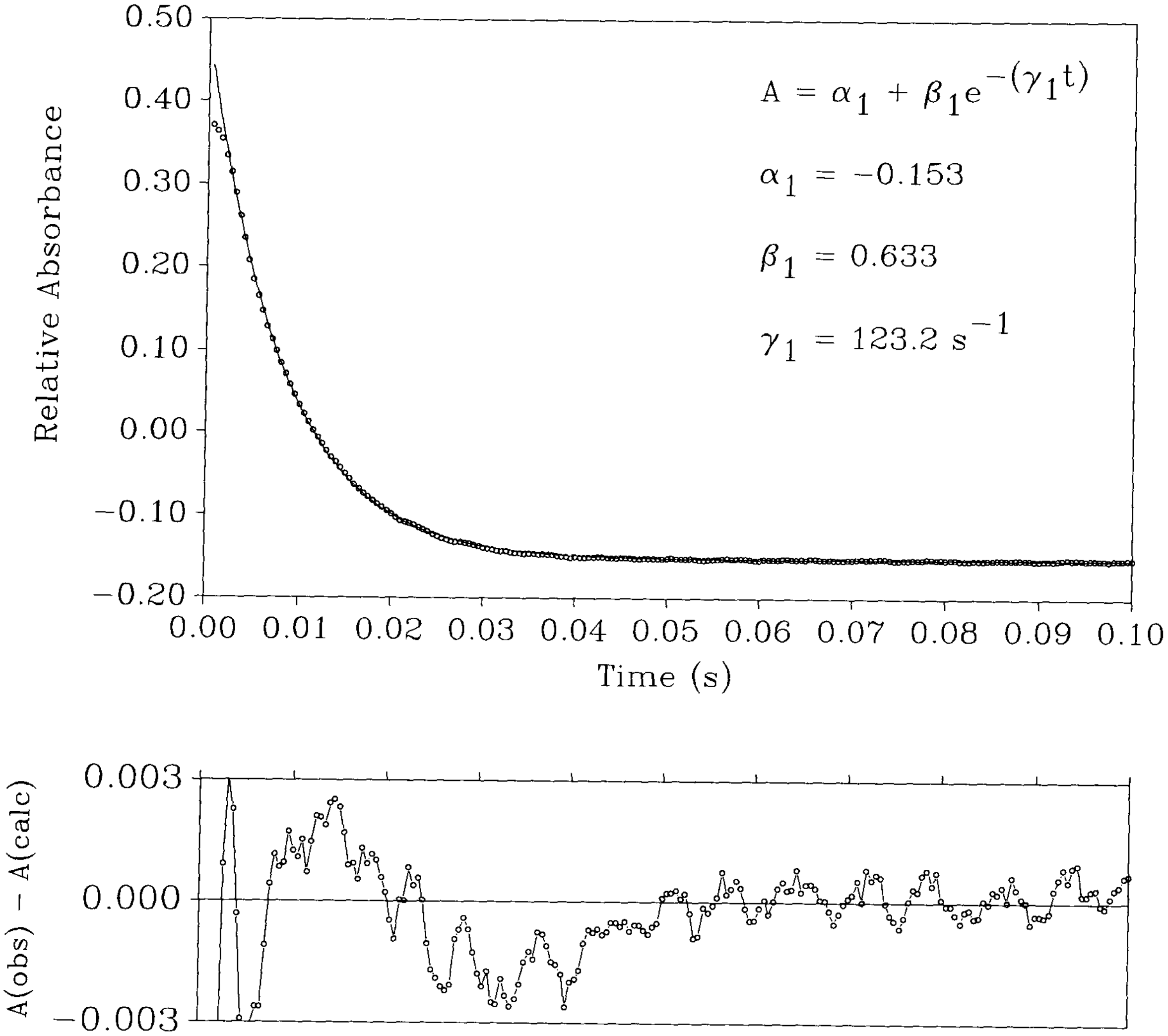

Figure 3.14. A typical, fitted stopped-flow trace of the change in absorbance over 100 ms, at λ = 400.5 nm, when $Et_2S$ is substituted for $Et_2SO$ in $Ru(OEP)(Et_2SO)_2$. $[Et_2S]$ = 9.27±0.09 mM; $[Et_2SO]$ = 1.18±0.03 mM; $[Ru]_o$ = $(3.44\pm0.07)\times10^{-6}$ M. The first four points likely are in the dead time of the instrument, and are neglected in the fit.

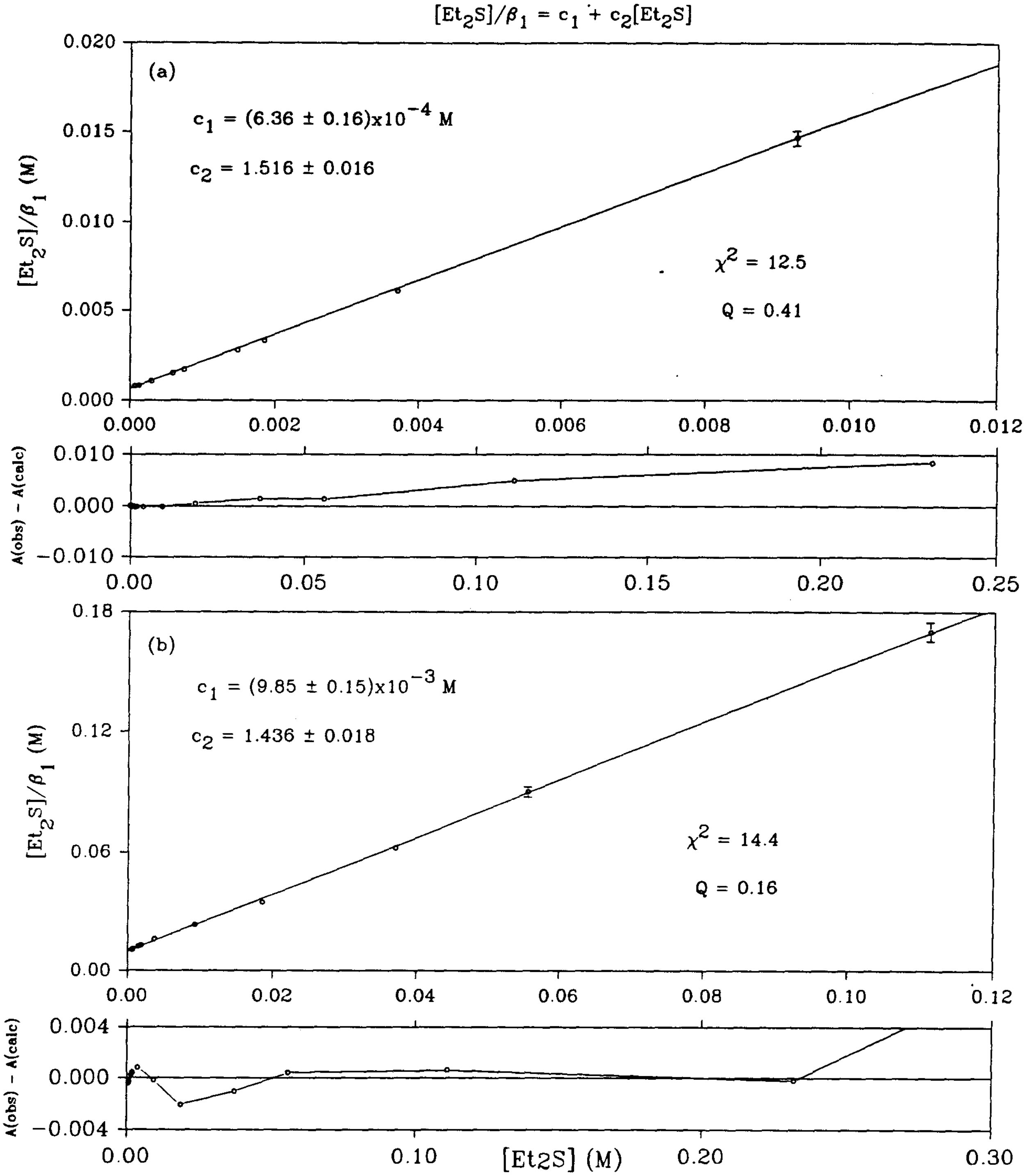

Figure 3.15. Portions of the plots of $[Et_2S]/\beta_1$ vs $[Et_2S]$ for data collected at λ = 400.5 nm over 100-ms time-frames. a) $[Et_2SO] = 1.18\pm0.03$ mM; b) $[Et_2SO] = 17.7\pm0.2$ mM. In each case $[Ru]_o = (3.44\pm0.07)\times10^{-6}$ M. The residual plots show the full range of data collected; the main plots show only the region in which $\beta_1$ increases (Q is the goodness of fit given the obtained $\chi^2$ value[14]).

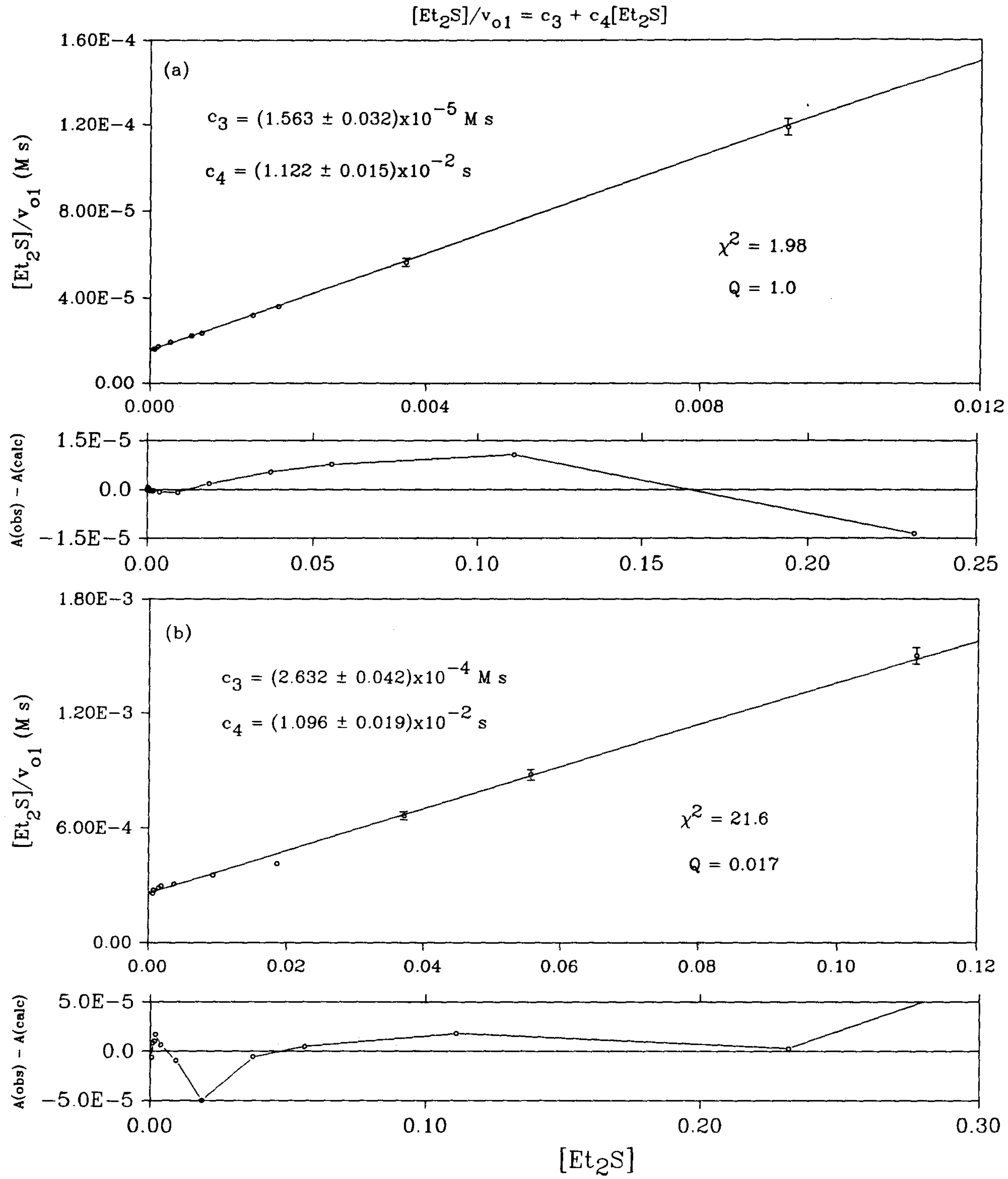

Figure 3.16. Portions of the plots of $[Et_2S]/v_{o1}$ vs $[Et_2S]$ for data collected at λ = 400.5 nm over 100-ms time-frames. a) $[Et_2SO]$ = 1.18±0.03 mM; b) $[Et_2SO]$ = 17.7±0.2 mM. In each case, $[Ru]_o = (3.44\pm0.07)\times10^{-6}$ M. The residual plots show the full range of data collected; the main plots show only the region in which $v_{o1}$ increases.

$[Ru]_o$ cannot be obtained. Nevertheless, analysis analogous to that which yielded equations 3.18 and 3.19 (see section 4.2) gives the following quadratic functions:

$$[Et_2S]^2/\beta_2 = d_1[Et_2S]^2 + d_2[Et_2S] + d_3 \qquad 3.24$$

$$[Et_2S]/v_{o2} = d_4[Et_2S]^2 + d_5[Et_2S] + d_6 \qquad 3.25$$

where

$$d_1 \equiv ([Ru]_o\Delta\epsilon_2')^{-1} \qquad 3.26$$

$$d_2 \equiv [Et_2SO]d_1/K_2 \qquad 3.27$$

$$d_3 \equiv d_2[Et_2SO]/K_{1App} \qquad 3.28$$

$$d_4 \equiv d_1/k_3 \qquad 3.29$$

$$d_5 \equiv (K_{m2} + (K_{1App})^{-1})[Et_2SO]d_4 \qquad 3.30$$

$$d_6 \equiv K_{m2}[Et_2SO]^2d_4/K_{1App} \qquad 3.31$$

$$\Delta\epsilon_2{}' \equiv (\epsilon_3 - \epsilon_2)\ell$$

$$= (\epsilon_3 - (\epsilon_1 + \epsilon_{1'}K')/(1 + K'))\ell$$

at the isosbestic wavelength λ = 402.8 nm 3.32

$$[\mathrm{Ru}]_o \equiv [\mathbf{1}] + [\mathbf{1'}] + [\mathbf{2}] + [\mathbf{3}] \qquad 3.33$$

$$K_{m2} \equiv k_{-3}/k_4 \qquad 3.34$$

$$K_2 \equiv k_3k_4/k_{-3}k_{-4} \qquad 3.35$$

Also, **3** represents Ru(OEP)$(Et_2S)_2$, and $\epsilon_3$ is its extinction coefficient. Functions 3.24 and 3.25 are linear in their dependence on the parameters $d_1$-$d_6$, and so it is still possible to do least-squares minimization without resorting to iterative methods.[5a,6] One set of experiments was carried out, with $[Et_2SO]$ = 1.18 ± 0.03 mM, and a varying $[Et_2S]$. Figure 3.17 shows a typical absorbance vs. time plot for λ = 402.8 nm; again, the remaining plots are collected in appendix 2, along with the tabulated values of $\alpha_2,\beta_2,\gamma_2$. Figure 3.18 shows the plots of equations 3.24 and 3.25, fitted to the data using the technique of singular value decomposition followed by back-substitution,[5a,5b,6] to obtain the least-squares fit parameters. Table 3.2 summarizes the values of the equilibrium constant and the rate constants obtained from equations 3.24 and 3.25; their significance is discussed in section 3.4.3.

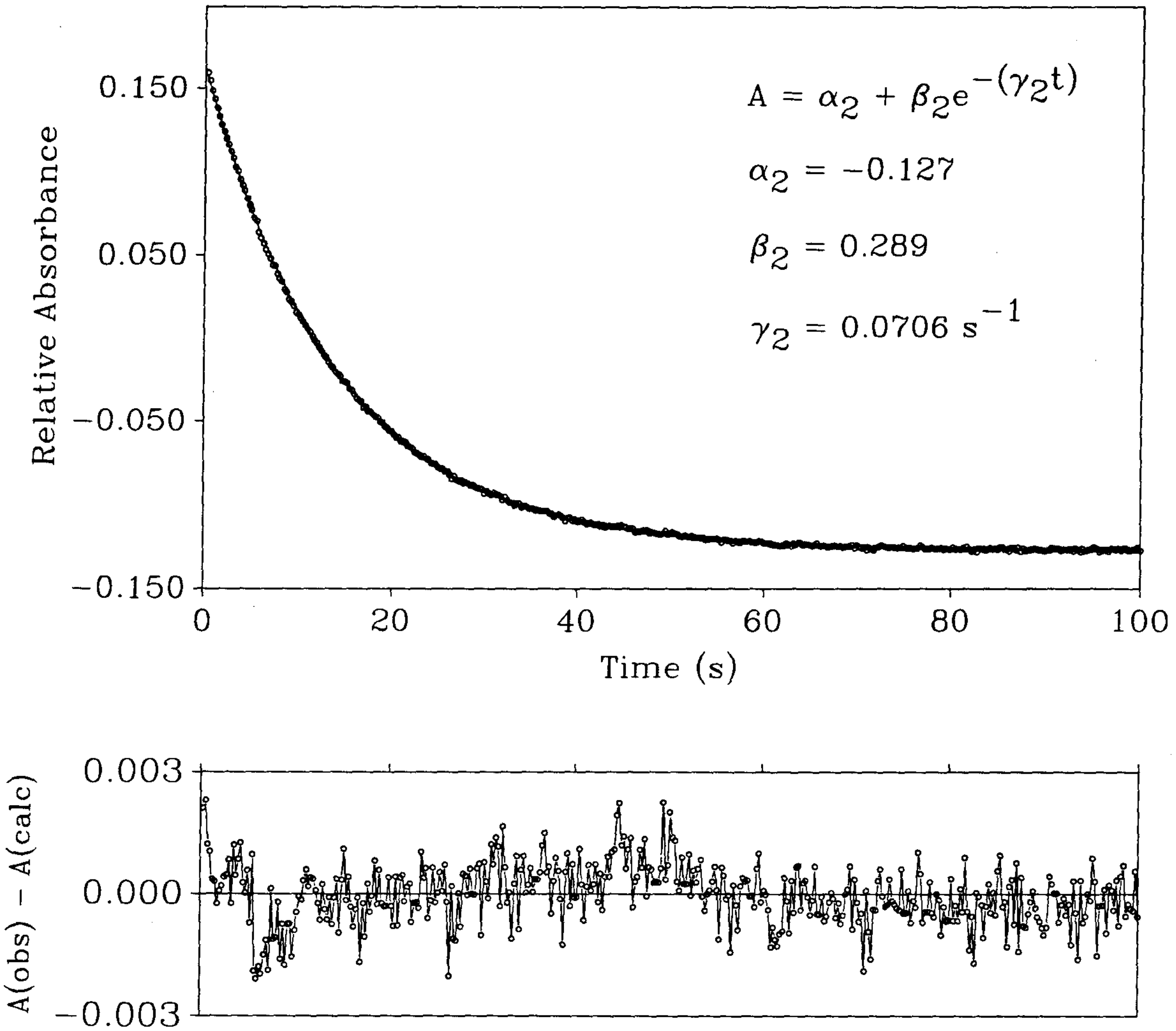

Figure 3.17. A typical, fitted stopped-flow trace of the change in absorbance over 100 s, at λ = 402.8 nm, when $Et_2S$ is substituted for $Et_2SO$ in Ru(OEP)($Et_2S$)($Et_2SO$). [$Et_2S$] = 18.6±0.2 mM; [$Et_2SO$] = 1.18±0.03 mM; $[Ru]_o$ = (3.44±0.07)x$10^{-6}$ M.

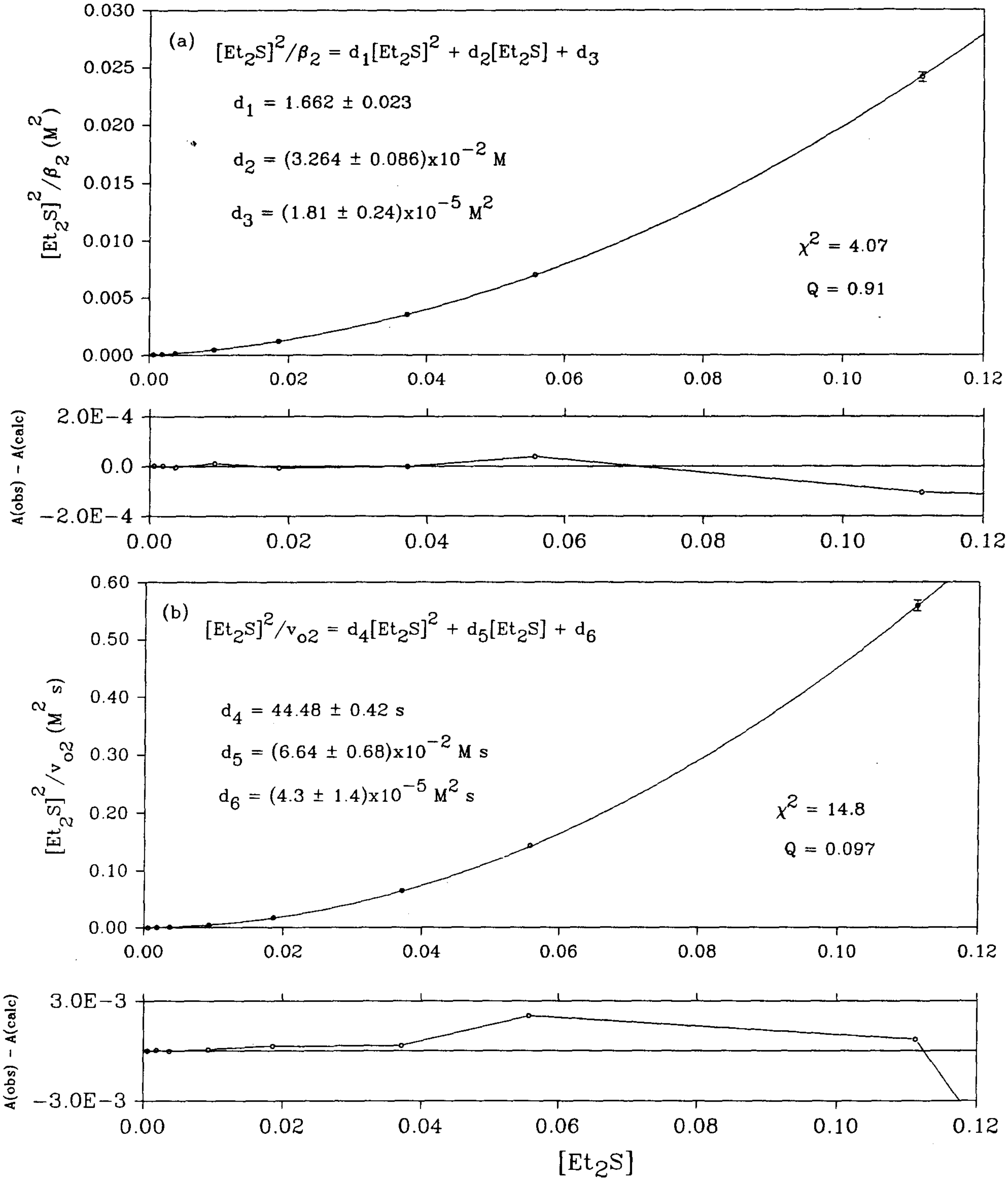

Figure 3.18. Portions of the plots of: a) $[Et_2S]^2/\beta_2$ vs $[Et_2S]$, and b) $[Et_2S]^2/v_{o2}$ vs $[Et_2S]$, for data collected at λ = 402.8 nm over 100-s time-frames. $[Et_2SO] = 1.18\pm0.03$ mM; $[Ru]_o = (3.44\pm0.07)\text{x}10^{-6}$ M. There is one off-scale point at $[Et_2S] = 0.232\pm0.002$ M for each plot; all of the data are tabulated in appendix 2.

**Table 3.2**
**Fundamental Parameters Derived from Equations 3.24 and 3.25**

| $[Et_2SO]x10^3$ (M) | $\Delta\epsilon_{402.8}'x10^{-5}$ ($M^{-1}cm^{-1}$) | $K_2x10^2$ | $k_3x10^2$ ($s^{-1}$) | $K_{m2}$ | $k_{-4}$ ($s^{-1}$) |
|---|---|---|---|---|---|
| 1.18±0.03 | -(1.75±0.04) | 6.0±0.2 | 3.74±0.06 | 1.1±0.2 | 0.7±0.1 |

### 3.4.2 Error Analysis

#### 3.4.2.1 Uncertainties in the Solution Concentrations

Small amounts of the pure reagents were used to make up the initial stock solutions. $Ru(OEP)(Et_2SO)_2$ was weighed out in approximately 5 mg quantities on an analytical balance with a precision of $\sigma = 1.9x10^{-4}$ g (based on 38 weighings of the same object over a time period of 1.5 months). The liquid reagents were measured out using Unimetrics microliter syringes with stated precisions of 1%. Once the stock solutions were made up, serial dilution using larger scale volumetric apparatus contributed little to increasing the uncertainties in the solution concentrations.

#### 3.4.2.2 Instrumental Uncertainties

Blank runs carried out with each series of experiments, both on the 100 ms and the 100 s timescales, showed that the baseline was not flat (see appendix 2). The raw data were therefore corrected by subtracting the blank from each individual run. No independent estimate of the measurement error in the absorbance was available, so a measure of the goodness of fit of the proposed exponential decay model to the data could not be obtained from the least squares analysis.[5a] Instead, an estimate of the measurement error was calculated from the least squares analysis *assuming* that the exponential decay model (given by equation 3.6) accurately described the absorbance change with time, instead of testing this as a hypothesis. Qualitatively one can say, from inspection of figures 3.14 and 3.17, that there is a good fit of the theoretical curves to the data, both on the 100 ms and the 100 s timescales. A minor oscillatory deviation of the experimentally observed data points from the theoretical values is consistently observed in all of the absorbance vs. time plots obtained on the 100 ms timescale (see figure 3.12 and appendix 2). This is probably an artifact, and is small enough to be ignored.

#### 3.4.2.2.1 Uncertainties on the Millisecond Timescale

Initially equations 3.18 and 3.19 were fitted to the data obtained by monitoring the 100 ms timescale, using the standard errors in $\alpha_1$, $\beta_1$, and $\gamma_1$, calculated from fitting equation 3.6, as weighting factors. The goodness of fit values (Q) that resulted from this procedure were unacceptably low (less than $10^{-5}$), which could not be accounted for by one or two outlier points.[14] Thus, either the model being used was wrong, or there were other sources of error beyond those already accounted for.[5a] Now if repeated stopped-flow experiments (5 run averages) were done without changing the concentration of any of the reagents, the variation in the calculated parameters $\alpha_1$, $\beta_1$, $\gamma_1$ from run to run was found to be much higher than the standard errors calculated for any given run (figure 3.19). Moreover, in the case of parameter $\beta_1$, the variation was not entirely random, with $\beta_1$ appearing to decrease slightly with with increasing number of runs. Two series of repeated runs were carried out, one at each end of the $Et_2S$ concentration range used. In the case of parameter $\beta_1$, the relative error is approximately the same (2.4%) at both

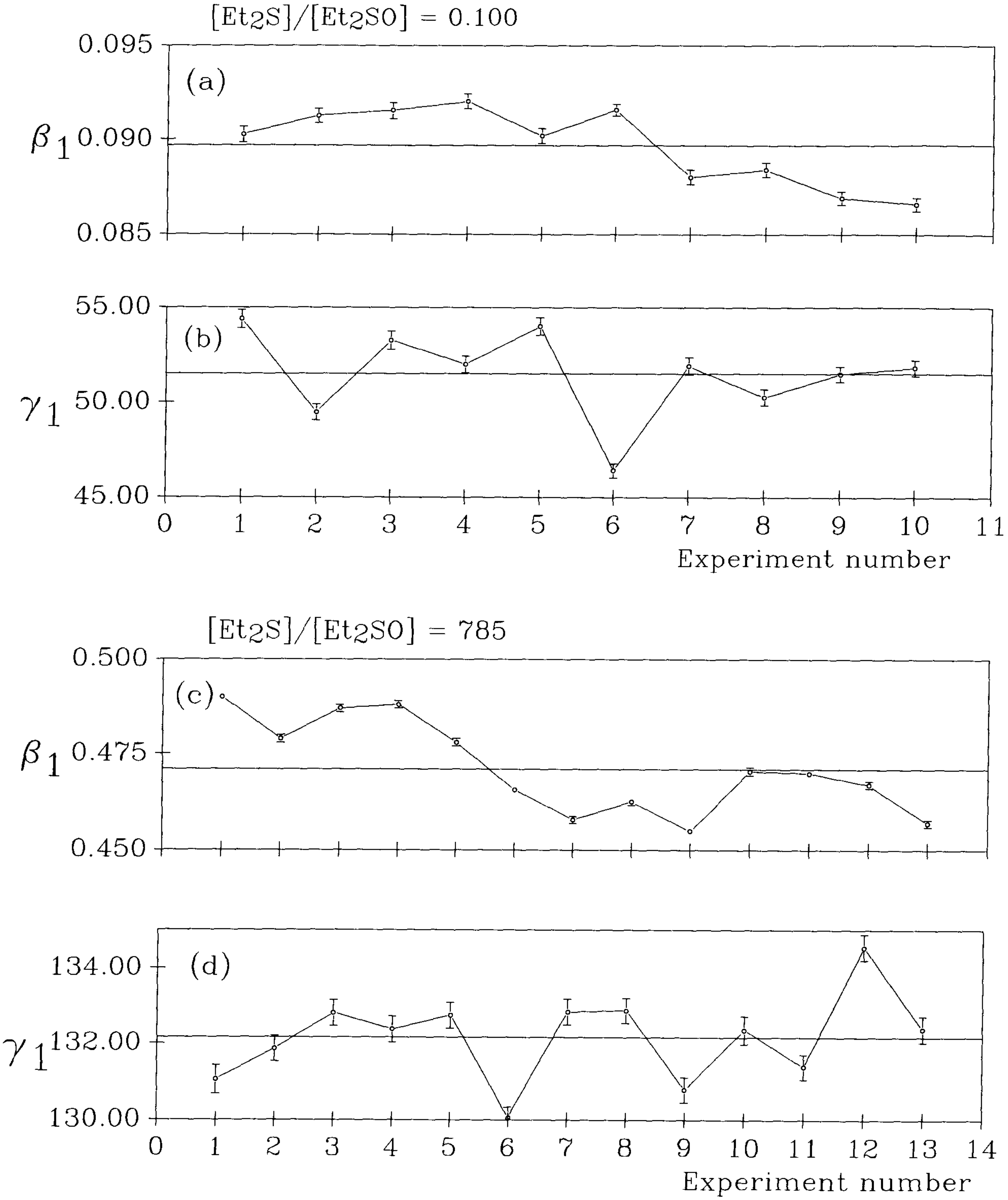

Figure 3.19. Variation of the parameters $\beta_1$ and $\gamma_1$ from experiment to experiment, when all reagent concentrations are held constant. The error bars represent the uncertainties estimated from fitting the raw stopped-flow data.

extremes, and this is considered to remain constant for experiments done at intermediate values of [$Et_2S$]. Therefore, in the fitting of equation 3.18 a relative uncertainty of ±2.4% was assumed for all $\beta_1$ values. For parameter $\gamma_1$ no such convenient trend exists, and a somewhat artificial convention was adopted by assigning a relative error of 2.5% to the points corresponding to the lowest three $Et_2S$ concentrations, one of 0.87% to the three highest concentration points, and the average value of 1.7% to the remainder. This provides an educated guess as to the proper weighting. In figures 3.15 and 3.16, the error bars represent the combination of the instrumental uncertainties as calculated by the above procedures, and the uncertainty in the thioether concentration for the experimental point in question. The goodness of fit values (reported in figures 3.15 and 3.16) are now between 0.02 and 1.0, which is quite acceptable given the relatively small sample sizes.[5a]

A comparison of the two sets of equilibrium and rate constant values listed in table 3.1 shows them to agree within 10% or better. This suggests that the proposed model, together with the concomitant assumptions, adequately describe the system under study, and the obtained values closely approximate the true equilibrium and rate constants. In particular, within the context of this thesis, the key parameter is $K_{1App}$, whose value affects the determination of all of the parameters in the second substitution reaction, which is of fundamental importance in the catalytic oxidation cycle (see section 3.5.1). Knowing $K_{1App}$ to within 10% accuracy is certainly adequate for estimating its relatively minor effect on the second reaction. The difference between the equilibrium and rate constant values obtained in the two series of experiments is significantly greater than the uncertainties resulting from the least-squares fitting; however, since the instrumental errors are not entirely random, one must be careful in assigning too much quantitative meaning to the uncertainties derived from this procedure. In fact, the main discrepancy between the two sets of results could well be due to a difference in the data collection method. For the experimental series which resulted in figures 3.15a and 3.16a, the data were collected sequentially starting at the lowest $Et_2S$ concentration, and ending with the highest. Probably as a result, the data points in these figures exhibit a slight underlying curvature relative to the theoretical lines. On the other hand, the series which resulted in figures 3.15b and 3.16b were collected in more random order, and the data points appear to be more randomly scattered about the theoretical line. As an indication that the uncertainties in the equilibrium and rate constant values are greater than suggested from the least squares analysis, the uncertainties reported with the average equilibrium and rate constants in table 3.1 are given as half the difference between the two sets of derived values.

As to the most probable source of the abnormally high instrumental variation, it was likely due to the Xenon arc lamp being quite old and deteriorating significantly during the time that the experiments were being carried out. This was evidenced by the fact that the photomultiplier gain had to be turned up quite frequently to obtain constant absorbance readings. Normally this must be done over a period of months; during the course of the reported experiments, it was not unusual to have to adjust the gain twice in the same day. As the gain is turned up, one expects the output signal to become less stable.

### 3.4.2.2.2 Uncertainties in the One Hundred Second Timescale

The error bars in figure 3.18 combine the uncertainty in the $Et_2S$ concentration and the instrumental uncertainties affecting the parameters $\alpha_2$, $\beta_2$, and $\gamma_2$, as calculated in the fitting of equation 3.6 to the data collected at $\lambda = 402.8$ nm. The goodness of fit values (Q) derived from fitting data to equations 3.24 and 3.25 suggest reasonable fits assuming these uncertainties, and the data points appear to be fairly randomly scattered above and below the theoretical curves in figure 3.18. Apparently, some of the sources of error affecting the millisecond timescale were somehow compensated for over the longer time frame.

Analysis of the intermediate results in the singular value decomposition solutions of equations 3.24 and 3.25 showed the parameters $d_1$-$d_6$ to be determined uniquely.[5a,b] The experimental uncertainty calculated for parameter $d_6$ is high enough to make the value worthless for extracting rate constant data; nevertheless, both $d_3$ and $d_6$ are significantly different from zero, and the temptation to neglect them, which would allow equations 3.24 and 3.25 to be linearized, was resisted.

For comparison with the values obtained over the 100 ms timescale, the value of $K_{1App}$ was independently determined to be 2.1 ± 0.3, by inserting the data collected in the analysis of the second substitution reaction into the equation:

$$K_{1App} = d_2\,[Et_2SO]/d_3 \qquad 3.36$$

Again, this value is significantly different statistically from the values calculated by studying the first substitution reactions directly, but is close enough to suggest that any uncertainties or mechanistic factors unaccounted for so far are relatively minor.

Finally, and of importance, $K_2$ was also determined independently from $^1$H-nmr experiments. Thus the $^1$H-nmr spectra of three solutions, initially containing 1-2 mM [$Ru(OEP)(Et_2S)_2$], 0.45 M [$Et_2S$], and 16, 40 and 79 mM [$Et_2SO$], respectively, were collected using an aquisition time of 1.5 s, and a 7 s delay between pulses. $K_2$ was then determined from the integral ratios of the meso signals ($T_1$ = 0.68 ±0.03 s) for $Ru(OEP)(Et_2S)_2$ and $Ru(OEP)(Et_2S)(Et_2\underline{S}O)$. These experiments were carried out at 20° C, rather than 35° C, but the average obtained value for $K_2$, 0.055 ± 0.005 is close to that obtained in the stopped-flow experiments.

### 3.4.3 Discussion of the Parameter Values

The equilibrium constants obtained for the first ($K_{1App}$) and second ($K_2$) substitution reactions (tables 3.1 and 3.2) show that, in a solution containing equal amounts of free $Et_2S$ and free $Et_2SO$, $Ru(OEP)(Et_2S)(Et_2\underline{S}O)$ is the predominant species in solution; i.e. it is the thermodynamically most stable of the four complexes which can possibly form. Kinetically, both substitution steps proceed via a dissociative mechanism; for both steps, the rate constants for binding to the five-coordinate intermediates ($k_{-1}$, $k_{-1'}$,$k_2$ for the $Ru(OEP)(Et_2\underline{S}O)$ species, and $k_{-3}$ and $k_4$ for $Ru(OEP)(Et_2S)$) are similar for $Et_2S$ and $Et_2SO$, as evidenced by $K_m$ values which are close to one. This means that the values of the equilibrium constants are essentially determined by the relative values of the dissociative rate constants for each reaction; i.e. $k_{1App}/k_{-2}$ for the first substitution, and $k_3/k_{-4}$ for the second.

The observed values of $K_2$, $k_3$ and $k_{-4}$ can be rationalized in terms of the sulfoxide's ability to act as a better $\pi$-electron acceptor from the metal center, relative to the sulfide (see section 2.4).[9a,15] The greater double-bond character of a $\mathrm{Ru\text{-}(Et_2\underline{S}O)}$ bond would make it stronger, and hence more difficult to break, than a $\mathrm{Ru\text{-}(Et_2S)}$ bond. Therefore it seems reasonable that $\mathrm{Et_2SO}$ should dissociate more slowly than $\mathrm{Et_2S}$ ($k_3 < k_{-4}$), and hence that the $\mathrm{Ru(OEP)(Et_2S)(Et_2\underline{S}O)}$ complex should be thermodynamically more stable than $\mathrm{Ru(OEP)(Et_2S)_2}$ ($K_2 < 1$).[†]

The large labilizing effect of a $\pi$-accepting ligand on the ligand *trans* to it has been well documented in Ru(Porp) systems,[16,17] and has been shown to be especially pronounced if the *trans* ligand is another $\pi$-acceptor.[18,19] This rationalizes why the $\mathrm{Et_2S}$ is more labile in $\mathrm{Ru(OEP)(Et_2S)(Et_2\underline{S}O)}$ than in $\mathrm{Ru(OEP)(Et_2S)_2}$ ($k_{-2} > k_{-4}$), and leads to the prediction that $\mathrm{Ru(OEP)(Et_2S)(Et_2\underline{S}O)}$ is more stable than $\mathrm{Ru(OEP)(Et_2\underline{S}O)_2}$ ($K_1 > 1$).[†] Without knowing what fraction of $\mathrm{Ru(OEP)(Et_2SO)_2}$ is present as $\mathrm{Ru(OEP)(Et_2\underline{S}O)(Et_2S\underline{O})}$ in solution, the prediction cannot be verified directly; however, the solid-state ir and electrochemical evidence from sections 2.3 and 2.4 suggest that $\mathrm{Ru(OEP)(Et_2\underline{S}O)(Et_2S\underline{O})}$ is a relatively minor species in solution. Furthermore, recall from section 1.2 that the most stable isomer of $\mathrm{Ru(TMP)(Et_2SO)_2}$ is known to be the bis(S-bound) one.[20] If the fraction of $\mathrm{Ru(OEP)(Et_2\underline{S}O)(Et_2S\underline{O})}$ is small ($K' << 1$), then $K_1 \approx K_{1App}$ (equation 3.14, p.119), and $K_{1App}$ is $>1$ (table 3.1).

The so-called "*trans effect*" (labilization of a mutually *trans* ligand) has been studied extensively in square-planar Pt complexes, and a good qualitative theory has been established.[21] In the present case, in which the ligand responsible for the *trans*

---

[†] This reflects the relative concentrations of the two metal complexes when equal concentrations of free $\mathrm{Et_2S}$ and $\mathrm{Et_2SO}$ are present.

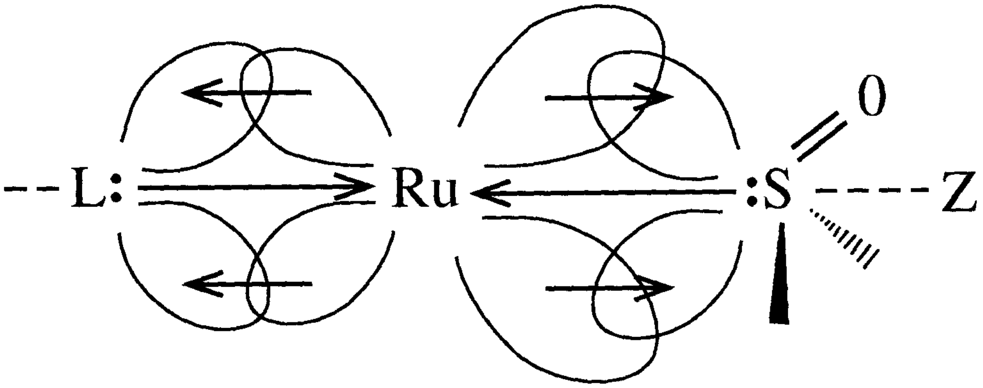

Figure 3.20. Weakening of $\pi$-bonds *trans* to a sulfoxide; $\sigma$ bonds *trans* to the sulfoxide will also be weakened, since the sulfoxide can transfer more $\sigma$-electron density to the Ru $d_{z^2}$ orbital than a comparable ligand incapable of $\pi$-bonding (see text).

labilization is a $\pi$-acceptor, the mechanism by which the phenomenon occurs can be visualized according to figure 3.20. When the sulfoxide accepts electron density from the ruthenium center via $\pi$-$\pi^*$ back-bonding, there will be less electron density left on the $\pi$-bonding metal orbital for back-bonding to another $\pi$-acceptor *trans* to the sulfoxide. Thus the bond of a sulfoxide trans to the first sulfoxide will be especially weak. At the same time, the back-bonding of the ruthenium to the sulfoxide has a synergistic effect on the Ru-S $\sigma$ bond; as more electron density is put on the sulfoxide via the $\pi$-bond, more of that density can be fed from the sulfur back to the ruthenium via the $\sigma$ bond. This will mean that the $d_{z^2}$ orbital of the ruthenium will also be monopolized by the sulfoxide, and less available for bonding with a *trans* ligand L. Therefore even a $\sigma$ bond *trans* to the sulfoxide will be weakened, but not as much as another $\pi$-bond.

## 3.5 Catalytic Oxidation of $Et_2S$ - Rate Dependence on $[O_2]$ [PhCOOH] and $[Ru(OEP)(Et_2S)_2]$

### 3.5.1 Data Treatment and Results

For carrying out a *quantitative* kinetic analysis of the catalytic oxidation, monitoring the oxygen uptake proved to be more convenient than following $Et_2SO$ production by gas chromatography. Although gc was useful in providing complementary information, it did not yield quantitatively reliable results consistently under conditions of higher PhCOOH ([PhCOOH] > 5 mM) or Ru(OEP) ($[Ru]_o$ > 0.5 mM) concentration. The presence of PhCOOH tends to broaden the $Et_2SO$ signals considerably when present in high concentrations. The effect of high concentrations of Ru(OEP) is more subtle; the appearance of the chromatograms remains unchanged by repeated injections of reaction mixtures initially containing higher concentrations of $Ru(OEP)(Et_2S)_2$, but standards run before and after monitoring the reactions show that the response factors for $Et_2SO$ change appreciably during the period of the monitoring process.

Based on the mechanism proposed in figure 3.8, a system of five differential equations can be derived (see section 4.3 for the derivations) to describe the rates of appearance and disappearance of the major species in solution:

$$\begin{aligned} d[\mathbf{2}]/dt = {} & k_{-4}[Et_2SO][\mathbf{3}]/[Et_2S]_o - k_3[Et_2S][\mathbf{2}]/[Et_2S]_o \\ & + k_{obs}[Et_2SO][\mathbf{3}]/([Et_2S]_o([\mathbf{3}] + \psi[\mathbf{2}])) \end{aligned} \tag{3.37}$$

$$-d[\mathbf{3}]/dt = d[\mathbf{2}]/dt \tag{3.38}$$

$$\begin{aligned} d[Et_2SO]/dt = {} & k_{obs}[\mathbf{3}](2[Et_2S]_o - [Et_2SO])/([Et_2S]_o([\mathbf{3}] + \psi[\mathbf{2}])) \\ & + k_3[Et_2S][\mathbf{2}]/[Et_2S]_o - k_{-4}[Et_2SO][\mathbf{3}]/[Et_2S]_o \end{aligned} \tag{3.39}$$

$$-d[Et_2S]/dt = d[Et_2SO]/dt \tag{3.40}$$

$$-d[O_2]/dt = 0.5d[Et_2SO]/dt \tag{3.41}$$

where

$$k_{obs} \equiv v_m(f[Ru]_o)[O_2][PhCOOH]/((K_{m4} + [PhCOOH])(K_{m3} + [O_2])) \tag{3.42}$$

$$[Et_2S]_o \equiv [Et_2S] + [Et_2SO] \tag{3.43}$$

and also

$$v_m \equiv 0.5c_1k_7/(k_{-6'} + k_7) \tag{3.44}$$

$$K_{m3} \equiv k_{-5}/k_6 \tag{3.45}$$

$$K_{m4} \equiv k_{-6'}k_{-7}/((k_{-6'} + k_7)k_8) \tag{3.46}$$

Again, **2** $\equiv$ Ru(OEP)($Et_2S$)($Et_2\underline{S}O$), and **3** $\equiv$ Ru(OEP)$(Et_2S)_2$. The constants $c_1$ and $\psi$, and the function $f[Ru]_o$ are all part of an empirical expression, the significance of which is discussed below.

Note that at $t = 0$, $[\mathbf{2}] = 0$, $[\mathbf{3}] = [Ru]_o$, $[Et_2SO] = 0$, and $[Et_2S] = [Et_2S]_o$. Therefore:

$$(d[\mathbf{2}]/dt)_{t=0} = 0 \tag{3.47}$$

$$(d[Et_2SO]/dt)_{t=0} = 2k_{obs} \tag{3.48}$$

i.e. the initial rate of $[Et_2SO]$ production is $2k_{obs}$. The forms of the initial rate equations 3.47 and 3.48 have an important theoretical significance, which is discussed in section 4.3.3.1.

Equations 3.37-3.41 were derived making all of the simplifying assumptions discussed in section 3.3: a) all species other than $Ru(OEP)(Et_2S)_2$ and $Ru(OEP)(Et_2S)(Et_2\underline{S}O)$ are present in negligible, steady state concentrations; b) only $Ru(OEP)(Et_2S)_2$ reacts with $O_2$; c) the photochemical effect is initiated by the $\pi$-$\pi^*$ transitions which give rise to the $\alpha,\beta$ bands in the uv/vis spectrum of $Ru(OEP)(Et_2S)_2$; d) no catalyst degradation takes place during reaction; e) reaction of $Ru(OEP)(Et_2S)_2$ with $O_2$ via direct coordination of $O_2$ to the metal center does not occur when excess thioether is present; f) rearrangement of $Ru(OEP)(Et_2S)(Et_2S\underline{O})$ to $Ru(OEP)(Et_2S)(Et_2\underline{S}O)$ occurs only via the five-coordinate $Ru(OEP)(Et_2S)$ intermediate (i.e. the reaction pathway in figure 3.8 labelled "internal rearrangement" does not occur). In addition to these six assumptions, based on the results of the stopped-flow studies described in the previous section, two additional simplifying assumptions were made. First, the concentrations of $Ru(OEP)(Et_2\underline{S}O)_2$ and $Ru(OEP)(Et_2\underline{S}O)(Et_2S\underline{O})$ produced during the reaction were neglected. For the fastest reactions studied, the ratio $[Et_2SO]/[Et_2S]$ at the end of the typical time period monitored (1.7-2.5 h) was at most 0.1, which means that the $[Ru(OEP)(Et_2SO)_2]$ would still be 30 times less than the $[Ru(OEP)(Et_2S)(Et_2\underline{S}O)]$, or 20 times less than the $[Ru(OEP)(Et_2S)_2]$ (using the values of $K_{1App}$ and $K_2$ listed in tables 3.1 and 3.2). The second assumption was that $K_{m2}$ is essentially equal to one, as determined experimentally ($1.1 \pm 0.2$, see section 3.4 and table 3.2).

The expression

$$c_1(f[Ru]_o)[3]/([3] + \psi[2]) \qquad 3.49$$

is an empirical one meant to approximate $I_a$, the amount of light absorbed by $Ru(OEP)(Et_2S)_2$, for each turn of the catalytic cycle ($I_a \equiv$ einsteins absorbed by $Ru(OEP)(Et_2S)_2$ per liter per second). The true form of the function $I_a$ will be complicated, and the theoretical problem of approximating it by a reasonably simple function is treated in detail in section 4.3.2; for the moment, only a summary is provided. The approximate function consists of two distinguishable sub-functions, and the constant $c_1$. The first sub-function is $f[Ru]_o$, which is intended to reflect what fraction of the total incident light will be absorbed by all the contents of the reaction flask for a given $[Ru]_o$. As will be seen below, when the one-parameter function

$$f[Ru]_o = 1 - \exp(-10c_2[Ru]_o) + \arctan(c_2[Ru]_o) \qquad 3.50$$

is used (where $c_2$ is the adjustable parameter), the resulting equation for $k_{obs}$ fits well all of the experimental data, although no doubt there are other suitable expressions for $f[Ru]_o$ (see section 4.3.2).

The second sub-function of $I_a$ is defined by

$$f_2 \equiv [3]/([3] + \psi[2]) \qquad 3.51$$

Where

$$\psi \equiv \int \epsilon_3 d\lambda / \int \epsilon_2 d\lambda \qquad 3.52$$

Thus $f_2$ represents what fraction of the total light absorbed by the solution is actually absorbed by $Ru(OEP)(Et_2S)_2$. Note that whereas $c_1$ and $c_2$ are empirical parameters whose value depends on the geometry of the experimental apparatus, the value of $\psi$ is dictated by assumption (c) above; therefore $\psi$ has chemical significance. Figure 3.21 illustrates the region of the spectrum over which the integrals in equation 3.52 were evaluated. The integral values were obtained as follows. First, the spectra of separate 0.0340 mM solutions of $Ru(OEP)(Et_2S)_2$ and $Ru(OEP)(Et_2SO)_2$, containing 74.2 mM $Et_2S$ and 2.22 mM $Et_2SO$, respectively, were collected. The desired region in each spectrum was then cut out and weighed; these weights represented, in effect, the integrated "absorbance" (in units of g) of each species, over the region of interest. Thus an integrated "extinction coefficient" (in units of g $M^{-1}$ $cm^{-1}$) was calculated for each species. Next, the spectrum of a solution initially containing 0.0340 mM $Ru(OEP)(Et_2S)_2$, 74.2 mM $Et_2S$ and 44.9 mM $Et_2SO$ was obtained, and the desired region cut out and weighed. The equilibrium concentrations of $Ru(OEP)(Et_2S)_2$, $Ru(OEP)(Et_2S)(Et_2\underline{S}O)$ and $Ru(OEP)(Et_2SO)_2$ were easily obtained from the known values of the equilibrium constants $K_{1App}$ and $K_2$ (see section 3.4, and tables 3.1 and 3.2); thus, the integrated extinction coefficient for $Ru(OEP)(Et_2S)(Et_2\underline{S}O)$ (in units of g $M^{-1}cm^{-1}$), being the only unknown value left, was obtained directly from the Beer-Lambert law. The unusual units of the integrated extinction coefficients do not pose a problem, because they cancel out when the desired ratio $\psi$ is calculated. The value of $\psi$ calculated using the above procedure was $0.86 \pm 0.07$.

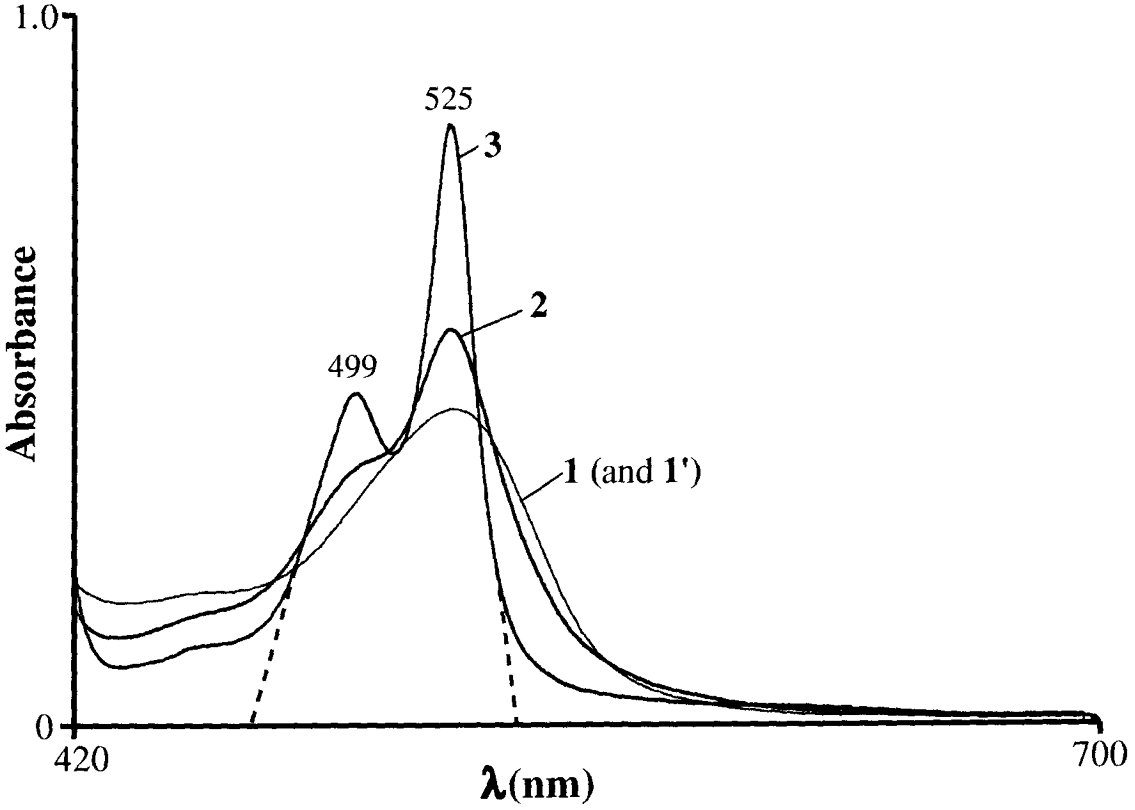

Figure 3.21. Visible spectra of pure Ru(OEP)$(Et_2S)_2$ (**3**), a solution containing mostly Ru(OEP)$(Et_2S)(Et_2\underline{S}O)$ (**2**, see text), and pure Ru(OEP)$(Et_2SO)_2$ (**1** and **1'**). The dashed lines indicate the region of all three spectra over which the integrated extinction coefficients were calculated (see text for details).

The constant $c_1$ is conceptually important in that it reflects the maximum attainable value of $I_a$. From equations 3.49 and 3.50, the maximum value of $I_a$ (when all of the light incident on the solution is absorbed) is given by

$$(I_a)_{max} = 3\pi c_1/2 \qquad 3.53$$

Note that $c_1$ is itself a function of $I_o$ (the intensity of the incident light, commonly given in einsteins $dm^{-2}\ s^{-1}$), the area of the cross-section of solution illuminated, and the solution volume (see section 4.3.2). Also, the area of the cross-section of solution illuminated is a function of various geometrical parameters such as flask size, lamp orientation and flask shaking speed. It was to keep $c_1$ constant over the whole series of experiments that all runs were carried out using the same solution volume, and great care was taken to keep every part of the apparatus, including the flask, bucket, shaking speed and illumination lamp orientation, the same from run to run. Some experiments were carried out in which either the volume or the shaking speed were deliberately varied; these will not be discussed further here, except to say that changing the shaking speed did not have a great effect on the observed results, but changing the volume did. The results of all the experiments in which either solution volume or shaking speed were varied are listed in appendix 3 (section A3.3). For the experiments discussed in this thesis, only $v_m$, rather than $c_1$, could be obtained (see equation 3.44); the relationship between $c_1$ and $v_m$ is further discussed at the end of section 3.5.2.2.

With $\psi$ calculated, and $k_3$, $k_{-4}$ known from the stopped-flow experiments, all of the unknown parameters in the differential equations 3.37-3.41 fall within the expression for

$k_{obs}$. Within any one experiment, [PhCOOH], $[O_2]$ and $[Ru]_o$ were held constant, and therefore $k_{obs}$ can be considered a pseudo rate constant, remaining unchanged for the duration of a single experiment. The initial conditions for the system of differential equations 3.37-3.41 are known experimentally, and so only $k_{obs}$ is needed to solve the system numerically for a given run. To find the best value of $k_{obs}$ for a given run, an iterative algorithm, composed mainly of sub-programs from "Numerical Recipes", was devised.[5c,6] The complete program is listed in appendix 1, but essentially it works as follows. The program is supplied with a copy of an experimentally derived $[Et_2SO]$ vs. time data set (where $[Et_2SO] = 2[O_2]_{absorbed}$), the initial conditions for the data set, and two initial guesses as to the best value of $k_{obs}$. The first part of the program, a standard numerical integrator, uses these trial $k_{obs}$ values to generate two theoretical $[Et_2SO]$ vs. time data sets. These data sets are individually compared with the experimental results in least-square fashion, and a $\chi^2$ value is generated for each initially guessed $k_{obs}$ value. The second part of the program then uses the first two $(k_{obs},\chi^2)$ pairs to generate new trial values of $k_{obs}$ according to a prescribed algorithm, and these are successively sent back to the integrator until the lowest possible value of $\chi^2$ is obtained. Figure 3.9, seen in section 3.3, shows a typical $[Et_2SO]$ vs. time plot, fitted using this $\chi^2$ minimization routine; another is given in figure 3.22. A total of about 50 experiments were carried out, and the rest of the corresponding plots are collected in appendix 3.

The experiments performed are divided into three categories; for any given category, one of $[Ru]_o$, [PhCOOH] or $[O_2]$ was varied, while the other two were held

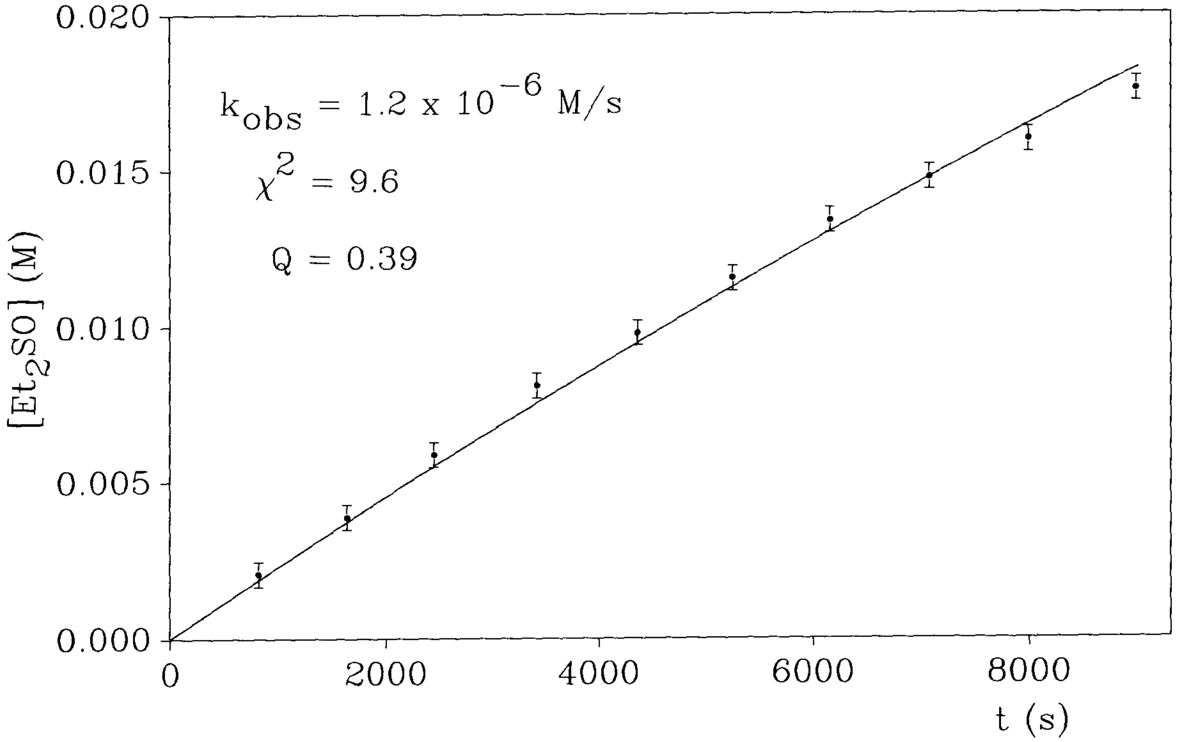

Figure 3.22. A plot of [$Et_2SO$] vs. time, fitted using the least squares procedure described in the text. For this experiment, the initial concentrations of the reagents are: [$Ru(OEP)(Et_2S)_2$] = 0.202 mM; [PhCOOH] = 2.31 mM; [$Et_2S$] = 0.742 M; $pO_2$ = 0.813 atm (corrected for benzene vapour pressure).

constant. Figure 3.23a shows a graph of $k_{obs}$ vs. $[Ru]_o$ for the data in which $[Ru]_o$ was varied while keeping $[O_2]$ and [PhCOOH] constant. Taking into account equations 3.42 and 3.50, the data were fitted to the equation

$$k_{obs} = p_1(1 - \exp(-10c_2[Ru]_o) + \arctan(c_2[Ru]_o) \qquad 3.54$$

using the Leavenberg-Marquardt algorithm.[5a,6] It follows directly from equations 3.42 and 3.50 that

$$p_1 \equiv v_m[O_2][PhCOOH]/((K_{m4} + [PhCOOH])(K_{m3} + [O_2])) \qquad 3.55$$

Figure 3.23b shows the graph of $k_{obs}$ vs. [PhCOOH] for the set of data in which [PhCOOH] was varied, while keeping $[O_2]$ and $[Ru]_o$ constant. These data were fitted to a rectangular hyperbola with zero intercept, again using the Leavenberg-Marquardt algorithm.

Thus

$$k_{obs} = p_2[PhCOOH]/(K_{m4} + [PhCOOH]) \qquad 3.56$$

where

$$p_2 \equiv v_m[O_2](1 - \exp(-10c_2[Ru]_o) + \arctan(c_2[Ru]_o)/(K_{m3} + [O]_2) \qquad 3.57$$

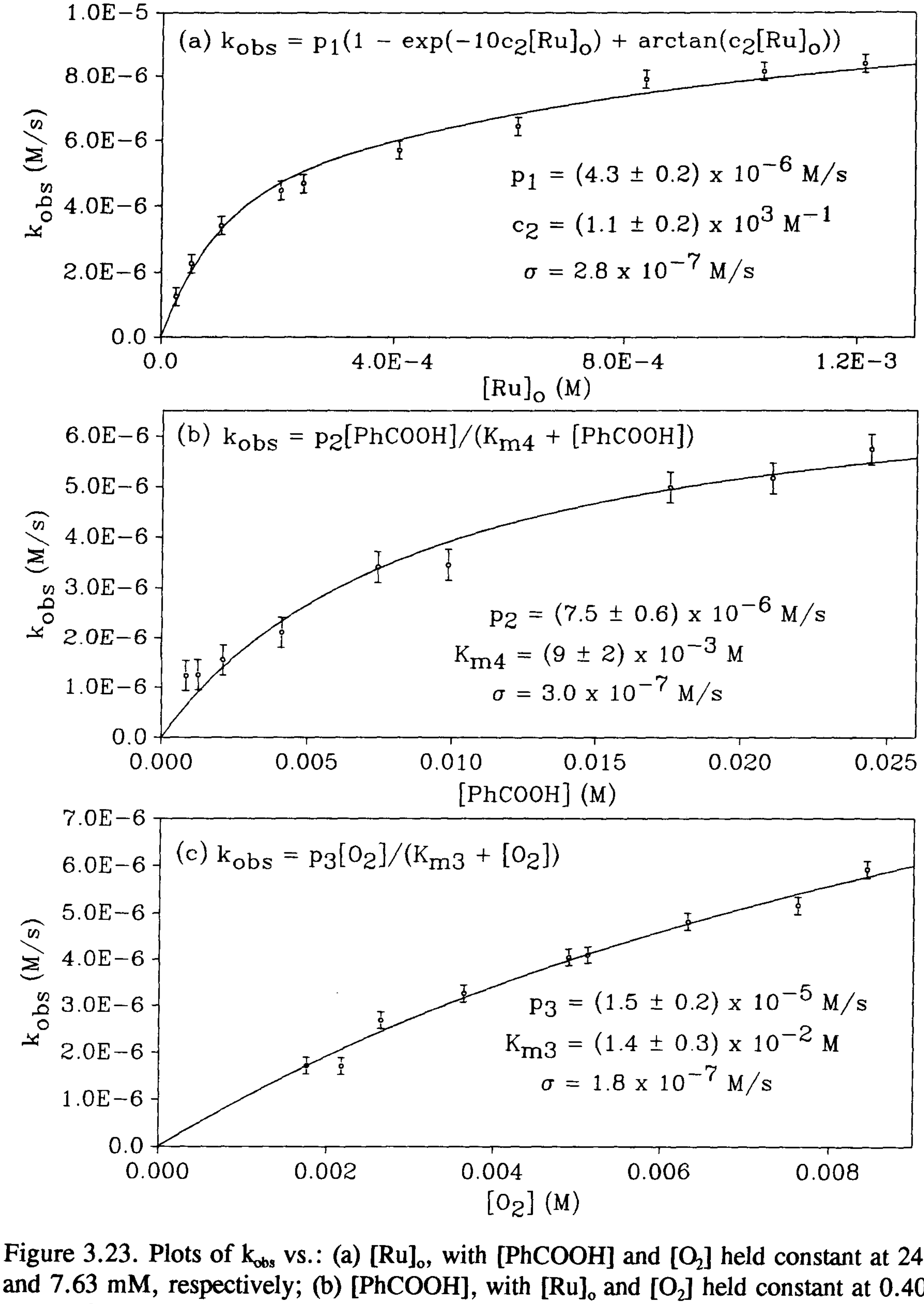

Figure 3.23. Plots of $k_{obs}$ vs.: (a) $[Ru]_o$, with [PhCOOH] and $[O_2]$ held constant at 24.4 and 7.63 mM, respectively; (b) [PhCOOH], with $[Ru]_o$ and $[O_2]$ held constant at 0.408 and 7.63 mM, respectively; (c) $[O_2]$ with $[Ru]_o$ and [PhCOOH] held constant at 0.408 and 24.4 mM, respectively. The error bar magnitude in each case is given by $\sigma$.

Finally, figure 3.23c illustrates the data obtained from experiments where $[O_2]$ was varied, keeping $[Ru]_o$ and [PhCOOH] constant. These data were also fitted to a rectangular hyperbola with zero intercept,

$$k_{obs} = p_3[O_2]/(K_{m3} + [O_2]) \qquad 3.58$$

where

$$p_3 \equiv v_m[PhCOOH](1 - \exp(-10c_2[Ru]_o) + \arctan(c_2[Ru]_o)/(K_{m4} + [PhCOOH]) \qquad 3.59$$

In addition to the data shown in figure 3.23, the experiments in which [PhCOOH] and $[Ru]_o$ were varied were repeated several months after the first set of experiments, with the apparatus set up slightly differently (it was impossible to set it up in exactly the same way). The results of these experiments are shown graphically in figure 3.24. Note that, as expected, the parameters $v_m$ and $c_2$ are different for these experiments, since the apparatus geometry was different (presumably it is the difference in the value of $c_1$ which makes the value of $v_m$ different). To avoid confusion, when referring to the second set of experiments, $c_{1'}$, $c_{2'}$, $p_{1'}$, $p_{2'}$ and $v_{m'}$ are used instead of $c_1$, $c_2$ $p_1$, $p_2$ and $v_m$. Thus, for example, for the $[Ru]_o$-dependence experiments, equations 3.54 and 3.55 become

$$k_{obs} = p_{1'}(1 - \exp(-10c_{2'}[Ru]_o) + \arctan(c_{2'}[Ru]_o) \qquad 3.60$$

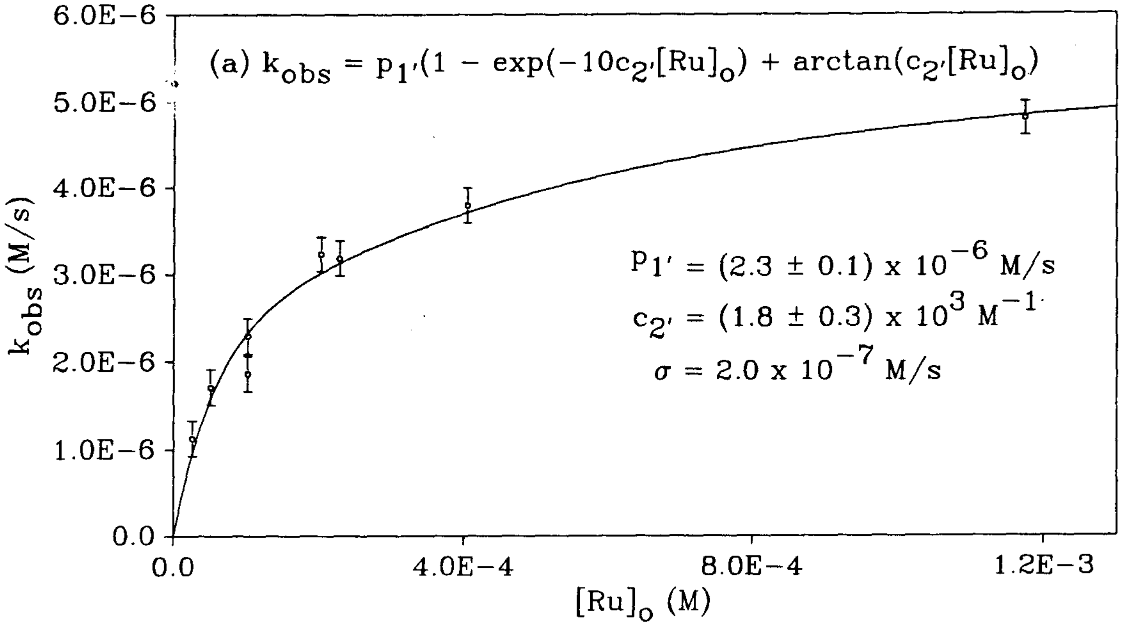

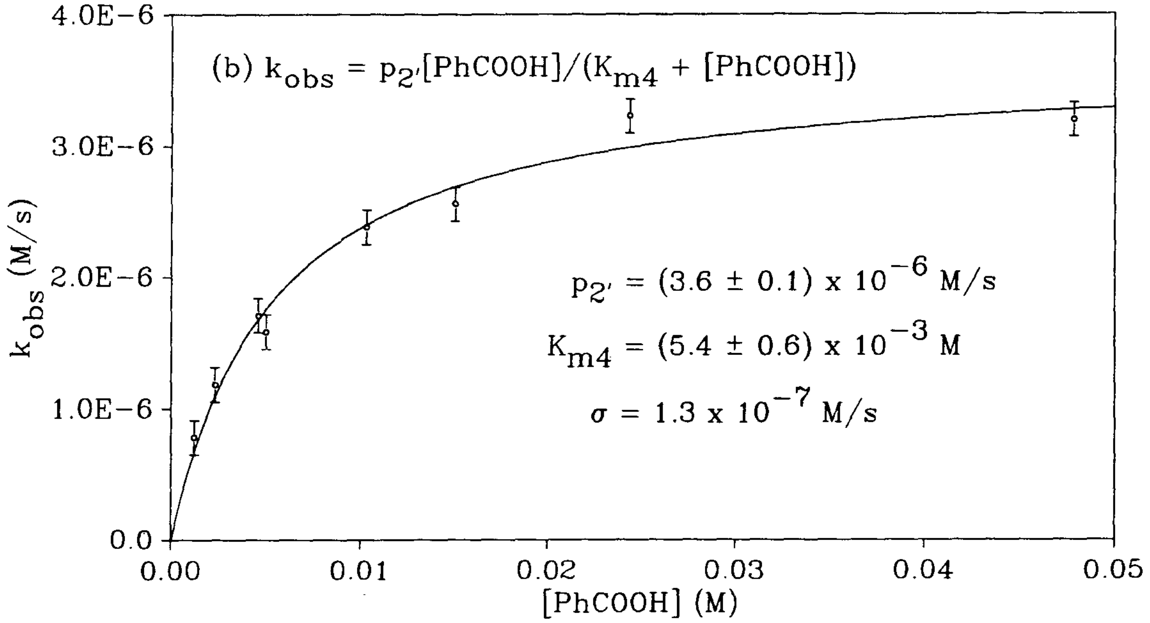

Figure 3.24. Plots of $k_{obs}$ vs.: (a) $[Ru]_o$, with [PhCOOH] and $[O_2]$ held constant at 24.4 and 7.63 mM, respectively; (b) [PhCOOH], with $[Ru]_o$ and $[O_2]$ held constant at 0.202 and 7.63 mM, respectively. The error bar magnitude in each case is given by $\sigma$.

where

$$p_{1'} \equiv v_{m'}[O_2][PhCOOH]/((K_{m4} + [PhCOOH])(K_{m3} + [O_2])) \qquad 3.61$$

and

$$v_{m'} \equiv 0.5c_{1'}k_7/(k_{-6'} + k_7) \qquad 3.62$$

The values for $K_{m3}$, $K_{m4}$, $v_m$ and $v_{m'}$ obtained in the two sets of experiments are tabulated in table 3.3.

### TABLE 3.3
### Fundamental Parameters Derived from the Plots of $k_{obs}$ vs. $[Ru]_o$, [PhCOOH] and $[O_2]$

| $K_{m3}$ (M) | $K_{m4}$ (M)[a] | $v_m$ (M/s)[b] | $v_{m'}$ (M/s)[c] |
|---|---|---|---|
| $(1.4 \pm 0.3)x10^{-2}$ | $(5.4 \pm 0.6)x10^{-3}$ | $(1.4 \pm 0.3)x10^{-5}$ | $(8 \pm 2)x10^{-6}$ |

a) Only the result obtained from figure 3.22 is considered.

b) The reported value is the average of the values obtained from a consideration of $p_1$, $p_2$ and $p_3$.

c) The reported value is the average of the values obtained from a consideration of $p_{1'}$ and $p_{2'}$.

### 3.5.2 Error Analysis and Discussion

#### 3.5.2.1 Experimental Uncertainties

The procedure used to weigh out reagents and prepare solutions was the same in the oxygen-uptake experiments as in the stopped-flow experiments, and so the uncertainties in the reagent concentrations are expected to be similar in both cases.

The major source of experimental uncertainty for the gas uptake experiments is undoubtedly associated with the gas uptake measurements themselves. It was estimated that the oil manometer on the apparatus could be levelled with an accuracy of ±1 mm, which translates to an uncertainty of ±0.1 mM in the measured uptake. This relationship holds, regardless of the pressure at which the reaction was carried out. As mentioned in section 3.2.4.2, the vapour pressures of [$Et_2S$] and benzene caused a cyclic variation in the oil manometer levels as the temperature cycled between 34.85 ± 0.15° C, which was compensated for by always levelling the manometer at the temperature minimum. Now if the oil manometer were levelled either slightly before or after the minimum, the temperature in the reaction flask would be higher than required, which would cause the uptake to be underestimated over that time period. Thus uncertainties due to non-levelling of the manometer exactly at the minimum should always lead to an underestimation of the uptake volume, *provided that the temperature never dropped below the average minimum*. Experimentally, the temperature fluctuation was found not to be perfectly predictable, and sometimes the minimum would drop below the average value (34.70° C) while the manometer was being levelled. This can be attributed to the complicated mixing process which takes place in the reaction oil bath, due to both stirring by the mechanical stirrer, and the shaking of the reaction flask. It is difficult to get a good feeling for the combined uncertainty due to the difficulties in always levelling the oil manometer at the same temperature. As an educated guess, the total uncertainty in the oxygen uptake measurement was estimated to be ±0.2 mM, twice the value suggested earlier for the levelling of the manometer in the absence of the temperature-induced pressure fluctuations. The error bars in figures 3.9 and 3.22 show an uncertainty in [$Et_2SO$] of ±0.4 mM, which is twice the postulated [$O_2$] uncertainty.

### 3.5.2.2 Evaluation of the Kinetic Model

The suitability of the proposed model can be evaluated at two distinct levels. At the first level, one wishes to asses how well the differential equations 3.37-3.41, as written, fit the raw data. At the second level, the question is how well does the proposed expression for $k_{obs}$ fit the replotted $k_{obs}$ vs. $[Ru]_o$, [PhCOOH], and [$O_2$] data?

Figure 3.25 shows plots of the goodness-of-fit parameter Q, vs. $[Ru]_o$, [PhCOOH], and [$O_2$], obtained in the evaluation of $k_{obs}$ for each uptake experiment. For the typical experiment performed, in which about 13-16 data points were collected, about 95% of the Q values should fall between .04 and .99, with an average around 0.4, assuming that the fitting model is correct, and the measurement errors are normally distributed.[5a,14] Most of the data points do indeed fall within this range, but there are some notable exceptions.

There are isolated data sets in figure 3.25 that have very low Q values (less than $10^{-3}$; see also appendix 3). When these data sets are examined (appendix 3), they are found to have unusually high, but random scatter about the theoretical curve. Thus for these data sets, the low Q values are almost certainly due to the fact that the measurement

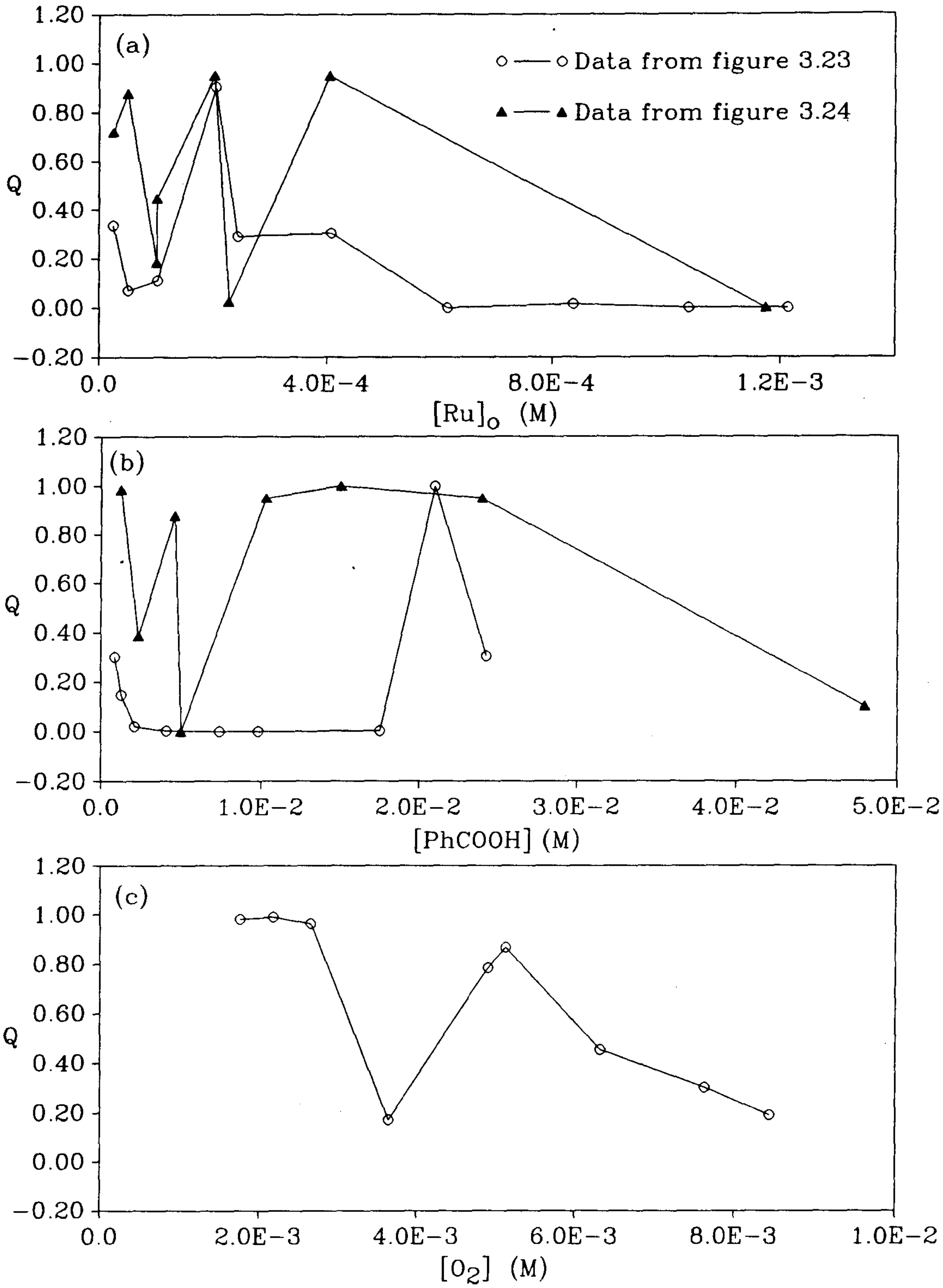

Figure 3.25. Plots of the goodness of fit parameter (Q) vs.: (a) $[Ru]_o$; (b) [PhCOOH]; (c) $[O_2]$ for the fitting procedures illustrated in figures 3.23 and 3.24, and assuming that $\psi$ = 0.85 (see text for details).

errors in the experiments were higher than normal, rather than to any flaw in the model. As mentioned in the previous section, the temperature cycle in the reaction vesssel was not entirely predictable, and sometimes the temperature minimum either went below that expected, or didn't quite reach the minimum. Generally the deviations from the typical cycle were not too bad, but occasionally the temperature minimum would be as much as 0.1° C off the average, sometimes for a few points in a row. What makes this phenomenon difficult to quantify is that the temperature cycle was clearly observed to be more chaotic in some experiments than in others. It is not obvious why this should be, but it does explain why the model fits some data sets more poorly than average. From a statistical point of view, the unpredicable temperature deviations represent a breakdown in the assumption that the measurement errors are normally distributed.

Of greater concern than isolated "bad" data points, are identifiable regions in which several points in a row have low Q values. There are two such regions: the first data set in which [PhCOOH] was varied (figure 3.23b) shows many bad data points in a row, and all of the data collected at high $[Ru]_o$ (figures 3.23a and 3.24a) have low Q values.

The fact that very poor fits were obtained for the first data set in which [PhCOOH] was varied (figure 3.23b) was what prompted the repetition of all these experiments, to see if this was a reproducible trend. The second set of data, however (figure 3.24b), was of quality comparable to the data obtained generally for the $[O_2]$ and $[Ru]_o$ dependence experiments. A careful examination of the plots of $[Et_2SO]$ vs. t for the first data set in which [PhCOOH] was varied (see appendix 3) shows no obvious systematic deviations of the theoretical curves from the experimentally obtained data points; however, the scatter of the data points is much greater in these plots than in other data sets. Moreover, the $k_{obs}$ vs. [PhCOOH] plots also show considerable scatter relative to the other data sets. The high scatter is most likely attributable to the fact that this was the first set of data collected, and the technique required to obtain reproducible data had not yet been "perfected". The second set of $k_{obs}$ vs. [PhCOOH] data, collected several months after the first, has generally higher Q values for the raw data, and much less scatter in the replotted data.

The cluster of low Q values observed at higher $[Ru]_o$ is of greater interest. In this case there is no obvious source of error which could account for the fact that in all of the experiments in which $[Ru]_o > 0.5$ mM, the $[Et_2SO]$ vs. t data (appendix 3) are poorly fitted by the proposed rate law. It appears that in these cases the low Q values may be indicating a real flaw in the proposed model, which becomes apparent at higher $[Ru]_o$ concentrations. Inspection of the complete set of graphs listed in appendix 3 shows that generally the theoretical curves arch over more than the experimental points. For experiments in which the total accumulation of $Et_2SO$ is small, the scatter due to experimental uncertainty tends to obscure this trend, but for experiments in which $Et_2SO$ accumulation over the course of the reaction is high (e.g. graphs A3.1.1.7-A3.1.1.10), the predicted curvature in the graphs is more pronounced, and the deviation of the experimental points from the predicted curve is clearly visible. In the case of experiments carried out at the highest $[Ru]_o$, the arch in the theoretical curves is such that the curves are outside the error bars of a significant number of the experimental points.

A smaller than predicted curvature in the experimental $[Et_2S]$ vs. t data means that the rate at which the reaction is slowing down with time is lower than predicted. Now recall that accumulation of supposedly unreactive Ru(OEP)($Et_2S$)($Et_2\underline{S}O$) as the reaction progresses is the only pathway included in the model by which $Et_2SO$ production can slow down. Therefore one possible explanation for the smaller than predicted curvature in the experimental [$Et_2SO$] vs. t data is that the mixed sulfide/sulfoxide complex perhaps reacts with $O_2$ to some degree; as mentioned in section 3.3, the energy provided by yellow light is sufficient to allow this process to occur. If $Ru^{III}(OEP)(Et_2S)(Et_2\underline{S}O)^+O_2^-$ is indeed produced, then the rate law expressed in equations 3.37-3.41 could be modified to include the reaction of Ru(OEP)($Et_2S$)($Et_2\underline{S}O$) with $O_2$, but there is a conceptually simple (and useful) way to correct for its effect, using the equations exactly as written. Combining equations 3.1 and 3.2 from section 3.3 gives the expression:

$$\begin{aligned}&Ru^{III}(OEP)(Et_2S)(Et_2\underline{S}O)^+X^- + Ru(OEP)(Et_2S)_2 \rightarrow \\ &\qquad Ru^{II}(OEP)(Et_2S)(Et_2\underline{S}O) + Ru^{III}(OEP)(Et_2S)_2{}^+X^- \quad \Delta G^\circ = -39\ \mathrm{kJ/mol} \qquad 3.63\end{aligned}$$

where X is either $O_2$ or PhCOO. Therefore the one-electron transfer from $Ru^{II}(OEP)(Et_2S)_2$ to $Ru^{III}(OEP)(Et_2S)(Et_2\underline{S}O)^+X^-$ is thermodynamically favoured. Furthermore, the electron exchange is likely to be fast, as transfer from $Ru(OEP)(Et_2S)_2$ to $Ru(OEP)(Et_2S)_2{}^+X^-$ is fast (see section 2.5). According to equation 3.63, $Ru^{II}(OEP)(Et_2S)(Et_2\underline{S}O)$ can be thought of as an "antenna", collecting the light energy required for electron transfer to occur, and eventually transferring it to $Ru(OEP)(Et_2S)_2$. Experimentally this energy transfer should have the effect of making $\psi$ lower than expected. Recall that $\psi$ is the ratio of the integral extinction coefficients of Ru(OEP)($Et_2S$)($Et_2\underline{S}O$) and $Ru(OEP)(Et_2S)_2$; if some of the light energy absorbed by

$Ru(OEP)(Et_2S)(Et_2\underline{S}O)$ eventually leads to the production of $Ru(OEP)(Et_2S)_2{}^+X^-$, it will appear as if $Ru(OEP)(Et_2S)_2$ is absorbing more strongly, and $Ru(OEP)(Et_2S)(Et_2\underline{S}O)$ less strongly than expected, thus resulting in a lower $\psi$ value.

To test this hypothesis, all of the calculations were repeated, but this time $\psi$ was left as an adjustable parameter, and a 2-dimensional $\chi^2$ minimization routine was used to simultaneously obtain the best values of $\psi$ and $k_{obs}$ (the program used for the minimization is reported in appendix 1). This procedure yielded an average $\psi$ value of $0.6 \pm 0.2$. An important observation about the results of this analysis is that the variation in $\psi$ was found to be independent of $[Ru]_o$, [PhCOOH], or $[O_2]$, while $k_{obs}$ increased with all three concentrations. According to the proposed model this is expected, since $\psi$ is a true constant, while $k_{obs}$ is only constant while $[Ru]_o$, [PhCOOH] and $[O_2]$ are held constant. Unfortunately, the rather large scatter seen for the values of both $\psi$ and $k_{obs}$ tends to obscure any trends which might be of interest. Therefore, instead of using these data for further analysis, the calculations were repeated again, this time fixing $\psi$ at 0.6, and varying only $k_{obs}$. Of course this means that the uncertainties obtained for the $k_{obs}$ values will be artificially low; however, the important question is whether choosing a $\psi$ value other than 0.86 gives better fits of the experimental data *overall.*

Figure 3.26 shows the Q vs. concentration plots, where Q is the goodness of fit parameter obtained by fitting equations 3.37-3.41 to the data, with $\psi$ fixed at 0.6, and $k_{obs}$ adjusted to minimize $\chi^2$. The Q values for the experiments carried out at high $[Ru]_o$ are now quite good, and in fact the Q values overall are better and more randomly distributed than those obtained for $\psi = 0.86$. Exceptions are the data obtained in the initial acid dependence studies but, as mentioned before, these data were probably perturbed by

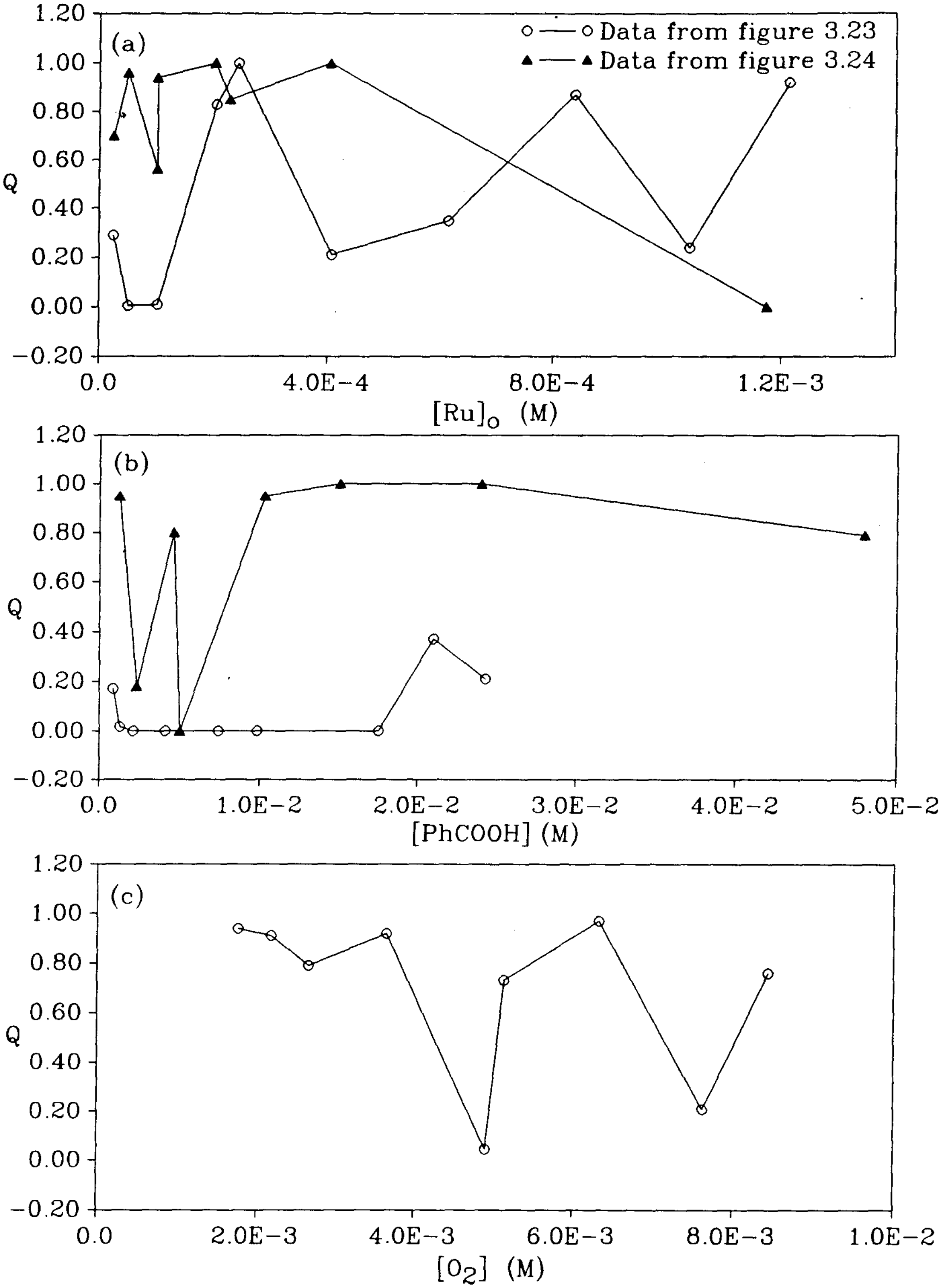

Figure 3.26. Plots of the goodness of fit parameter (Q) vs.: (a) $[Ru]_o$; (b) [PhCOOH]; (c) $[O_2]$ for the fitting procedures illustrated in figures 3.21 and 3.22, and assuming that $\psi$ = 0.6 (see text for details).

uncharacteristically high experimental errors.

There is, of course, another possible explanation for why equations 3.37-3.41 fit the data better if $\psi$ is set at 0.6 rather than 0.85, and that is that the photochemical effect could be initiated by a charge-transfer transition (or transitions) rather than by the $\pi$-$\pi^*$ transitions which give rise to the $\alpha,\beta$ bands (i.e. assumption (c) from the begining of this section could be wrong). If there is in fact a band hidden under the $\alpha,\beta$ envelope originating from a metal-to porphyrin charge-transfer, it is impossible to directly evaluate $\psi$ for this band. Therefore, if this charge transfer is responsible for initiating the photochemical reaction, $\psi$ would have to be treated as an adjustable parameter in a kinetic analysis, as described in the previous paragraphs. Further evidence that a charge-transfer transition is indeed responsible for the observed photochemistry is presented later in this section.

Another simplification made in deriving the rate law was that no irreversible decomposition of the Ru(OEP)($Et_2S$)$_2$ catalyst occurred (assumption (d)). Any such degradation would cause the experimentally observed rate of $Et_2SO$ production to decrease more rapidly than predicted. As mentioned above, the experimentally observed rate actually decreased *less* rapidly than predicted. This doesn't rule out catalyst degradation (indeed, slow degradation is observed experimentally by uv/vis spectroscopy; section 3.3), but it does mean that any effect on the $O_2$-uptake due to the degradation is experimentally undetectable, or masked.

In conclusion, in order for the mechanism in figure 3.8 to explain the kinetic data, one or both of the assumptions (b) and (c), listed at the beginning of the section, must be relaxed. In so doing, the resultant modification in the rate law (i.e. empirically changing the value of $\psi$ to fit the data) will automatically compensate for any effect which catalyst degradation might have upon the change in reaction rate with time. Note that the values of $K_{m3}$, $K_{m4}$ and $v_m$, derived by plotting $k_{obs}$ vs. $[Ru]_o$, [PhCOOH] and $[O_2]$ (figures 3.23 and 3.24), are only marginally affected by using $\psi = 0.6$ rather than $\psi = 0.86$.

The conclusions from the above analysis may appear somewhat inexplicit; however, the fact that equations 3.37-3.41 can be made to fit the kinetic data is significant, even if this could only be done by adjusting $\psi$ arbitrarily. One important point is that even if equations 3.37-3.41 are considered to be completely empirical, they still give values of the initial rates (i.e. $2k_{obs}$) which are much better than could be obtained from estimating tangent lines at the origin.

Another point worth mentioning is that not all of the mechanisms which could be reasonably proposed in the absence of a kinetic analysis will fit the experimental data. For example, figure 3.8 shows an alternate pathway (labelled "internal rearrangement"), by which $Ru(OEP)(Et_2S)(Et_2S\underline{O})$ isomerizes directly to $Ru(OEP)(Et_2S)(Et_2\underline{S}O)$, without the sulfoxide dissociating into the bulk of the solution. A rate law was derived allowing for internal sulfoxide rearrangement, and tested in the same way as the dissociative model described thus far (this represents a relaxation of assumption (f), listed at the begining of this section). The results of this analysis clearly show that the internal rearrangement cannot be an important pathway, assuming that the scheme proposed in figure 3.8 is otherwise a reasonable interpretation of the reaction mechanism. A detailed discussion of the analysis will not be included here (some theoretical elaboration is included in section 4.3.3.1), but the results can be easily understood by looking at one of the experiments in which the alternate model fails most noticeably. Consider the case in which internal rearrangement is assumed to be the only pathway by which $Ru(OEP)(Et_2S)(Et_2S\underline{O})$ can rearrange to $Ru(OEP)(Et_2S)(Et_2\underline{S}O)$ (i.e. $k_{14} = 0$). If this were the situation, then the maximum rate for the oxidation reaction would be given by $2k_3[Ru]_o$. This rate would be attained for a rate determining loss of $Et_2SO$ from the mixed thioether/sulfoxide species; i.e. $k_{obs}$ has to be sufficiently large, so that all of the $Ru(OEP)(Et_2S)_2$ is rapidly converted to $Ru(OEP)(Et_2S)(Et_2\underline{S}O)$. Figure 3.27 shows the results obtained for an experiment in which the reaction mixture initially contained 0.0255 mM $[Ru(OEP)(Et_2S)_2]$, 24.4 mM [PhCOOH], and 0.742 M $[Et_2S]$, under 0.813 atm $O_2$. The solid curve in the figure represents the fit obtained from equations 3.37-3.41 (with $\psi = 0.85$), while the dashed line is the line obtained for

$$[Et_2SO] = 2k_3[Ru]_o t \tag{3.64}$$

This line falls somewhat below the experimental data, meaning that the rate at which $[Et_2SO]$ is produced exceeds that which is possible if $k_3$ is the rate limiting step. This in itself is significant, but not conclusive evidence that the internal rearrangement model does not work. After all, if the assumption that $Ru(OEP)(Et_2S)(Et_2\underline{S}O)$ does not react with $O_2$ is relaxed, then the theoretical line could be made to go through the experimental points. The main problem is that if the internal rearrangement route is assumed, modelling studies show that $Ru(OEP)(Et_2S)(Et_2\underline{S}O)$ rapidly builds up to a near steady state in the first few seconds of reaction, after which the rate of $Et_2SO$ production should be much closer to linear than is observed experimentally. Note that relaxing the assumption that $Ru(OEP)(Et_2S)(Et_2\underline{S}O)$ does not react with $O_2$ does not correct this

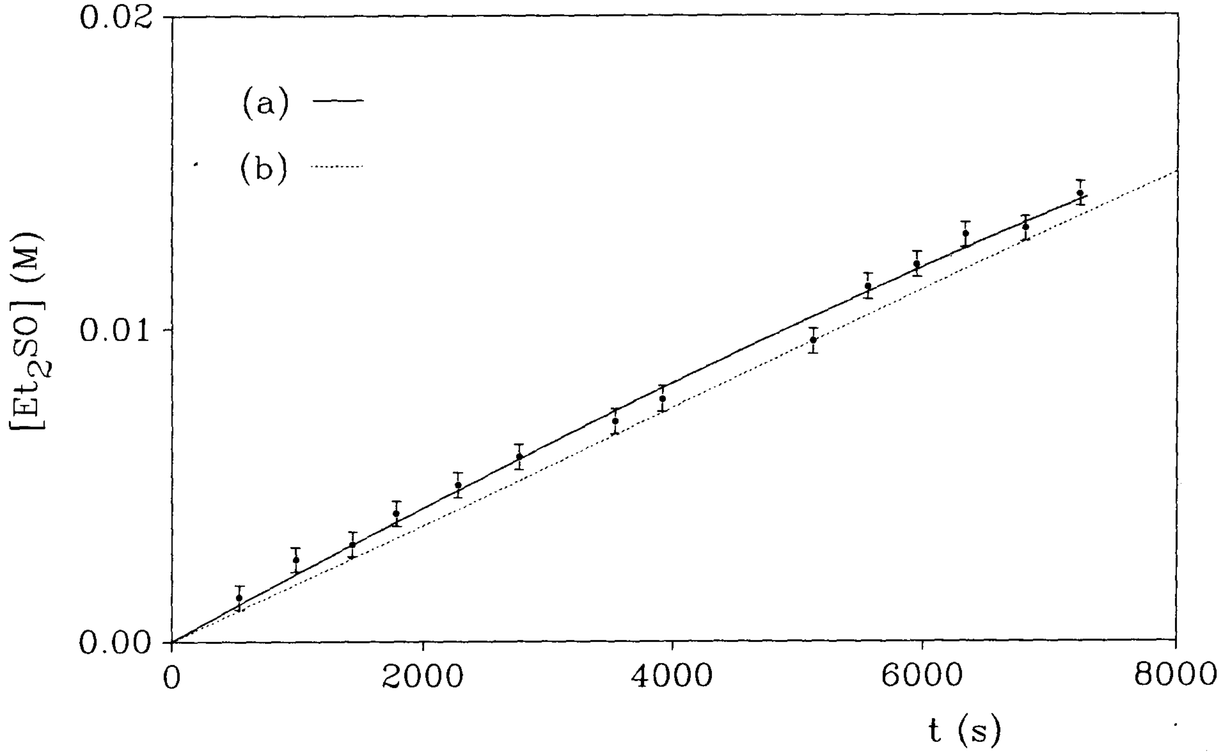

Figure 3.27. A plot of $[Et_2SO]$ vs. time, fitted using: (a) the least squares procedure described in the text; (b) the function $[Et_2SO] = 2k_3[Ru]_ot$. For this experiment, the initial concentrations of all the reagents are: $[Ru(OEP)(Et_2S)_2]$ = 0.0253 mM; [PhCOOH] = 24.4 mM; $[O_2]$ = 7.63 mM; $[Et_2S]$ = 0.742 M.

problem; Ru(OEP)($Et_2S$)($Et_2\underline{S}O$) will still accumulate to a maximum value within a few seconds, after which the rate of $Et_2SO$ production will be essentially linear. If the internal rearrangement step is assumed to be significant, then it is necessary to invoke irreversible catalyst degradation (or some other, as yet unidentified mechanism) as a cause for the observed decrease in [$Et_2SO$] production with time. Given that the rate law derived without invoking internal rearrangement fits the collected data quite well, there seems no reason to consider these possibilities.

The next point of discussion is an analysis of the parameters obtained from fitting the plots of $k_{obs}$ vs. $[Ru]_o$, [PhCOOH], and [$O_2$]. Table 3.3 lists these parameters. No effort was made to estimate the uncertainty in the $k_{obs}$ values directly from the raw data; the error bars in figures 3.23 and 3.24 were calculated during the least-squares fitting procedures, assuming that the proposed models accurately described the data. This means that no independent statistical estimate of the goodness-of fit can be made for the replot analyses. Note, however, that the scatter of the experimental points about the theoretical lines is fairly random, which tends to suggest that any deviations of the experimental points from the theoretical curve are due to experimental errors, rather than to a failure of the model (the latter would generally lead to systematic over- or undershooting by the theoretical curve of several experimental points in a row).

As previously mentioned, the first $k_{obs}$ vs. [PhCOOH] data set obtained were of rather poor quality, and so only the parameters obtained from the analysis of the second data set are referred to in subsequent discussions. The calculated uncertainties in the parameters obtained from fitting the $k_{obs}$ vs. [$O_2$] plots are also quite large (14 % for $p_3$ and 20 % for $K_{m3}$). In this case the large uncertainties do not arise from unusually high scatter of the data, but rather from the fact that the $[O_2]$ concentration range studied was fairly small; at the highest $[O_2]$ studied, $k_{obs}$ was only about 40% of its maximum value. In effect this means that the maximum value of $k_{obs}$ is being estimated by a rather long extrapolation, and the degree of curvature in the plot (reflected by $K_{m3}$) is being estimated from the curvature in a comparatively straight segment of the total curve.

Despite the uncertainty in the calculated value of $K_{m3}$, this value provides some interesting insights. Recall that $K_{m3}$ is the ratio $k_{-5}/k_6$ (equation 3.45), where $k_{-5}$ is the first order rate constant for the decay of the $Ru^{II}(OEP)^*(Et_2S)_2$ species back to the ground state, and $k_6$ is the second order rate constant governing the reaction of the excited species with $O_2$ (see figures 3.5a and 3.8). The value obtained for $K_{m3}$ ($0.014 \pm 0.003$ M) means that $k_6$ is about 70 times greater than $k_{-5}$. As $k_6$ is a second order rate constant, its magnitude cannot be greater than about $10^{10}$ $M^{-1}s^{-1}$, which is the upper limit imposed by the rate at which two species in solution diffuse towards each other.[13b] This in turn means that $k_{-5}$ cannot be greater than about $10^8$ $s^{-1}$; however, as the following analysis suggests, the assumption made so far, that the $\alpha$, $\beta$ absorbance bands for the porphyrin $\pi$-$\pi^*$ transitions are responsible for the observed photochemistry, leads to the conclusion that $k_{-5}$ should actually be $>>10^8$ $s^{-1}$.

The rate constant for the decay of a photoexcited state can be expressed as the sum of various more elementary rate constants; for $k_{-5}$ one could write

$$k_{-5} = k_f + k_{other} \qquad 3.65$$

where $k_f$ is the rate constant for fluorescence emmission, and $k_{other}$ is the rate constant for deactivation via other processes, such as intersystem crossing/phosphorescence, and various radiationless processes.[7,8,22a] There is a useful approximate relationship between the magnitude of $k_f$ and that of the extinction coefficient at the absorbance peak:[22b]

$$k_f \approx (10^4 \epsilon_{max})\ s^{-1} \qquad 3.66$$

For the $\alpha$ band at 525 nm, $\epsilon_{max}$ is $2.5 \times 10^4\ M^{-1}cm^{-1}$ (see section 2.2.4.2), and so $k_f$ should be about $2\text{-}3 \times 10^8\ s^{-1}$. Experiments to investigate the optical emission properties of the synthesized Ru(OEP) complexes were not done, but previous studies by other groups have found that Ru(Porp) complexes in general show negligible fluorescence.[8] This implies that the rate constant for the decay of the photoexcited state by processes other than fluorescence must be several orders of magnitude > $k_f$, i.e. the excited state is quenched via pathways alternative to fluorescence. This in turn suggests that $k_{-5}$ should be $>> 10^8\ s^{-1}$, which is in contradiction with the conclusions drawn from the value of $K_{m3}$.

This analysis provides evidence that the observed photochemistry is not due to $\pi$-$\pi^*$ transitions (as suggested in figures 3.5a and 3.8), but rather to a weaker metal-to-porphyrin charge-transfer transition, hidden under the $\alpha/\beta$ absorption manifold (as suggested in figure 3.5b, p. 98). A charge transfer transition such as the one pictured in figure 3.5b ($k_5$ step) would be symmetry forbidden (see figure 3.4);[8] accordingly, $\epsilon_{max}$ and therefore $k_{-5}$ would be much smaller, and more reconcilable with the calculated $K_{m3}$ value. Furthermore, if a specific charge transfer band is responsible for the observed photochemistry, this provides a more logical explanation as to why it is specifically light above 480 nm which is necessary, even though the Soret band at 407 nm is both more energetic and more intense (see section 3.3).

Modifying the overall mechanism proposed in figure 3.8 with the photochemistry of figure 3.5b does not affect the form of the rate equations; however, the parameters $K_{m4}$, $v_m$ (and $v_{m'}$) have new meanings (cf. section 4.3.3):

$$K_{m4} \equiv k_{-5'}k_{-6'}/(k_7(k_{6'} + k_{-5'})) \quad \text{(cf. equation 3.46)} \qquad 3.67$$

$$v_m \equiv 0.5c_l \quad \text{(cf. equation 3.44)} \qquad 3.68$$

$$v_{m'} \equiv 0.5c_{l'} \quad \text{(cf. equation 3.62)} \qquad 3.69$$

The fact that modifying the light dependence does not affect the form of the derived rate equations, given the data available, shows that it is unwise to attempt further interpretation of the data, without first doing more detailed experiments focussed on the photochemical phenomenon. However, it is worth considering one point, which could be of importance in designing future experiments.

If the expressions obtained for $v_m$ and $v_{m'}$ in equations 3.68 and 3.69 are compared with those obtained for the mechanism of figure 3.8 (equations 3.44 and 3.62, respectively), an important difference is noted. In the case of the modified mechanism, $v_m$ and $v_{m'}$ are simply equal to half of the geometrical parameters $c_l$ and $c_{l'}$, while in the original mechanism these parameters were each multiplied by a factor of $k_7/(k_{-6'} + k_7)$. Now, because the $c_l$ (or $c_{l'}$) parameter is dependent only on the geometry of the apparatus and on the intensity of the light source, this parameter could be obtained experimentally for a given apparatus setup by measuring the rate of a completely different photochemical reaction, for which the maximum rate was known to be dependent solely on the geometry of the apparatus. Then, the calculated value of $v_m$ could be checked to see if it was equal to $0.5c_1$, or whether it was significantly lower. In practice, this experiment would be much simpler if a monochromatic light source were utilized; however, in other respects, a crude apparatus such as the one used for this thesis work would be adequate.

# NOTES AND REFERENCES
# FOR CHAPTER 3

1. This pressure was high enough to drive the syringes at the 35° C temperature reported in this work; studies not reported here showed that for higher temperatures the drive syringes become stiffer, and higher pressures are necessary.

2. See for example: Thorburn, I. S. M.Sc. Dissertation, The University of British Columbia, Vancouver, B. C., 1980.

3. a) *The Handbook for Chemistry and Physics*, 62nd ed., Weast, R. C.; Astle, M. J. Eds., Chemical Rubber Company, Boca Raton, Fla., 1981; p. D-192. The effect of diethylsulfide on the total solvent vapour pressure was neglected in this series of experiments. b) *IUPAC Solubility Data Series*, Battino, R., Kertes, A. S., Eds., Pergamon Press, Elmsford, N. Y., 1981; Vol. 7, p. 250.

4. Bevington, Philip R. *Data Reduction and Error Analysis for the Physical Sciences*, McGraw-Hill, New York, N. Y., 1969, Chapter 11.

5.Press, W. H.; Flannery, B. P.; Teukolsky, S. A.; Vetterling, W. T. *Numerical Recipes (the Art of Scientific Computing)*, Cambridge University Press, New York, N. Y., 1987. (a) Chapter 14; this chapter is an excellent treatise on data modelling. (b) Chapter 2 discusses singular value decomposition, and solution of linear equations in general. (c) Chapters 10 (function minimization) and 15 (solution of differential equations).

6. Reference (4) is for the main book, which contains extensive mathematical background for the relevant programs. It is available in three different versions, with the routines in Fortran, Pascal, or C. The Quick Basic versions are found in a separate book: Sprott, J. C. *Numerical Recipes in Basic (Routines and Examples)*, Cambridge University Press: New York, N. Y., 1991. The latter does not contain a detailed mathematical background of the programs. All four books have the same chapters.

7. Gouterman, M. In *The Porphyrins*, Dolphin, D., Ed., Academic Press, New York, N. Y., 1978; Vol. III, Chapter 1.

8. Antipas, A.; Buchler, J. W.; Gouterman, M.; Smith, P. D. *J. Am. Chem. Soc.* **1978**, *100*, 3015.

9. (a) James, B. R.; Pacheco, A. A.; Rettig, S. J.; Ibers, J. A. *Inorg. Chem.* **1988**, *27*, 2414.
(b) Barley, M.; Becker, J. Y.; Domazetis, G.; Dolphin, D.; James, B. R. *Can. J. Chem.* **1983**, *61*, 2389.

10. Brown, G. M.; Hopf, F. R.; Ferguson, J. A.; Meyer, T. J.; Whitten, D. G. *J. Am. Chem. Soc.* **1973**, *95*, 5939.

11. Barnard, D.; Bateman, L.; Cuneen, J. I. In *Organic Sulfur Compounds*, Kharasch, N., Ed., Pergamon Press, New York, N. Y., 1961; Vol. I, Chapter 21.

12. Pacheco, A. A. M. Sc. Dissertation, The University of British Columbia, Vancouver, B. C., 1986.

13. Laidler, K. J. *Chemical Kinetics*, 3rd ed, Harper and Row, New York, N. Y., 1987. a) e.g. Chapter 10; b) pp. 212-222.

14. For a full discussion on the meanings of $\chi^2$ and Q, see reference 5a; however, the following summary may prove useful. Suppose we have a set of data points, each denoted by $(y_{obs})_i$, and each with an associated measurement error $\sigma_i$. Now suppose that, according to a theoretical model, we calculate values $(y_{cal})_i$, corresponding to each of the $(y_{obs})_i$. Then, assuming that the measurement errors are random and normally distributed, a) $\chi^2 \equiv \sum (((y_{obs})_i-(y_{cal})_i)^2/\sigma_i)$; b) Q gives the probability (as a number between 0 and 1) of obtaining this $\chi^2$ value (or a higher one) if the model is assumed to be correct. Clearly, if Q is very low, then the model could be wrong. In practice, reference 5a suggests that the odd Q value as low as $10^{-3}$ may be tolerated if the distribution of the measurement errors is not perfectly normal.

15. Jaswal, J. S.; Rettig, S. J.; James, B. R. *Can. J. Chem.* **1990**, *68*, 1808.

16. Eaton, S. S.; Eaton, G. R.; Holm, R. H. *J. Organometal. Chem.* **1972**, *39*, 179.

17. Bonnet, J. J.; Eaton, S. S.; Eaton, G. R.; Holm, R. H.; Ibers, J. A. *J. Am. Chem. Soc.* **1973**, *95*, 2141.

18. Eaton, G. R.; Eaton, S. S. *J. Am. Chem. Soc.* **1975**, *97*, 235.

19. Buchler, J. W.; Kokisch, W.; Smith, P. D. *Struct. Bonding* **1978**, *34*, 79.

20. Rajapakse, N.; James, B. R.; Dolphin, D. *Catal. Lett.* **1989**, *2*, 219.

21. Huheey, J. E. *Inorganic Chemistry*, 2nd ed., Harper and Row, New York, N. Y., 1978; Chapter 11.

22. Turro, N. J. *Modern Molecular Photochemistry*, University Science Books, Mill Valley, CA., 1991; a) p. 176; b) p. 90.

# CHAPTER 4

# RATE LAW DERIVATION FOR THE $O_2$-OXIDATION OF DIETHYLSULFIDE CATALYZED BY $Ru(OEP)(Et_2S)_2$

## 4.1 Introduction

In the last chapter a mechanism was suggested to account for the catalytic oxidation of $Et_2S$ to $Et_2SO$ by $Ru(OEP)(Et_2S)_2$, and a rate law based on this mechanism was shown to accurately describe the quantitative production of $Et_2SO$ under a variety of experimental conditions, at least over a time period of 2h. In addition, the equilibria between $Ru(OEP)(Et_2S)_2$, $Ru(OEP)(Et_2S)(Et_2SO)$ and $Ru(OEP)(Et_2SO)_2$ were studied independently, and rate laws for the net substitution processes verified experimentally. This chapter gives the mathematical derivation of the rate laws for both the overall catalytic cycle and the isolated equilibria. Most of the manipulations described are based on well established kinetic data treatments (see for example, reference 13 in the previous chapter). An exception is in the empirical treatment of the $Et_2S$ oxidation rate dependence on light, so this topic is given special attention.

## 4.2 The Equilibria between $Ru(OEP)(Et_2S)_2$, $Ru(OEP)(Et_2S)(Et_2SO)$ and $Ru(OEP)(Et_2SO)_2$

### 4.2.1 Rate Law Derivations

In the stopped-flow experiments described in the previous chapter, a solution containing $Ru(OEP)(Et_2SO)_2$ and $Et_2SO$ was mixed with another containing $Et_2S$. It was suggested that the ensuing pair of substitution reactions proceeded according the scheme outlined in figure 3.12, and shown again in figure 4.1. Experimentally, the first substitution of a coordinated $\mathrm{Et_2SO}$ by $\mathrm{Et_2S}$ was found to progress much faster than the second, so the assumption is made that $\mathrm{Ru(OEP)(Et_2SO)_2}$ and $\mathrm{Ru(OEP)(Et_2S)(Et_2\underline{S}O)}$ will achieve their equilibrium concentrations before the second substitution reaction has proceeded to any appreciable extent. This allows the rate laws for the two substitution processes to be derived independently, and the successful quantitative analysis of the kinetic data, described in section 3.4, substantiates this assumption.

For the purpose of the derivations that follow, some shorthand notation will be used to make the equations less cumbersome. Thus:

$\mathrm{Ru(OEP)(Et_2\underline{S}O)_2} \equiv \mathbf{1}$;    $\mathrm{Ru(OEP)(Et_2\underline{S}O)(Et_2S\underline{O})} \equiv \mathbf{1'}$;

$\mathrm{Ru(OEP)(Et_2\underline{S}O)} \equiv \mathbf{I_1}$,    first 5-coordinate intermediate;

$\mathrm{Ru(OEP)(Et_2S)(Et_2\underline{S}O)} \equiv \mathbf{2}$;

$\mathrm{Ru(OEP)(Et_2S)} \equiv \mathbf{I_2}$,    second 5-coordinate intermediate;

$\mathrm{Ru(OEP)(Et_2S)_2} \equiv \mathbf{3}$.

First Substitution Equilibrium

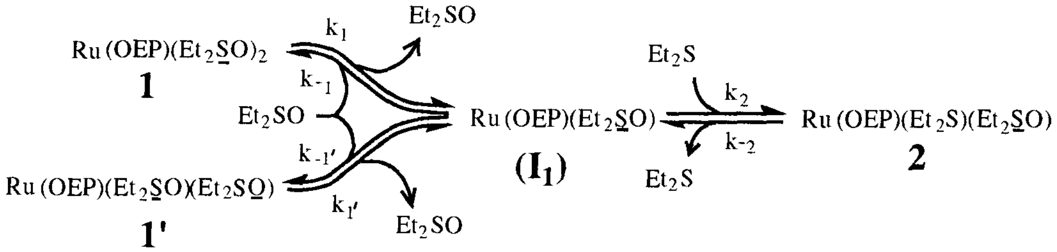
Ru(OEP)(Et$_2$SO)$_2$
1
$k_1$
$k_{-1}$
Et$_2$SO
Et$_2$SO
$k_{-1'}$
Ru(OEP)(Et$_2$SO)(Et$_2$SO)
1'
$k_{1'}$
Et$_2$SO
Ru(OEP)(Et$_2$SO)
(I$_1$)
Et$_2$S
$k_2$
$k_{-2}$
Et$_2$S
Ru(OEP)(Et$_2$S)(Et$_2$SO)
2

Second Substitution Equilibrium

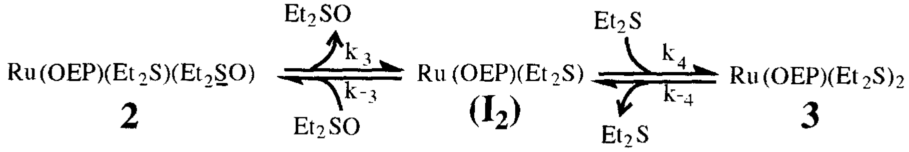
Ru(OEP)(Et$_2$S)(Et$_2$SO)
2
Et$_2$SO
$k_3$
$k_{-3}$
Et$_2$SO
Ru(OEP)(Et$_2$S)
(I$_2$)
Et$_2$S
$k_4$
$k_{-4}$
Et$_2$S
Ru(OEP)(Et$_2$S)$_2$
3

Figure 4.1. Mechanism proposed for the sequential substitution of two Et$_2$SO ligands by Et$_2$S, assuming that in solution the bis(sulfoxide) species exists as a mixture of the S- and O-bound linkage isomers.

For the first substitution process, the rate of appearance of **2** is described by the differential equation

$$d[\mathbf{2}]/dt = k_2[\mathbf{I_1}][Et_2S] - k_{-2}[\mathbf{2}] \tag{4.1}$$

Under conditions of high $[Et_2SO]$ and $[Et_2S]$, $\mathbf{I_1}$ is not expected to accumulate to any appreciable extent, so the following steady state approximation is made:

$$\begin{aligned} d[\mathbf{I_1}]/dt &= 0 \\ &= k_1[\mathbf{1}] + k_{1'}[\mathbf{1'}] + k_{-2}[\mathbf{2}] - [\mathbf{I_1}]((k_{-1} + k_{-1'})[Et_2SO] + k_2[Et_2S])) \end{aligned} \tag{4.2}$$

Thus the concentration of $\mathbf{I_1}$ will be given by

$$\mathbf{I_1} = (k_1[\mathbf{1}] + k_{-1'}[\mathbf{1'}] + k_{-2}[\mathbf{2}])/((k_{-1} + k_{-1'})[Et_2SO] + k_2[Et_2S]) \tag{4.3}$$

Using

$$k_{-1App} \equiv k_{-1} + k_{-1'} \tag{4.4}$$

and combining 4.3 and 4.4, and then substituting for $\mathbf{I}_1$ in 4.1 yields, after rearrangement,

$$\begin{aligned} d[\mathbf{2}]/dt = {} & k_2[Et_2S](k_1[\mathbf{1}] + k_{1'}[\mathbf{1'}])/(k_{-1App}[Et_2SO] + k_2[Et_2S]) \\ & - k_{-1App}k_{-2}[Et_2SO][\mathbf{2}]/(k_{-1App}[Et_2SO] + k_2[Et_2S]) \end{aligned} \qquad 4.5$$

Now, because the equilibrium between **1** and **1′** is independent of [Et$_2$S] and [Et$_2$SO], and because the stopped-flow analysis of section 3.4 showed that the equilibrium is not disturbed, even transiently, during the substitution process, the following relation holds at all times during the first substitution (and of course also the second) reaction:

$$K' = [\mathbf{1'}]/[\mathbf{1}] \qquad 4.6$$

where

$$K' \equiv k_1k_{-1'}/k_{1'}k_{-1} \qquad 4.7$$

Equation 4.6 can be used to eliminate [**1′**] from 4.5. Straightforward algebra results in the expression

$$\begin{aligned} d[\mathbf{2}]/dt = {} & k_1k_2k_{-1App}[Et_2S][\mathbf{1}]/(k_{-1}(k_{-1App}[Et_2SO] + k_2[Et_2S])) \\ & - k_{-1App}k_{-2}[Et_2SO][\mathbf{2}]/(k_{-1App}[Et_2SO] + k_2[Et_2S]) \end{aligned} \qquad 4.8$$

For any given experiment, the concentrations of [$Et_2S$] and [$Et_2SO$] remain essentially unchanged throughought; we therefore define two pseudo rate constants,

$$k_{1f} \equiv k_1k_2k_{-1App}[Et_2S]/(k_{-1}(k_{-1App}[Et_2SO] + k_2[Et_2S])) \qquad 4.9$$

$$k_{1r} \equiv k_{-1App}k_{-2}[Et_2SO]/(k_{-1App}[Et_2SO] + k_2[Et_2S]) \qquad 4.10$$

On defining $[Ru]_o$ as

$$[Ru]_o \equiv [1] + [1'] + [2] + [3] \qquad 4.11$$

and remembering that before the first equilibrium is established, the concentration of [**3**] is assumed to be zero, the combination of 4.6 and 4.11 yields

$$[1] = ([Ru]_o - [2])/(1 + K') \qquad 4.12$$

Now equations 4.8, 4.9, 4.10 and 4.12 can be combined to give

$$d[2]/dt = k_{1f}[Ru]_o/(1 + K') - [2](k_{1f}/(1 + K') + k_{1r}) \qquad 4.13$$

[**2**] is the only variable on the right hand side of equation 4.13, so it is convenient to define two more parameters; let

$$\theta_1 \equiv k_{1f}[Ru]_o/(1 + K') \qquad 4.14$$

$$\theta_2 \equiv k_{1f}/(1 + K') + k_{1r} \qquad 4.15$$

so that

$$d[\mathbf{2}]/dt = \theta_1 - \theta_2[\mathbf{2}] \qquad 4.16$$

This equation is integrated to give the desired expression for [**2**] as a function of time:

$$[\mathbf{2}] = (\theta_1/\theta_2)(1 - \exp(-\theta_2 t)) \qquad 4.17$$

Derivation of the rate law for the second substitution reaction begins by assuming that **1,1′** and **2** are in equilibrium, and that the concentration of **3** equals zero at the start of this reaction. The rate of appearance of **3** is then described by the differential equation

$$d[\mathbf{3}]/dt = k_4[\mathbf{I_2}][Et_2S] - k_{-4}[\mathbf{3}] \qquad 4.18$$

A treatment analogous to that used for the first equilibrium allows us to rewrite equation 4.18 in the form

$$d[\mathbf{3}]/dt = k_{2f}[\mathbf{2}] - k_{2r}[\mathbf{3}] \qquad 4.19$$

where

$$k_{2f} \equiv k_3k_4[Et_2S]/(k_{-3}[Et_2SO] + k_4[Et_2S]) \qquad 4.20$$

$$k_{2r} \equiv k_{-3}k_{-4}[Et_2SO]/(k_{-3}[Et_2SO] + k_4[Et_2S]) \qquad 4.21$$

$K_1$ is defined as the equilibrium constant between **1** and **2**, and therefore

$$K_1 = [\mathbf{2}][Et_2SO]/[\mathbf{1}][Et_2S] \qquad 4.22$$

Rearranging this expression and combining it with equations 4.6 and 4.11 gives

$$[Ru]_o = [\mathbf{2}][Et_2SO](1 + K')/K_1[Et_2S] + [\mathbf{2}] + [\mathbf{3}] \qquad 4.23$$

And on defining

$$K_{1App} \equiv K_1/(1 + K') \qquad 4.24$$

equation 4.23 becomes

$$[Ru]_o = [\mathbf{2}]([Et_2SO] + K_{1App}[Et_2S])/K_{1App}[Et_2S] + [\mathbf{3}] \qquad 4.25$$

which gives, after solving for **[2]**,

$$[\mathbf{2}] = ([\mathrm{Ru}]_o - [\mathbf{3}])K_{1App}[\mathrm{Et_2S}]/([\mathrm{Et_2SO}] + K_{1App}[\mathrm{Et_2S}]) \qquad 4.26$$

Let

$$\Lambda \equiv K_{1App}[\mathrm{Et_2S}]/([\mathrm{Et_2SO}] + K_{1App}[\mathrm{Et_2S}]) \qquad 4.27$$

Thus equation 4.19 can be rewritten as

$$d[\mathbf{3}]/dt = k_{2f}\Lambda[\mathrm{Ru}]_o - (k_{2f}\Lambda + k_{2r})[\mathbf{3}] \qquad 4.28$$

This equation is identical in form to equation 4.13, and integrates to

$$[\mathbf{3}] = (\theta_3/\theta_4)(1 - \exp(-\theta_4 t)) \qquad 4.29$$

where

$$\theta_3 \equiv k_{2f}\Lambda[\mathrm{Ru}]_o \qquad 4.30$$

$$\theta_4 \equiv k_{2f}\Lambda + k_{2r} \qquad 4.31$$

## 4.2.2 Correlation of Uv/Vis Absorbance Changes to the Derived Rate Laws

### 4.2.2.1 First Substitution Reaction

Experimentally, the reaction of $Ru(OEP)(Et_2SO)_2$ with $Et_2S$ was monitored by visible absorption spectroscopy. The first substitution was followed at 400.5 nm, which is the absorbance maximum for $Ru(OEP)(Et_2SO)_2$ solutions at 35° C. From the Beer-Lambert law we can write

$$\begin{aligned} A &= \epsilon_1'[\mathbf{1}] + \epsilon_{1'}'[\mathbf{1'}] + \epsilon_2'[\mathbf{2}] \\ &= (\epsilon_1' + \epsilon_{1'}'K')[\mathbf{1}] + \epsilon_2'[\mathbf{2}] \\ &= (\epsilon_1' + \epsilon_{1'}'K')[Ru]_o/(1 + K') + [\mathbf{2}](\epsilon_2' - (\epsilon_1' + \epsilon_{1'}'K')/(1 + K')) \qquad 4.32 \end{aligned}$$

The final form of equation 4.32 is obtained by substituting 4.6 for [**1'**], and then 4.12 for [**1**]. As defined, $\epsilon_n' \equiv \epsilon_n l$, where $l$ is the path length of the solution whose absorbance is being measured.

If $A_o$ is defined as the absorbance at t = 0, and $[\mathbf{1}]_o$,$[\mathbf{1'}]_o$ are the initial concentrations of **1** and **1'**, then

$$A_o = \epsilon_1'[\mathbf{1}]_o + \epsilon_{1'}'[\mathbf{1'}]_o \qquad 4.33$$

$$[Ru]_o = [\mathbf{1}]_o + [\mathbf{1'}]_o \qquad 4.34$$

Since **1** and **1'** are in equilibrium, equations 4.33,4.34 can be rewritten as

$$A_o = (\epsilon_1' + \epsilon_{1'}'K')[\mathbf{1}]_o \tag{4.35}$$

$$[Ru]_o = (1 + K')[\mathbf{1}]_o \tag{4.36}$$

Solving equation 4.36 for $[\mathbf{1}]_o$ and substituting into equation 4.33 yields

$$A_o = (\epsilon_1' + \epsilon_{1'}'K')[Ru]_o/(1 + K') \tag{4.37}$$

Let

$$\epsilon_{1App}' \equiv (\epsilon_1' + \epsilon_{1'}'K')/(1 + K') \tag{4.38}$$

then

$$A_o = \epsilon_{1App}'[Ru]_o \tag{4.39}$$

The last two expressions can be used to simplify equation 4.32:

$$A = A_o + (\epsilon_2' - \epsilon_{1App}')[\mathbf{2}] \tag{4.40}$$

If we define

$$\Delta\epsilon_1' \equiv \epsilon_2' - \epsilon_{1App}' \tag{4.41}$$

then equations 4.17, 4.40 and 4.41 can be combined to give the desired expression for the change in absorbance as a function of time:

$$A = \theta_1\Delta\epsilon_1'/\theta_2 + A_o - \theta_1\Delta\epsilon_1'\exp(-\theta_2 t)/\theta_2 \qquad 4.42$$

This equation is equivalent to equation 3.6 (p. 118) if we define

$$\alpha_1 \equiv \theta_1\Delta\epsilon_1'/\theta_2 + A_o \qquad 4.43$$

$$\begin{aligned}\beta_1 &\equiv A_o - \alpha_1 \\ &= -\theta_1\Delta\epsilon_1'/\theta_2 \qquad 4.44\end{aligned}$$

$$\gamma_1 \equiv \theta_2 \qquad 4.45$$

Equation 3.9 (p. 119), the expression for the initial rate of change of absorbance with time, also follows directly from equation 4.42:

$$\begin{aligned}v_{o1} &= -\gamma_1\beta_1 \\ &= \theta_1\Delta\epsilon_1' \qquad 4.46\end{aligned}$$

Rearranging equations 4.44 and 4.46 into the forms of equations 3.10 and 3.11 (p. 119) is straightforward, but somewhat tedious. The key steps are:

$$\beta_1 = -\theta_1\Delta\epsilon_1'/\theta_2$$

$$= -k_{1f}[Ru]_o\Delta\epsilon_1'/(k_{1f} + k_{1r}(1 + K'))$$

$$= -[Ru]_o\Delta\epsilon_1'/(1 + (k_{1r}/k_{1f})(1 + K')) \qquad 4.47$$

$$k_{1r}/k_{1f} = (k_{-1App}k_{-2}[Et_2SO]/(k_{-1App}[Et_2SO] + k_2[Et_2S]))$$

$$x(k_1k_2k_{-1App}[Et_2S]/(k_{-1}(k_{-1App}[Et_2SO] + k_2[Et_2S]))^{-1}$$

$$= k_{-1}k_{-2}[Et_2SO]/k_1k_2[Et_2S]$$

$$= [Et_2SO]/K_1[Et_2S] \qquad 4.48$$

Substituting 4.48 into 4.47, and rearranging, gives the final desired expression for $\beta$:

$$\beta_1 = -[Ru]_o\Delta\epsilon_1'[Et_2S]/((K_{1App})^{-1}[Et_2SO] + [Et_2S]) \qquad (3.10)\ 4.49$$

Similarly for $v_{o1}$:

$$v_{o1} = \theta_1\Delta\epsilon_1'$$

$$= k_{1f}[Ru]_o\Delta\epsilon_1'/(1 + K')$$

$$= (k_1k_2k_{-1App}[Et_2S]/(k_{-1}(k_{-1App}[Et_2SO] + k_2[Et_2S])))([Ru]_o\Delta\epsilon_1'/(1 + K'))$$

$$= (k_{-1App}/(k_{-1}(1 + K')))(k_1[Et_2S][Ru]_o\Delta\epsilon_1'/(K_{m1}[Et_2SO] + [Et_2S]) \qquad 4.50$$

$$\begin{aligned} k_1k_{-1App}/k_{-1}(1 + K') &= k_1/(1 + K') + k_{-1'}k_1/(k_{-1}(1 + K')) \\ &= k_1/(1 + K') + k_{1'}/(1 + (K')^{-1}) \\ &\equiv k_{1App} \end{aligned} \qquad 4.51$$

Therefore

$$v_{o1} = k_{1App}[Ru]_o\Delta\epsilon_1'[Et_2S]/(K_{m1}[Et_2SO] + [Et_2S]) \qquad (3.11)\ 4.52$$

The subscript *App* emphasizes an important feature of equations 4.49 and 4.52; the two equations have forms identical to those which would be obtained if $Ru(OEP)(Et_2SO)_2$ were present as a single isomer; in this case, $K_{1App}$ would be replaced simply by $K_1$. In the same way, the parameter $\epsilon_{1App}'$ behaves like an extinction coefficient for a single species, $Ru(OEP)(Et_2SO)_2$, provided that all the experiments are being carried out at one temperature.

#### 4.2.2.2 Second Substitution Reaction

The second substitution reaction was followed at 402.8 nm, which is an isosbestic point for a mixture of $Ru(OEP)(Et_2SO)_2$ and $Ru(OEP)(Et_2S)(Et_2SO)$ at a total fixed concentration. The Beer-Lambert expression at any wavelength will be

$$A = (\epsilon_1' + \epsilon_{1'}'K')[1] + \epsilon_2'[2] + \epsilon_3'[3] \qquad 4.53$$

If equations 4.6 and 4.11 are used to eliminate [1] from equation 4.53, a little rearranging simplifies the latter to

$$A = A_o - \epsilon_{1App}'([2] + [3]) + \epsilon_2'[2] + \epsilon_3'[3] \tag{4.54}$$

At the isosbestic point chosen, $\epsilon_2' - \epsilon_{1App}' = 0$, and thus

$$A = A_o + [3](\epsilon_3' - \epsilon_{1App}') \tag{4.55}$$

Now if $\Delta\epsilon_2'$ is defined as

$$\Delta\epsilon_2' \equiv \epsilon_3' - \epsilon_{1App}' \tag{4.56}$$

the desired expression for [3] as a function of absorbance is obtained:

$$[3] = (A - A_o)/\Delta\epsilon_2' \tag{4.57}$$

which, when combined with equation 4.29, gives the absorbance change as a function of time:

$$A = \theta_3\Delta\epsilon_2'/\theta_4 + A_o - (\theta_3\Delta\epsilon_2'\exp(-\theta_4 t))/\theta_4 \tag{4.58}$$

Again this equation has the form of equation 3.6 (p. 118). For this particular system,

$$\alpha_2 = \theta_3\Delta\epsilon_2'/\theta_4 + A_o \qquad 4.59$$

$$\begin{aligned}\beta_2 &= A_o - \alpha_2 \\ &= -\theta_3\Delta\epsilon_2'/\theta_4\end{aligned} \qquad 4.60$$

$$\gamma_2 = \theta_4 \qquad 4.61$$

Also

$$v_{o2} = -\gamma\beta = \theta_3\Delta\epsilon_2' \qquad 4.62$$

Equations 4.60 and 4.62 need to be expanded to show the dependences of $\beta_2$ and $v_{o2}$ on $[Et_2S]$ and $[Et_2SO]$; again, this is a long but straightforward process, and only a sketch of the procedure need be given. From equations 4.20, 4.21, 4.27 and 4.60,

$$\begin{aligned}\beta_2 &= k_{2f}\Lambda\Delta\epsilon_2'[Ru_o]/(k_{2f}\Lambda + k_{2r}) \\ &= k_3k_4[Et_2S][Ru]_o\Lambda\Delta\epsilon_2'/(k_3k_4\Lambda[Et_2S] + k_{-3}k_{-4}[Et_2SO]) \\ &= [Et_2S][Ru]_o\Delta\epsilon_2'/([Et_2S] + [Et_2SO]\Lambda^{-1}K_2^{-1}) \\ \\ &= K_{1App}K_2[Ru]_o\Delta\epsilon_2'[Et_2S]^2/(K_{1App}K_2[Et_2S]^2 \\ &\quad + K_{1App}[Et_2S][Et_2SO] + [Et_2SO])\end{aligned} \qquad 4.63$$

Similarly, from equations 4.20, 4.27, and 4.62,

$$\begin{aligned} v_{o2} &= k_{2f}\Lambda[Ru]_o\Delta\epsilon_2' \\ &= (k_3[Ru]_o\Delta\epsilon_2'[Et_2S]/(K_{m2}[Et_2SO] + [Et_2S])) \\ &\quad x(K_{1App}[Et_2S]/([Et_2SO] + K_{1App}[Et_2S])) \\ &= k_3[Ru]_o\Delta\epsilon_2'[Et_2S]^2/((K_{m2}[Et_2SO] + [Et_2S])((K_{1App})^{-1}[Et_2SO] + [Et_2S]) \qquad 4.64 \end{aligned}$$

In theory, all of the desired equilibrium and rate constants should be obtainable from equations 4.63 and 4.64 (the value of $K_{1App}$ could also be determined independently from the study of the first substitution reaction). In practice, these equations prove to be very awkward to deal with numerically, but fortunately they are easily rearranged to the more tractable quadratic forms shown in equations 3.24 and 3.25 (p. 125):

$$[Et_2S]^2/\beta_2 = d_1[Et_2S]^2 + d_2[Et_2S] + d_3 \qquad (3.24)\ 4.65$$

$$[Et_2S]^2/v_{o2} = d_4[Et_2S]^2 + d_5[Et_2S] + d_6 \qquad (3.25)\ 4.66$$

where the parameters $d_1$-$d_6$ were previously defined in chapter 3 (p. 125). An analysis of the dependences of $[Et_2S]^2/\beta_2$ and $[Et_2S]^2/v_{o2}$ on $[Et_2S]$ at constant $[Et_2SO]$ yields the desired equilibrium and rate constants. Note, that if $d_3$ and $d_6$ are negligible relative to the other terms in equations 4.65 and 4.66, these equations simplify to the same linear form as equations 4.49 and 4.50.

## 4.3 Catalytic $O_2$-Oxidation of $Et_2S$ by $Ru(OEP)(Et_2S)_2$

### 4.3.1 General Rate Law Derivation

In section 3.3 a mechanism was proposed, by which $Ru(OEP)(Et_2S)_2$ could catalyze $O_2$-oxidation of $Et_2S$ in acidic benzene. Throughout section 3.5, several modifications to this mechanism were suggested, in order to account for some of the experimentally derived results. In this section and the next, only the original mechanism, outlined in figure 3.8 and reproduced on the following page for convenience, is considered. Using the methodology provided, it is not difficult to derive rate laws for the modified mechanisms; a brief sketch of the procedures involved, together with some additional theoretical considerations, are given in section 4.3.3.

According to the assumptions summarized in section 3.5.1 (pp. 140-141), the only Ru(OEP) species present in significant amounts during any given reaction are $Ru(OEP)(Et_2S)_2$ (**3**) and $Ru(OEP)(Et_2S)(Et_2\underline{S}O)$ (**2**); the $Ru(OEP)(Et_2SO)_2$ species (**1** and **1′**) are assumed to accumulate only negligibly over the time period monitored, and all other Ru(OEP) species are assumed to remain in small, steady state concentrations. The rates of change in concentration of the two major Ru(OEP) species are governed by the differential equations:

$$d[\mathbf{2}]/dt = k_{-3}[I_2][Et_2SO] - k_3[\mathbf{2}] \qquad 4.67$$

$$-d[\mathbf{3}]/dt = d[\mathbf{2}]/dt \qquad (3.38)\ 4.68$$

(where $I_2 \equiv Ru(OEP)(Et_2S)_2$). Again some shorthand notation will be used to make the

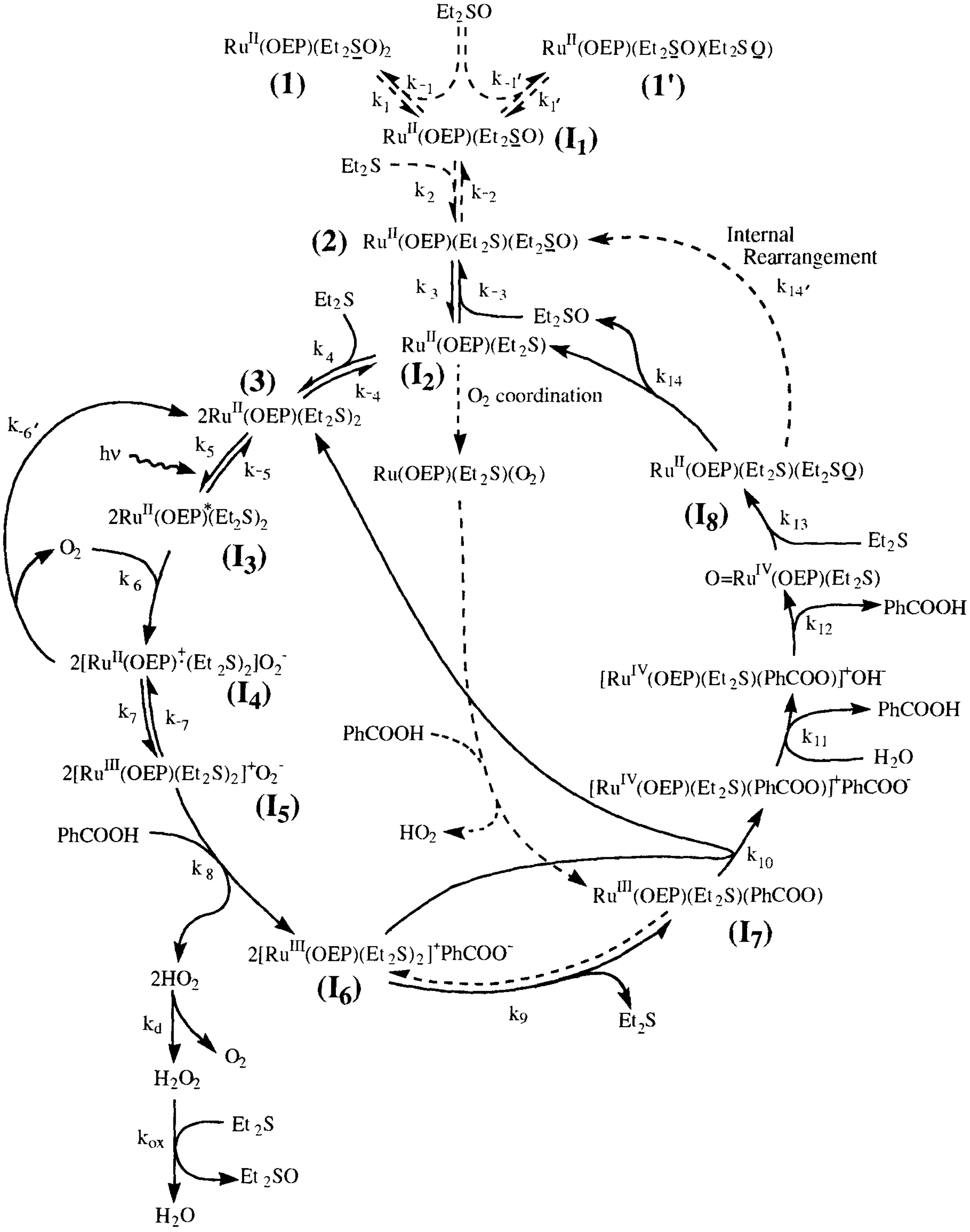

$Et_2SO$
$Ru^{II}(OEP)(Et_2\underline{S}O)_2$
(1)
$k_{-1}$
$k_1$
$k_{-1'}$
$k_{1'}$
$Ru^{II}(OEP)(Et_2\underline{S}O)(Et_2S\underline{O})$
(1')
$Ru^{II}(OEP)(Et_2\underline{S}O)$ ($I_1$)
$Et_2S$
$k_2$
$k_{-2}$
(2) $Ru^{II}(OEP)(Et_2S)(Et_2\underline{S}O)$
Internal Rearrangement
$k_{14'}$
$k_3$
$k_{-3}$
$Et_2SO$
$Et_2S$
$k_4$
$Ru^{II}(OEP)(Et_2S)$
($I_2$)
$k_{-4}$
$O_2$ coordination
$k_{14}$
(3)
$2Ru^{II}(OEP)(Et_2S)_2$
$k_{-6'}$
hν
$k_5$
$k_{-5}$
$Ru(OEP)(Et_2S)(O_2)$
$Ru^{II}(OEP)(Et_2S)(Et_2S\underline{O})$
($I_8$)
$k_{13}$
$Et_2S$
$2Ru^{II}(OEP)^*(Et_2S)_2$
($I_3$)
$O_2$
$k_6$
$O{=}Ru^{IV}(OEP)(Et_2S)$
$k_{12}$
PhCOOH
$2[Ru^{II}(OEP)^{+\cdot}(Et_2S)_2]O_2^-$
($I_4$)
$[Ru^{IV}(OEP)(Et_2S)(PhCOO)]^+OH^-$
$k_7$
$k_{-7}$
PhCOOH
PhCOOH
$k_{11}$
$H_2O$
$2[Ru^{III}(OEP)(Et_2S)_2]^+O_2^-$
($I_5$)
$[Ru^{IV}(OEP)(Et_2S)(PhCOO)]^+PhCOO^-$
PhCOOH
$HO_2$
$k_{10}$
$k_8$
$Ru^{III}(OEP)(Et_2S)(PhCOO)$
($I_7$)
$2[Ru^{III}(OEP)(Et_2S)_2]^+PhCOO^-$
$2HO_2$
($I_6$)
$k_9$
$Et_2S$
$k_d$
$O_2$
$H_2O_2$
$k_{ox}$
$Et_2S$
$Et_2SO$
$H_2O$

Figure 4.2. Mechanism proposed for the $O_2$-oxidation of $Et_2S$ to $Et_2SO$, catalyzed by $Ru(OEP)(Et_2S)_2$ and PhCOOH (dotted pathways imply that these processes can be neglected, or do not occur, under catalytic conditions; see the assumptions on pp. 140-141).

equations less cumbersome. Thus:

$I_3 \equiv \mathrm{Ru^{II}(OEP)^{*}(Et_2S)_2}$

$I_4 \equiv \mathrm{Ru^{II}(OEP)^{+\cdot}(Et_2S)_2O_2^{-}}$

$I_5 \equiv \mathrm{Ru^{III}(OEP)(Et_2S)_2{}^{+}O_2^{-}}$

$I_6 \equiv \mathrm{Ru^{III}(OEP)(Et_2S)_2{}^{+}PhCOO^{-}}$

$I_7 \equiv \mathrm{Ru^{III}(OEP)(Et_2S)(PhCOO)}$

$I_8 \equiv \mathrm{Ru^{II}(OEP)(Et_2S)(Et_2S\underline{O})}$

The steady state equation for $[I_2]$ will be:

$$k_{14}[I_8] + k_3[\mathbf{2}] + k_{-4}[\mathbf{3}] = [I_2](k_{-3}[\mathrm{Et_2SO}] + k_4[\mathrm{Et_2S}]) \tag{4.69}$$

All of the reactions between $k_{10}$ and $k_{14}$ are unbranched, and are assumed to be irreversible; therefore, $k_{14}[I_8] = k_{10}[I_6][I_7]$. Upon substituting for $k_{14}[I_8]$ and rearranging, equation 4.69 becomes

$$[I_2] = (k_{10}[I_6][I_7] + k_3[\mathbf{2}] + k_{-4}[\mathbf{3}])/(k_{-3}[\mathrm{Et_2SO}] + k_4[\mathrm{Et_2S}]) \tag{4.70}$$

Substituting for $[I_2]$ in equation 4.67 yields

$$d[\mathbf{2}]/dt = k_{-3}[Et_2SO](k_{10}[I_6][I_7] + k_3[\mathbf{2}] + k_{-4}[\mathbf{3}])/(k_{-3}[Et_2SO] + k_4[Et_2S]) - k_3[\mathbf{2}] \quad 4.71$$

Rearranging 4.71 and using $K_{m2} \equiv (k_{-3}/k_4)$ gives

$$\begin{aligned} d[\mathbf{2}]/dt = {} & k_{10}[Et_2SO][I_6][I_7]/([Et_2SO] + (K_{m2})^{-1}[Et_2S]) \\ & + k_{-4}[\mathbf{3}][Et_2SO]/([Et_2SO] + (K_{m2})^{-1}[Et_2S]) \\ & - k_3[Et_2S][\mathbf{2}]/(K_{m2}[Et_2SO] + [Et_2S]) \end{aligned} \quad 4.72$$

Recalling that $K_{m2}$ was found experimentally to be very close to 1 (table 3.2, p. 129), equation 4.72 can be simplified to

$$\begin{aligned} d[\mathbf{2}]/dt = {} & k_{10}[Et_2SO][I_6][I_7]/[Et_2S]_o + k_{-4}[Et_2SO][\mathbf{3}]/[Et_2S]_o \\ & - k_3[Et_2S][\mathbf{2}]/[Et_2S]_o \end{aligned} \quad 4.73$$

where $[Et_2S]_o \equiv [Et_2S] + [Et_2SO]$. The steady state relationships for $[I_3]$-$[I_7]$ are given by the following equations:

$$[I_3] = I_a/(k_{-5} + k_6[O_2]) \quad 4.74$$

(where $I_a$ is the amount of light absorbed by $Ru(OEP)(Et_2S)_2$ for each turn of the catalytic cycle; $I_a \equiv$ einsteins absorbed per liter per second).

$$k_6[O_2][I_3] + k_{-7}[I_5] = [I_4](k_{-6'} + k_7) \qquad 4.75$$

$$k_7[I_4] = [I_5](k_{-7} + k_8[PhCOOH]) \qquad 4.76$$

$$k_8[PhCOOH][I_5] = [I_6](k_9 + k_{10}[I_7]) \qquad 4.77$$

$$k_9[I_6] = k_{10}[I_6][I_7] \qquad 4.78$$

Combining equations 4.77 and 4.78 gives

$$k_8[PhCOOH][I_5] = 2k_{10}[I_6][I_7] \qquad 4.79$$

At the same time, combining equations 4.74, 4.75 and 4.76 gives

$$k_6[O_2]I_a/(k_{-5} + k_6[O_2]) + k_{-7}[I_5] = [I_5](k_{-7} + k_8[PhCOOH])(k_{6'} + k_7)/k_7 \qquad 4.80$$

A series of algebraic manipulations converts this last expression to

$$[I_5] = k_6k_7[O_2]I_a/((k_{-6'}k_{-7} + (k_{-6'}k_8 + k_7k_8)[PhCOOH])(k_{-5} + k_6[O_2])) \qquad 4.81$$

which, when combined with expression 4.79, yields

$$k_{10}[I_6][I_7] = 0.5k_6k_7k_8[PhCOOH][O_2]I_a \div((k_{-6'}k_{-7} + k_8(k_{-6'} + k_7)[PhCOOH])(k_{-5} + k_6[O_2])) \qquad 4.82$$

Now we can substitute for $k_{10}[I_6][I_7]$ in equation 4.73:

$$d[\mathbf{2}]/dt = 0.5k_6k_7k_8[PhCOOH][O_2][Et_2SO]I_a \div([Et_2S]_o(k_{-6'}k_{-7} + k_8(k_{-6'} + k_7)[PhCOOH])(k_{-5} + k_6[O_2])) + k_4[Et_2SO][\mathbf{3}]/[Et_2S]_o - k_3[Et_2S][\mathbf{2}]/[Et_2S]_o \qquad 4.83$$

Upon defining

$$K_{m3} \equiv k_{-5}/k_6 \qquad 4.84$$

$$K_{m4} \equiv k_{-6'}k_{-7}/((k_{-6'} + k_7)k_8 \qquad 4.85$$

$$v_{max} \equiv 0.5k_7/(k_{-6'} + k_7) \qquad 4.86$$

equation 4.83 can be rewritten in a somewhat more compact form:

$$d[\mathbf{2}]/dt = v_{max}[PhCOOH][O_2][Et_2SO]I_a \div([Et_2S]_o(K_{m3} + [O_2])(K_{m4} + [PhCOOH])) + k_4[Et_2SO][\mathbf{3}]/[Et_2S]_o - k_3[Et_2S][\mathbf{2}]/[Et_2S]_o \qquad 4.87$$

Expressions for the rate of change in $[Et_2SO]$, $[Et_2S]$ and $[O_2]$ are now required. For $[Et_2SO]$:

$$\begin{aligned} d[Et_2SO]/dt &= k_{ox}[Et_2S][H_2O_2] + k_{14}[I_8] - k_{-3}[Et_2SO][I_2] + k_3[\mathbf{2}] \\ &= k_8[PhCOOH][I_5] - d[\mathbf{2}]/dt \end{aligned} \qquad 4.88$$

Substituting expression 4.81 for $[I_5]$ in equation 4.88, and taking into account the definitions 4.84-4.86, we can write:

$$\begin{aligned} d[Et_2SO]/dt = {} & 2v_{max}[PhCOOH][O_2]I_a/((K_{m3} + [O_2])(K_{m4} + [PhCOOH])) \\ & -d[\mathbf{2}]/dt \end{aligned} \qquad 4.89$$

Finally, combining equations 4.87 and 4.89 gives, after rearrangement:

$$\begin{aligned} d[Et_2SO]/dt = {} & v_{max}[PhCOOH][O_2]I_a/(K_{m3} + [O_2])(K_{m4} + [PhCOOH]) \\ & x(2[Et_2S]_o - [Et_2SO])/[Et_2S]_o \\ & -k_{-4}[Et_2SO][\mathbf{3}]/[Et_2S]_o + k_3[Et_2S][\mathbf{2}]/[Et_2S]_o \end{aligned} \qquad 4.90$$

For $[Et_2S]$ and $[O_2]$,

$$-d[Et_2S]/dt = d[Et_2SO]/dt \qquad (3.40) \quad 4.91$$

$$-d[O_2]/dt = 0.5d[Et_2SO]/dt \qquad (3.41) \quad 4.92$$

Equations 4.68, 4.87 and 4.90-4.92 are very close to the desired expressions, given in equations 3.37-3.41 (p.139); however, one problem remains: that of finding a suitable expression to describe $I_a$.

### 4.3.2 An Approximate Expression for $I_a$

In the system of interest, a solution contained in a spherical vessel was irradiated by polychromatic light. The vessel was shaken at a fixed rate, and the light source was mounted at an angle to the solution surface. In such a system, any function describing the amount of light ($I_a$) absorbed by a solution species is expected to have a complicated form. Nevertheless, empirical funtions to approximate $I_a$ can be suggested, based on the form which $I_a$ would have if a more simple apparatus had been used.

Suppose, for instance, that a quiescent solution of $Ru(OEP)(Et_2S)_2$ and $Ru(OEP)(Et_2S)(Et_2SO)$ was contained in a rectangular reaction vessel, and illuminated by monochromatic light striking the vessel normal to a wall. From the exponential form of the Beer-Lambert law,

$$I_t = I_o\exp(-2.303(\epsilon_2'[2] + \epsilon_3'[3]) \qquad 4.93$$

where $I_o$ is the intensity of the incident light, $I_t$ is the intensity of the transmitted light, and $\epsilon_2'$ and $\epsilon_3'$ are the extinction coefficients of each species, multiplied by the path length $l$. The typical units for both these quantities are (einsteins $dm^{-2}$ $s^{-1}$); i.e. moles of photons transmitted per unit area, per unit time. It follows directly from equation 4.93 that the intensity of light absorbed by the solution is simply

$$I_{abs} = I_o(1 - \exp(-2.303(\epsilon_2'[2] + \epsilon_3'[3]))$$ 4.94

In studies of homogeneous reactions, it is customary to deal with units of mol $l^{-1}$; we therefore define:

$$I_{abs'} \equiv I_{abs}(A/V)$$ 4.95

where A is the surface area being irradiated ( in $dm^2$), and V is the volume of the solution being irradiated (in $dm^3$, or l). It is important to emphasize this point: $I_{abs'}$, unlike $I_{abs}$, is *not* in units of intensity.

$I_{abs'}$ represents the total amount of light that would be absorbed by a solution containing $Ru(OEP)(Et_2S)_2$ and $Ru(OEP)(Et_2S)(Et_2\underline{S}O)$; the required variable is the amount of light absorbed only by $Ru(OEP)(Et_2S)_2$, in a solution containing both species. Consider an infinitessimally small cross-section, perpendicular to the incident radiation, located somewhere in the irradiated solution. Let I be the intensity of the light incident on this plane. The following relationship will hold:

$$-dI/d\ell = -(dI_2/d\ell + dI_3/d\ell)$$ 4.96

where

$$-dI_2/d\ell \equiv \epsilon_2 I[2]$$ 4.97

$$-dI_3/dl \equiv \epsilon_3 I[3] \qquad 4.98$$

Equation 4.96 is simply the differential form of the Beer-Lambert law, which requires that the exponential decrease in light intensity, as it passes through a unit length of a solution containing several absorbing species, depends on how much the light intensity decreases exponentially due to each indiviual species. The fractional contribution to the decrease in light intensity by $Ru(OEP)(Et_2S)_2$, which is equivalent to the fraction of the total light absorbed by $Ru(OEP)(Et_2S)_2$, will be given by

$$X_3 \equiv \epsilon_3[3]/(\epsilon_2[2] + \epsilon_3[3]) \qquad 4.99$$

and the total amount of light $I_a$ absorbed by $Ru(OEP)(Et_2S)_2$ (in units of einsteins $l^{-1}$ $s^{-1}$) will be given by

$$I_a = X_3 I_{abs'} \qquad 4.100$$

Upon defining the constants

$$\psi \equiv \epsilon_2/\epsilon_3 \qquad 4.101$$

$$c_1 \equiv I_oA/V \text{ (constant only for any one particular apparatus)} \qquad 4.102$$

equation 4.100 can be written in the desired form:

$$I_a = c_1[3](1 - \exp(-2.303(\epsilon_2'[2] + \epsilon_3'[3]))/([3] + \psi[2]) \qquad 4.103$$

Now in the experiments described in section 3.5.1 it was seen that $\epsilon_2$ and $\epsilon_3$ (actually the integrated forms of these parameters over the absorption region of interest; see below) differ only by a factor of around 0.6-0.8; furthermore, in all of the experiments described, a substantial proportion of the incident light was absorbed (e.g. for the most dilute reaction solution studied, $[Ru(OEP)(Et_2S)_2] = 2.55 \times 10^{-5}M$ and $A_{525nm} \approx 0.6$ for a 1 cm cell; in this situation, 75% of the 525nm incident light would be absorbed). Under these conditions, the total amount of light absorbed by the solution will not change very much provided that $[Ru]_o$ remains constant. Therefore equation 4.103 should be well approximated by

$$I_a \approx c_1[3](1 - \exp(-c_2[Ru]_o))/([3] + \psi[2]) \qquad 4.104$$

where

$$c_2 \equiv 2.303\epsilon_{av}' \qquad 4.105$$

and

$$\epsilon_{av} = (\epsilon_2' + \epsilon_3')/2 \qquad 4.106$$

Equation 4.104 describes the amount of *monochromatic* light which would be absorbed by $Ru(OEP)(Et_2S)_2$, in a solution containing both $Ru(OEP)(Et_2S)_2$ and $Ru(OEP)(Et_2S)(Et_2\underline{S}O)$, *if the solution were in a rectangular reaction vessel, with the incident light striking the vessel normal to a wall.* We now consider the real apparatus setup, shown in figure 3.1 (p. 89), and consider qualitatively what changes need to be made to equation 4.104 as the experimental setup is made more complicated. The discussion considers the effects of each change in the apparatus on $I_{abs'}$ (equations 4.94 and 4.95) and $X_3$ (equation 4.99) separately (see equation 4.100).

Making the light source polychromatic will not affect the form of either $I_{abs'}$ or $X_3$, but the molar extinction coefficients for **2** and **3** must be replaced by their equivalent forms integrated over all of the absorbing wavelengths, as was done in the data analysis of section 3.5.1 (equation 3.52, p. 142). Neither shaking the solution nor switching from a rectangular to a spherical vessel will affect $X_3$, but both these changes will have effects on $I_{abs'}$. Switching to a spherical vessel means that the path length is no longer constant over the reaction solution; shaking the solution makes the determination of the solution surface area exposed to the light very difficult or impossible, and means that scattering effects due to the bubbles produced by the shaking of the solution will have to be contended with.

Despite the expected complicated nature of $I_{abs'}$ in the real experimental system, one thing is certain: regardless of the experimental setup, any equation proposed to describe $I_{abs'}$ must behave the same under limiting conditions as the equation derived for the rectangular system; that is, it must drop to zero as either $[Ru]_o$ or $\ell$ drops to zero (i.e. when no solution is present, the transmittance must be 100%), and it must approach a maximum value as either $[Ru]_o$ or $\ell$ becomes very large (i.e. when the solution becomes infinitely concentrated, the transmittance must be 0%). The latter means that $c_1$ still reflects the maximum attainable value of $I_a$, and although A is no longer a parameter which can be directly obtained, $c_1$ will still be a linear function of $I_oA/V$. To summarize, in the real system $I_a$ should still be describable by a function of the form

$$I_a = c_1 f[Ru]_o[3]/([3] + \psi[2]) \qquad 4.107$$

where $c_1$ is a constant dependent only on the geometry of the experimental setup, the solution stirring rate, and on the intensity of the incident light, $\psi$ is the ratio of the molar absorption coefficients of $Ru(OEP)(Et_2S)_2$ and $Ru(OEP)(Et_2S)(Et_2\underline{S}O)$ integrated over all absorbing wavelengths, and $f[Ru]_o$ is a function of $[Ru]_o$, which has a value of zero when $[Ru]_o = 0$, and approaches a constant value asymptotically as $[Ru]_o$ becomes very large. The equation given in section 3.5.1 (p. 142)

$$1 - \exp(-10c_2[Ru]_o) + \arctan(c_2[Ru]_o) \qquad (3.50)\ 4.108$$

was arrived at through trial and error; it has the disadvantage that its range is from 0 to $1 + (\pi/2)$ which makes the expression for the maximum value of $I_a$ somewhat cumbersome ($=3\pi c_1/2$, instead of $c_1$ which would be more convenient); however, the equation proved easy to work with, and has only one adjustable parameter. Now, upon defining

$$v_m \equiv v_{max}c_1 \qquad 4.109$$

and

$$k_{obs} \equiv v_m(f[Ru]_o)[O_2][PhCOOH]/((K_{m3} + [O_2])(K_{m4} + [PhCOOH])) \qquad 4.110$$

equations 4.87 and 4.90 can be written in the form of equations 3.37 and 3.39 (p.139), respectively:

$$\begin{aligned} d[\mathbf{2}]/dt = {} & k_{-4}[Et_2SO][\mathbf{3}]/[Et_2S]_o - k_3[Et_2S][\mathbf{2}]/[Et_2S]_o \\ & + k_{obs}[Et_2SO][\mathbf{3}]/([Et_2S]_o([\mathbf{3}] + \psi[\mathbf{2}])) \qquad (3.37) \quad 4.111 \end{aligned}$$

$$\begin{aligned} d[Et_2SO]/dt = {} & k_{obs}[\mathbf{3}](2[Et_2S]_o - [Et_2SO])/([Et_2S]_o([\mathbf{3}] + \psi[\mathbf{2}])) \\ & -k_{-4}[Et_2SO][\mathbf{3}]/[Et_2S]_o + k_3[Et_2S][\mathbf{2}]/[Et_2S]_o \qquad (3.39) \quad 4.112 \end{aligned}$$

### 4.3.3. Modifications to the Proposed Mechanism

In sections 3.3 and 3.5.2.2, two possible modifications to the mechanism discussed so far (for the $O_2$-oxidation of $Et_2S$ catalyzed by $Ru(OEP)(Et_2S)_2$) were proposed. In one of the modifications it was postulated that $Ru(OEP)(Et_2S)(Et_2S\underline{O})$ could be rearranging to the $Ru(OEP)(Et_2S)(Et_2\underline{S}O)$ isomer without dissociation of $Et_2SO$ into the bulk of the solution (this "internal rearrangement" is labelled $k_{14'}$ in figure 4.2, p.190). In the other modification it was postulated that perhaps the initial photoactivation step ($k_5$ in figure 4.2) involved a direct, light-induced metal-to-porphyrin d-$\pi^*$ charge transfer, rather than a porphyrin $\pi$-$\pi^*$ transition, as implied in figure 4.2. The procedures used to derive rate laws for the alternative mechanisms parallel those described in detail in sections

4.3.1 and 4.3.2, so only a summary is provided here. In addition, some important features of the derived rate laws are considered.

### 4.3.3.1 Internal Rearrangement

If $\mathrm{Ru(OEP)(Et_2S)(Et_2S\underline{O})}$ were isomerizing directly to $\mathrm{Ru(OEP)(Et_2S)(Et_2\underline{S}O)}$, without intermediate dissociation of $\mathrm{Et_2SO}$ into the bulk solution, then the rate of change in $\mathrm{Ru(OEP)(Et_2S)(Et_2\underline{S}O)}$ would be governed by the differential equation:

$$\begin{aligned} d[\mathbf{2}]/dt &= k_{14'}[I_8] + k_{-3}[\mathrm{Et_2SO}][I_2] - k_3[\mathbf{2}] \\ &= k_{10}[I_6][I_7] + k_{-3}[\mathrm{Et_2SO}][I_2] - k_3[\mathbf{2}] \qquad 4.113 \end{aligned}$$

The steady-state expression for $[I_2]$ would be

$$[I_2] = (k_3[\mathbf{2}] + k_{-4}[\mathbf{3}])/(k_{-3}[\mathrm{Et_2SO}] + k_4[\mathrm{Et_2S}]) \qquad 4.114$$

Substituting equation 4.114 into 4.113 yields, after several steps (cf. steps 4.70-4.73):

$$d[\mathbf{2}]/dt = k_{10}[I_6][I_7] + k_{-4}[\mathrm{Et_2SO}][\mathbf{3}]/[\mathrm{Et_2S}]_o - k_3[\mathrm{Et_2S}][\mathbf{2}]/[\mathrm{Et_2S}]_o \qquad 4.115$$

Substituting expression 4.82 for $k_{10}[I_6][I_7]$, and keeping in mind the definition of $k_{obs}$ (cf. equation 4.110), yields the counterpart to equation 4.111:

$$d[\mathbf{2}]/dt = k_{-4}[\mathrm{Et_2SO}][\mathbf{3}]/[\mathrm{Et_2S}]_o - k_3[\mathrm{Et_2S}][\mathbf{2}]/[\mathrm{Et_2S}]_o + k_{obs}[\mathbf{3}]/([\mathbf{3}] + \psi[\mathbf{2}]) \qquad 4.116$$

For the alternative mechanism, the differential equation governing the appearance of $Et_2SO$ would be:

$$d[Et_2SO]/dt = 0.5k_8[PhCOOH][I_5] + k_3[\mathbf{2}] - k_{-3}[Et_2SO][I_2] \qquad 4.117$$

A series of substitutions analogous to those used for the previous derivations yield the expression:

$$\begin{aligned} d[Et_2SO]/dt = {} & k_{obs}[\mathbf{3}]/([\mathbf{3}] + \psi[\mathbf{2}]) \\ & + k_3[Et_2S][\mathbf{2}]/[Et_2S]_o - k_{-4}[Et_2SO][\mathbf{3}]/[Et_2S]_o \end{aligned} \qquad 4.118$$

which is the counterpart of equation 4.112.

Equations 4.116 and 4.118 may appear somewhat similar to equations 4.111 and 4.112, but they are fundamentally different. The difference is best seen by considering the initial values of the differentials $d[\mathbf{2}]/dt$ and $d[Et_2SO]/dt$ for each of the mechanisms. For the dissociative mechanism,

$$(d[\mathbf{2}]/dt)_{t=0} = 0 \qquad 4.119$$

$$(d[Et_2SO]/dt)_{t=0} = 2k_{obs} \qquad 4.120$$

For the internal rearrangement mechanism,

$$(d[\mathbf{2}]/dt)_{t=0} = k_{obs} \tag{4.121}$$

$$(d[Et_2SO]/dt)_{t=0} = k_{obs} \tag{4.122}$$

The important difference between the first and second set of initial rate equations is that the internal rearrangement mechanism predicts that [**2**] should begin to build up immediately, and independently from [$Et_2SO$]. Because of this, the appearance of the integrated [$Et_2SO$] vs. time curves are very different for the two models. Experimentally, the original mechanism (i.e. isomerization of Ru(OEP)($Et_2S$)($Et_2S\underline{O}$) to Ru(OEP)($Et_2S$)($Et_2\underline{S}O$) via a five-coordinate intermediate) is found to fit the data much better (see also the discussion in section 3.5.2.2).

### 4.3.3.2 Photoactivation Via Metal-to-Porphyrin Charge Transfer

The alternative mechanism proposed in section 4.3.3.1 affected the shape of the theoretical [$Et_2SO$] vs. time plots, but not the form of $k_{obs}$. The alternative photoactivation mechanism, first illustrated in figure 3.5b, and reproduced in figure 4.3 for easy reference, affects only $k_{obs}$. This allows a convenient shortcut to be employed in deriving the form of $k_{obs}$. From equation 4.120 and figure 4.3,

$$(d[Et_2SO]/dt)_{t=0} = 2k_{obs} = k_7[PhCOOH][I_5] \tag{4.123}$$

therefore,

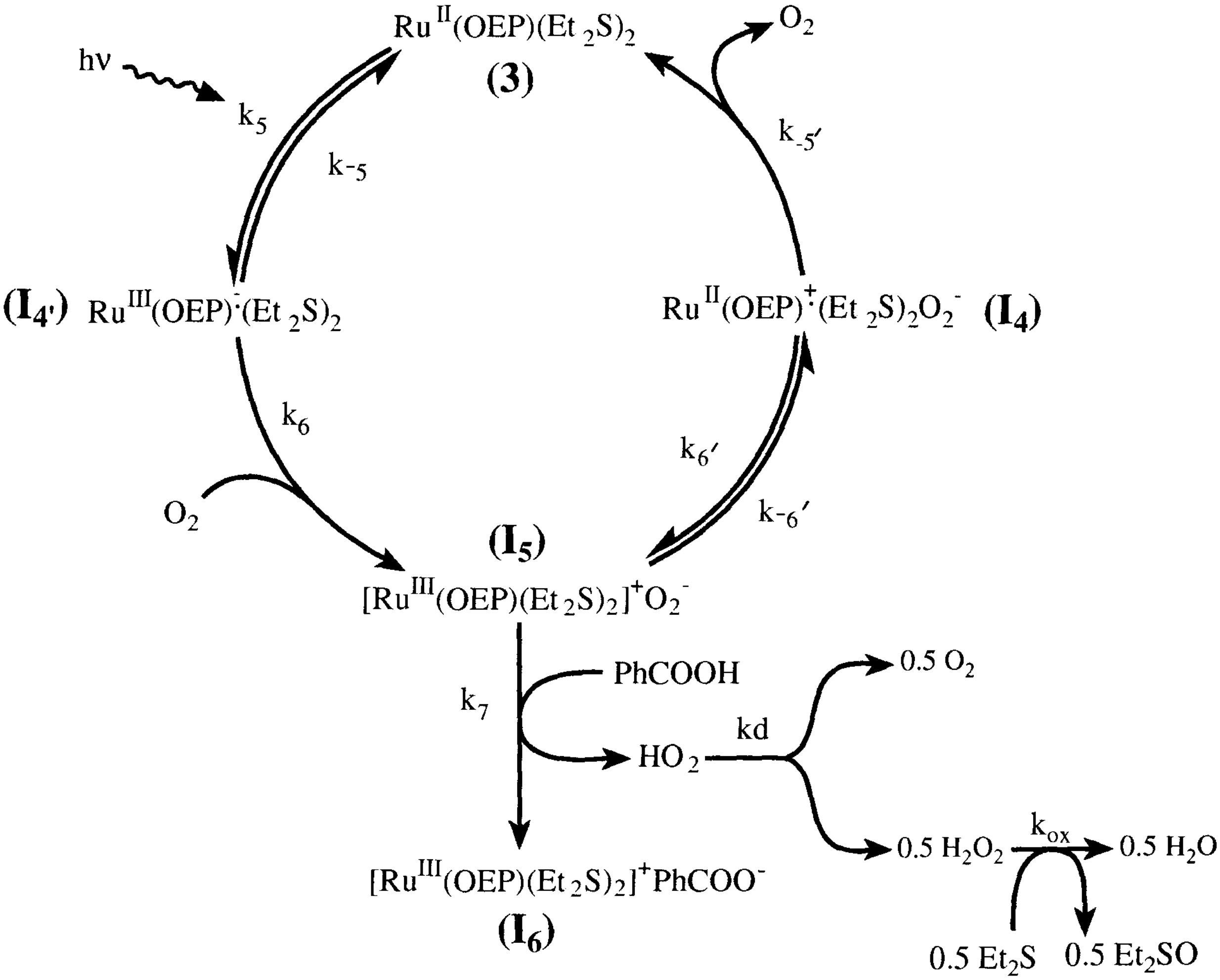
hν
$k_5$
$k_{-5}$
$Ru^{II}(OEP)(Et_2S)_2$
(3)
$O_2$
$k_{-5'}$
$(I_{4'})$ $Ru^{III}(OEP)^{\cdot}(Et_2S)_2$
$Ru^{II}(OEP)^{+\cdot}(Et_2S)_2O_2^-$ $(I_4)$
$k_6$
$k_{6'}$
$k_{-6'}$
$O_2$
$(I_5)$
$[Ru^{III}(OEP)(Et_2S)_2]^+O_2^-$
$k_7$
PhCOOH
$HO_2$
kd
0.5 $O_2$
0.5 $H_2O_2$
$k_{ox}$
0.5 $H_2O$
0.5 $Et_2S$
0.5 $Et_2SO$
$[Ru^{III}(OEP)(Et_2S)_2]^+PhCOO^-$
$(I_6)$

Figure 4.3. Alternative mechanism for the photochemical stage of the $O_2$-oxidation of $Et_2S$ catalyzed by $Ru(OEP)(Et_2S)_2$; see text for details.

$$k_{obs} = 0.5k_7[PhCOOH][I_5] \tag{4.124}$$

The steady-state conditions for $[I_4]$, $[I_{4'}]$, and $[I_5]$ are (recall that at t=0, [**3**] = $[Ru]_o$):

$$[I_4](k_{-5'} + k_{6'}) = k_{-6'}[I_5] \tag{4.125}$$

$$[I_{4'}](k_{-5} + k_6[O_2] = c_1f[Ru]_o \tag{4.126}$$

$$[I_5](k_{-6'} + k_7[PhCOOH]) = k_6[O_2][I_{4'}] + k_{-6'}[I_4] \tag{4.127}$$

where $f[Ru]_o$ is the light absorption function (see equation 4.108). Combining expressions 4.125-4.127 yields, after rearrangement,

$$[I_5] = c_1[O_2]f[Ru]_o/(k_7(K_{m3} + [O_2])(K_{m4} + [PhCOOH])) \tag{4.128}$$

where $K_{m3}$ is still $k_{-5}/k_6$ (equation 4.84), but $K_{m4}$ is now defined as:

$$K_{m4} \equiv k_{-5'}k_{-6'}/(k_7(k_{-5'} + k_{6'})) \tag{4.129}$$

Finally, substituting 4.128 into 4.124 yields:

$$k_{obs} = v_m[PhCOOH][O_2]f[Ru]_o/((K_{m3} + [O_2])(K_{m4} + [PhCOOH])) \tag{4.130}$$

where $v_m$ is now defined as $0.5c_1$.

# CHAPTER 5

# GENERAL CONCLUSIONS AND SUGGESTIONS FOR FURTHER STUDIES

Exposure to $O_2$ or air of a benzene, toluene or methylene chloride solution containing PhCOOH and Ru(OEP)(RR'S)$_2$ (where R = methyl, ethyl or decyl, and R' = methyl or ethyl) results in selective oxidation of the axial ligands to the corresponding sulfoxides. A $^1$H-nmr study of this reaction in $CD_2Cl_2$ for the case where RR'S = dms, indicated the presence of reaction intermediates. Attempts to identify these intermediates led to the synthesis and characterization, by $^1$H-nmr, uv/vis and ir spectroscopy, and CV, of a variety of Ru$^{II}$(OEP) and Ru$^{III}$(OEP) complexes; of these, Ru(OEP)(dms)(dmso), Ru(OEP)(dms)$_2^+$ and Ru(OEP)(dms)(PhCOO) are found to be present during the $O_2$ -oxidation of Ru(OEP)(dms)$_2$ to Ru(OEP)(dmso)$_2$.

Based on the identities and properties of the reaction intermediates, a mechanism is proposed for the $O_2$-oxidation of Ru(OEP)(RR'S)$_2$ complexes, which can be broken down into three stages. In the first stage, $O_2$ coordinates to the Ru$^{II}$(OEP)(dms) intermediate formed by dissociation of a dms ligand from Ru(OEP)(dms)$_2$. This is followed by electron transfer from the metal to $O_2$; the $O_2^-$ so formed is protonated by PhCOOH, yielding Ru$^{III}$(OEP)(dms)(PhCOO) and $HO_2$. The protonated superoxoxide disproportionates to give 0.5 equivalents each of $O_2$ and $H_2O_2$, and the latter oxidizes 0.5 equivalents of $Et_2S$ to $Et_2SO$. This first stage results in the oxidation of one mole of thioether for every two moles of Ru(OEP)(dms)$_2$ initially oxidized. In the second stage, a Ru$^{III}$(OEP) species (possibly Ru$^{III}$(OEP)(dms)(PhCOO)), which has had its oxidation potential lowered by coordination of an anionic ligand, is oxidized to $Ru^{IV}(OEP)$ by another species (possibly $Ru^{III}(OEP)(dms)_2{}^+PhCOO^-$), which has two neutral axial ligands. During the third stage, the $Ru^{IV}(OEP)$ species is eventually converted to $O{=}Ru^{IV}(OEP)(dms)$, which then reacts with one equivalent of dms to produce $Ru^{II}(OEP)(dms)(dm\underline{s}o)$. One mole of $O{=}Ru^{IV}(OEP)(dms)$ is produced for every two moles of $Ru(OEP)(dms)_2$ initially oxidized. The net reaction results in two moles of dms being oxidized to dmso for every mole of $O_2$ consumed, with no net consumption of PhCOOH. The basic mechanism appears to be the same for the oxidation of coordinated $Et_2S$ or decMS, regardless of whether the reaction is performed in $CH_2Cl_2$, benzene or toluene; however, differences in detail are observed between systems.

In the presence of excess thioether, solutions of $Ru(OEP)(RR'S)_2$ and PhCOOH, in $CH_2Cl_2$, benzene or toluene, catalyze the $O_2$-oxidation of free thioether to sulfoxide; however, under these conditions, light of wavelength above 480 nm is required for the reaction to proceed. The catalysis is quite efficient, with initial turnovers of up to 350 $h^{-1}$ being observed under favourable circumstances (i.e. high $[O_2]$ and [PhCOOH], but low $[Ru]_o$, so that a greater fraction of the metalloporphyrin molecules in the reaction vessel are exposed to the light). The catalytic system was studied in detail for the case in which RR'S = $Et_2S$; again, the basic mechanism appears to be the same whether RR'S= dms, $Et_2S$ or decMS. The stoichiometry of two moles of sulfoxide produced for every mole of $O_2$ used was verified by monitoring a reaction simultaneously by gc and by oxygen-uptake experiments. The light dependence observed under catalytic conditions is believed to arise from the fact that $O_2$ coordination to the metal is inhibited by the presence of excess thioether; light is then required to provide energy for an otherwise highly unfavourable outer-sphere electron transfer from the metal to $O_2$. After the initial electron transfer, the reaction is believed to follow the same course in both the stoichiometric and catalytic oxidations.

A detailed kinetic analysis of the gas uptake data shows that, under the experimental conditions used, a maximum value for the initial rate is approached at $[Ru]_o > 2$ mM, $[O_2] > 0.14$ M, and $[PhCOOH] > 54$ mM, respectively. The limit to the value of the initial rate appears to be imposed by the complete absorption by the reaction solution of the incident light by the metalloporphyrin species. The results of the kinetic analysis also suggest two other conclusions. The first conclusion is that whichever electronic transition is responsible for the observed photochemistry, it cannot have a lifetime lower than about $10^{-8}$ s (corresponding to a decay rate constant of $10^{8}$ $s^{-1}$), in the absence of $O_2$. According to a qualitative molecular orbital picture, this suggests that the photochemical reaction is initiated by a metal-to-porphyrin charge-transfer transition (rather than a $\pi$-$\pi^*$ ring-centered transition), which is followed by transfer of the excited electron from the porphyrin ring to $O_2$. The second conclusion is that $Ru(OEP)(Et_2S)(Et_2\underline{S}O)$, although seen to accumulate as $Et_2SO$ builds up with time, is outside of the catalytic cycle (i.e. it is not an intermediate in the reaction pathway).

To our knowledge, photoactivated electron transfer has not been reported previously for ruthenium porphyrin systems; however, a neglected, possible light dependence probably explains the irreproducibility encountered in studies of the $O_2$-oxidation of $PPh_3$ catalyzed by $Ru(OEP)(PPh_3)_2$.[1] A light dependence could also explain the irreproducibility encountered in the apparently unrelated investigations of aldehyde decarbonylation catalyzed by Ru(Porp) complexes, although some data suggested that the catalysis was a purely thermal process;[2] of note, Ru(OEP)(CO)L complexes (L = a neutral axial ligand) appear to be minor side products in both the stoichiometric and catalytic oxidations described in this thesis. When successfully initiated, the catalytic decarbonylation reactions were reported to be quite efficient,[2] and it may be worth re-investigating these reactions to see if they behave more consistently under steady illumination.

The possible commercial value of a catalyst which could selectively oxidize thioethers to sulfoxides was a consideration in the initial decision to investigate the reactivity of Ru(OEP)(RR'S)$_2$ complexes with $O_2$. Two general commercial applications can be envisioned for a catalyst which oxidizes thioethers to sulfoxides. The first is to oxidize simple thioethers such as dms, which are often waste products in industrial processes,[3] to the more valuable sulfoxides. The second commercial application would be to convert prochiral thioethers into chiral sulfoxides, which could then be used as chiral synthetic reagents in organic synthesis.[4] For the oxidation of simple thioethers, the system described in this thesis could probably be reasonably effective if efforts were made to optimize the geometry of the reaction apparatus for light absorption; however,the eventual decomposition of the catalyst would always be a problem. Furthermore, the cerium-based system of Riley et al. (see section 1.3) currently appears to show more promise, despite requiring high temperatures (100° C) and $O_2$ pressures (14 bar).[3]

As a model system for future developement of a chiral oxidant, the Ru(OEP)(RR'S)$_2$/PhCOOH system is fundamentally flawed in that half of the thioether is oxidized by the achiral $H_2O_2$. For chiral oxidation of thioethers, a chiral Ru(Porp) system based on the Ru(OCP)(O)$_2$ system previously studied in our laboratories (see section

1.2)[5] could be investigated. For such a system, care would have to be taken to avoid side reaction via the mechanism reported in this thesis.

An especially intriguing direction for future study of the reaction of Ru(OEP)(RR'S)$_2$ complexes (and possibly other Ru$^{II}$(Porp) complexes) with O$_2$, in acidic media, would be to use the reaction as a probe, as part of a detailed investigation of the electronic structure of these complexes. In particular, it would be interesting to combine an investigation of the photochemistry described in this thesis with photophysical experiments, such as those recently reported by Holten et al., in which the photophysical properties of a variety of Ru(Porp) complexes were investigated by picosecond laser techniques.[6]

## REFERENCES FOR CHAPTER 5

1. James, B. R.; Mikkelsen, S. R.; Leung, T. W.; Wiliams, G. M.; Wong, R. *Inorg. Chim. Acta* **1984**, *85*, 209.

2.a) Domazetis, G.; James, B. R.; Tarpey, B.; Dolphin, D. *ACS Symp. Ser.*, **1981**, *152*, 243. b) Domazetis, G.; Tarpey, B.; Dolphin, D.; James, B. R. *J. Chem. Soc., Chem. Commun.* **1980**, 939. c) Tarpey, B. M.Sc. Dissertation, The University of British Columbia, Vancouver, B. C., 1982.

3. Riley, D. P.; Smith, M. R.; Correa, P. E. *J. Am. Chem. Soc.* **1988**, *110*, 177.

4. a) Pitchen, P.; Dunak, E.; Deshmukh, M. N.; Kagan, H. B. *J. Am. Chem. Soc.* **1984**, *106*, 8188. b) Mikolajcyk, M.; Drabowicz, J. *Top. Stereochem.* **1982**, *13*, 333.

5. a) James, B. R. *Chem. Ind.* **1992**, *47*, 245. b) Rajapakse, N. Ph.D. Dissertation, The University of British Columbia, Vancouver, B. C., 1990.

6. a) Tait, C. D.; Holten, D.; Barley, M. H.; Dolphin, D.; James, B. R. *J. Am. Chem. Soc.* **1985**, *107*, 1930. b) Levine, L. M. A.; Holten, D. *J. Phys. Chem.* **1988**, *92*, 714.

# APPENDIX 1

# QUICK BASIC PROGRAMS

This appendix lists all of the Quick Basic programs that were used for the data analyses discussed in chapter 3 of this thesis. In all cases the programs consist of one or more modules which were specifically written for the tasks performed in the thesis, and several generic modules obtained from "Numerical Recipes In Basic" (reference 6 in chapter 3). Only the parts of the programs tailored specifically for this thesis are included here. A complete list of the modules taken from Numerical Recipes, along with the chapter in which the modules can be found, is included after each program.

## A1.1 LINFIT

This is a program for fitting an experimentally derived data set (x, y, $\sigma_y$) (where $\sigma_y$ is the uncertainty in y) to a straight line, y = a + bx. The program returns the best values of a and b, the value of $\chi^2$ given these values, and the goodness of fit parameter Q. In addition, the theoretical line and the experimental data points can be displayed graphically on the screen, and the theoretical points can be saved for future inclusion in a graphical print-out.

```
DECLARE SUB FIT (X!(), Y!(), NDATA!, SIG!(), MWT!, A!, B!, SIGA!, SIGB!,
CHI2!, Q!)
DECLARE SUB PLOT (XDAT(), YDAT(), XP(), YP(), NPT, NTHEOR, SIG())

'Driver for routine FIT
CLS
LINE INPUT "Filename:", dum$
```

```
OPEN dum$ FOR INPUT AS #1
LINE INPUT #1, dum$
INPUT #1, NPT
DIM X(NPT), Y(NPT), SIG(NPT)
LINE INPUT #1, dum$
LINE INPUT #1, dum$
FOR I = 1 TO NPT
  INPUT #1, X(I), Y(I), SIG(I)
NEXT I
PRINT "If you wish to leave the first m data points out of the least squares"
PRINT "calculation, input m at this point (m=0 to include all points):"
INPUT M
NDAT = NPT - M
DIM XDEL(NDAT), YDEL(NDAT), SIGDEL(NDAT)
NDEL = M + 1
FOR J = NDEL TO NPT
  XDEL(J - M) = X(J)
  YDEL(J - M) = Y(J)
  SIGDEL(J - M) = SIG(J)
NEXT J
FOR MWT = 0 TO 1
  CALL FIT(XDEL(), YDEL(), NDAT, SIGDEL(), MWT, A, B, SIGA, SIGB, CHI2,
  Q)
  IF MWT = 0 THEN
    PRINT "Ignoring standard deviation"
  ELSE
    PRINT "Including standard deviation"
  END IF
  PRINT "   A = ";
  PRINT USING "#.#####^^^^"; A;
  PRINT "      Uncertainty:   ";
  PRINT USING "#.#####^^^^"; SIGA
  PRINT "   B = ";
  PRINT USING "#.#####^^^^"; B;
  PRINT "      Uncertainty:   ";
  PRINT USING "#.#####^^^^"; SIGB
  PRINT "   Chi-squared: ";
  PRINT USING "#.#####^^^^"; CHI2
  PRINT "   Goodness-of-fit: ";
  PRINT USING "#.##^^^^"; Q
  PRINT
  PRINT
NEXT MWT
PRINT "Do you want to see a plot of the data (y/n)"
INPUT dum$
```

```
IF dum$ = "n" THEN END
NTHEOR = 2
DIM XP(NTHEOR), YP(NTHEOR)
XP(1) = 0
YP(1) = A
PRINT XP(1); YP(1)
XP(NTHEOR) = 2 * X(NPT)
YP(NTHEOR) = A + B * XP(NTHEOR)
PRINT XP(NTHEOR); YP(NTHEOR)
INPUT "Press return to continue", dum$
CALL PLOT(X(), Y(), XP(), YP(), NPT, NTHEOR, SIG())
END



SUB PLOT (XDAT(), YDAT(), X(), Y(), NDATA, NTHEOR, SIG())
DO
 SCREEN 2
 CLS 2
 VIEW PRINT 1 TO 4
 LOCATE 1, 1
 PRINT "Enter  X1,X2 (X1=X2 to stop)"
 INPUT X1, X2
 IF X1 = X2 THEN EXIT SUB
 PRINT "Enter Y1,Y2"
 INPUT Y1, Y2
 CLS
 VIEW (50, 35)-(550, 180)
 WINDOW (0, 0)-(500, 145)
 LINE (0, 0)-(500, 145), , B
 DX = (X2 - X1) / 500 ’X Units per pixel
 DY = (Y2 - Y1) / 145 ’Y Units per pixel
 FOR K = 1 TO NDATA
   SX = INT((XDAT(K) - X1) / DX)
   SY = INT((YDAT(K) - Y1) / DY)
   ERRY = INT(SIG(K) / DY)
   CIRCLE (SX, SY), 1
   LINE (SX, SY + ERRY)-(SX, SY - ERRY)
 NEXT K
 FOR L = 1 TO NTHEOR
   C1X = INT((X(L) - X1) / DX)
   C1Y = INT((Y(L) - Y1) / DY)
   IF L < > 1 THEN LINE (C2X, C2Y)-(C1X, C1Y)
   C2X = C1X
   C2Y = C1Y
```

```
  NEXT L
LOOP
END SUB
```

The following modules were incorporated, directly and without any modification, from "Numerical Recipes In Basic" into the program:

FIT (Chapter 14);

GAMMLN, GAMMQ, GCF, GSER (Chapter 6).

The (x, y, $\sigma_y$) experimental data file should be in the ASCII format given by the following example:

```
NPT=
14

X,Y,SIG(Y)
5.934E-5,.0007805,2.90E-5
.00011868,.00083401,3.10E-5
.00029669,.0010711,2.98E-5
.0005934,.0015153,4.22E-5
.0007417,.001709,4.76E-5
.0014835,.0028049,7.81E-5
.0018543,.0033231,9.26E-5
.0037086,.0061133,1.70E-4
.0092715,.014638,4.08E-4
.01855,.029296,8.16E-4
.0371,.058381,1.63E-3
.05563,.086382,2.41E-3
.11126,0.17426,4.85E-3
.23179,.36055,1.00E-2
'DATA FOR K1 DETERMINATION; [Et2S]/P(1) vs [Et2S]
```

## A1.2 POLFIT

This is a program for fitting an experimentally derived data set (x, y, $\sigma_y$) (where $\sigma_y$ is the uncertainty in y) to a polynomial, using the method of singular value decomposition. The program first returns the diagonal values of the **W** matrix (see chapters 2 and 14 of numerical recipes), and prompts the user for the maximum tolerated value of the condition number. If this value is exceeded, the appropriate $w_i$ values are set to zero; in either case, the program then returns the best values of a, b, c... in $y = a + bx + cx^2 + \ldots$, the value of $\chi^2$ given these values, and the goodness of fit parameter Q. In addition, the theoretical curve and the experimental data points can be displayed graphically on the screen, and the theoretical points can be saved for future inclusion in a graphical print-out.

```
DECLARE SUB SVDVAR (V!(), MA!, NP!, W!(), CVM!(), NCVM!)
DECLARE SUB SVDFIT (X!(), Y!(), SIG!(), NDATA!, A!(), MA!, U!(), V!(), W!(),
MP!, NP!, CHISQ!, FUNCS$, Q!)
DECLARE SUB PLOT (XDAT(), YDAT(), X(), Y(), NDATA, SIG())

'Driver for routine SVDFIT
CLS
LINE INPUT "Filename?:", dum$
OPEN dum$ FOR INPUT AS #1
LINE INPUT #1, dum$
INPUT #1, NPT
LINE INPUT #1, dum$
LINE INPUT #1, dum$
INPUT #1, NPOL
DIM X(NPT), Y(NPT), SIG(NPT), A(NPOL), CVM(NPOL, NPOL)
DIM U(NPT, NPOL), V(NPOL, NPOL), W(NPOL)
LINE INPUT #1, dum$
LINE INPUT #1, dum$
FOR I = 1 TO NPT
  INPUT #1, X(I), Y(I), SIG(I)
NEXT I
```

```
CALL SVDFIT(X(), Y(), SIG(), NPT, A(), NPOL, U(), V(), W(), MP, NP, CHISQ,
"FPOLY", Q)
CALL SVDVAR(V(), NPOL, NP, W(), CVM(), NPOL)
PRINT "Polynomial fit:"
FOR I = 1 TO NPOL
  PRINT "A("; I; ") =";
  PRINT USING "#.#####^^^^"; A(I);
  PRINT "  +-";
  PRINT USING "#.#####^^^^"; SQR(CVM(I, I))
NEXT I
PRINT "Chi-squared";
PRINT USING "#.#####^^^^"; CHISQ
PRINT "Goodness of fit";
PRINT USING "#.##^^^^"; Q
PRINT
PRINT "Do you want to see a plot of the data (y/n)"
INPUT dum$
IF dum$ = "y" THEN
  DIM XP(NPT), YP(NPT)
  FOR J = 1 TO NPT
    XP(J) = X(J)
    YP(J) = A(1) + X(J) * (A(2) + X(J) * A(3))
  NEXT J
  CALL PLOT(X(), Y(), XP(), YP(), NPT, SIG())
END IF
PRINT "Do you want to save the theoretical points (y/n)?"
INPUT dum$
IF dum$ = "y" THEN
  INPUT "Filename?", filename$
  OPEN filename$ FOR OUTPUT AS #2
  FOR I = 1 TO NPT
    WRITE #2, X(I), Y(I), SIG(I), XP(I), YP(I)
  NEXT I
END IF
END



SUB SVDFIT (X(), Y(), SIG(), NDATA, A(), MA, U(), V(), W(), MP, NP, CHISQ,
FUNCS$, Q)
DIM B(NDATA), AFUNC(MA)
FOR I = 1 TO NDATA
  IF FUNCS$ = "FPOLY" THEN CALL FPOLY(X(I), AFUNC(), MA)
  TMP = 1! / SIG(I)
  FOR J = 1 TO MA
```

```
    U(I, J) = AFUNC(J) * TMP
   NEXT J
   B(I) = Y(I) * TMP
  NEXT I
  CALL SVDCMP(U(), NDATA, MA, MP, NP, W(), V())
  PRINT "DIAGONAL OF MATRIX W"
  FOR K = 1 TO MA
   PRINT USING "#.#####^^^^"; W(K)
  NEXT K
  INPUT "HOW SMALL A FRACTION OF WMAX WILL YOU ACCEPT?", TOL
  WMAX = 0!
  FOR J = 1 TO MA
   IF W(J) > WMAX THEN WMAX = W(J)
  NEXT J
  THRESH = TOL * WMAX
  FOR J = 1 TO MA
   IF W(J) < THRESH THEN W(J) = 0!
   IF W(J) = 0! THEN PRINT "Resetting W(J)="; J; "equal to zero"
  NEXT J
  CALL SVBKSB(U(), W(), V(), NDATA, MA, MP, NP, B(), A())
  CHISQ = 0!
  FOR I = 1 TO NDATA
   IF FUNCS$ = "FPOLY" THEN CALL FPOLY(X(I), AFUNC(), MA)
   SUM = 0!
   FOR J = 1 TO MA
    SUM = SUM + A(J) * AFUNC(J)
   NEXT J
   CHISQ = CHISQ + ((Y(I) - SUM) / SIG(I)) ^ 2
  NEXT I
  Q = GAMMQ(.5 * (NDATA - NPOL), .5 * CHISQ)
  ERASE AFUNC, B
  END SUB
```

The supprogram SVDFIT listed above was taken directly from "Numerical Recipes" with only minor modifications.

The subprogram PLOT was the same one used in the program LINFIT described earlier.

The following modules were incorporated, directly and without any modification, from "Numerical Recipes In Basic" into the program:

SVDVAR (Chapter 14);
GAMMLN, GAMMQ, GCF, GSER (Chapter 6);
SVDCMP, SVDVAR (Chapter 2).

The (x, y, $\sigma_y$) experimental data file should be in the ASCII format given by the following example:

```
NPT=
9

NPOL=
3

X,Y,SIG(Y)
.0005934,.0000393,3.72E-6
.0018543,.000085194,1.92E-6
.0037086,.00015811,2.89E-6
.0092715,.00047466,8.48E-6
.01855,.0011898,2.10E-5
.0371,.0035157,6.22E-5
.05563,.0070143,1.24E-4
.11126,.024116,4.27E-4
.23179,.096683,1.71E-3
DATA FOR FITTING [Et2S]^2/P(1) vs [Et2S]
```

## A1.3 ONEDMIN

This is the iterative program which was used to find the best value for $k_{obs}$, in section 3.5.1 of the thesis. The user provides: 1) a set of experimentally derived data points (t, $[Et_2SO]$, $\sigma_{[Et_2SO]}$) (where $\sigma_{[Et_2SO]}$ is the uncertainty in $[Et_2SO]$ produced); 2) a set of initial conditions $[Ru(OEP)(Et_2S)(Et_2\underline{S}O)]_o$ = [A] (INIT), $[Ru(OEP)(Et_2S)_2]_o$ = [B] (INIT), $[Et_2SO]_o$ = [Et2SO] (INIT), $[Et_2S]_o$ = [Et2S] (INIT), $t_o$ = X1; 3) a final time X2 to stop the integrator, and an estimate of an appropriate step size for the integrator; 4) a value for the integrated extinction coefficient ratio $\psi$; 5) two initial guesses as to the value of $k_{obs}$. Along with the best value of $k_{obs}$, the program also returns the value of $\chi^2_{min}$.

```
DECLARE FUNCTION BRENT! (XDAT!(), YDAT!(), SIG!(), NPT!, YSTART!(),
NVAR!, X1!, X2!, AX!, BX!, CX!, DUM!, TOL!, XMIN!, H1)
DECLARE SUB MNBRAK (XDAT!(), YDAT!(), SIG!(), NPT!, YSTART!(), NVAR!,
X1!, X2!, AX!, BX!, CX!, DUM!, H1)
DECLARE SUB HUNT (XX!(), N!, X!, JLO!)
DECLARE SUB ODEINT (YSTART!(), NVAR!, X1!, X2!, EPS!, H1!, HMIN!, NOK!,
NBAD!, DUM1!, DUM2!)
DECLARE SUB RATINT (XP(), YTHEOR(), KOUNT, X, Y, DY)
DECLARE FUNCTION RKCHI2 (W, XDAT(), YDAT(), SIG(), NPT, YSTART(),
NVAR, X1, X2, H1)
COMMON SHARED KMAX, KOUNT, DXSAV, XP(), YP()
COMMON SHARED KOBS, PSI, Et2S


CLS
NVAR = 4
DIM YSTART(NVAR), XP(200), YP(10, 200)
INPUT "What is the initial time in seconds?", X1
INPUT "What is the final time in seconds?", X2
INPUT "[A] (INIT)?", YSTART(1)
INPUT "[B] (INIT)?", YSTART(2)
INPUT "[Et2SO] (INIT)?", YSTART(3)
INPUT "[Et2S] (INIT)?", YSTART(4)
```

```
Et2S = YSTART(4)
INPUT "Estimate PSI", PSI
INPUT "Estimate the required stepsize for the integration sequence", H1
PRINT "Input a filename containing raw data for comparison"
INPUT DUM$
OPEN DUM$ FOR INPUT AS #1
LINE INPUT #1, DUM$
INPUT #1, NPT
DIM XDAT(NPT), YDAT(NPT), SIG(NPT)
LINE INPUT #1, DUM$
LINE INPUT #1, DUM$
FOR I = 1 TO NPT
  INPUT #1, XDAT(I), YDAT(I), SIG(I)
NEXT I
PRINT "Input two trial values for kobs: a,b"
INPUT AX, BX
CALL MNBRAK(XDAT(), YDAT(), SIG(), NPT, YSTART(), NVAR, X1, X2, AX,
BX, CX, DUM, H1)
B = BRENT(XDAT(), YDAT(), SIG(), NPT, YSTART(), NVAR, X1, X2, AX, BX,
CX, DUM, TOL, XMIN, H1)
PRINT "Chi2 Min ="; B
PRINT "kobs="; XMIN
END

FUNCTION BRENT (XDAT(), YDAT(), SIG(), NPT, YSTART(), NVAR, X1, X2,
AX, BX, CX, DUM, TOL, XMIN, H1)
ITMAX = 100
CGOLD = .381966#
ZEPS = 1E-10
A = AX
IF CX < AX THEN A = CX
B = AX
IF CX > AX THEN B = CX
V = BX
W = V
X = V
E = 0!
FX = RKCHI2(X, XDAT(), YDAT(), SIG(), NPT, YSTART(), NVAR, X1, X2, H1)
FV = FX
FW = FX
FOR ITER = 1 TO ITMAX
  PRINT ITER
  XM = .5 * (A + B)
  TOL1 = TOL * ABS(X) + ZEPS
  TOL2 = 2! * TOL1
```

```
 IF ABS(X - XM) < = TOL2 - .5 * (B - A) THEN EXIT FOR
 DONE% = -1
 IF ABS(E) > TOL1 THEN
   R = (X - W) * (FX - FV)
   Q = (X - V) * (FX - FW)
   P = (X - V) * Q - (X - W) * R
   Q = 2! * (Q - R)
   IF Q > 0! THEN P = -P
   Q = ABS(Q)
   ETEMP = E
   E = D
   DUM = ABS(.5 * Q * ETEMP)
   IF ABS(P) < DUM AND P > Q * (A - X) AND P < Q * (B - X) THEN
     D = P / Q
     U = X + D
     IF U - A < TOL2 OR B - U < TOL2 THEN D = ABS(TOL1) * SGN(XM - X)
     DONE% = 0
   END IF
 END IF
 IF DONE% THEN
   IF X > = XM THEN
     E = A - X
   ELSE
     E = B - X
   END IF
   D = CGOLD * E
 END IF
 IF ABS(D) > = TOL1 THEN
   U = X + D
 ELSE
   U = X + ABS(TOL1) * SGN(D)
 END IF
 FU = RKCHI2(U, XDAT(), YDAT(), SIG(), NPT, YSTART(), NVAR, X1, X2, H1)
 IF FU < = FX THEN
   IF U > = X THEN
     A = X
   ELSE
     B = X
   END IF
   V = W
   FV = FW
   W = X
   FW = FX
   X = U
   FX = FU
```

```
  ELSE
    IF U < X THEN
      A = U
    ELSE
      B = U
    END IF
    IF FU <= FW OR W = X THEN
      V = W
      FV = FW
      W = U
      FW = FU
    ELSEIF FU <= FV OR V = X OR V = W THEN
      V = U
      FV = FU
    END IF
  END IF
NEXT ITER
IF ITER > ITMAX THEN PRINT "Brent exceed maximum iterations.": END
XMIN = X
BRENT = FX
END FUNCTION
```

```
SUB DERIVS (X, Y(), DYDX())
DYDX(1) = .7 * Y(3) * Y(2) / Et2S - .0374 * Y(4) * Y(1) / Et2S + KOBS * (Y(2) /
(Y(2) + PSI * Y(1))) * (Y(3) / Et2S)
DYDX(2) = -DYDX(1)
DYDX(3) = KOBS * (2 - Y(3) / Et2S) * (Y(2) / (Y(2) + PSI * Y(1))) + .0374 * Y(4)
* Y(1) / Et2S - .7 * Y(3) * Y(2) / Et2S
DYDX(4) = -DYDX(3)
END SUB
```

```
SUB HUNT (XX(), N, X, JLO)
ASCND% = XX(N) > XX(1)
IF JLO <= 0 OR JLO > N THEN
  JLO = 0
  JHI = N + 1
ELSE
  INC = 1
  IF X >= XX(JLO) EQV ASCND% THEN
```

```
 1  JHI = JLO + INC
    IF JHI > N THEN
      JHI = N + 1
    ELSEIF X >= XX(JHI) EQV ASCND% THEN
      JLO = JHI
      INC = INC + INC
      GOTO 1
    END IF
  ELSE
    JHI = JLO
 2  JLO = JHI - INC
    IF JLO < 1 THEN
      JLO = 0
    ELSEIF X < XX(JLO) EQV ASCND% THEN
      JHI = JLO
      INC = INC + INC
      GOTO 2
    END IF
  END IF
END IF
DO
  IF JHI - JLO = 1 THEN EXIT SUB
  JM = INT((JHI + JLO) / 2)
  IF X > XX(JM) EQV ASCND% THEN
    JLO = JM
  ELSE
    JHI = JM
  END IF
LOOP
END SUB



SUB MNBRAK (XDAT(), YDAT(), SIG(), NPT, YSTART(), NVAR, X1, X2, AX, BX,
CX, DUM, H1)
GOLD = 1.618034
GLIMIT = 100!
TINY = 1E-20
FA = RKCHI2(AX, XDAT(), YDAT(), SIG(), NPT, YSTART(), NVAR, X1, X2, H1)
FB = RKCHI2(BX, XDAT(), YDAT(), SIG(), NPT, YSTART(), NVAR, X1, X2, H1)
IF FB > FA THEN
  DUM = AX
  AX = BX
  BX = DUM
  DUM = FB
  FB = FA
  FA = DUM
END IF
CX = BX + GOLD * (BX - AX)
FC = RKCHI2(CX, XDAT(), YDAT(), SIG(), NPT, YSTART(), NVAR, X1, X2, H1)
DO
  IF FB < FC THEN EXIT DO
  DONE% = -1
  R = (BX - AX) * (FB - FC)
  Q = (BX - CX) * (FB - FA)
  DUM = Q - R
  IF ABS(DUM) < TINY THEN DUM = TINY
  U = BX - ((BX - CX) * Q - (BX - AX) * R) / (2! * DUM)
  ULIM = BX + GLIMIT * (CX - BX)
  IF (BX - U) * (U - CX) > 0! THEN
    FU = RKCHI2(U, XDAT(), YDAT(), SIG(), NPT, YSTART(), NVAR, X1, X2,
    H1)
    IF FU < FC THEN
      AX = BX
      FA = FB
      BX = U
      FB = FU
      EXIT SUB
    ELSEIF FU > FB THEN
      CX = U
      FC = FU
      EXIT SUB
    END IF
    U = CX + GOLD * (CX - BX)
    FU = RKCHI2(U, XDAT(), YDAT(), SIG(), NPT, YSTART(), NVAR, X1, X2,
    H1)
  ELSEIF (CX - U) * (U - ULIM) > 0! THEN
    FU = RKCHI2(U, XDAT(), YDAT(), SIG(), NPT, YSTART(), NVAR, X1, X2,
    H1)
    IF FU < FC THEN
      BX = CX
      CX = U
      U = CX + GOLD * (CX - BX)
      FB = FC
      FC = FU
      FU = RKCHI2(U, XDAT(), YDAT(), SIG(), NPT, YSTART(), NVAR, X1, X2,
      H1)
    END IF
  ELSEIF (U - ULIM) * (ULIM - CX) >= 0! THEN
    U = ULIM
    FU = RKCHI2(U, XDAT(), YDAT(), SIG(), NPT, YSTART(), NVAR, X1, X2,
    H1)
   ELSE
    U = CX + GOLD * (CX - BX)
    FU = RKCHI2(U, XDAT(), YDAT(), SIG(), NPT, YSTART(), NVAR, X1, X2,
    H1)
   END IF
   IF DONE% THEN
    AX = BX
    BX = CX
    CX = U
    FA = FB
    FB = FC
    FC = FU
   ELSE
    DONE% = 0
   END IF
LOOP WHILE NOT DONE%
END SUB
```

```
FUNCTION RKCHI2 (W, XDAT(), YDAT(), SIG(), NPT, YSTART(), NVAR, X1, X2,
H1)
KOBS = W
DIM YCOPY(NVAR)
FOR K = 1 TO NVAR
  YCOPY(K) = YSTART(K)
NEXT K
EPS = .0001
KMAX = 200
HMIN = 0
DXSAV = 1
CALL ODEINT(YSTART(), NVAR, X1, X2, EPS, H1, HMIN, NOK, NBAD, DUM,
RKQC)
FOR K = 1 TO NVAR
  YSTART(K) = YCOPY(K)
NEXT K
DIM YINT(NPT), YTHEOR(KOUNT), XTHEOR(KOUNT), XTABL(4), YTABL(4)
FOR I = 1 TO KOUNT
  YTHEOR(I) = YP(3, I)
  XTHEOR(I) = XP(I)
NEXT I
JLO = 0
KPASS = KOUNT
```

```
FOR I = 1 TO NPT
  CALL HUNT(XTHEOR(), KPASS, XDAT(I), JLO)
  FOR K = 1 TO 4
    IF JLO <= KOUNT - 2 THEN
      XTABL(K) = XP(JLO - 2 + K)
      YTABL(K) = YTHEOR(JLO - 2 + K)
    ELSE
      XTABL(K) = XP(JLO - 3 + K)
      YTABL(K) = YTHEOR(JLO - 3 + K)
    END IF
  NEXT K
  CALL RATINT(XTABL(), YTABL(), 4, XDAT(I), Y, DY)
  YINT(I) = Y
  JLO = INT(JLO + KOUNT / NPT)
NEXT I
CHI2 = 0
FOR J = 1 TO NPT
  CHI2 = CHI2 + ((YDAT(J) - YINT(J)) / SIG(J)) ^ 2
NEXT J
RKCHI2 = CHI2
ERASE YINT, YTHEOR, YTABL, XTHEOR, XTABL
END FUNCTION
```

Of the subprograms and functions listed above, the following were taken directly from "Numerical Recipes" with only minor modifications:

BRENT, MNBRAK, (Chapter 10);

HUNT (Chapter 3).

The following modules were incorporated, directly and without any modification, from "Numerical Recipes In Basic" into the program:

ODEINT, RKQC, RK4 (Chapter 15);

RATINT (Chapter 3).

The (t, $[Et_2SO]$, $\sigma_{[Et_2SO]}$) experimental data file should be in the ASCII format illustrated by the following example:

```
NPT=
12

X               Y               SIG(Y)
821,.0030894,.0004
1200,.0042814,.0004
1615,.0056192,.0004
2031,.0067806,.0004
2516,.0083214,.0004
2972,.0094714,.0004
3436,.010583,.0004
3835,.011614,.0004
4229,.0124036,.0004
5000,.0142396,.0004
5790,.015424,.0004
6261,.016413,.0004
```

## A1.4 TWODMIN

This program is exactly analogous to ONEDMIN, but in this case $\psi$ is treated as an adjustable parameter, and the program iteratively seeks the values of both $k_{obs}$ and $\psi$ for which $\chi^2$ is a minimum. Three initial guesses as to the value of the set ($k_{obs}$,$\psi$) are fed into the program, and three ($k_{obs}$,$\psi$) values for which $\chi^2$ differs by less than 1% are returned.

```
DECLARE SUB HUNT (XX!(), N!, X!, JLO!)
DECLARE FUNCTION AMOEB! (X(), NP, XDAT(), YDAT(), SIG(), NPT,
YSTART(), NVAR, X1, X2, H1)
DECLARE SUB ODEINT (YSTART!(), NVAR!, X1!, X2!, EPS!, H1!, HMIN!, NOK!,
NBAD!, DUM1!, DUM2!)
DECLARE SUB RATINT (XA!(), YA!(), N!, X!, Y!, DY!)
DECLARE FUNCTION RKCHI2! (W, Z, XDAT!(), YDAT!(), SIG!(), NPT!,
YSTART!(), NVAR!, X1!, X2!, H1!)
DECLARE SUB AMOEBA (P(), Y(), MP, NP, NDIM, FTOL, DUM, ITER, XDAT(),
YDAT(), SIG(), NPT, YSTART(), NVAR, X1, X2, H1)
COMMON SHARED KMAX, KOUNT, DXSAV, XP(), YP()
COMMON SHARED KOBS, PSI, Et2S


CLS
NVAR = 4
NP = 2
MP = 3
FTOL = .0001
DIM YSTART(NVAR), XP(200), YP(10, 200), P(MP, NP), X(NP), Y(MP)
INPUT "What is the initial time in seconds?", X1
INPUT "What is the final time in seconds?", X2
INPUT "[A] (INIT)?", YSTART(1)
INPUT "[B] (INIT)?", YSTART(2)
INPUT "[Et2SO] (INIT)?", YSTART(3)
INPUT "[Et2S] (INIT)?", YSTART(4)
Et2S = YSTART(4)
INPUT "First guess at kobs,PSI?", P(1, 1), P(1, 2)
INPUT "Second guess at kobs,PSI?", P(2, 1), P(2, 2)
INPUT "Third guess at kobs,PSI?", P(3, 1), P(3, 2)
INPUT "Estimate the required stepsize for the integration sequences", H1
NDIM = NP
PRINT "Input a filename containing raw data for comparison"
INPUT DUM$
OPEN DUM$ FOR INPUT AS #1
LINE INPUT #1, DUM$
INPUT #1, NPT
DIM XDAT(NPT), YDAT(NPT), SIG(NPT)
LINE INPUT #1, DUM$
LINE INPUT #1, DUM$
FOR I = 1 TO NPT
  INPUT #1, XDAT(I), YDAT(I), SIG(I)
NEXT I
FOR I = 1 TO MP
  FOR J = 1 TO NP
    X(J) = P(I, J)
  NEXT J
  Y(I) = AMOEB(X(), NP, XDAT(), YDAT(), SIG(), NPT, YSTART(), NVAR, X1,
  X2, H1)
  PRINT Y(I)
NEXT I
CALL AMOEBA(P(), Y(), MP, NP, NDIM, FTOL, DUM, ITER, XDAT(), YDAT(),
SIG(), NPT, YSTART(), NVAR, X1, X2, H1)
PRINT "Iterations:"; ITER
PRINT
PRINT "Vertices of final 2-D simplex and"
PRINT "function values at the vertices:"
PRINT
PRINT "  I    X(I)      Y(I)      CHISQUARE"
PRINT
FOR I = 1 TO MP
  PRINT USING "###"; I;
  FOR J = 1 TO NP
    PRINT USING "##.#####^^^^"; P(I, J);
  NEXT J
  PRINT USING "##.#####^^^^"; Y(I)
NEXT I
PRINT
END



FUNCTION AMOEB (X(), NP, XDAT(), YDAT(), SIG(), NPT, YSTART(), NVAR,
X1, X2, H1)
IF X(1) < = 0 OR X(2) < = .1 OR X(2) > 1 THEN
  AMOEB = 10000
ELSE
  AMOEB = RKCHI2(X(1), X(2), XDAT(), YDAT(), SIG(), NPT, YSTART(), NVAR,
  X1, X2, H1)
END IF
END FUNCTION
```

```
SUB AMOEBA (P(), Y(), MP, NP, NDIM, FTOL, DUM, ITER, XDAT(), YDAT(),
SIG(), NPT, YSTART(), NVAR, X1, X2, H1)
ALPHA = 1!
BETA = .5
GAMMA = 2!
ITMAX = 500
DIM PR(NDIM), PRR(NDIM), PBAR(NDIM)
MPTS = NDIM + 1
ITER = 0
DO
  ILO = 1
  IF Y(1) > Y(2) THEN
    IHI = 1
    INHI = 2
  ELSE
    IHI = 2
    INHI = 1
  END IF
  FOR I = 1 TO MPTS
    IF Y(I) < Y(ILO) THEN ILO = I
    IF Y(I) > Y(IHI) THEN
      INHI = IHI
      IHI = I
    ELSEIF Y(I) > Y(INHI) THEN
      IF I < > IHI THEN INHI = I
    END IF
  NEXT I
  RTOL = 2! * ABS(Y(IHI) - Y(ILO)) / (ABS(Y(IHI)) + ABS(Y(ILO)))
  IF RTOL < FTOL THEN ERASE PBAR, PRR, PR: EXIT SUB
  IF ITER = ITMAX THEN PRINT "Amoeba exceeding maximum iterations.": EXIT
  SUB
  ITER = ITER + 1
  FOR J = 1 TO NDIM
    PBAR(J) = 0!
  NEXT J
  FOR I = 1 TO MPTS
    IF I < > IHI THEN
      FOR J = 1 TO NDIM
        PBAR(J) = PBAR(J) + P(I, J)
      NEXT J
    END IF
  NEXT I
  FOR J = 1 TO NDIM
    PBAR(J) = PBAR(J) / NDIM
    PR(J) = (1! + ALPHA) * PBAR(J) - ALPHA * P(IHI, J)
```

```
NEXT J
YPR = AMOEB(PR(), NDIM, XDAT(), YDAT(), SIG(), NPT, YSTART(), NVAR,
X1, X2, H1)
PRINT "YPR= ", YPR
IF YPR <= Y(ILO) THEN
  FOR J = 1 TO NDIM
    PRR(J) = GAMMA * PR(J) + (1! - GAMMA) * PBAR(J)
  NEXT J
  YPRR = AMOEB(PRR(), NDIM, XDAT(), YDAT(), SIG(), NPT, YSTART(),
  NVAR, X1, X2, H1)
  PRINT "YPRR= ", YPRR
  IF YPRR < Y(ILO) THEN
    FOR J = 1 TO NDIM
      P(IHI, J) = PRR(J)
    NEXT J
    Y(IHI) = YPRR
  ELSE
    FOR J = 1 TO NDIM
      P(IHI, J) = PR(J)
    NEXT J
    Y(IHI) = YPR
  END IF
ELSEIF YPR >= Y(INHI) THEN
  IF YPR < Y(IHI) THEN
    FOR J = 1 TO NDIM
      P(IHI, J) = PR(J)
    NEXT J
    Y(IHI) = YPR
  END IF
  FOR J = 1 TO NDIM
    PRR(J) = BETA * P(IHI, J) + (1! - BETA) * PBAR(J)
  NEXT J
  YPRR = AMOEB(PRR(), NDIM, XDAT(), YDAT(), SIG(), NPT, YSTART(),
  NVAR, X1, X2, H1)
  PRINT "YPRR= ", YPRR
  IF YPRR < Y(IHI) THEN
    FOR J = 1 TO NDIM
      P(IHI, J) = PRR(J)
    NEXT J
    Y(IHI) = YPRR
  ELSE
    FOR I = 1 TO MPTS
      IF I <> ILO THEN
        FOR J = 1 TO NDIM
          PR(J) = .5 * (P(I, J) + P(ILO, J))
          P(I, J) = PR(J)
         NEXT J
         Y(I) = AMOEB(PR(), NDIM, XDAT(), YDAT(), SIG(), NPT, YSTART(),
         NVAR, X1, X2, H1)
         PRINT "Y("; I; ")=", Y(I)
        END IF
       NEXT I
      END IF
     ELSE
      FOR J = 1 TO NDIM
       P(IHI, J) = PR(J)
      NEXT J
      Y(IHI) = YPR
     END IF
    PRINT ITER
    LOOP
    END SUB



    SUB DERIVS (X, Y(), DYDX())
    DYDX(1) = .7 * Y(3) * Y(2) / Et2S - .0374 * Y(4) * Y(1) / Et2S + KOBS * (Y(2) /
    (Y(2) + PSI * Y(1))) * (Y(3) / Et2S)
    DYDX(2) = -DYDX(1)
    DYDX(3) = KOBS * (2 - Y(3) / Et2S) * (Y(2) / (Y(2) + PSI * Y(1))) + .0374 * Y(4)
    * Y(1) / Et2S - .7 * Y(3) * Y(2) / Et2S
    DYDX(4) = -DYDX(3)
    END SUB



    SUB HUNT (XX(), N, X, JLO)
    ASCND% = XX(N) > XX(1)
    IF JLO <= 0 OR JLO > N THEN
     JLO = 0
     JHI = N + 1
    ELSE
     INC = 1
     IF X >= XX(JLO) EQV ASCND% THEN
    1  JHI = JLO + INC
      IF JHI > N THEN
       JHI = N + 1
      ELSEIF X >= XX(JHI) EQV ASCND% THEN
       JLO = JHI
       INC = INC + INC
    GOTO 1
   END IF
  ELSE
   JHI = JLO
2  JLO = JHI - INC
   IF JLO < 1 THEN
    JLO = 0
   ELSEIF X < XX(JLO) EQV ASCND% THEN
    JHI = JLO
    INC = INC + INC
    GOTO 2
   END IF
  END IF
END IF
DO
  IF JHI - JLO = 1 THEN EXIT SUB
  JM = INT((JHI + JLO) / 2)
  IF X > XX(JM) EQV ASCND% THEN
   JLO = JM
  ELSE
   JHI = JM
  END IF
LOOP
END SUB
```

```
FUNCTION RKCHI2 (W, Z, XDAT(), YDAT(), SIG(), NPT, YSTART(), NVAR, X1,
X2, H1)
KOBS = W
PSI = Z
DIM YCOPY(NVAR)
FOR K = 1 TO NVAR
 YCOPY(K) = YSTART(K)
NEXT K
EPS = .0001
KMAX = 200
HMIN = 0
DXSAV = 1
CALL ODEINT(YSTART(), NVAR, X1, X2, EPS, H1, HMIN, NOK, NBAD, DUM,
RKQC)
FOR K = 1 TO NVAR
 YSTART(K) = YCOPY(K)
NEXT K
DIM YINT(NPT), YTHEOR(KOUNT), XTHEOR(KOUNT), XTABL(4), YTABL(4)
```

```
FOR I = 1 TO KOUNT
  YTHEOR(I) = YP(3, I)
  XTHEOR(I) = XP(I)
NEXT I
JLO = 0
KPASS = KOUNT
FOR I = 1 TO NPT
  CALL HUNT(XTHEOR(), KPASS, XDAT(I), JLO)
  FOR K = 1 TO 4
    IF JLO <= KOUNT - 2 THEN
      XTABL(K) = XP(JLO - 2 + K)
      YTABL(K) = YTHEOR(JLO - 2 + K)
    ELSE
      XTABL(K) = XP(JLO - 3 + K)
      YTABL(K) = YTHEOR(JLO - 3 + K)
    END IF
  NEXT K
  CALL RATINT(XTABL(), YTABL(), 4, XDAT(I), Y, DY)
  YINT(I) = Y
  JLO = INT(JLO + KOUNT / NPT)
NEXT I
CHI2 = 0
FOR J = 1 TO NPT
  CHI2 = CHI2 + ((YDAT(J) - YINT(J)) / SIG(J)) ^ 2
NEXT J
RKCHI2 = CHI2
ERASE YINT, YTHEOR, YTABL, XTHEOR, XTABL
END FUNCTION
```

Of the subprograms and functions listed above, the following were taken directly from "Numerical Recipes" with only minor modifications:

AMOEBA (Chapter 10);

HUNT (Chapter 3).

The following modules were incorporated, directly and without any modification, from "Numerical Recipes In Basic" into the program:

ODEINT, RKQC, RK4 (Chapter 15)
RATINT (Chapter 3)

The (t, $[Et_2SO]$, $\sigma_{[Et_2SO]}$) experimental data file should be in the same format as that required by the ONEDMIN program.

## A1.5 ODEGRPH

This is a program which can be used to display graphically the results of a numerical integration of the equations 3.37-3.40 (see section 3.5.1). The user provides: 1) a set of experimentally derived data points (t, $[Et_2SO]$, $\sigma_{[Et_2SO]}$); 2) a set of initial conditions $[Ru(OEP)(Et_2S)(Et_2\underline{S}O)]_o$ = [A] (INIT), $[Ru(OEP)(Et_2S)_2]_o$ = [B] (INIT), $[Et_2SO]_o$ = [Et2SO] (INIT), $[Et_2S]_o$ = [Et2S] (INIT), $t_o$ = X1; 3) a final time X2 to stop the integrator, and an estimate of an appropriate step size for the integrator; 4) a value for the integrated extinction coefficient ratio $\psi$; 5) a value for $k_{obs}$. Note that this program does not find the best values of $k_{obs}$ as do the previous two; this program simply integrates equations 3.37-3.40 once, using the $k_{obs}$ and $\psi$ values provided. However, the program allows any one of the generated concentration vs. time data pairs to be displayed graphically on the screen; in the case of $[Et_2SO]$ vs. t, the experimentally derived data set will be displayed along with the theoretical curve. Also, the program provides the opportunity of saving the theoretical [$Et_2SO$] vs. t data set, for later inclusion in a graphical print-out.

```
DECLARE SUB RKPLOT (YSTART!(), YCOPY!(), X1!, X2!, XDAT!(), YDAT!(),
SIG!(), NPT, NVAR!)
DECLARE SUB PLOT (XDAT!(), YDAT!(), X!(), Y!(), NDATA!, NTHEOR!, SIG!())
DECLARE SUB ODEINT (YSTART!(), NVAR!, X1!, X2!, EPS!, H1!, HMIN!, NOK!,
NBAD!, DUM1!, DUM2!)
COMMON SHARED KMAX, KOUNT, DXSAV, XP(), YP()
COMMON SHARED KOBS, PSI, Et2S


DO
 CLS
 DIM XP(200), YP(10, 200)
 NVAR = 4
 DIM YSTART(NVAR)
 DIM YCOPY(NVAR)
 INPUT "What is the initial time in seconds?", X1
 INPUT "What is the final time in seconds?", X2
 INPUT "[A] (INIT)?", YSTART(1)
 INPUT "[B] (INIT)?", YSTART(2)
 INPUT "[Et2SO] (INIT)?", YSTART(3)
 INPUT "[Et2S] (INIT)?", YSTART(4)
 FOR K = 1 TO NVAR
  YCOPY(K) = YSTART(K)
 NEXT K
 PRINT "Input a filename containing raw data for comparison"
 INPUT DUM$
 OPEN DUM$ FOR INPUT AS #1
 LINE INPUT #1, DUM$
 INPUT #1, NPT
 DIM XDAT(NPT), YDAT(NPT), SIG(NPT)
 LINE INPUT #1, DUM$
 LINE INPUT #1, DUM$
 FOR I = 1 TO NPT
  INPUT #1, XDAT(I), YDAT(I), SIG(I)
 NEXT I
 DO
  CALL RKPLOT(YSTART(), YCOPY(), X1, X2, XDAT(), YDAT(), SIG(), NPT,
    NVAR)
    PRINT "Do you want to do further analysis on this data set (y/n)?"
    INPUT DUM$
    IF DUM$ = "n" THEN EXIT DO
  LOOP
  PRINT "Any other data you wish to analyse (y/n)?"
  INPUT DUM$
  IF DUM$ = "n" THEN END
  ERASE XP, YP, XDAT, YDAT, SIG, YSTART, YCOPY
  CLOSE #1
LOOP
END



SUB DERIVS (X, Y(), DYDX())
DYDX(1) = .7 * Y(3) * Y(2) / Et2S - .0374 * Y(4) * Y(1) / Et2S + KOBS * (Y(2) /
(Y(2) + PSI * Y(1))) * (Y(3) / Et2S)
DYDX(2) = -DYDX(1)
DYDX(3) = KOBS * (2 - Y(3) / Et2S) * (Y(2) / (Y(2) + PSI * Y(1))) + .0374 * Y(4)
* Y(1) / Et2S - .7 * Y(3) * Y(2) / Et2S
DYDX(4) = -DYDX(3)
END SUB

SUB RKPLOT (YSTART(), YCOPY(), X1, X2, XDAT(), YDAT(), SIG(), NPT,
NVAR)
DO
 DO
     INPUT "Estimate kobs", KOBS
     INPUT "Estimate PSI", PSI
     Et2S = YSTART(4)
     EPS = .0001
     INPUT "Estimate the required stepsize", H1
     HMIN = 0!
     KMAX = 200
     DXSAV = (X2 - X1) / (X2 - X1)
     CALL ODEINT(YSTART(), NVAR, X1, X2, EPS, H1, HMIN, NOK, NBAD,
     DUM, RKQC)
     PRINT "Successful steps:          "; NOK
     PRINT "Bad steps:                 "; NBAD
     PRINT "Stored intermediate values:"; KOUNT
     PRINT "Press return to continue"
     INPUT DUM$
     PRINT "     t       [A]       [B]        [Et2SO]       [Et2S]       "
     FOR I = 1 TO KOUNT
```

```
      PRINT USING "####.#  "; XP(I);
      PRINT USING "#.####^^^^  "; YP(1, I); YP(2, I); YP(3, I); YP(4, I)
    NEXT I
    FOR K = 1 TO NVAR
      YSTART(K) = YCOPY(K)
    NEXT K
    PRINT "Do you wish to try another value of kobs (y/n)?"
    INPUT FLAG$
    IF FLAG$ = "n" THEN EXIT DO
  LOOP
  PRINT "Do you wish to see a plot of the data (y/n)?"
  INPUT FLAG$
  DO
    IF FLAG$ = "n" THEN EXIT DO
    PRINT "Which variable? (Input as a number 1-4)"
    INPUT VAR#
    DIM YTHEOR(KOUNT)
    FOR I = 1 TO KOUNT
      YTHEOR(I) = YP(VAR#, I)
    NEXT I
    CALL PLOT(XDAT(), YDAT(), XP(), YTHEOR(), NPT, KOUNT, SIG())
    SCREEN 0
    PRINT "Do you wish to save the calculated data set (y/n)?"
    INPUT FLAG$
    IF FLAG$ = "y" THEN
      INPUT "Document to be saved:", DUM$
      OPEN DUM$ FOR OUTPUT AS #2
      FOR I = 1 TO KOUNT
        WRITE #2, XP(I), YTHEOR(I)
      NEXT I
      CLOSE #2
    END IF
    PRINT "Do you wish to try another variable? (y/n)"
    INPUT FLAG$
    ERASE YTHEOR
  LOOP
  PRINT "Do you wish to plot another value of kobs (y/n)?"
  INPUT FLAG$
  IF FLAG$ = "n" THEN EXIT DO
LOOP
END SUB
```

The subprogram PLOT was the same one used in the program LINFIT described earlier.

The following modules were incorporated, directly and without any modification, from "Numerical Recipes In Basic" into the program:

ODEINT, RKQC, RK4 (Chapter 15).

The (t, [$Et_2SO$], $\sigma_{[Et_2SO]}$) experimental data file should be in the same format as that required by the ONEDMIN program.

# APPENDIX 2

# RESULTS OF STOPPED-FLOW EXPERIMENTS

## A2.1 Experiments Carried Out Using Light of 400.5 nm Wavelength

The two tables that follow give the numerical values of the parameters $\alpha_1$, $\beta_1$ $\gamma_1$, used to obtain the data points in figures 3.15 and 3.16. Following each table are the relative absorbance vs. time raw data plots (corrected for a non-level baseline; see section A2.3) to which the equation

$$A = \alpha_1 + \beta_1 e^{-(\gamma_1 t)}$$

was fitted, to obtain each set of $\alpha_1$, $\beta_1$, $\gamma_1$ values. For each experiment, the relative absorbance change was monitored over a period of 100 ms; the first four points of every experiment appear to be within the dead time of the instrument, and were neglected in the fit. The initial concentration of $Ru(OEP)(Et_2SO)_2$ in each case was $(3.44 \pm 0.07)\times10^{-6}$ M (note: all of the concentrations reported in this appendix take into account the 50% dilution in the stopped-flow reaction chamber).

### A2.1.1 Experiments Carried Out Using a Constant [$Et_2SO$] of 1.18 ± 0.03 mM

Relative uncertainty in [$Et_2S$] for each experiment ≈ 1-2%.

200 Data points were collected in the 0-200 ms time range.

| Graph # | [$Et_2S$] (M) | $\alpha_1$ | $\beta_1$ | $\gamma_1$ ($s^{-1}$) |
|---|---|---|---|---|
| A2.1.1.1 | $5.93 \times 10^{-5}$ | -0.009 | 0.076 | 48.2 |
| A2.1.1.2 | $1.19 \times 10^{-4}$ | -0.050 | 0.142 | 48.3 |
| A2.1.1.3 | $2.97 \times 10^{-4}$ | -0.024 | 0.277 | 55.0 |
| A2.1.1.4 | $5.93 \times 10^{-4}$ | -0.152 | 0.392 | 67.4 |
| A2.1.1.5 | $7.42 \times 10^{-4}$ | -0.123 | 0.434 | 72.6 |
| A2.1.1.6 | $1.48 \times 10^{-3}$ | -0.171 | 0.529 | 88.1 |
| A2.1.1.7 | $1.85 \times 10^{-3}$ | -0.154 | 0.558 | 92.3 |
| A2.1.1.8 | $3.71 \times 10^{-3}$ | -0.148 | 0.607 | 108 |
| A2.1.1.9 | $9.27 \times 10^{-3}$ | -0.153 | 0.633 | 123 |
| A2.1.1.10 | $1.85 \times 10^{-2}$ | -0.169 | 0.633 | 130 |
| A2.1.1.11 | $3.71 \times 10^{-2}$ | -0.174 | 0.636 | 134 |
| A2.1.1.12 | $5.56 \times 10^{-2}$ | -0.179 | 0.644 | 133 |
| A2.1.1.13 | 0.111 | -0.176 | 0.639 | 137 |
| A2.1.1.14 | 0.231 | -0.176 | 0.643 | 139 |

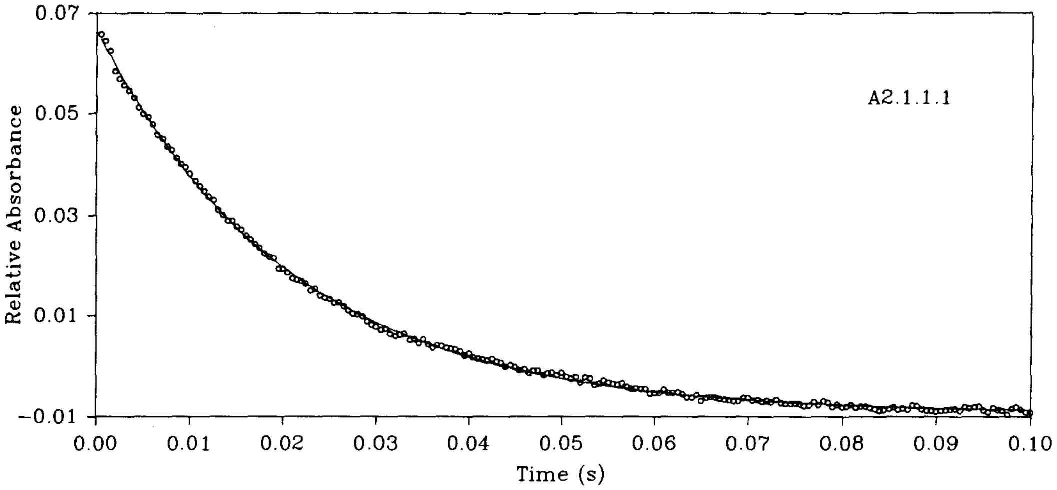
A2.1.1.1
Relative Absorbance
0.07
0.05
0.03
0.01
−0.01
Time (s)
0.00
0.01
0.02
0.03
0.04
0.05
0.06
0.07
0.08
0.09
0.10

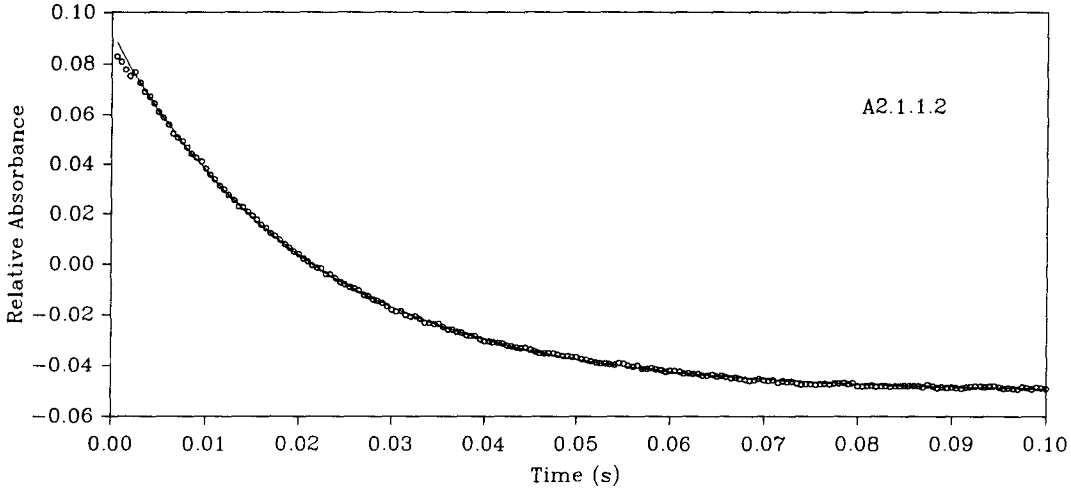
A2.1.1.2
Relative Absorbance
0.10
0.08
0.06
0.04
0.02
0.00
−0.02
−0.04
−0.06
Time (s)
0.00
0.01
0.02
0.03
0.04
0.05
0.06
0.07
0.08
0.09
0.10

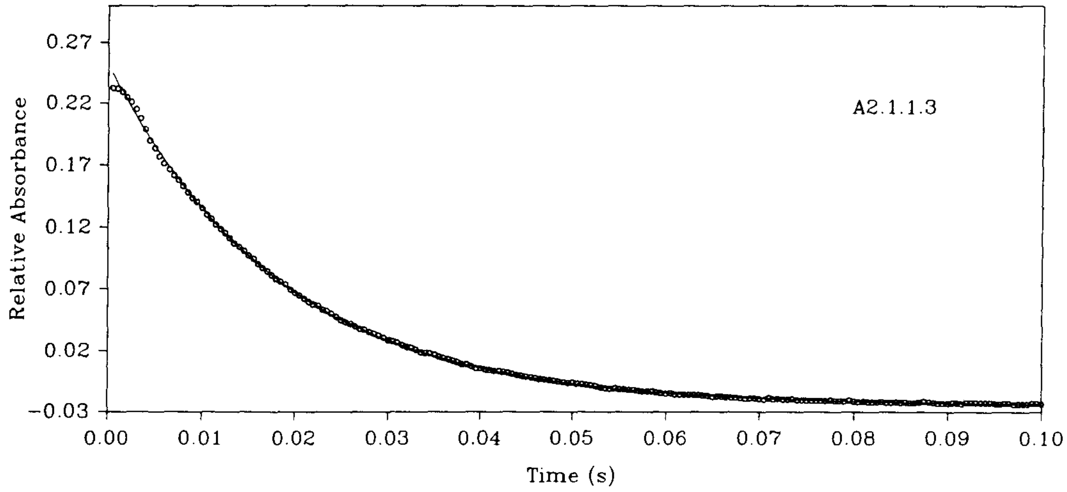
A2.1.1.3
Relative Absorbance
0.27
0.22
0.17
0.12
0.07
0.02
−0.03
Time (s)
0.00
0.01
0.02
0.03
0.04
0.05
0.06
0.07
0.08
0.09
0.10

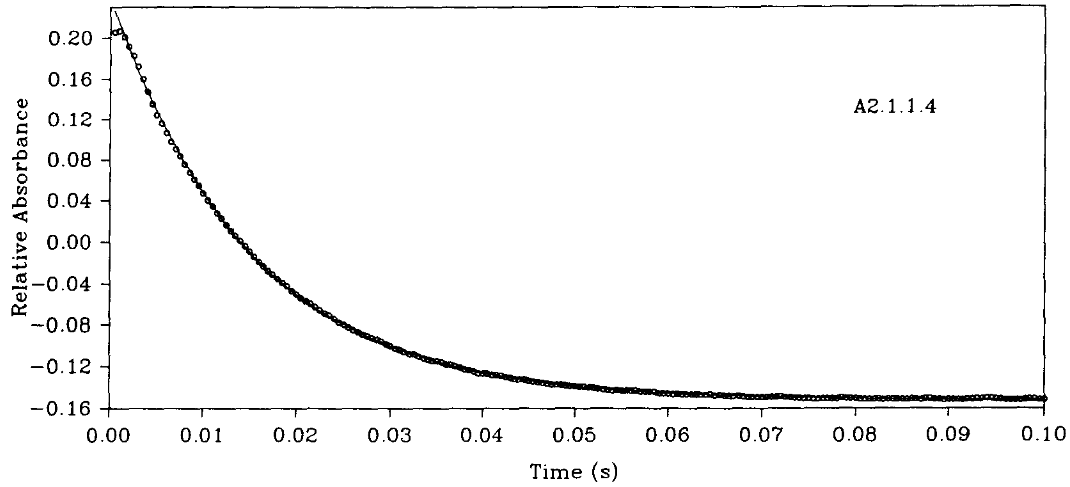
A2.1.1.4
Relative Absorbance
0.20
0.16
0.12
0.08
0.04
0.00
−0.04
−0.08
−0.12
−0.16
0.00
0.01
0.02
0.03
0.04
0.05
0.06
0.07
0.08
0.09
0.10
Time (s)

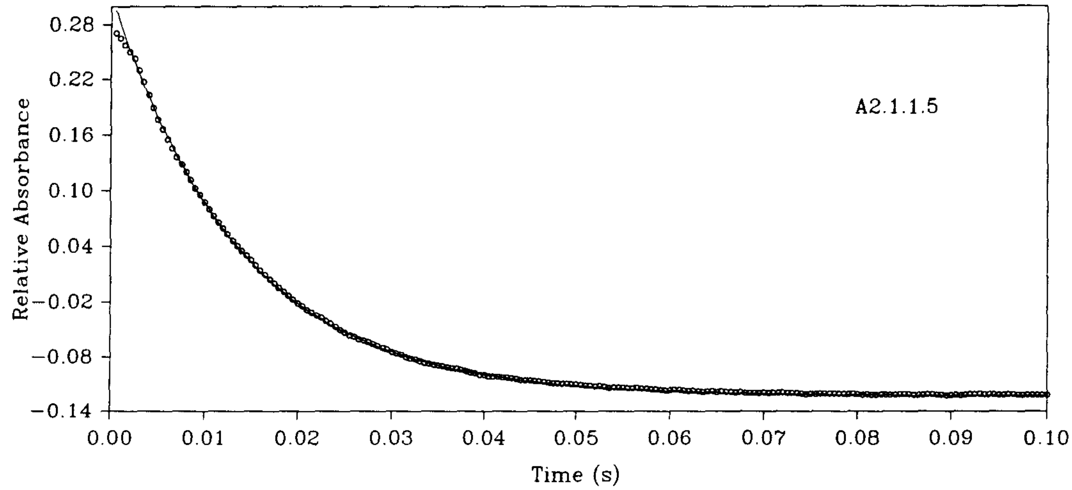
A2.1.1.5
Relative Absorbance
0.28
0.22
0.16
0.10
0.04
−0.02
−0.08
−0.14
0.00
0.01
0.02
0.03
0.04
0.05
0.06
0.07
0.08
0.09
0.10
Time (s)

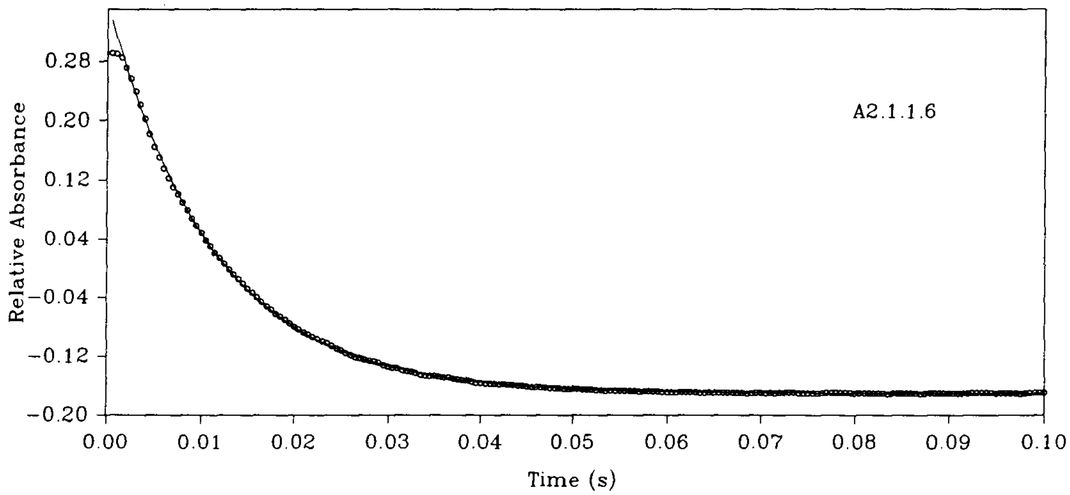
A2.1.1.6
Relative Absorbance
0.28
0.20
0.12
0.04
−0.04
−0.12
−0.20
0.00
0.01
0.02
0.03
0.04
0.05
0.06
0.07
0.08
0.09
0.10
Time (s)

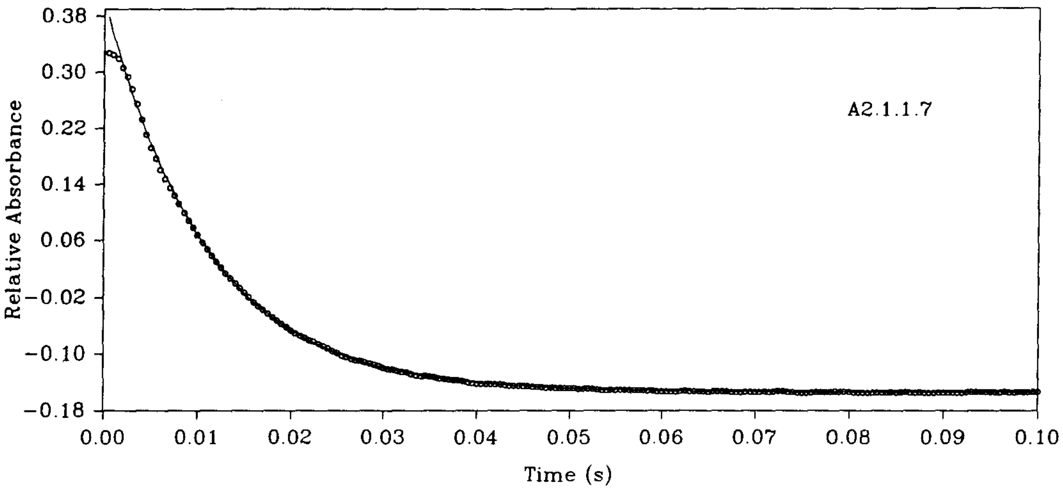
A2.1.1.7
Relative Absorbance
0.38
0.30
0.22
0.14
0.06
−0.02
−0.10
−0.18
0.00
0.01
0.02
0.03
0.04
0.05
0.06
0.07
0.08
0.09
0.10
Time (s)

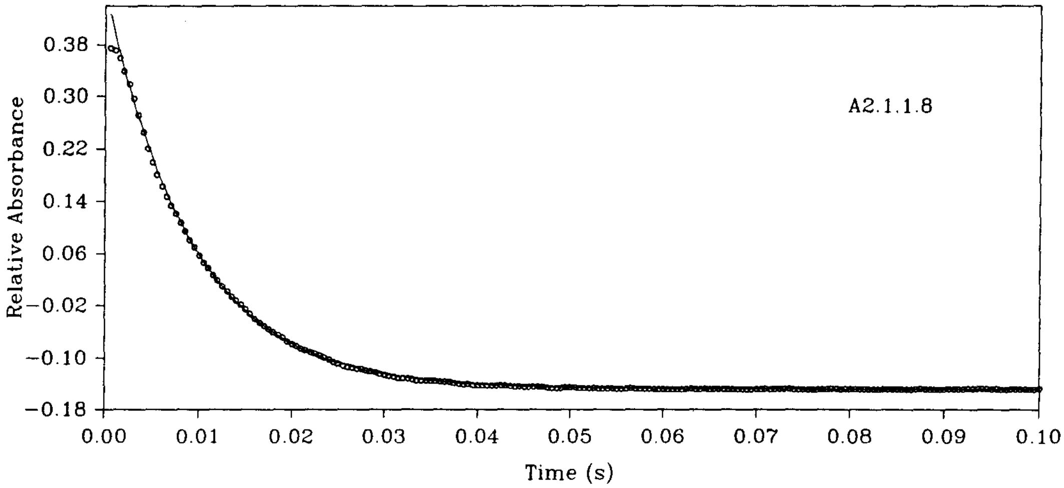
A2.1.1.8
Relative Absorbance
0.38
0.30
0.22
0.14
0.06
−0.02
−0.10
−0.18
0.00
0.01
0.02
0.03
0.04
0.05
0.06
0.07
0.08
0.09
0.10
Time (s)

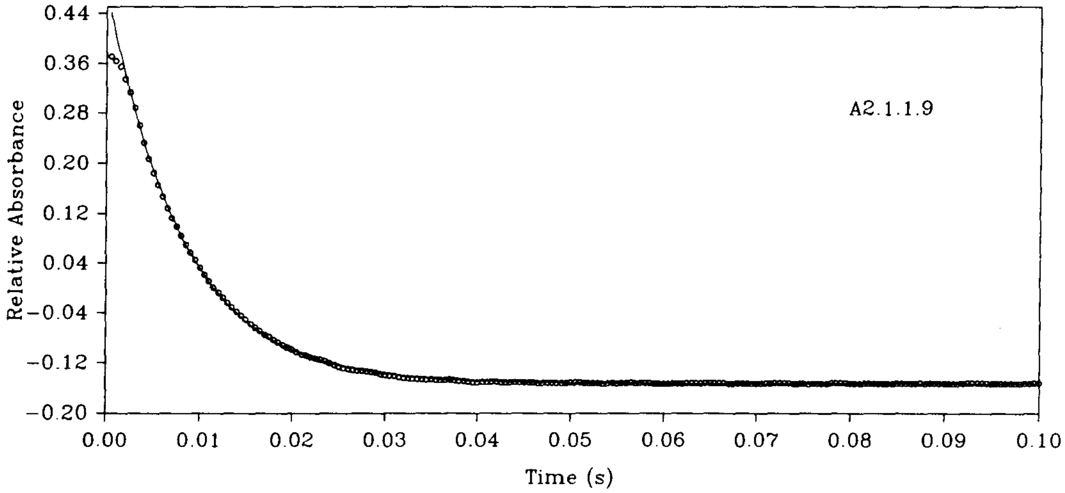
A2.1.1.9
Relative Absorbance
0.44
0.36
0.28
0.20
0.12
0.04
−0.04
−0.12
−0.20
0.00
0.01
0.02
0.03
0.04
0.05
0.06
0.07
0.08
0.09
0.10
Time (s)

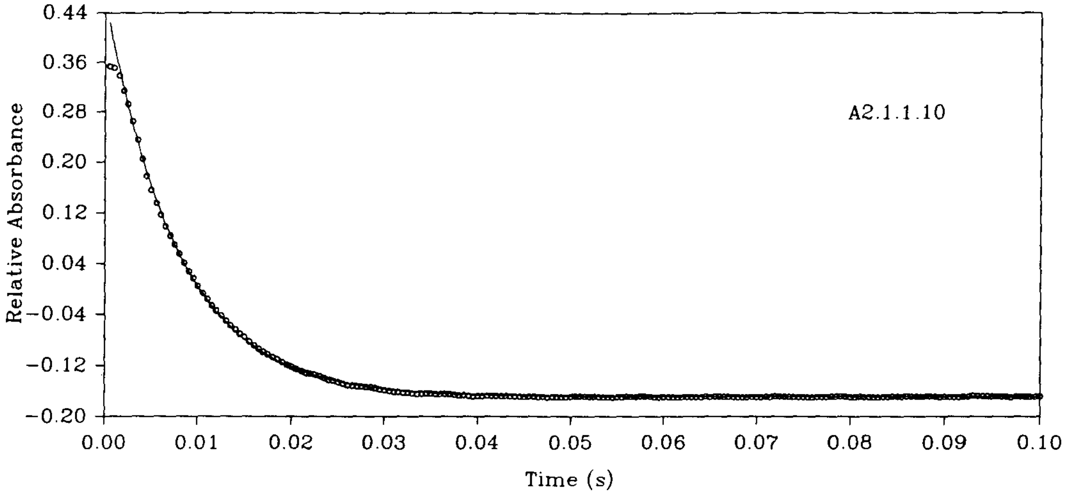
A2.1.1.10
Relative Absorbance
0.44
0.36
0.28
0.20
0.12
0.04
−0.04
−0.12
−0.20
0.00
0.01
0.02
0.03
0.04
0.05
0.06
0.07
0.08
0.09
0.10
Time (s)

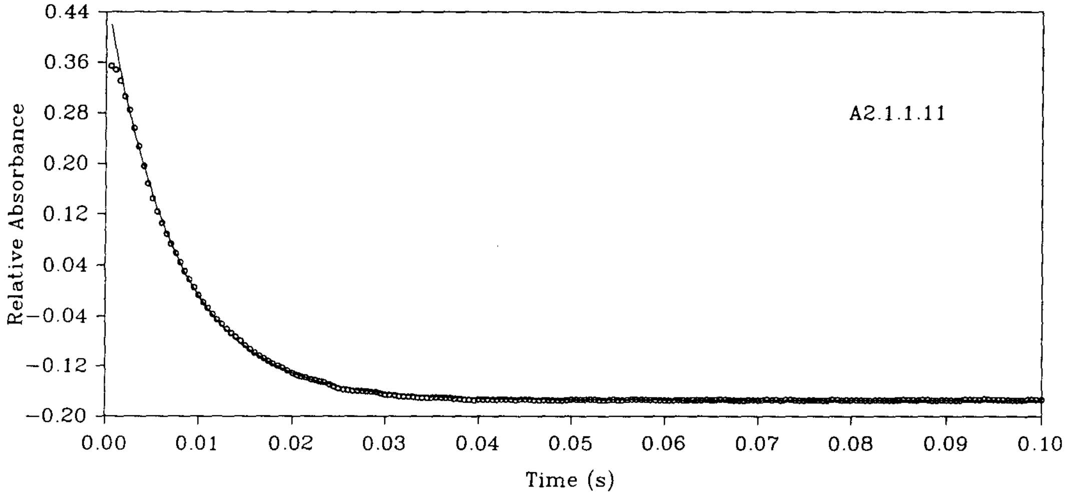
A2.1.1.11
Relative Absorbance
0.44
0.36
0.28
0.20
0.12
0.04
−0.04
−0.12
−0.20
0.00
0.01
0.02
0.03
0.04
0.05
0.06
0.07
0.08
0.09
0.10
Time (s)

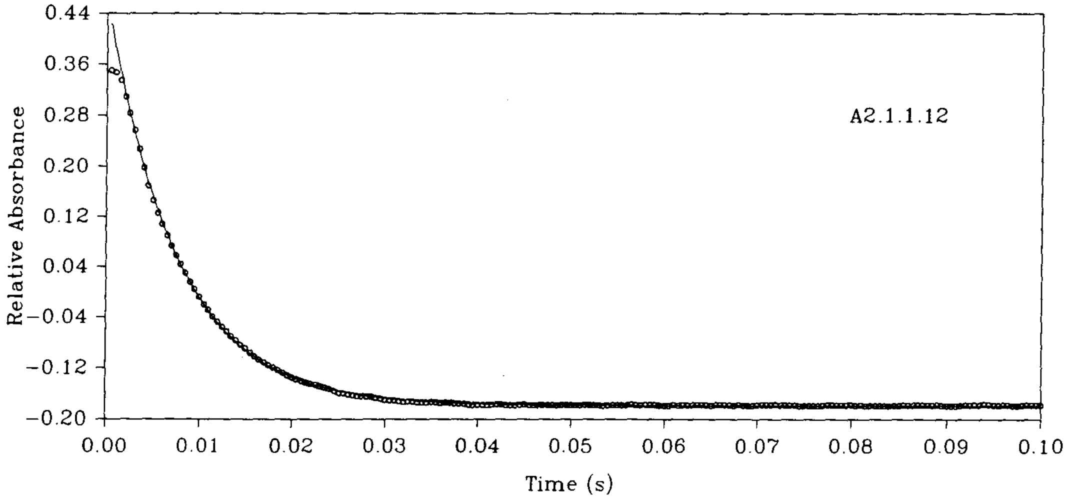
A2.1.1.12
Relative Absorbance
0.44
0.36
0.28
0.20
0.12
0.04
−0.04
−0.12
−0.20
0.00
0.01
0.02
0.03
0.04
0.05
0.06
0.07
0.08
0.09
0.10
Time (s)

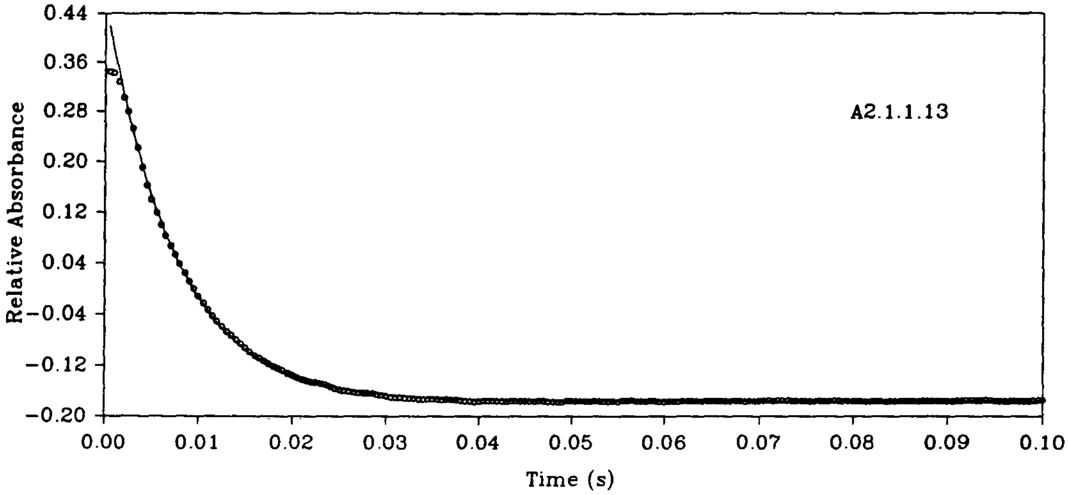
A2.1.1.13
Relative Absorbance
0.44
0.36
0.28
0.20
0.12
0.04
−0.04
−0.12
−0.20
0.00
0.01
0.02
0.03
0.04
0.05
0.06
0.07
0.08
0.09
0.10
Time (s)

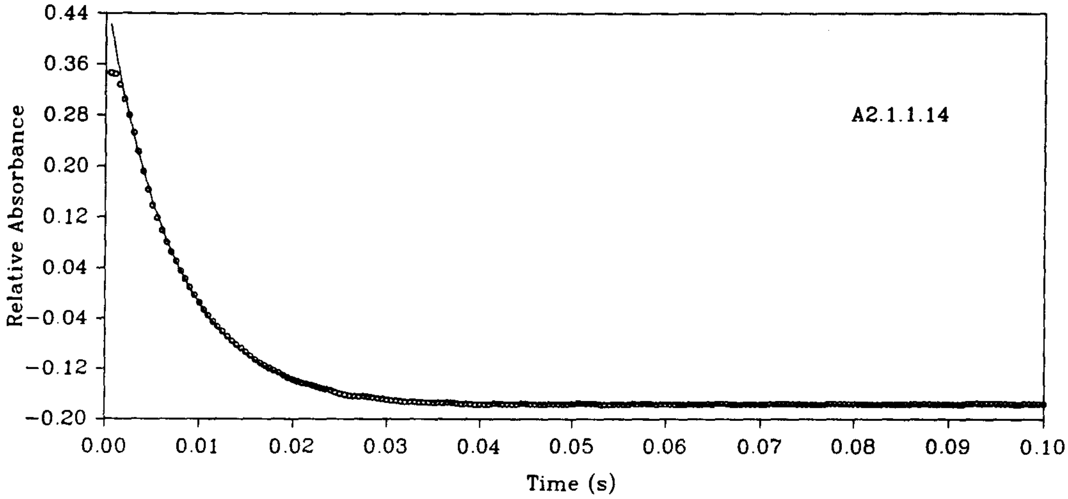
A2.1.1.14
Relative Absorbance
0.44
0.36
0.28
0.20
0.12
0.04
−0.04
−0.12
−0.20
0.00
0.01
0.02
0.03
0.04
0.05
0.06
0.07
0.08
0.09
0.10
Time (s)

### A2.1.2 Experiments Carried Out Using a Constant [$Et_2SO$] of 17.7 ± 0.2 mM

Relative uncertainty in [$Et_2S$] for each experiment ≈ 1-2%.

400 data points were collected in the 0-100 ms time range.

| Graph # | [$Et_2S$] (M) | $\alpha_1$ | $\beta_1$ | $\gamma_1$ ($s^{-1}$) |
|---|---|---|---|---|
| A2.1.2.1 | $5.93x10^{-4}$ | -0.034 | 0.057 | 39.2 |
| A2.1.2.2 | $7.42x10^{-4}$ | -0.023 | 0.069 | 38.3 |
| A2.1.2.3 | $1.48x10^{-3}$ | -0.049 | 0.121 | 42.3 |
| A2.1.2.4 | $1.85x10^{-3}$ | -0.079 | 0.143 | 43.1 |
| A2.1.2.5 | $3.71x10^{-3}$ | -0.097 | 0.232 | 51.6 |
| A2.1.2.6 | $9.27x10^{-3}$ | -0.128 | 0.403 | 64.7 |
| A2.1.2.7 | $1.86x10^{-2}$ | -0.088 | 0.539 | 82.7 |
| A2.1.2.8 | $3.71x10^{-2}$ | -0.188 | 0.597 | 93.6 |
| A2.1.2.9 | $5.57x10^{-2}$ | -0.176 | 0.617 | 103 |
| A2.1.2.10 | 0.111 | -0.179 | 0.654 | 113 |
| A2.1.2.11 | 0.232 | -0.198 | 0.677 | 122 |
| A2.1.2.12 | 0.464 | -0.178 | 0.662 | 126 |

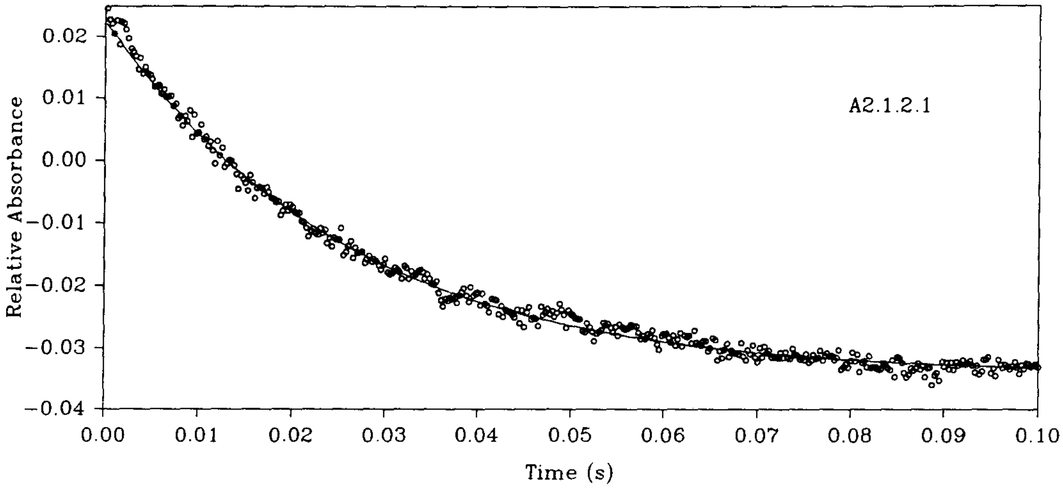
A2.1.2.1
Relative Absorbance
0.02
0.01
0.00
−0.01
−0.02
−0.03
−0.04
0.00
0.01
0.02
0.03
0.04
0.05
0.06
0.07
0.08
0.09
0.10
Time (s)

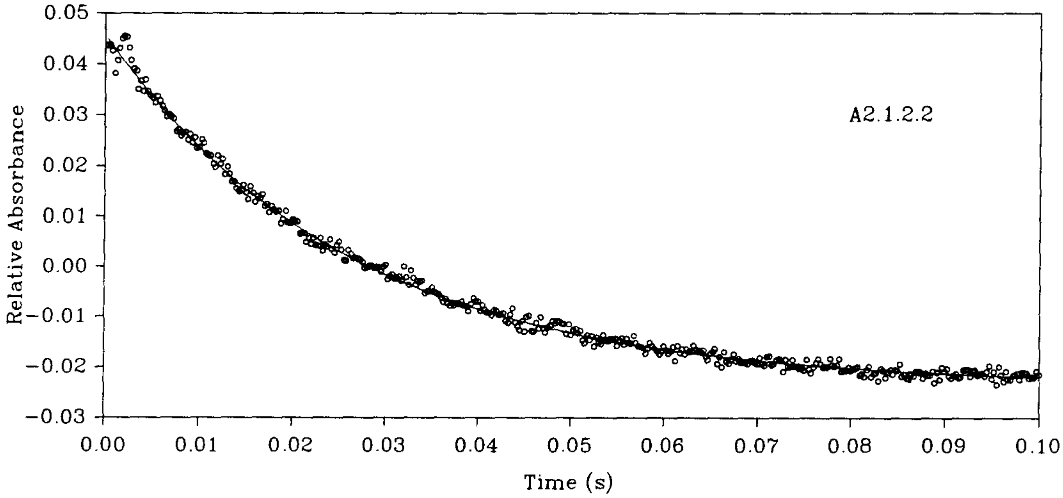
A2.1.2.2
Relative Absorbance
0.05
0.04
0.03
0.02
0.01
0.00
−0.01
−0.02
−0.03
0.00
0.01
0.02
0.03
0.04
0.05
0.06
0.07
0.08
0.09
0.10
Time (s)

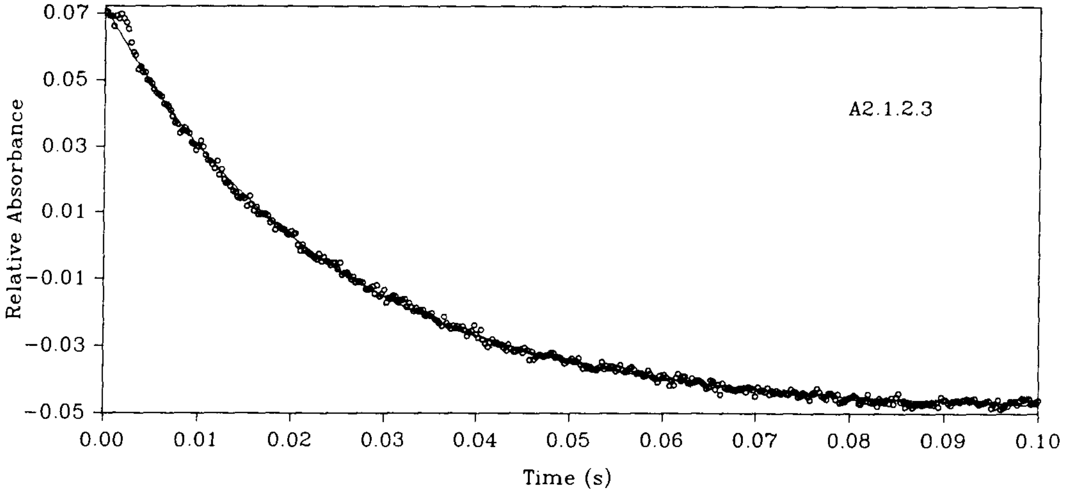
A2.1.2.3
Relative Absorbance
0.07
0.05
0.03
0.01
−0.01
−0.03
−0.05
0.00
0.01
0.02
0.03
0.04
0.05
0.06
0.07
0.08
0.09
0.10
Time (s)

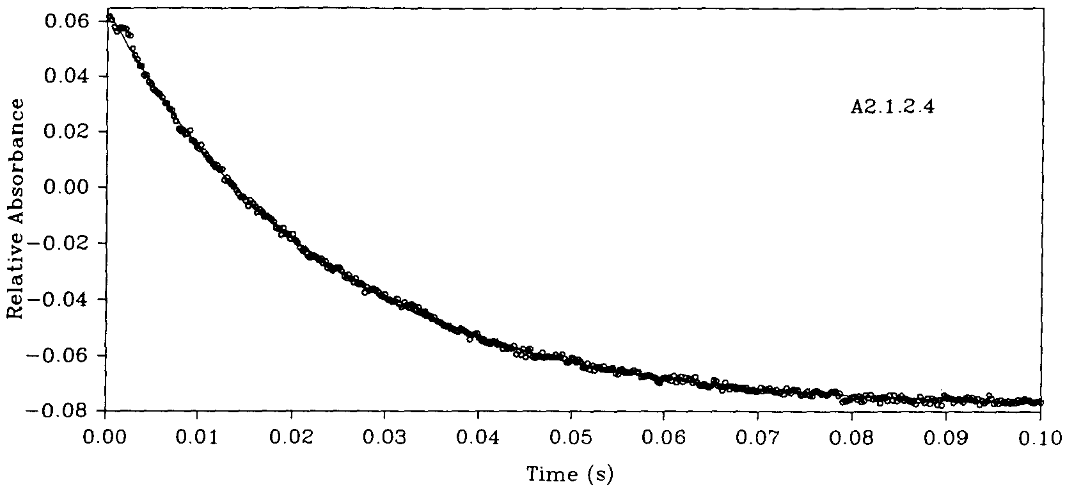
0.06
0.04
0.02
0.00
−0.02
−0.04
−0.06
−0.08
Relative Absorbance
A2.1.2.4
0.00
0.01
0.02
0.03
0.04
0.05
0.06
0.07
0.08
0.09
0.10
Time (s)

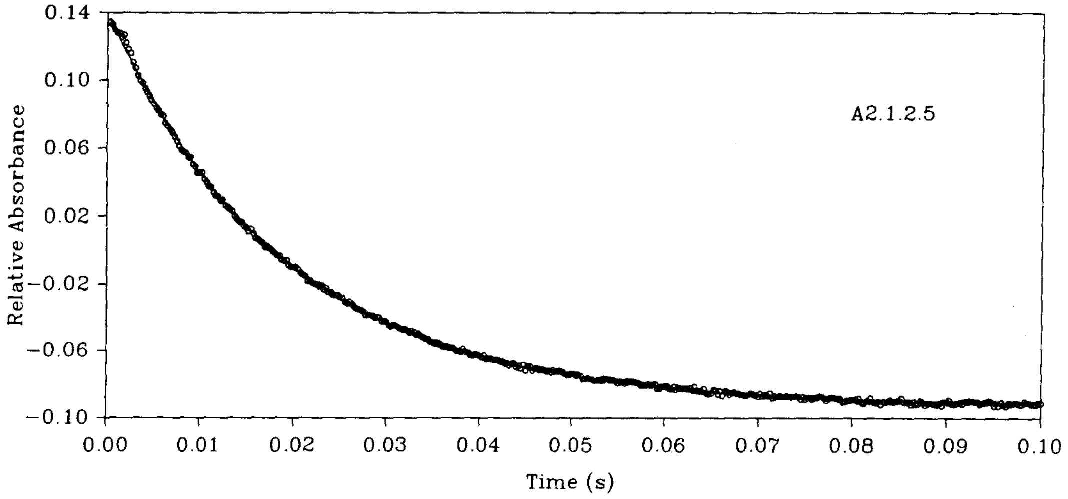
0.14
0.10
0.06
0.02
−0.02
−0.06
−0.10
Relative Absorbance
A2.1.2.5
0.00
0.01
0.02
0.03
0.04
0.05
0.06
0.07
0.08
0.09
0.10
Time (s)

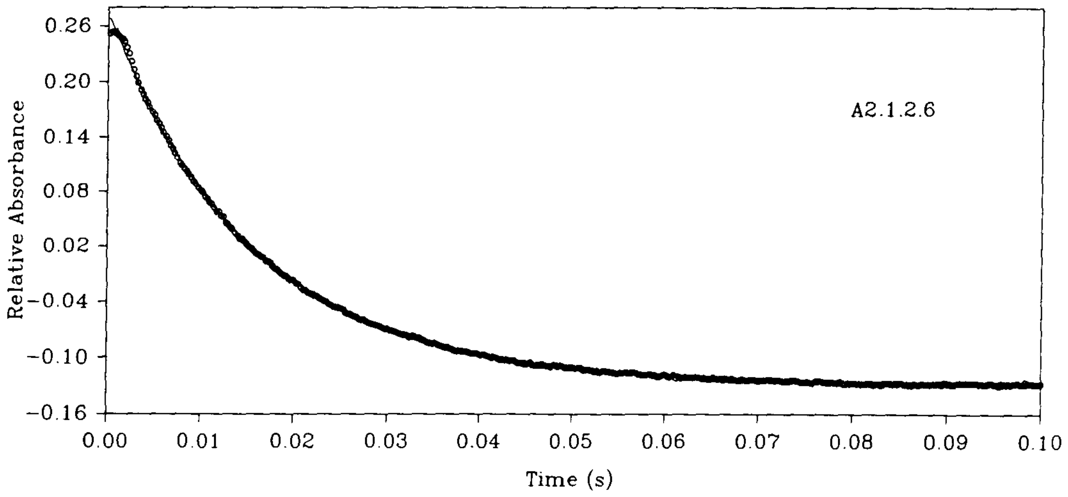
0.26
0.20
0.14
0.08
0.02
−0.04
−0.10
−0.16
Relative Absorbance
A2.1.2.6
0.00
0.01
0.02
0.03
0.04
0.05
0.06
0.07
0.08
0.09
0.10
Time (s)

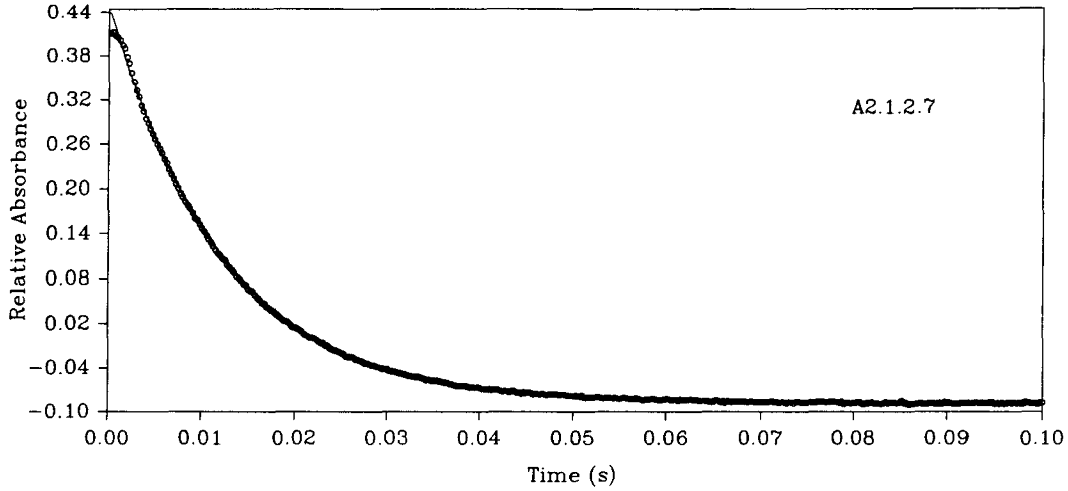
A2.1.2.7
Relative Absorbance
0.44
0.38
0.32
0.26
0.20
0.14
0.08
0.02
−0.04
−0.10
0.00
0.01
0.02
0.03
0.04
0.05
0.06
0.07
0.08
0.09
0.10
Time (s)

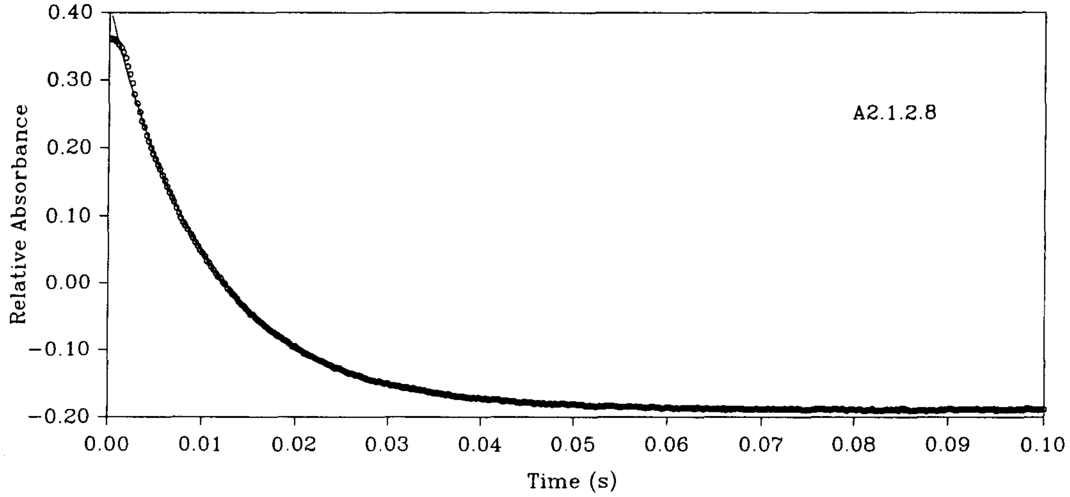
A2.1.2.8
Relative Absorbance
0.40
0.30
0.20
0.10
0.00
−0.10
−0.20
0.00
0.01
0.02
0.03
0.04
0.05
0.06
0.07
0.08
0.09
0.10
Time (s)

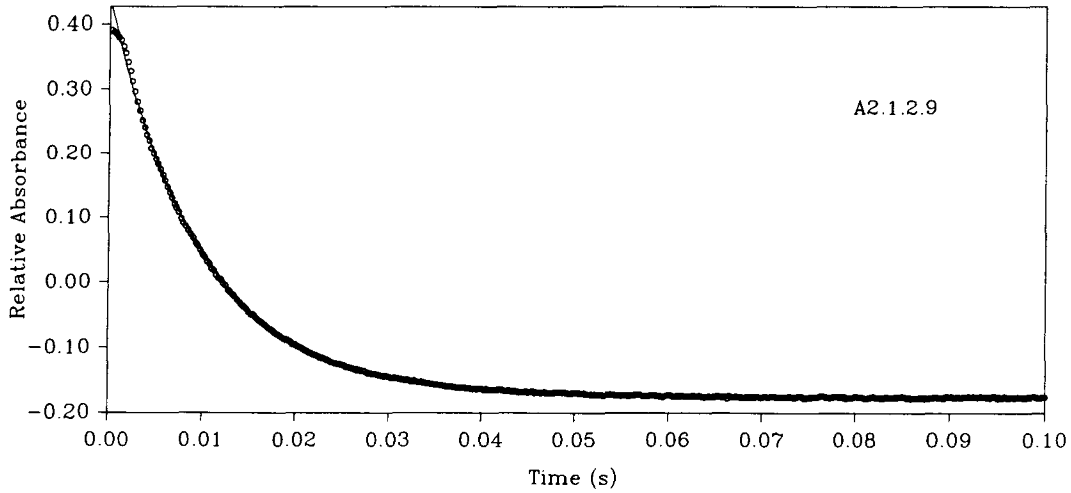
A2.1.2.9
Relative Absorbance
0.40
0.30
0.20
0.10
0.00
−0.10
−0.20
0.00
0.01
0.02
0.03
0.04
0.05
0.06
0.07
0.08
0.09
0.10
Time (s)

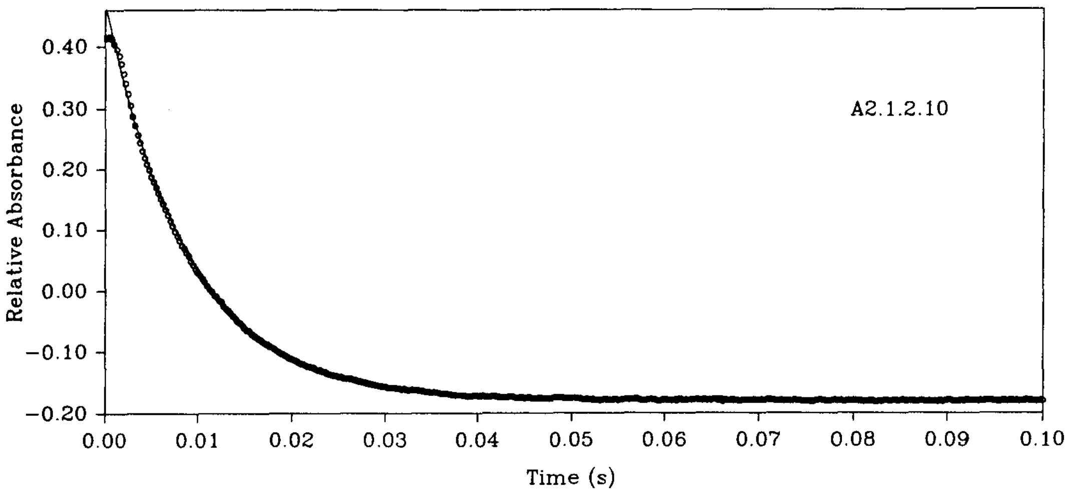
A2.1.2.10
Relative Absorbance
0.40
0.30
0.20
0.10
0.00
−0.10
−0.20
0.00
0.01
0.02
0.03
0.04
0.05
0.06
0.07
0.08
0.09
0.10
Time (s)

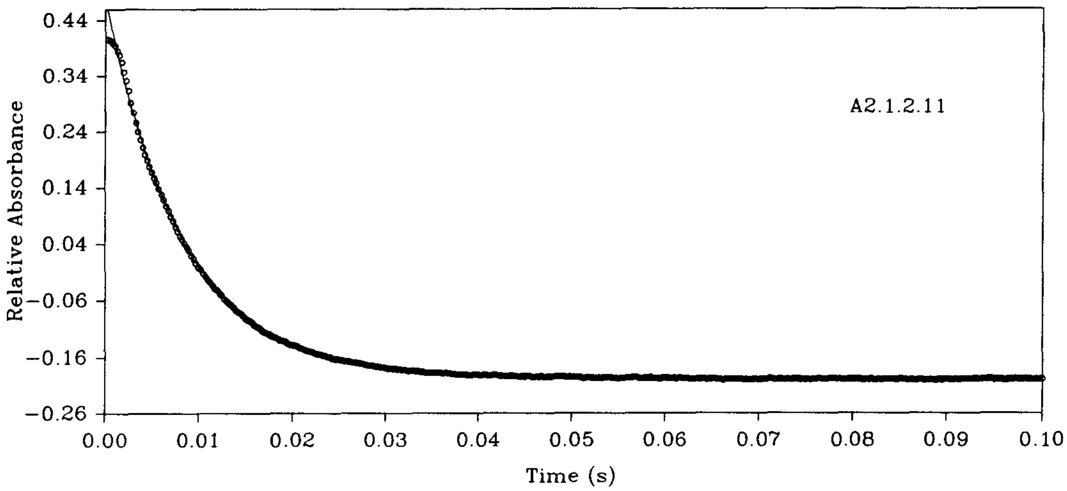
A2.1.2.11
Relative Absorbance
0.44
0.34
0.24
0.14
0.04
−0.06
−0.16
−0.26
0.00
0.01
0.02
0.03
0.04
0.05
0.06
0.07
0.08
0.09
0.10
Time (s)

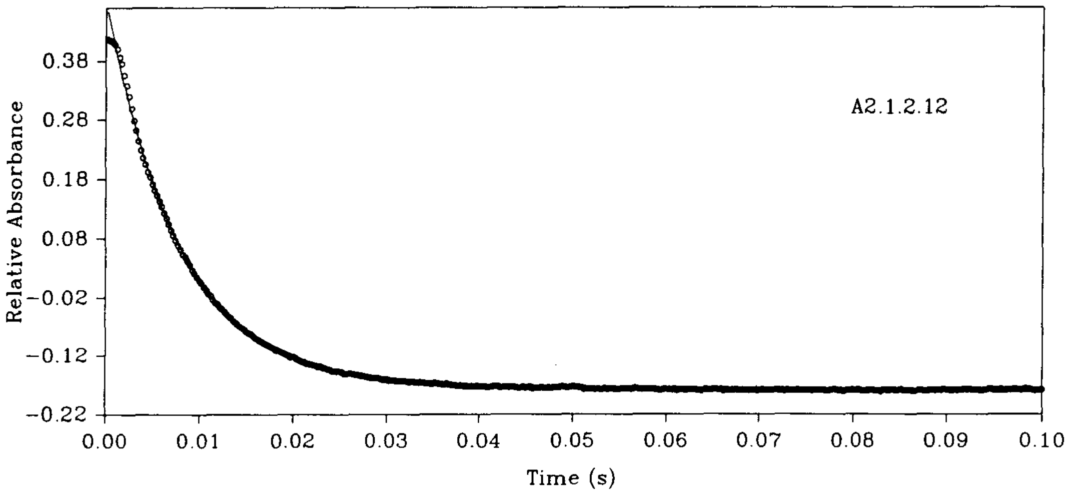
A2.1.2.12
Relative Absorbance
0.38
0.28
0.18
0.08
−0.02
−0.12
−0.22
0.00
0.01
0.02
0.03
0.04
0.05
0.06
0.07
0.08
0.09
0.10
Time (s)

## A2.2 Experiments Carried Out Using Light of 402.8 nm Wavelength

The table that follows gives the numerical values of the parameters $\alpha_2$, $\beta_2$ $\gamma_2$, used to obtain the data points in figure 3.18. Following the table are the relative absorbance vs. time raw data plots (corrected for a non-level baseline; see section A2.3) to which the equation

$$A = \alpha_2 + \beta_2 e^{-(\gamma_2 t)}$$

was fitted, to obtain each set of $\alpha_2$, $\beta_2$, $\gamma_2$ values. For each experiment, the relative absorbance change was monitored over a period of 100 s. The initial concentration of $Ru(OEP)(Et_2SO)_2$ in each case was $(3.44 \pm 0.07) \times 10^{-6}$ M.

### A2.2.1 Experiments Carried Out Using a Constant [$Et_2SO$] of 1.18 ± 0.03 mM

Relative uncertainty in [$Et_2S$] for each experiment ≈ 1-2%.

400 data points were collected in the 0-100 s time range.

| Graph # | [$Et_2S$] (M) | $\alpha_2$ | $\beta_2$ | $\gamma_2$ ($s^{-1}$) |
|---|---|---|---|---|
| A2.2.1.1 | $5.93 x 10^{-4}$ | 0.0344 | 0.0090[a] | 0.47[a] |
| A2.2.1.2 | $1.85 x 10^{-3}$ | 0.0073 | 0.0404 | 0.251 |
| A2.2.1.3 | $3.71 x 10^{-3}$ | -0.059 | 0.0870 | 0.183 |
| A2.2.1.4 | $9.27 x 10^{-3}$ | -0.093 | 0.181 | 0.104 |
| A2.2.1.5 | $1.86 x 10^{-2}$ | -0.127 | 0.289 | 0.0706 |
| A2.2.1.6 | $3.71 x 10^{-2}$ | -0.086 | 0.391 | 0.0549 |
| A2.2.1.7 | $5.56 x 10^{-2}$ | -0.139 | 0.441 | 0.0489 |
| A2.2.1.8 | 0.111 | -0.180 | 0.513 | 0.0432 |
| A2.2.1.9 | 0.231 | -0.185 | 0.556 | 0.0414 |

a) The calculated uncertainites in these values are about 10%; for the remaining $\beta_2$ and $\gamma_2$ values, the calculated uncertainties were about 1%.

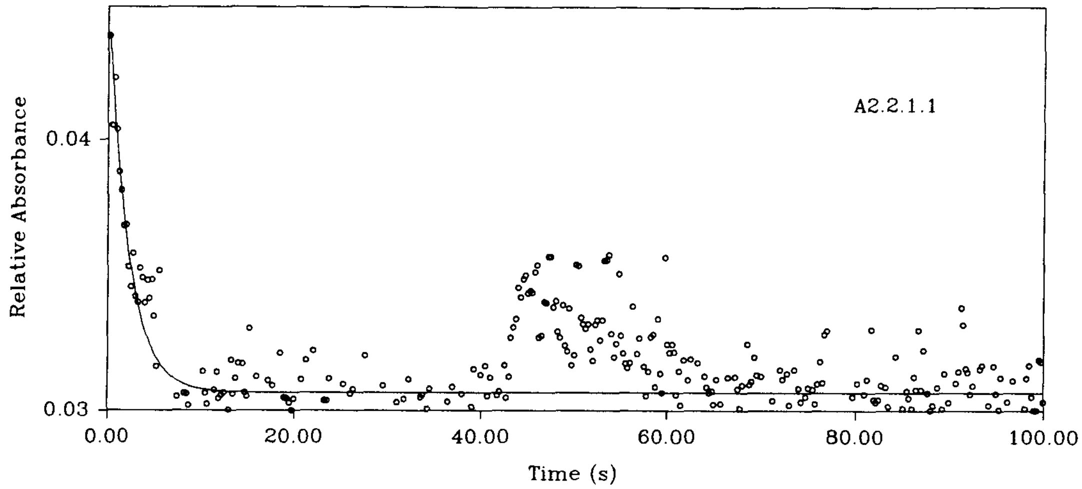
A2.2.1.1
Relative Absorbance
0.04
0.03
0.00
20.00
40.00
60.00
80.00
100.00
Time (s)

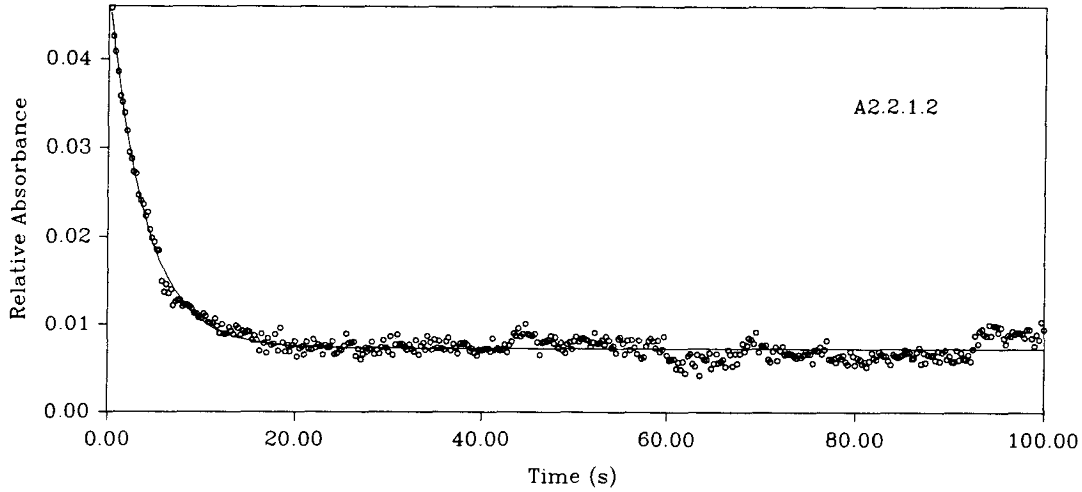
A2.2.1.2
Relative Absorbance
0.04
0.03
0.02
0.01
0.00
0.00
20.00
40.00
60.00
80.00
100.00
Time (s)

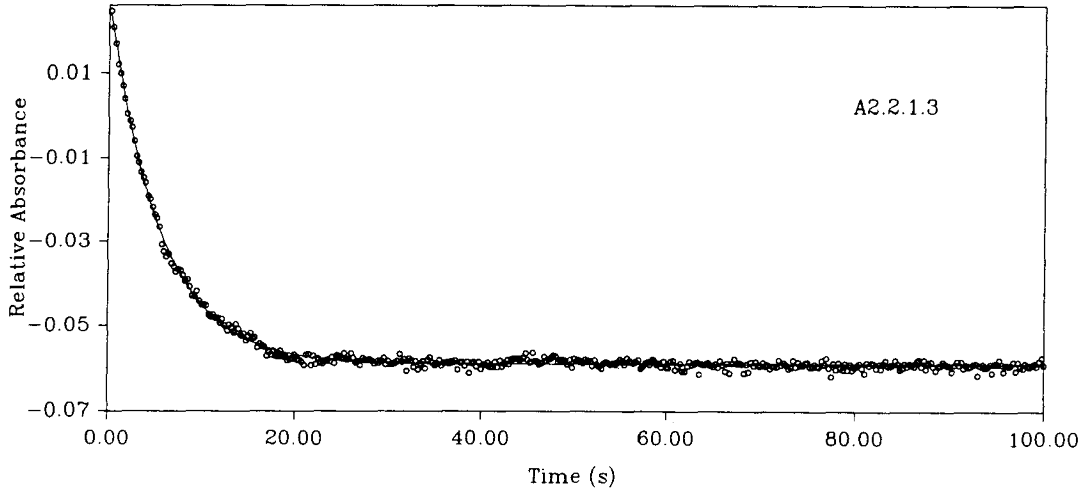
A2.2.1.3
Relative Absorbance
0.01
−0.01
−0.03
−0.05
−0.07
0.00
20.00
40.00
60.00
80.00
100.00
Time (s)

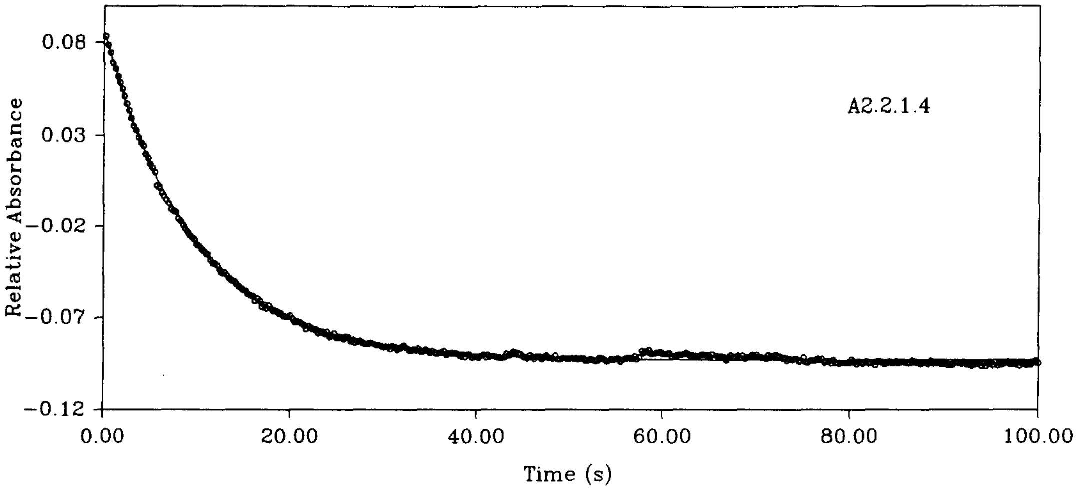
0.08
0.03
-0.02
-0.07
-0.12
Relative Absorbance
A2.2.1.4
0.00
20.00
40.00
60.00
80.00
100.00
Time (s)

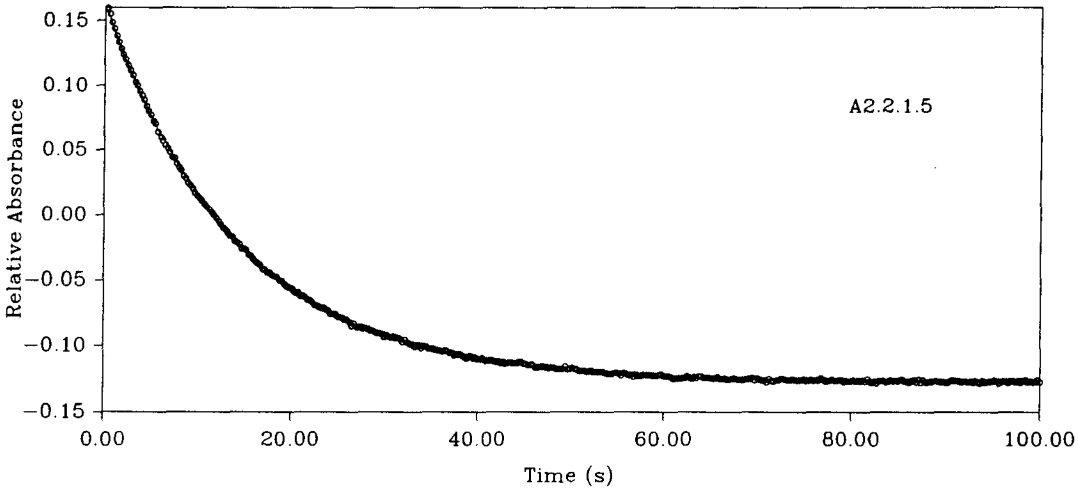
0.15
0.10
0.05
0.00
-0.05
-0.10
-0.15
Relative Absorbance
A2.2.1.5
0.00
20.00
40.00
60.00
80.00
100.00
Time (s)

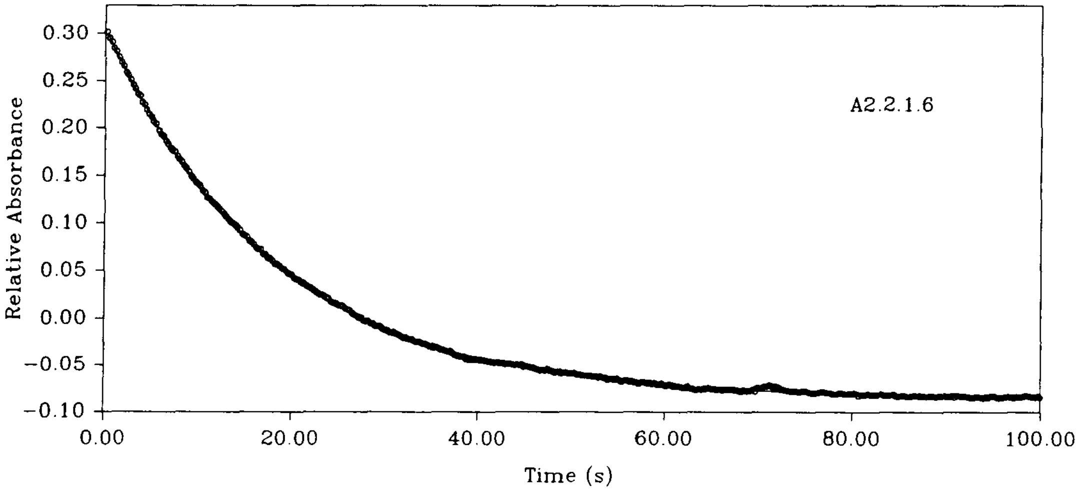
0.30
0.25
0.20
0.15
0.10
0.05
0.00
-0.05
-0.10
Relative Absorbance
A2.2.1.6
0.00
20.00
40.00
60.00
80.00
100.00
Time (s)

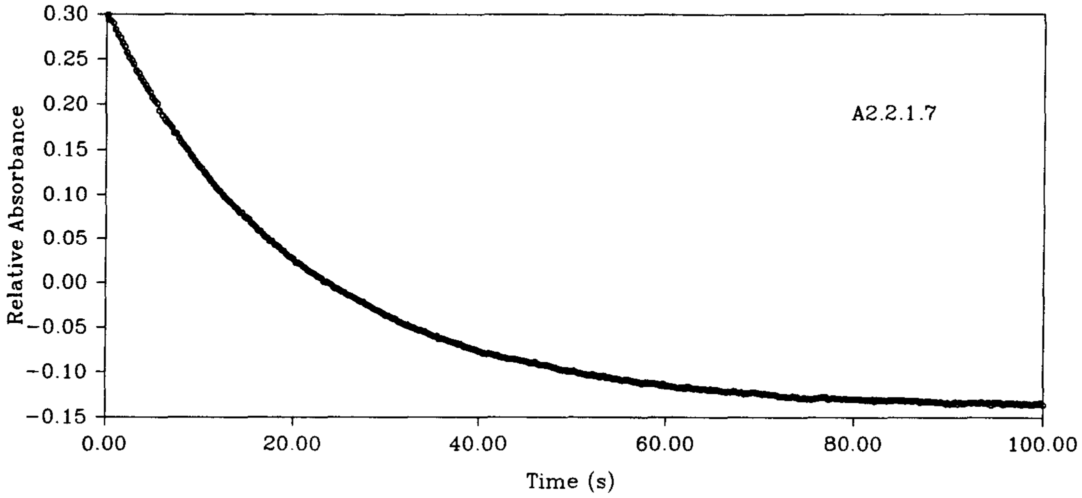
0.30
0.25
0.20
0.15
0.10
0.05
0.00
−0.05
−0.10
−0.15
Relative Absorbance
A2.2.1.7
0.00
20.00
40.00
60.00
80.00
100.00
Time (s)

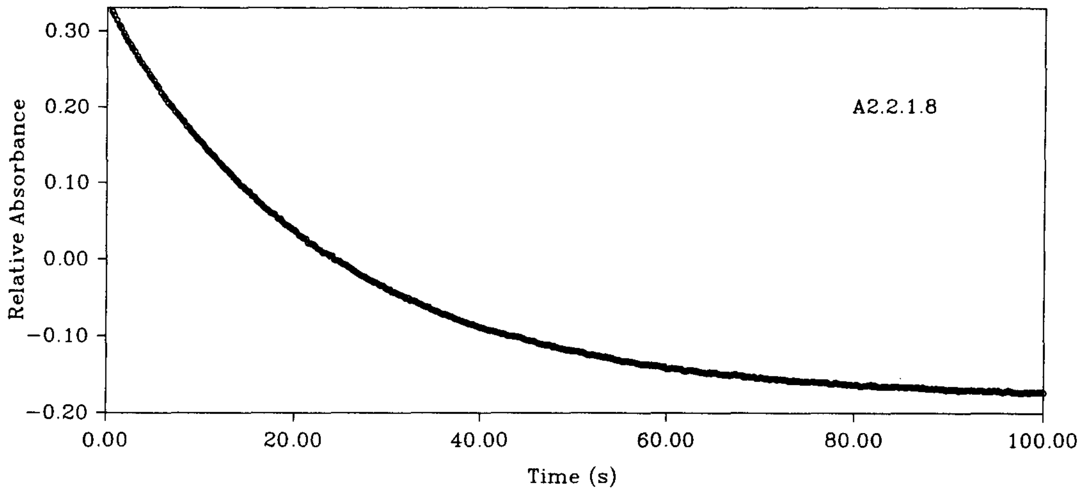
0.30
0.20
0.10
0.00
−0.10
−0.20
Relative Absorbance
A2.2.1.8
0.00
20.00
40.00
60.00
80.00
100.00
Time (s)

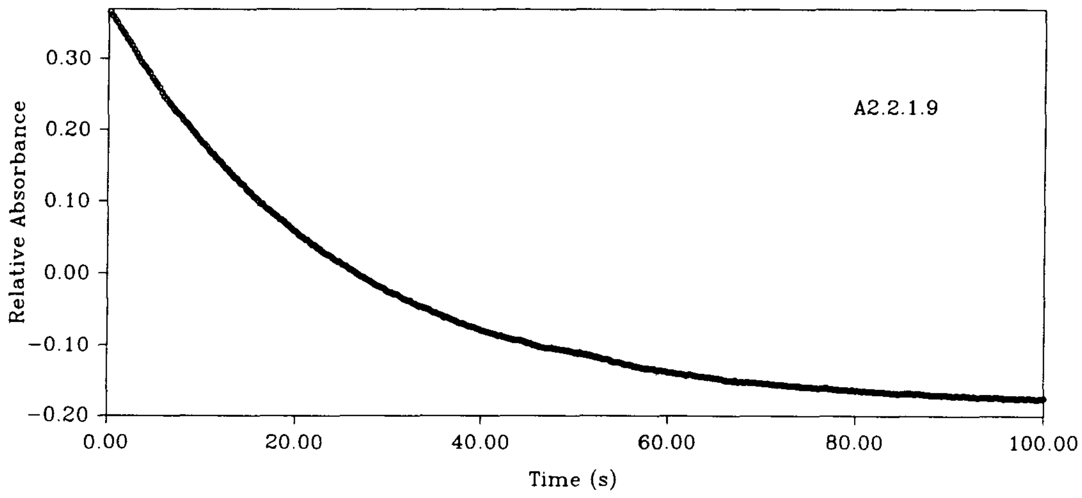
0.30
0.20
0.10
0.00
−0.10
−0.20
Relative Absorbance
A2.2.1.9
0.00
20.00
40.00
60.00
80.00
100.00
Time (s)

## A2.3 Blank Experiments

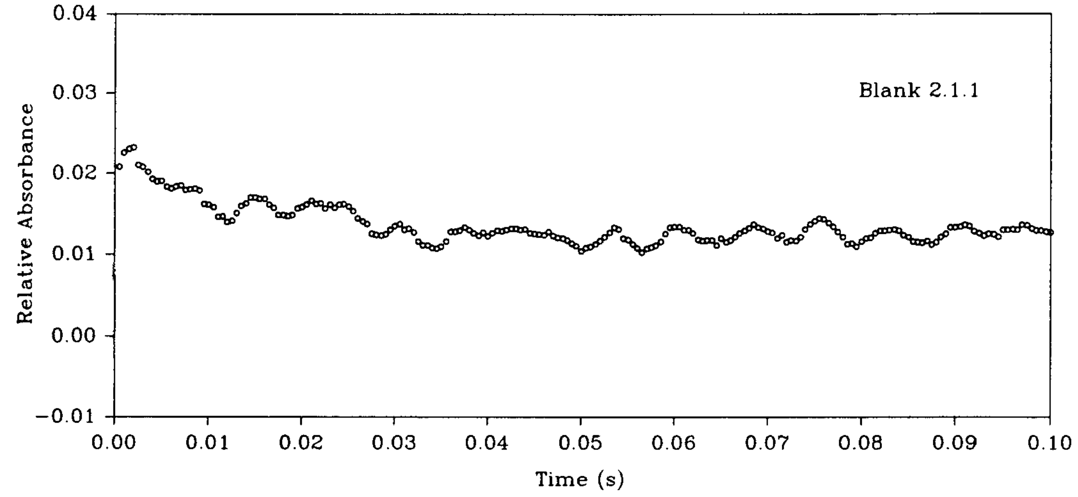

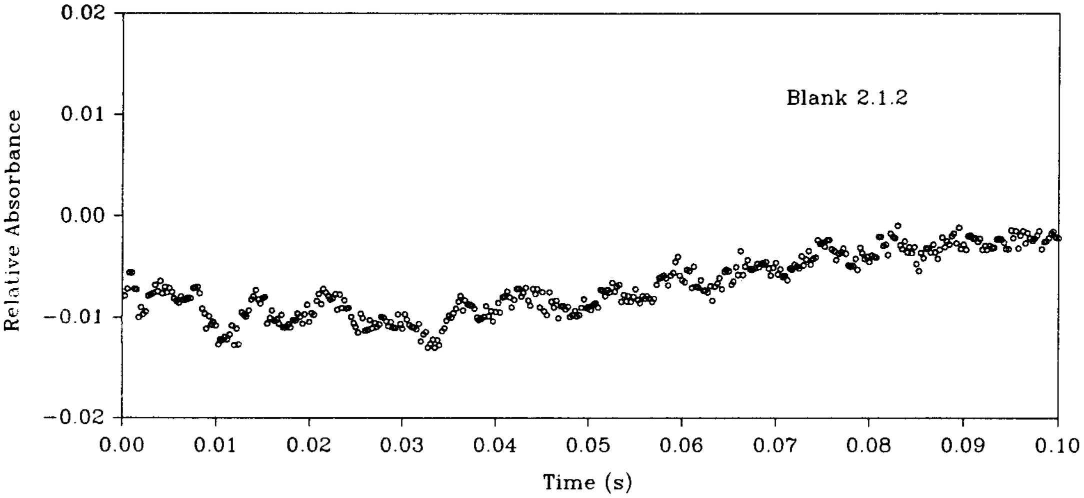

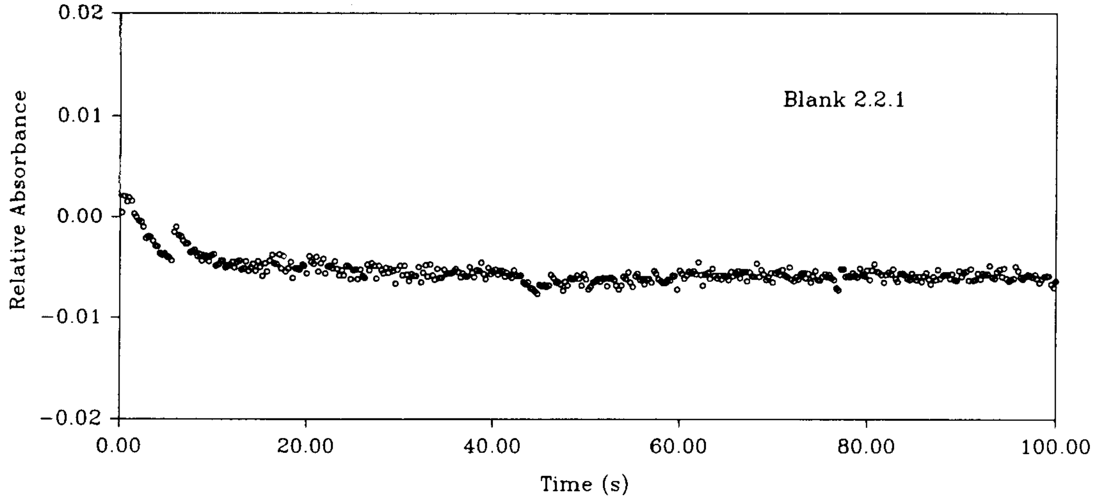

# APPENDIX 3

# RESULTS OF OXYGEN UPTAKE EXPERIMENTS

## A3.1 First Data Set

The three tables that follow give the numerical values of the data points shown in figures 3.23 and 3.25. Following each table are the [$Et_2SO$] vs. time raw data plots which gave rise to each data point in figures 3.23 and 3.25.

### A3.1.1 $[Ru]_o$ Dependence Studies

[PhCOOH] = 24.4 ± 0.1 mM

$[O_2]$ = 7.63 ± 0.07 mM

$[Et_2S]$ = 0.742 ± 0.006 M

Shaking rate = 164 ± 10 cycles/min

Solution volume = 10.0 ± 0.1 mL

Relative uncertainty in $[Ru]_o$ ≈ 1%

| Graph # | $[Ru]_o$ (M) | $k_{obs}x10^6$ | $\chi^2$ | Q |
|---|---|---|---|---|
| A3.1.1.1 | $2.55x10^{-5}$ | 1.26 | 8.0 | 0.34 |
| A3.1.1.2 | $5.10x10^{-5}$ | 2.26 | 19 | 0.071 |
| A3.1.1.3 | $1.02x10^{-4}$ | 3.41 | 17 | 0.11 |
| A3.1.1.4 | $2.04x10^{-4}$ | 4.48 | 6.2 | 0.90 |
| A3.1.1.5 | $2.43x10^{-4}$ | 4.68 | 11 | 0.29 |
| A3.1.1.6 | $4.08x10^{-4}$ | 5.72 | 10 | 0.30 |
| A3.1.1.7 | $6.15x10^{-4}$ | 6.42 | 36 | $2x10^{-4}$ |
| A3.1.1.8 | $8.37x10^{-4}$ | 7.91 | 25 | 0.014 |
| A3.1.1.9 | $1.04x10^{-3}$ | 8.14 | 34 | $3x10^{-4}$ |
| A3.1.1.10 | $1.21x10^{-3}$ | 8.38 | 33 | $9x10^{-4}$ |

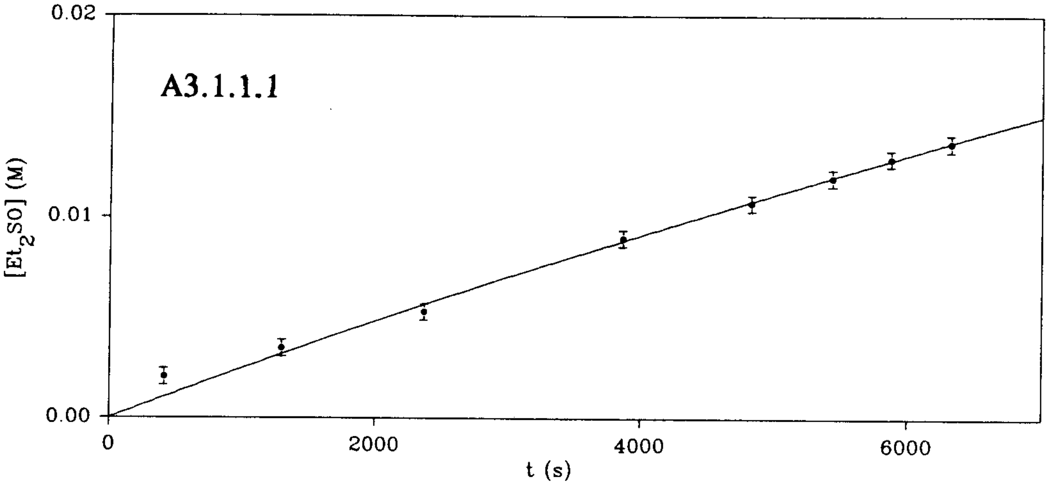
A3.1.1.1
0.02
0.01
0.00
[Et$_2$SO] (M)
0
2000
4000
6000
t (s)

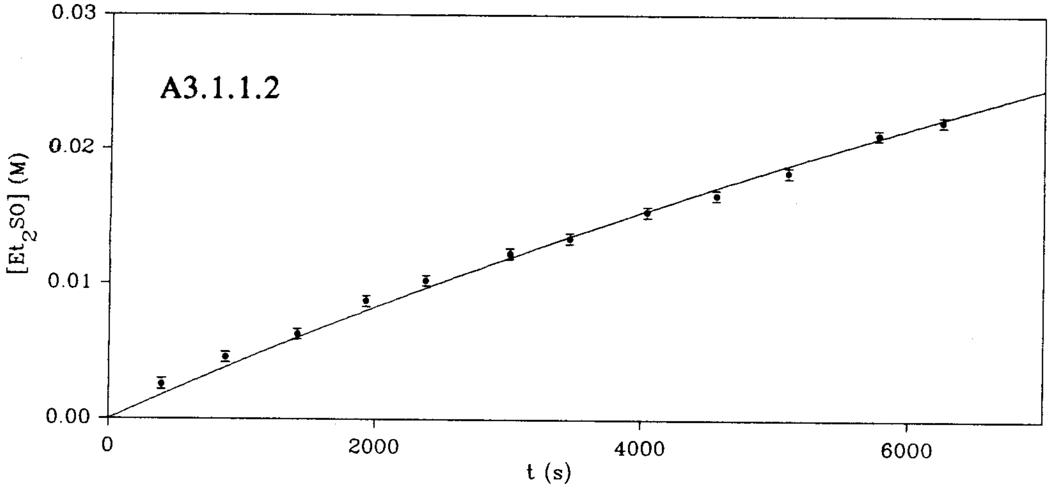
A3.1.1.2
0.03
0.02
0.01
0.00
[Et$_2$SO] (M)
0
2000
4000
6000
t (s)

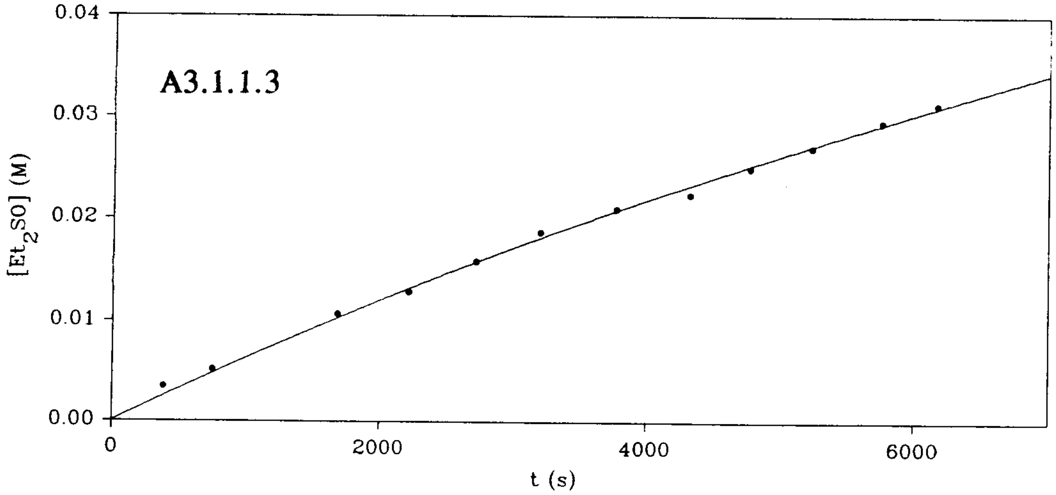
A3.1.1.3
0.04
0.03
0.02
0.01
0.00
[Et$_2$SO] (M)
0
2000
4000
6000
t (s)

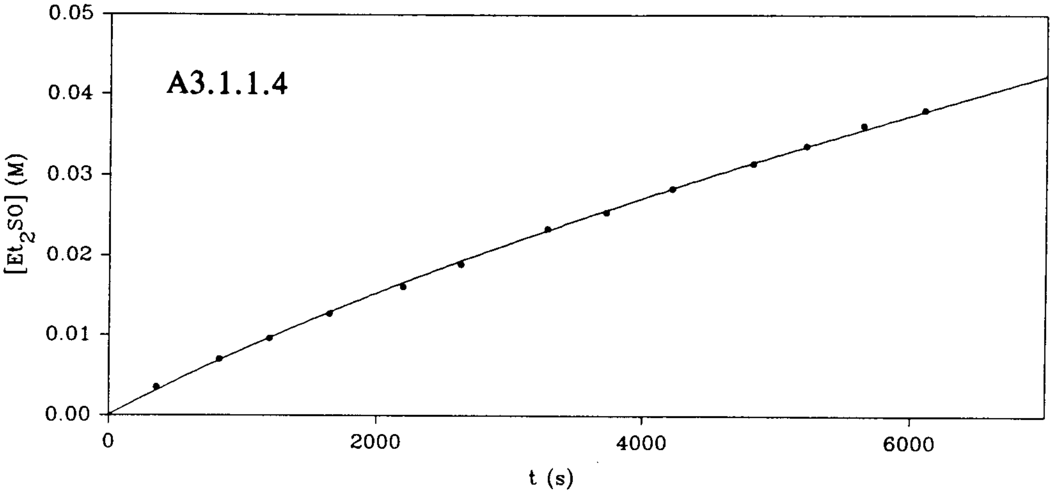
A3.1.1.4
[Et$_2$SO] (M)
0.05
0.04
0.03
0.02
0.01
0.00
0
2000
4000
6000
t (s)

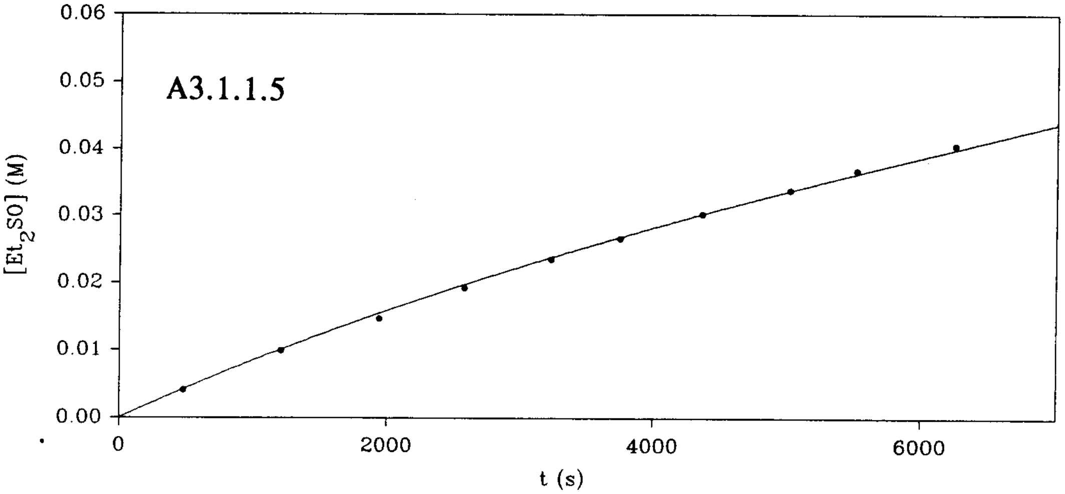
A3.1.1.5
[Et$_2$SO] (M)
0.06
0.05
0.04
0.03
0.02
0.01
0.00
0
2000
4000
6000
t (s)

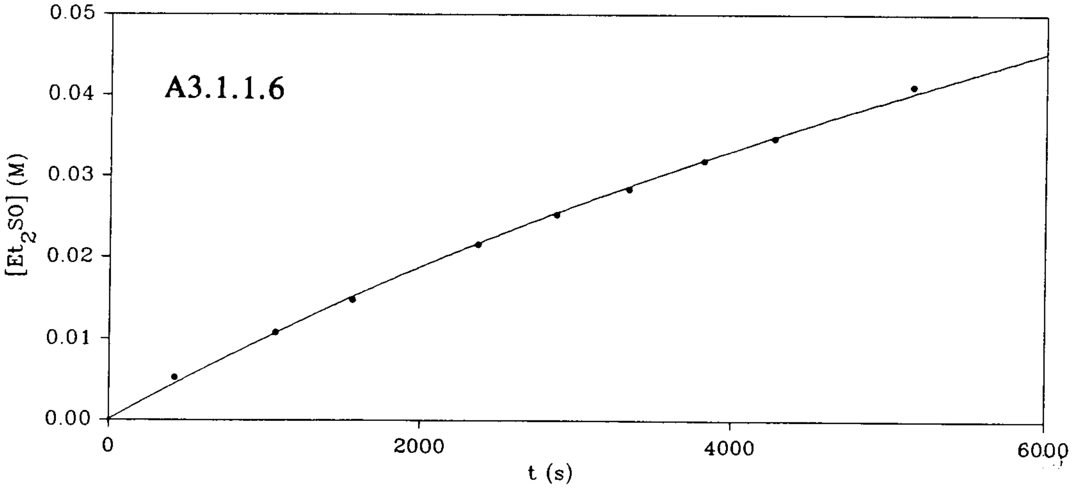
A3.1.1.6
[Et$_2$SO] (M)
0.05
0.04
0.03
0.02
0.01
0.00
0
2000
4000
6000
t (s)

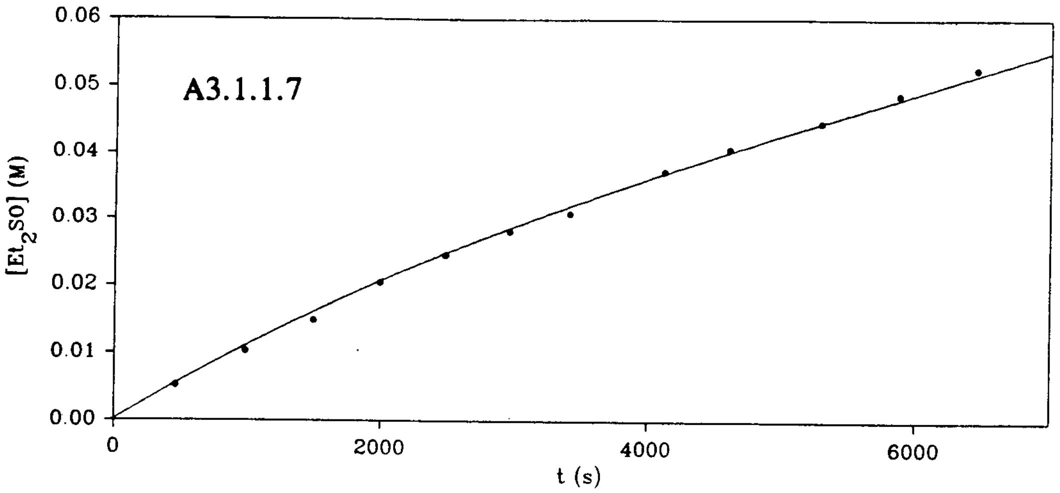
A3.1.1.7
[Et$_2$SO] (M)
0.06
0.05
0.04
0.03
0.02
0.01
0.00
0
2000
4000
6000
t (s)

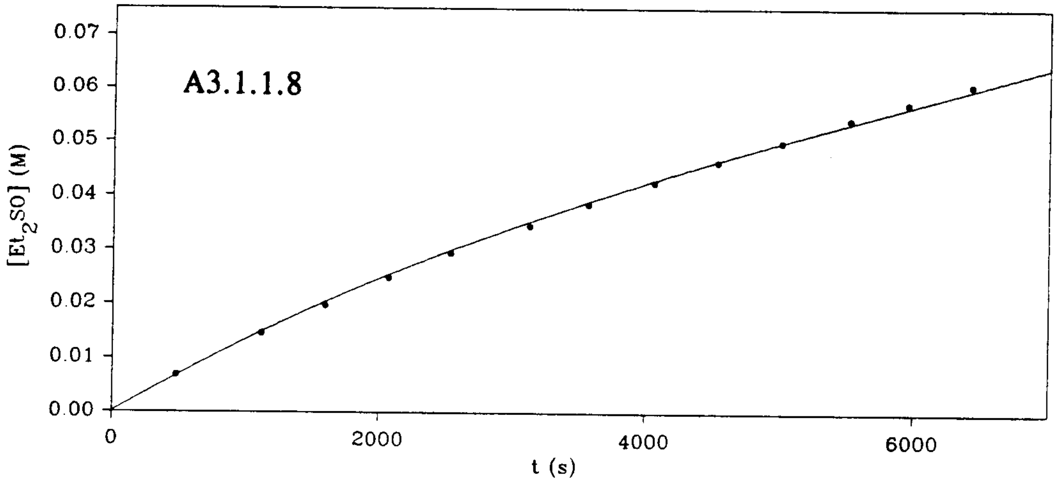
A3.1.1.8
[Et$_2$SO] (M)
0.07
0.06
0.05
0.04
0.03
0.02
0.01
0.00
0
2000
4000
6000
t (s)

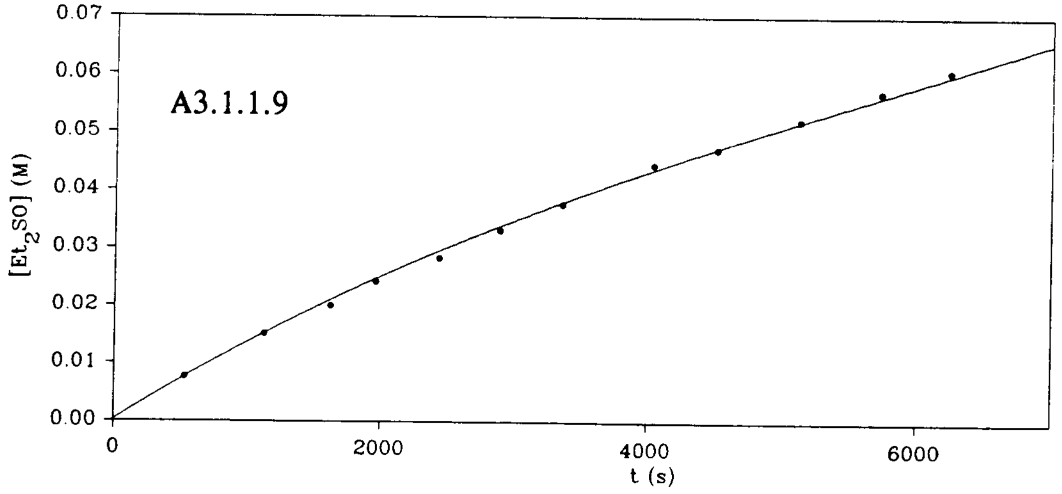
A3.1.1.9
[Et$_2$SO] (M)
0.07
0.06
0.05
0.04
0.03
0.02
0.01
0.00
0
2000
4000
6000
t (s)

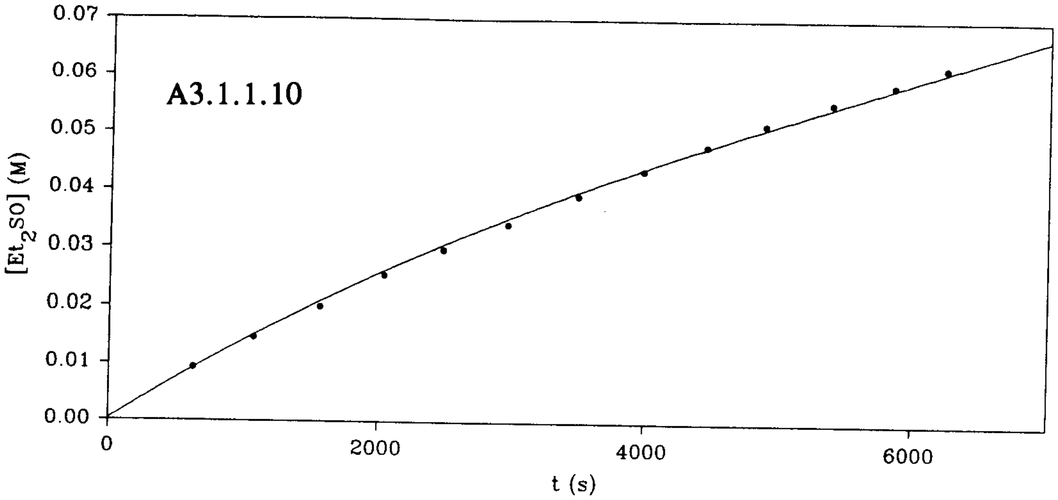
A3.1.1.10
[Et$_2$SO] (M)
0.07
0.06
0.05
0.04
0.03
0.02
0.01
0.00
0
2000
4000
6000
t (s)

### A3.1.2 [PhCOOH] Dependence Studies

$[Ru]_o$ = 0.408 ± 0.004 mM

$[O_2]$ = 7.63 ± 0.07 mM

$[Et_2S]$ = 0.742 ± 0.006 M

Shaking rate = 164 ± 10 cycles/min

Solution volume = 10.0 ± 0.1 mL

Relative uncertainty in [PhCOOH] ≈ 0.5-1%

| Graph # | [PhCOOH] (M) | $k_{obs}x10^6$ | $\chi^2$ | Q |
|---|---|---|---|---|
| A3.1.2.1 | $8.35x10^{-4}$ | 1.24 | 14 | 0.30 |
| A3.1.2.2 | $1.25x10^{-3}$ | 1.25 | 16 | 0.15 |
| A3.1.2.3 | $2.09x10^{-3}$ | 1.55 | 25 | 0.020 |
| A3.1.2.4 | $4.09x10^{-3}$ | 2.11 | 29 | $2.1x10^{-3}$ |
| A3.1.2.5 | $7.42x10^{-3}$ | 3.41 | 56 | $1.4x10^{-7}$ |
| A3.1.2.6 | $9.86x10^{-3}$ | 3.46 | 39 | $3.5x10^{-4}$ |
| A3.1.2.7 | $1.75x10^{-2}$ | 4.98 | 30 | $1.8x10^{-3}$ |
| A3.1.2.8 | $2.11x10^{-2}$ | 5.16 | 2.2 | 1.0 |
| A3.1.2.9 | $2.44x10^{-2}$ | 5.72 | 9.5 | 0.30 |

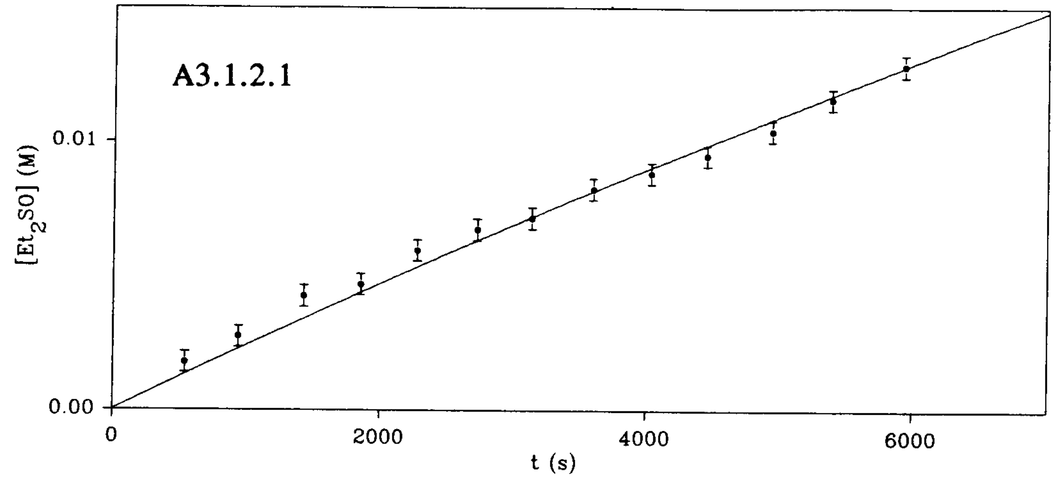
A3.1.2.1
[Et$_2$SO] (M)
0.01
0.00
0
2000
4000
6000
t (s)

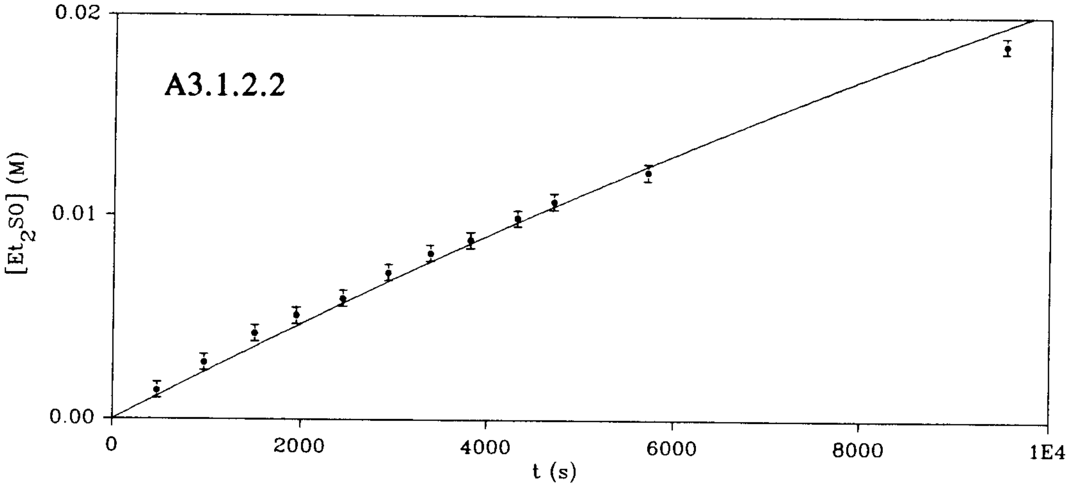
A3.1.2.2
[Et$_2$SO] (M)
0.02
0.01
0.00
0
2000
4000
6000
8000
1E4
t (s)

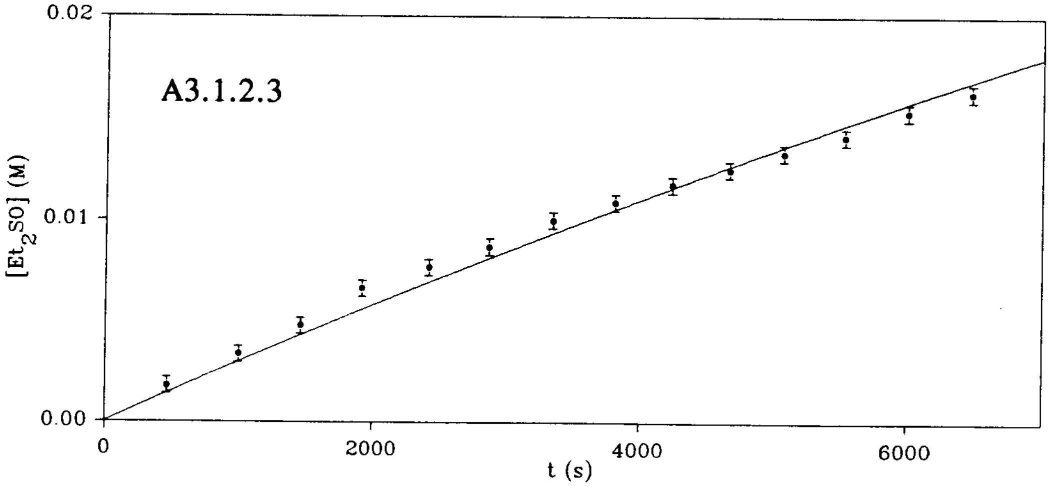
A3.1.2.3
[Et$_2$SO] (M)
0.02
0.01
0.00
0
2000
4000
6000
t (s)

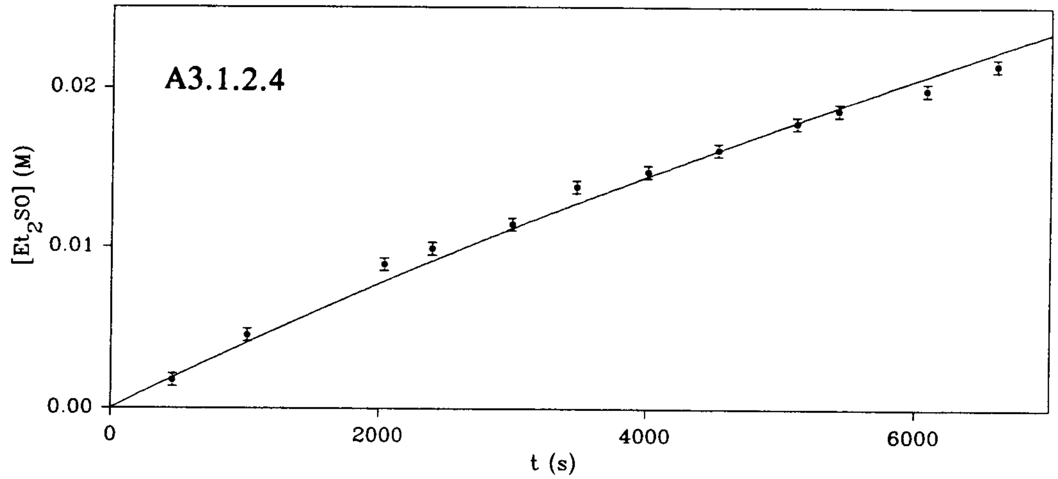
A3.1.2.4
$[Et_2SO]$ (M)
0.00
0.01
0.02
0
2000
4000
6000
t (s)

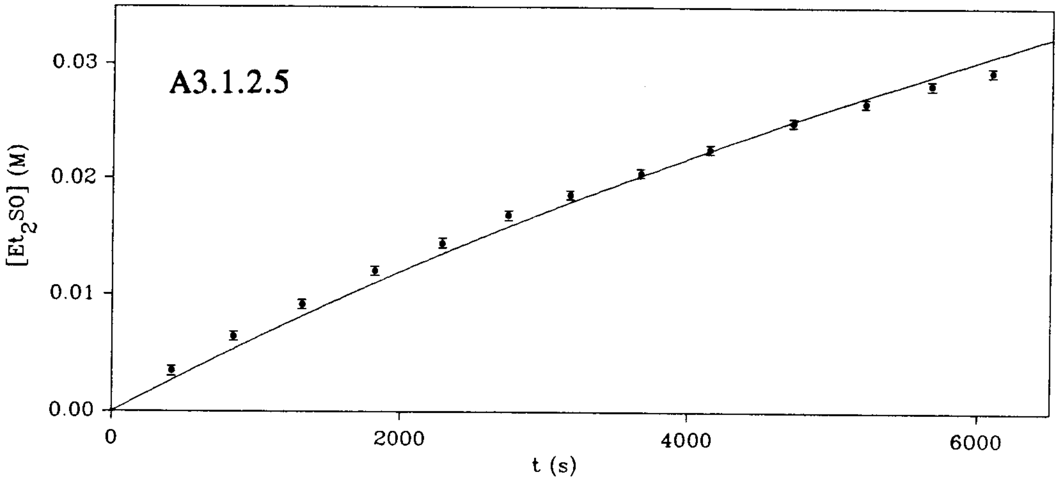
A3.1.2.5
$[Et_2SO]$ (M)
0.00
0.01
0.02
0.03
0
2000
4000
6000
t (s)

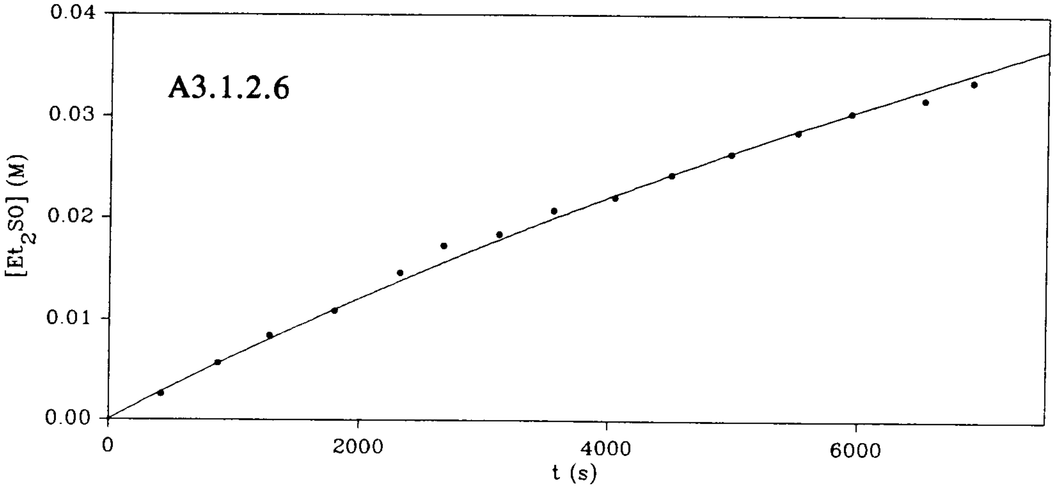
A3.1.2.6
$[Et_2SO]$ (M)
0.00
0.01
0.02
0.03
0.04
0
2000
4000
6000
t (s)

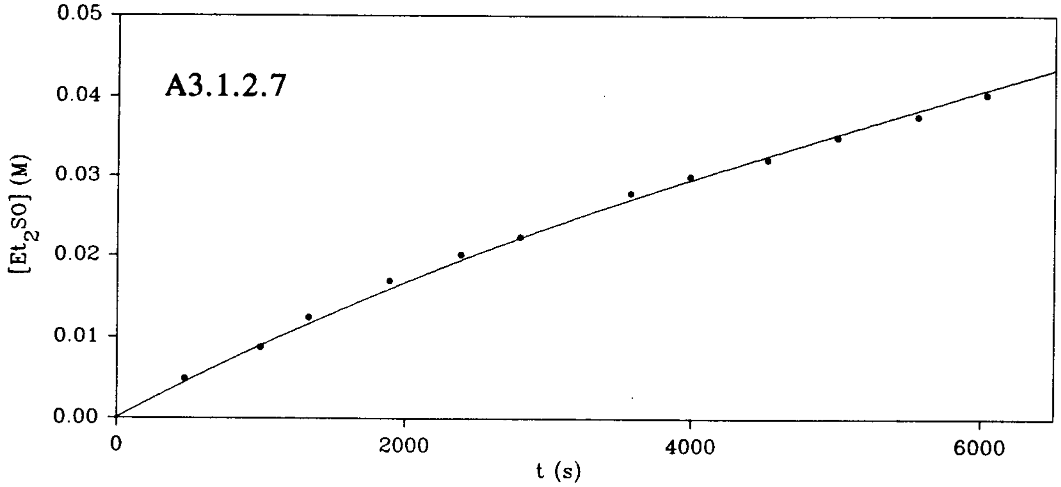
A3.1.2.7
0.05
0.04
0.03
0.02
0.01
0.00
$[Et_2SO]$ (M)
0
2000
4000
6000
t (s)

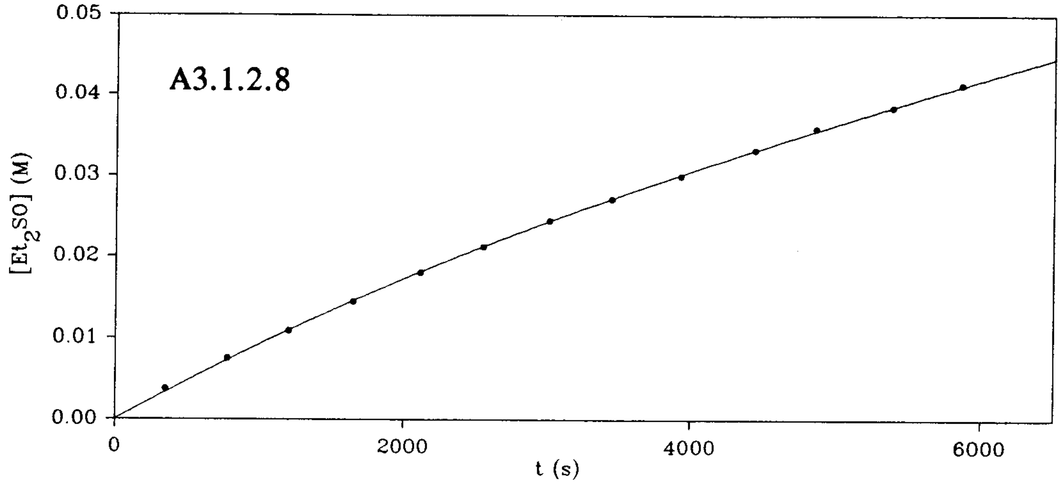
A3.1.2.8
0.05
0.04
0.03
0.02
0.01
0.00
$[Et_2SO]$ (M)
0
2000
4000
6000
t (s)

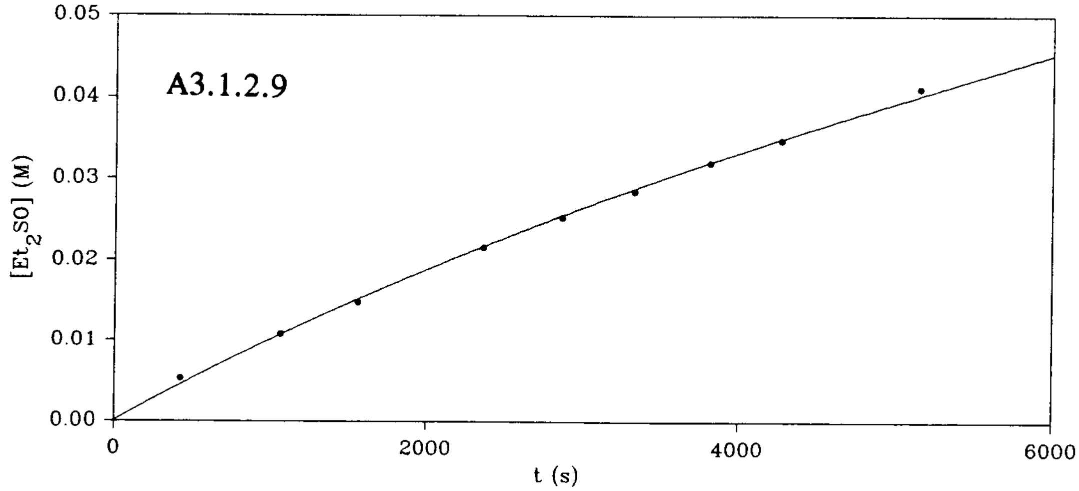
A3.1.2.9
0.05
0.04
0.03
0.02
0.01
0.00
$[Et_2SO]$ (M)
0
2000
4000
6000
t (s)

### A3.1.3 $[O_2]$ Dependence Studies

$[Ru]_o$ = 0.408 ± 0.004 mM

[PhCOOH] = 24.4 ± 0.1 mM

$[Et_2S]$ = 0.742 ± 0.006 M

Shaking rate = 164 ± 10 cycles/min

Solution volume = 10.0 ± 0.1 mL

Relative uncertainty in $[O_2]$ ≈ 1%

| Graph # | $[O_2]$ (M) | $k_{obs}x10^6$ | $\chi^2$ | Q |
|---|---|---|---|---|
| A3.1.3.1 | $1.76x10^{-3}$ | 1.72 | 3.5 | 0.98 |
| A3.1.3.2 | $2.18x10^{-3}$ | 1.71 | 2.2 | 0.99 |
| A3.1.3.3 | $2.65x10^{-3}$ | 2.69 | 3.6 | 0.96 |
| A3.1.3.4 | $3.64x10^{-3}$ | 3.26 | 15 | 0.17 |
| A3.1.3.5 | $4.90x10^{-3}$ | 4.05 | 7.2 | 0.78 |
| A3.1.3.6 | $5.13x10^{-3}$ | 4.10 | 6.1 | 0.87 |
| A3.1.3.7 | $6.32x10^{-3}$ | 4.82 | 9.9 | 0.45 |
| A3.1.3.8 | $7.63x10^{-3}$ | 5.16 | 9.5 | 0.30 |
| A3.1.3.9 | $8.44x10^{-3}$ | 5.93 | 16 | 0.19 |

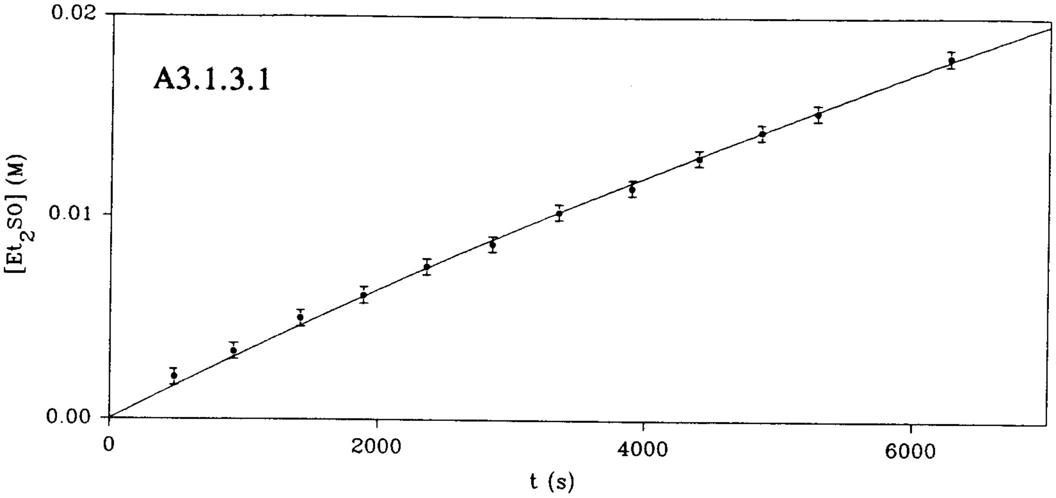
A3.1.3.1

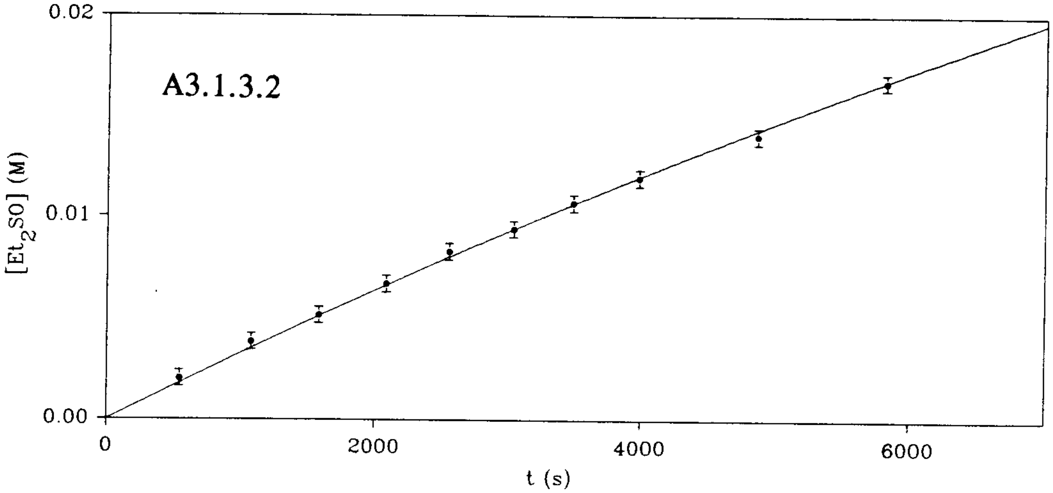
A3.1.3.2

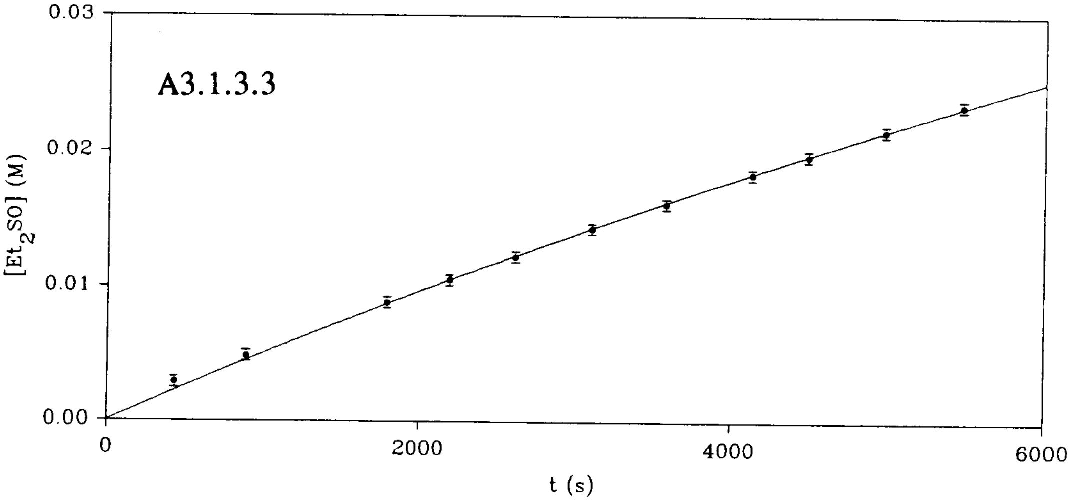
A3.1.3.3

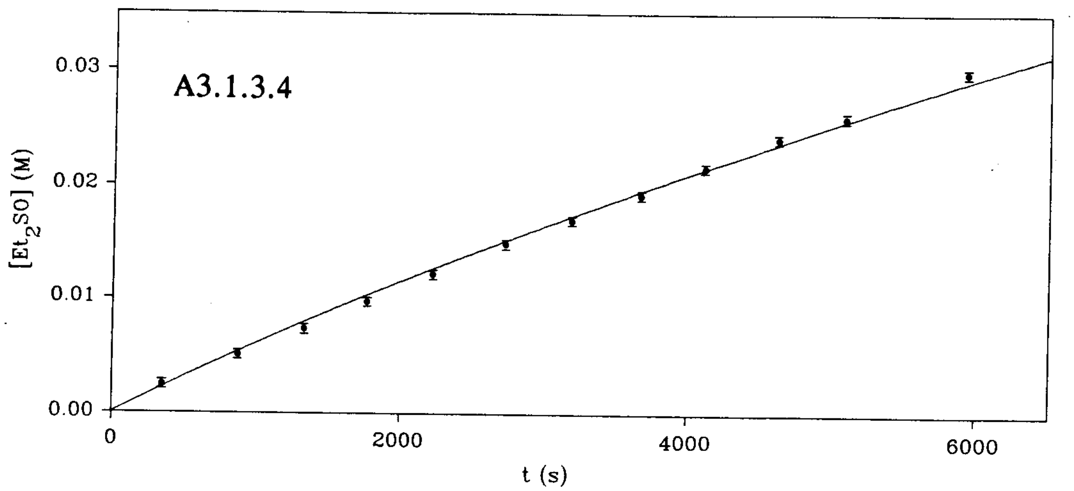
A3.1.3.4
[Et$_2$SO] (M)
0.00
0.01
0.02
0.03
0
2000
4000
6000
t (s)

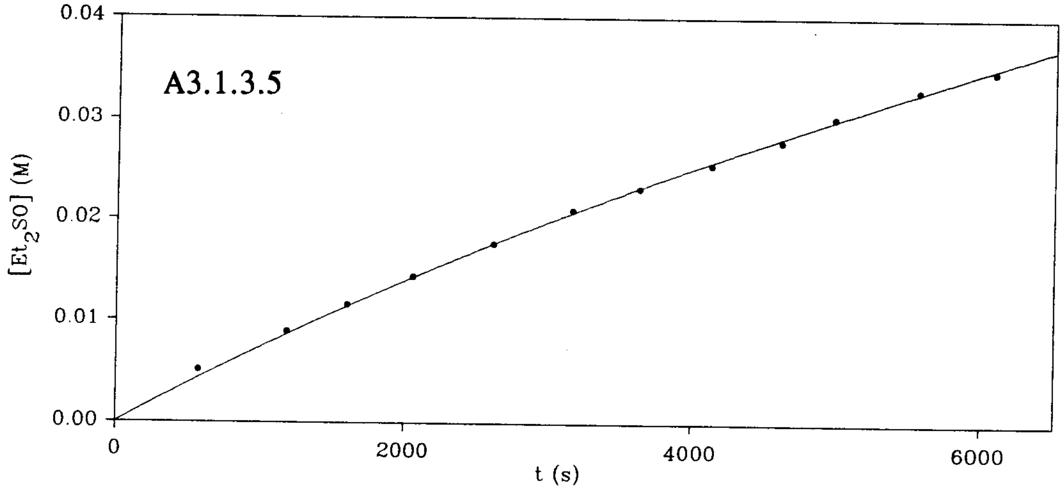
A3.1.3.5
[Et$_2$SO] (M)
0.00
0.01
0.02
0.03
0.04
0
2000
4000
6000
t (s)

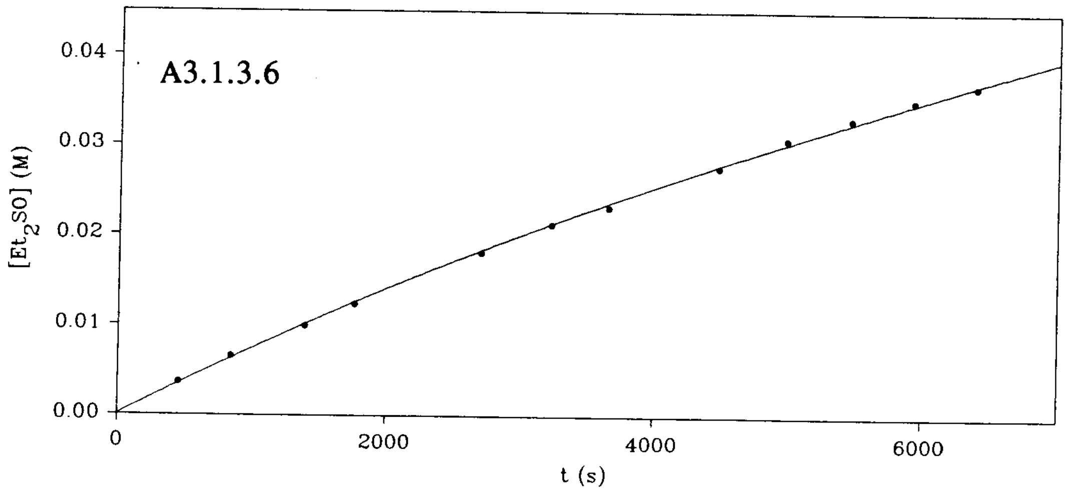
A3.1.3.6
[Et$_2$SO] (M)
0.00
0.01
0.02
0.03
0.04
0
2000
4000
6000
t (s)

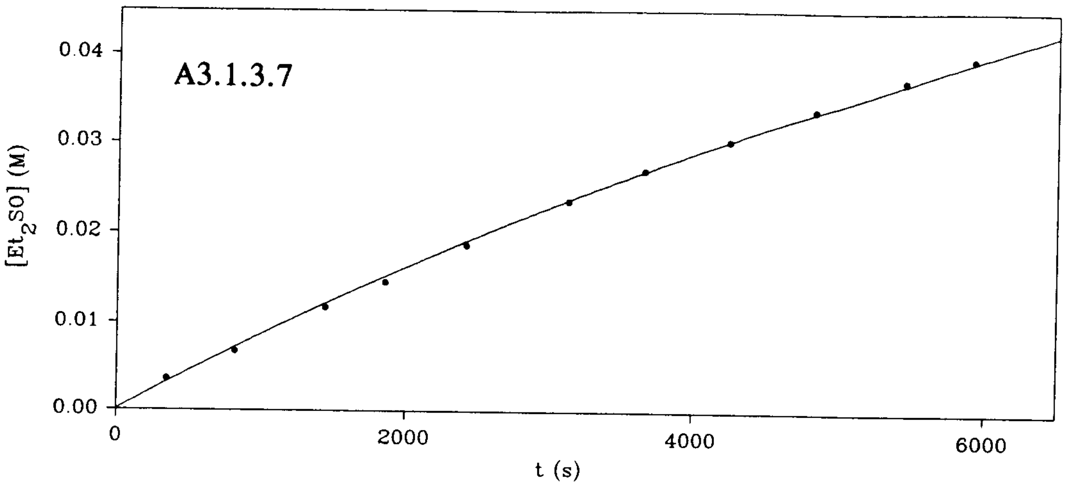
A3.1.3.7
[Et$_2$SO] (M)
0.00
0.01
0.02
0.03
0.04
0
2000
4000
6000
t (s)

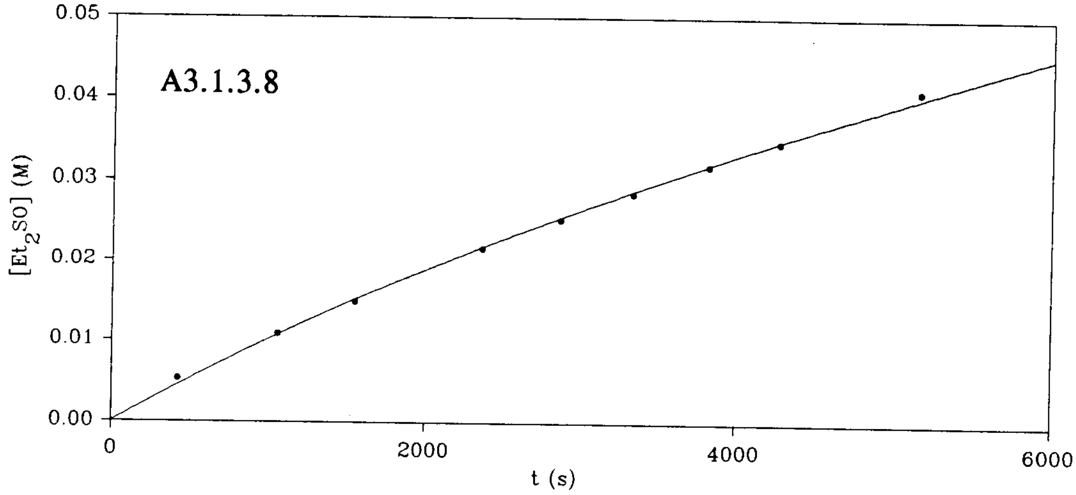
A3.1.3.8
[Et$_2$SO] (M)
0.00
0.01
0.02
0.03
0.04
0.05
0
2000
4000
6000
t (s)

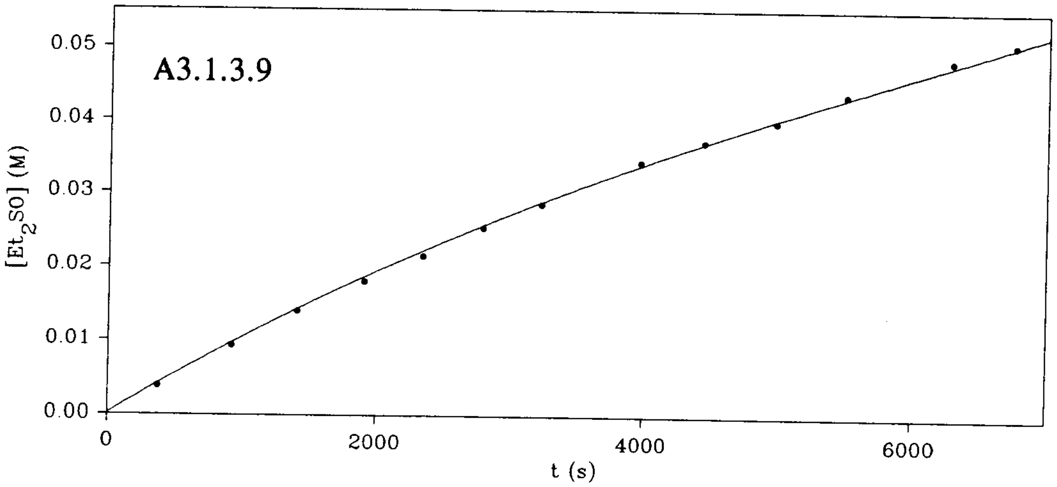
A3.1.3.9
[Et$_2$SO] (M)
0.00
0.01
0.02
0.03
0.04
0.05
0
2000
4000
6000
t (s)

## A3.2 Second Data Set

The two tables that follow give the numerical values of the data points shown in figures 3.24 and 3.25. Following each table are the $[Et_2SO]$ vs. time raw data plots which gave rise to each data point in figures 3.24 and 3.25.

### A3.2.1 $[Ru]_o$ Dependence Studies

[PhCOOH] = 24.4 ± 0.1 mM

$[O_2]$ = 7.63 ± 0.07 mM

$[Et_2S]$ = 0.742 ± 0.006 M

Shaking rate = 164 ± 10 cycles/min

Solution volume = 10.0 ± 0.1 mL

Relative uncertainty in $[Ru]_o$ ≈ 1%

| Graph # | $[Ru]_o$ (M) | $k_{obs}x10^6$ | $\chi^2$ | Q |
|---|---|---|---|---|
| A3.2.1.1 | $2.53x10^{-5}$ | 1.23 | 9.7 | 0.72 |
| A3.2.1.2 | $5.06x10^{-5}$ | 1.71 | 8.2 | 0.88 |
| A3.2.1.3 | $1.01x10^{-4}$ | 1.86 | 14 | 0.18 |
| A3.2.1.4 | $1.01x10^{-4}$ | 2.29 | 15 | 0.45 |
| A3.2.1.5 | $2.02x10^{-4}$ | 3.23 | 7.9 | 0.95 |
| A3.2.1.6 | $2.28x10^{-4}$ | 3.18 | 29 | 0.023 |
| A3.2.1.7 | $4.05x10^{-4}$ | 3.79 | 6.6 | 0.95 |
| A3.2.1.8 | $1.18x10^{-3}$ | 4.80 | 125 | 0 |

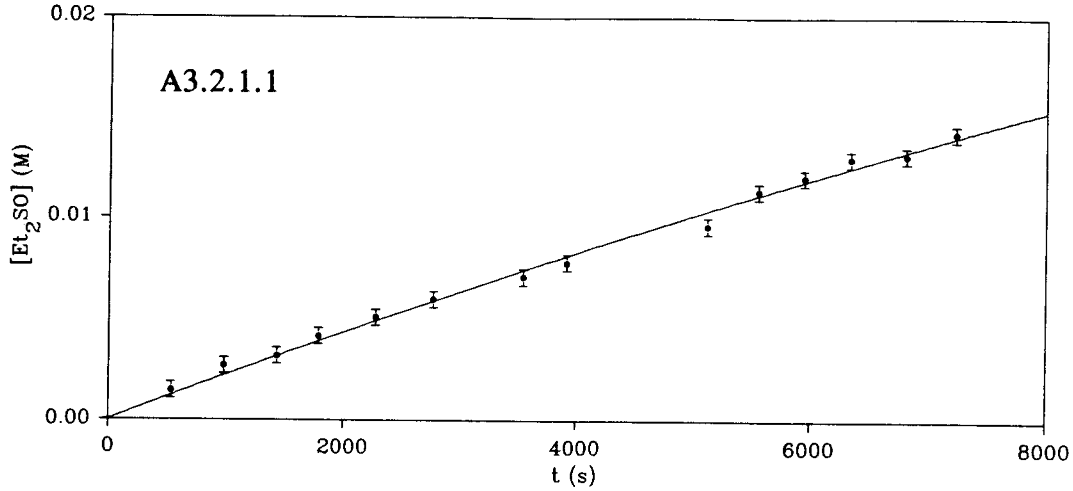
A3.2.1.1
[Et$_2$SO] (M)
0.02
0.01
0.00
0
2000
4000
6000
8000
t (s)

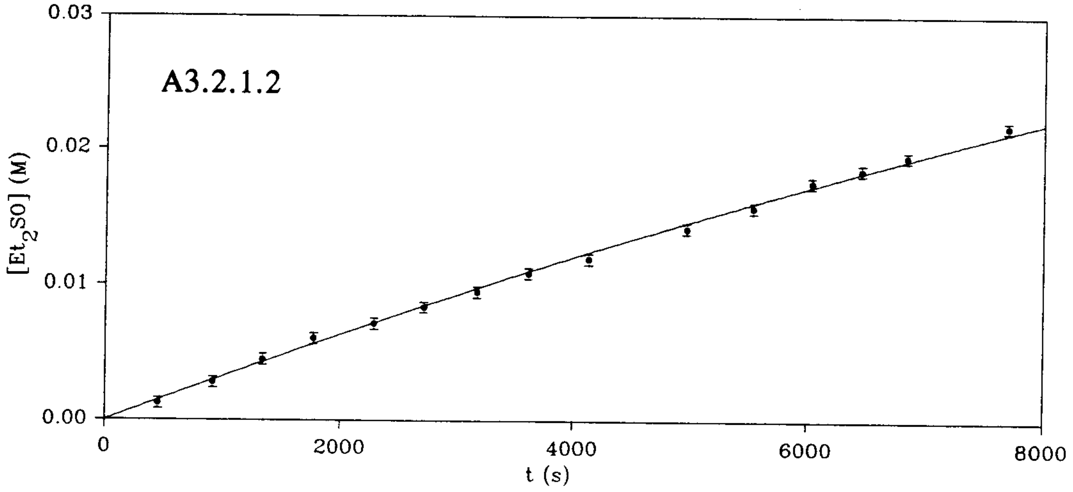
A3.2.1.2
[Et$_2$SO] (M)
0.03
0.02
0.01
0.00
0
2000
4000
6000
8000
t (s)

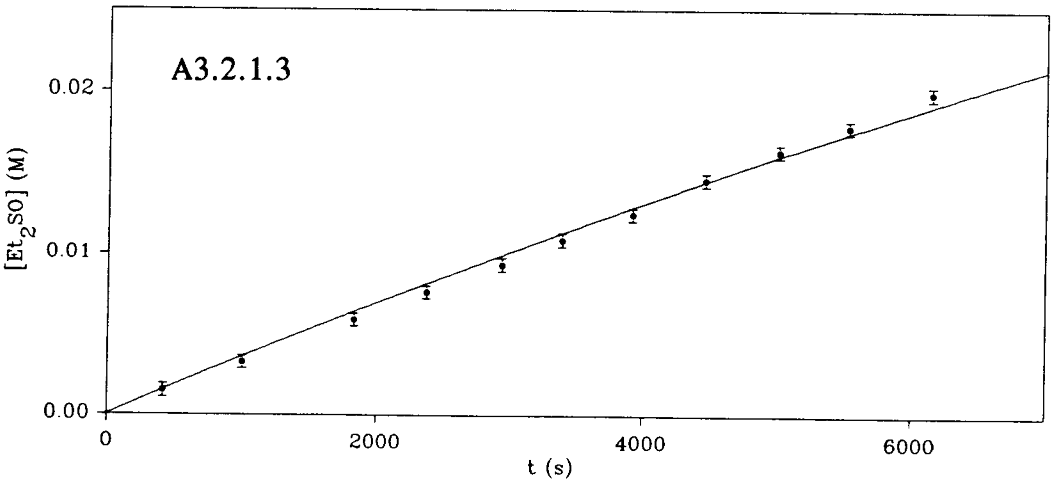
A3.2.1.3
[Et$_2$SO] (M)
0.02
0.01
0.00
0
2000
4000
6000
t (s)

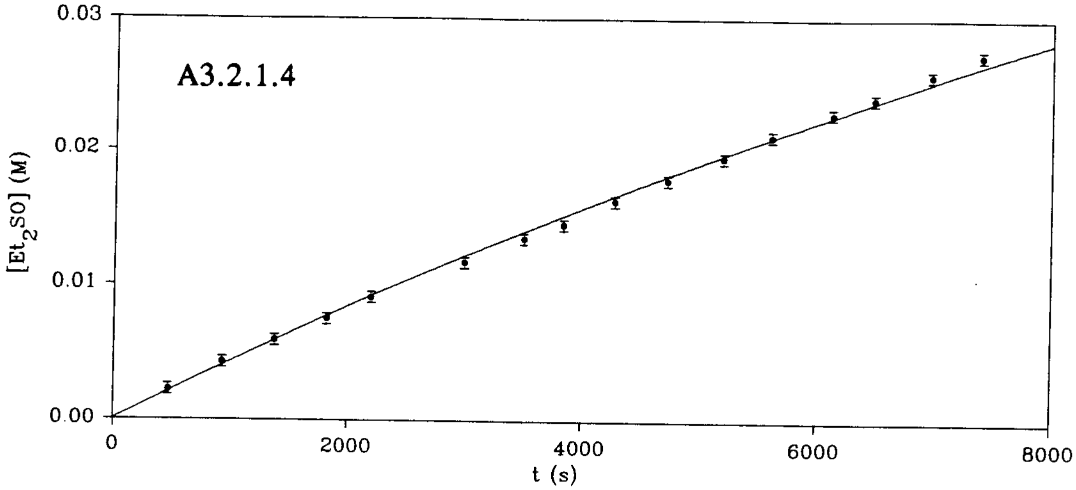
A3.2.1.4
[Et$_2$SO] (M)
0.00
0.01
0.02
0.03
t (s)
0
2000
4000
6000
8000

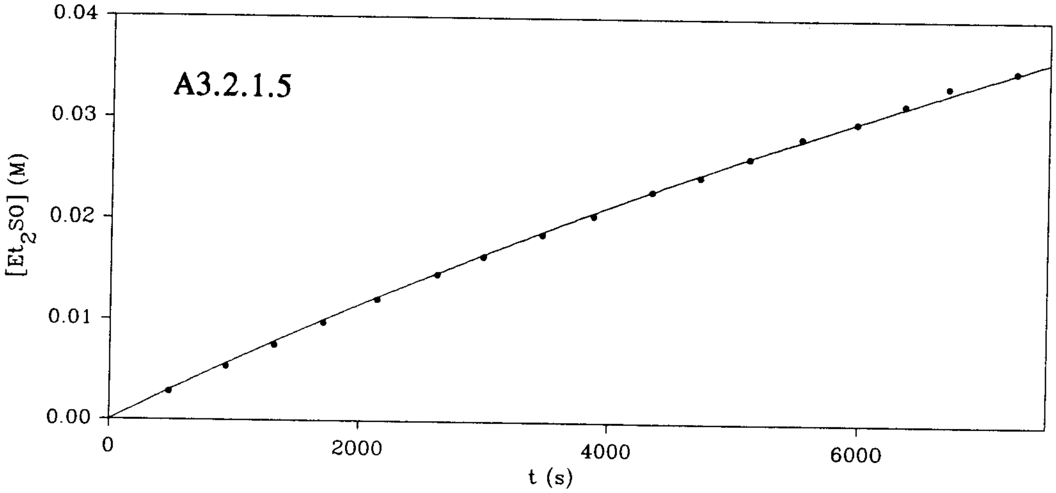
A3.2.1.5
[Et$_2$SO] (M)
0.00
0.01
0.02
0.03
0.04
t (s)
0
2000
4000
6000

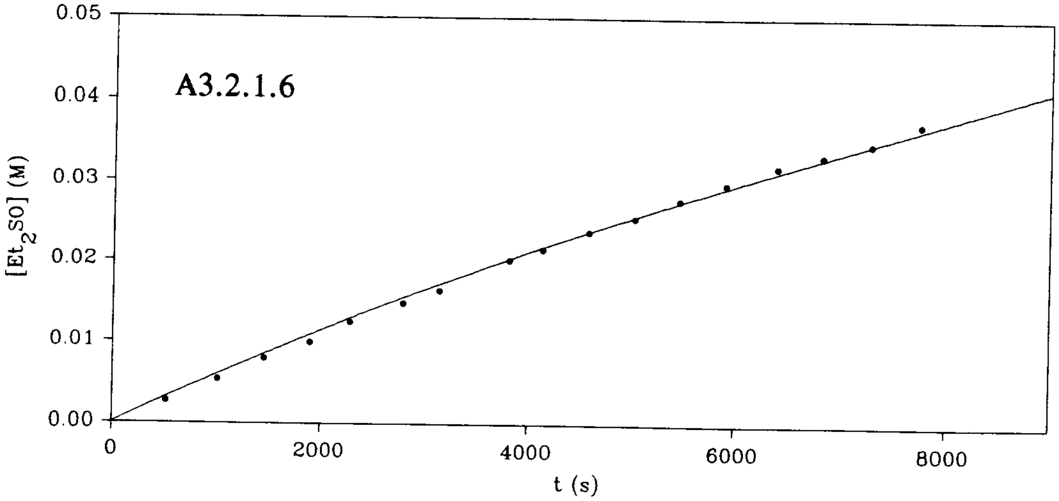
A3.2.1.6
[Et$_2$SO] (M)
0.00
0.01
0.02
0.03
0.04
0.05
t (s)
0
2000
4000
6000
8000

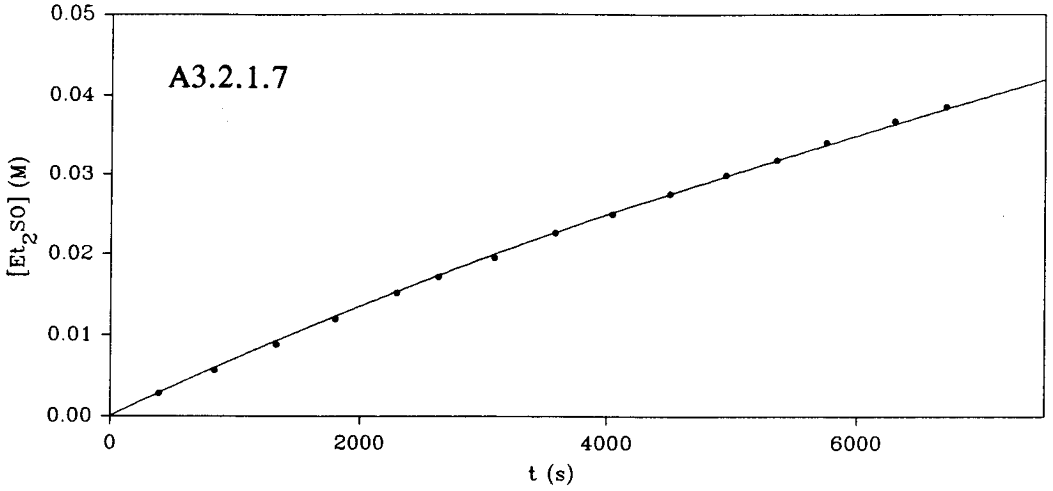
A3.2.1.7
[Et$_2$SO] (M)
0.05
0.04
0.03
0.02
0.01
0.00
0
2000
4000
6000
t (s)

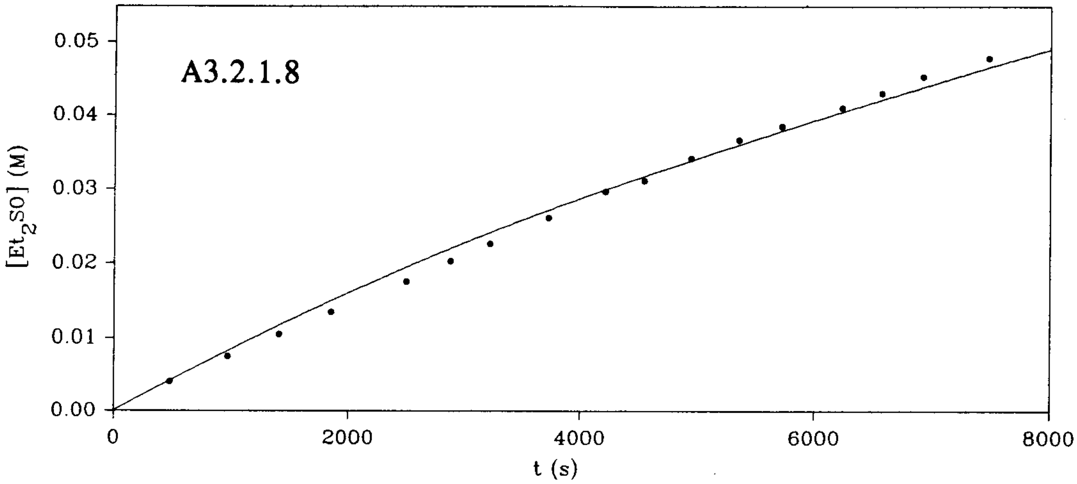
A3.2.1.8
[Et$_2$SO] (M)
0.05
0.04
0.03
0.02
0.01
0.00
0
2000
4000
6000
8000
t (s)

### A3.2.2 [PhCOOH] Dependence Studies

$[Ru]_o = 0.202 \pm 0.002$ mM

$[O_2] = 7.63 \pm 0.07$ mM

$[Et_2S] = 0.742 \pm 0.006$ M

Shaking rate = 164 ± 10 cycles/min

Solution volume = 10.0 ± 0.1 mL

Relative uncertainty in [PhCOOH] ≈ 0.5-1%

| Graph # | [PhCOOH] (M) | $k_{obs}x10^6$ | $\chi^2$ | Q |
|---|---|---|---|---|
| A3.2.2.1 | $1.21x10^{-3}$ | 0.786 | 2.9 | 0.99 |
| A3.2.2.2 | $2.31x10^{-3}$ | 1.18 | 9.6 | 0.39 |
| A3.2.2.3 | $4.59x10^{-3}$ | 1.71 | 6.7 | 0.88 |
| A3.2.2.4 | $4.99x10^{-3}$ | 1.58 | 40 | $1.6x10^{-4}$ |
| A3.2.2.5 | $1.03x10^{-2}$ | 2.38 | 4.2 | 0.95 |
| A3.2.2.6 | $1.50x10^{-2}$ | 2.55 | 0.89 | 1.0 |
| A3.2.2.7 | $2.44x10^{-2}$ | 3.23 | 7.9 | 0.95 |
| A3.2.2.8 | $4.79x10^{-2}$ | 3.20 | 21 | 0.10 |

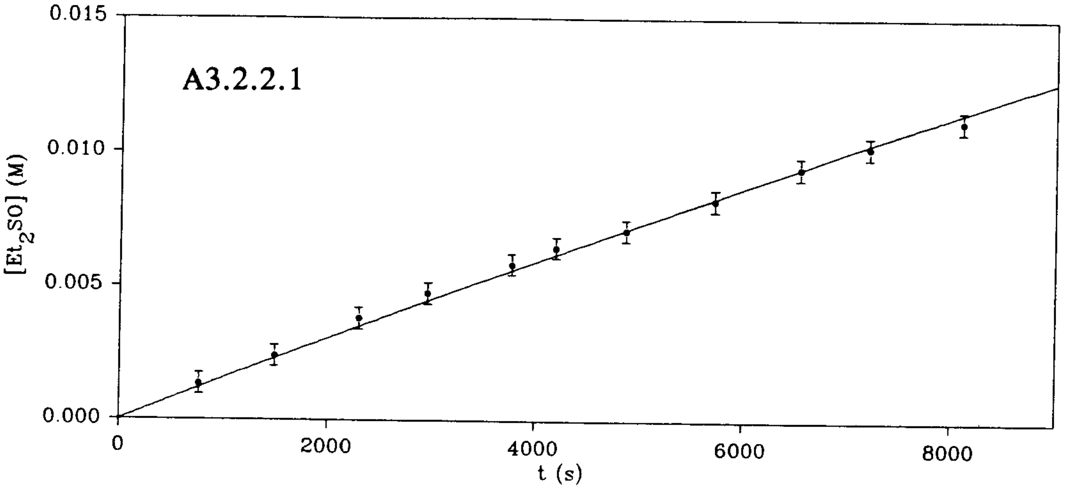
A3.2.2.1
[Et$_2$SO] (M)
0.015
0.010
0.005
0.000
0
2000
4000
6000
8000
t (s)

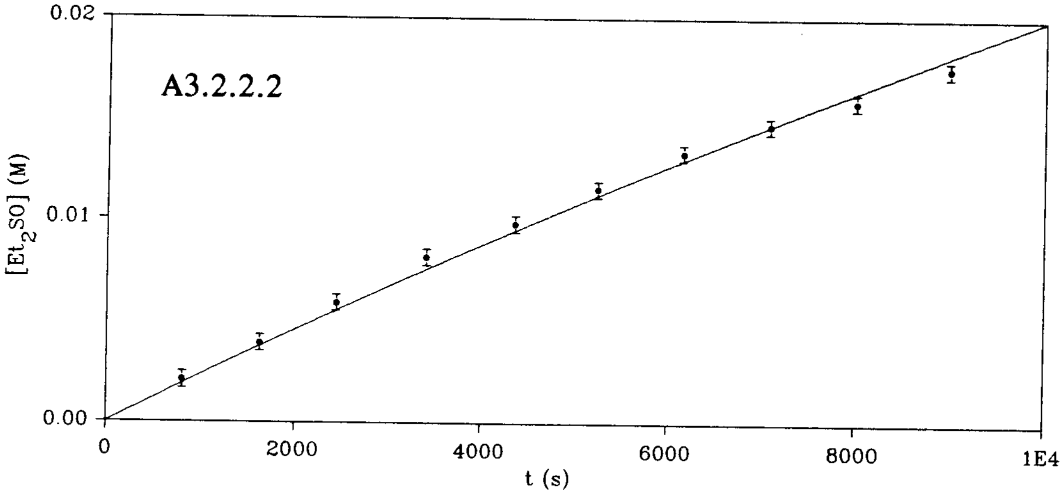
A3.2.2.2
[Et$_2$SO] (M)
0.02
0.01
0.00
0
2000
4000
6000
8000
1E4
t (s)

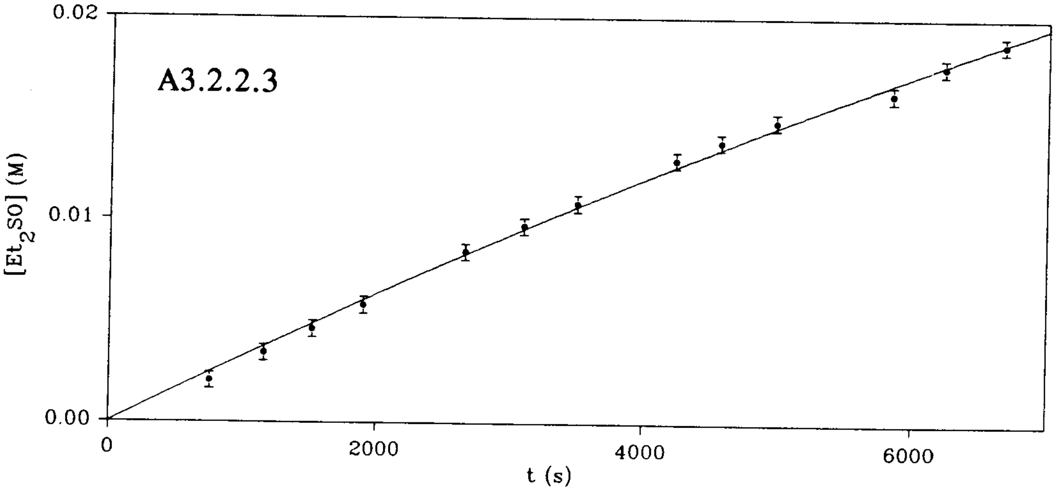
A3.2.2.3
[Et$_2$SO] (M)
0.02
0.01
0.00
0
2000
4000
6000
t (s)

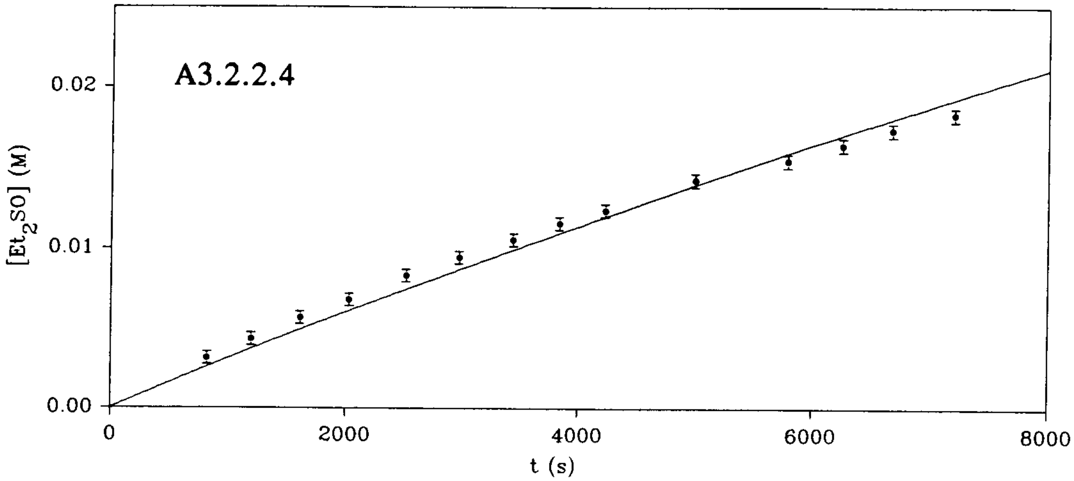
A3.2.2.4
0.02
0.01
0.00
[Et$_2$SO] (M)
0
2000
4000
6000
8000
t (s)

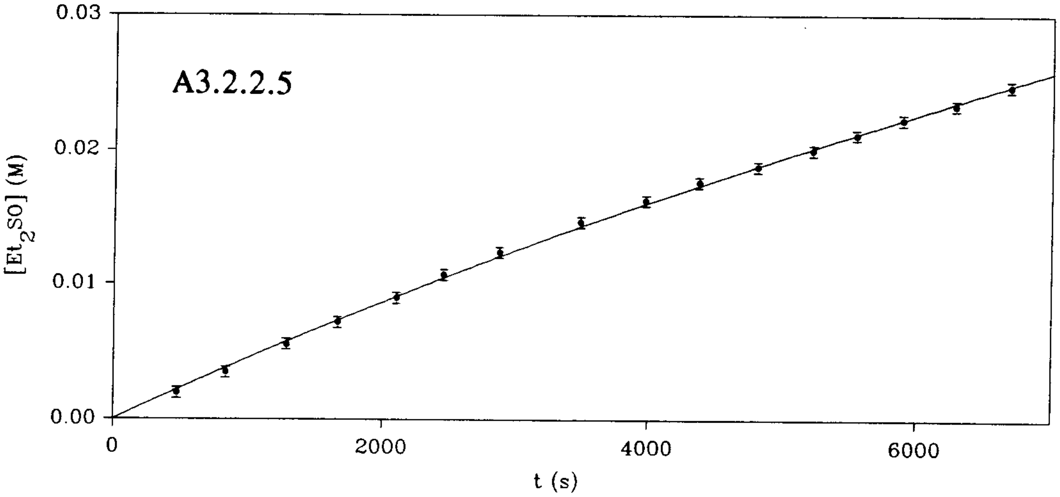
A3.2.2.5
0.03
0.02
0.01
0.00
[Et$_2$SO] (M)
0
2000
4000
6000
t (s)

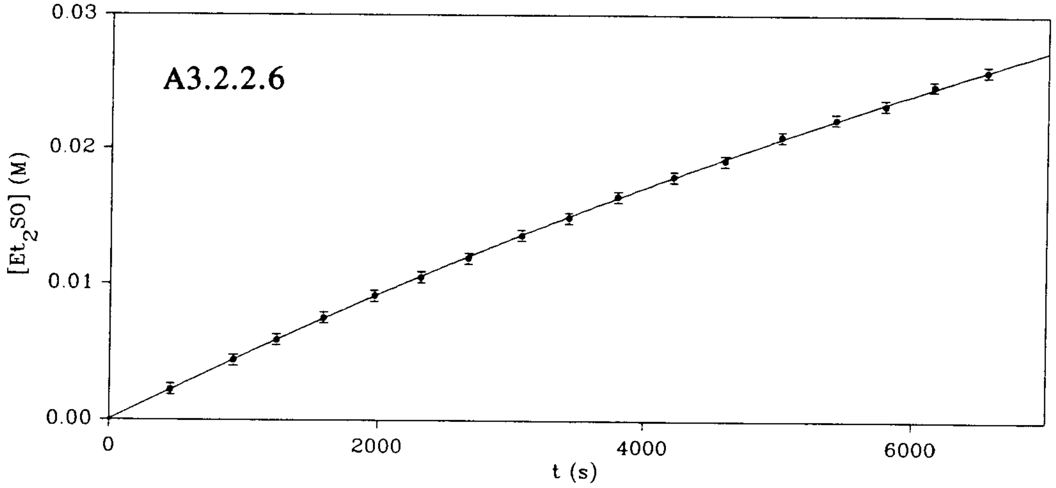
A3.2.2.6
0.03
0.02
0.01
0.00
[Et$_2$SO] (M)
0
2000
4000
6000
t (s)

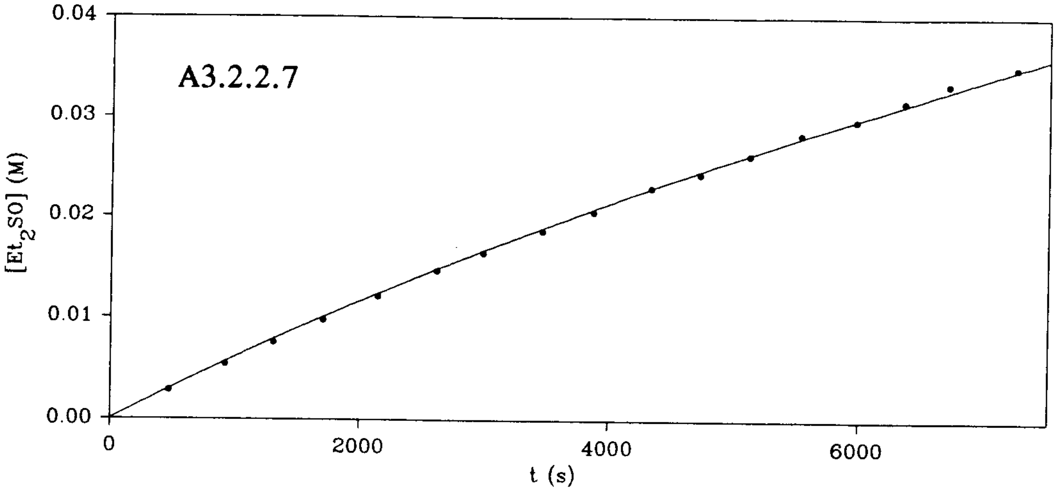
A3.2.2.7
0.04
0.03
0.02
0.01
0.00
$[Et_2SO]$ (M)
0
2000
4000
6000
t (s)

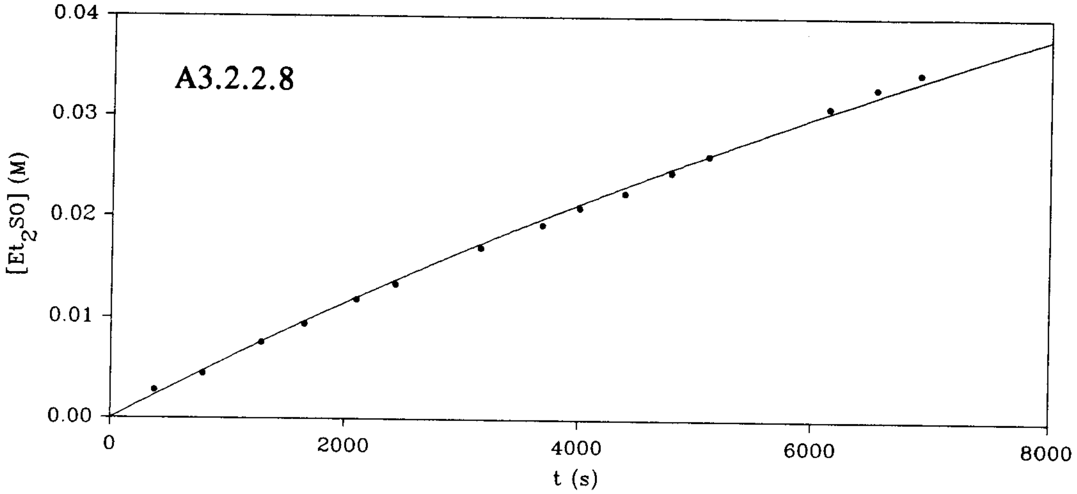
A3.2.2.8
0.04
0.03
0.02
0.01
0.00
$[Et_2SO]$ (M)
0
2000
4000
6000
8000
t (s)

## A3.3 Additional Data Sets

The two tables that follow give the numerical values of the data points for some experiments not discussed in the body of the thesis. The first gives the results of a series of experiments in which the reaction vessel shaking rate was varied from one experiment to the next. The second table lists the results of a series of experiments in which the volume of the reaction solution was varied from one experiment to the next. Following each table are the [$Et_2SO$] vs. time raw data plots which gave rise to each $k_{obs}$ value in the table.

### A3.3.1 Dependence of the Reaction Rates on the Reaction Vessel Shaking Speed

$[Ru]_o$ = 0.202 ± 0.002 mM

[$O_2$] = 7.63 ± 0.07 mM

[PhCOOH] = 24.4 ± 0.1 mM

[$Et_2S$] = 0.742 ± 0.006 M

Solution volume = 10.0 ± 0.1 mL

Relative uncertainty in the shaking rate ≈ 5-8%

| Graph # | Shaking Rate | $k_{obs} x 10^6$ | $\chi^2$ | Q |
|---|---|---|---|---|
| A3.3.1.1 | 133 | $3.04 x 10^{-6}$ | 11.8 | 0.62 |
| A3.3.1.2 | 164 | $3.23 x 10^{-6}$ | 7.9 | 0.95 |
| A3.3.1.3 | 186 | $2.61 x 10^{-6}$ | 22 | 0.10 |

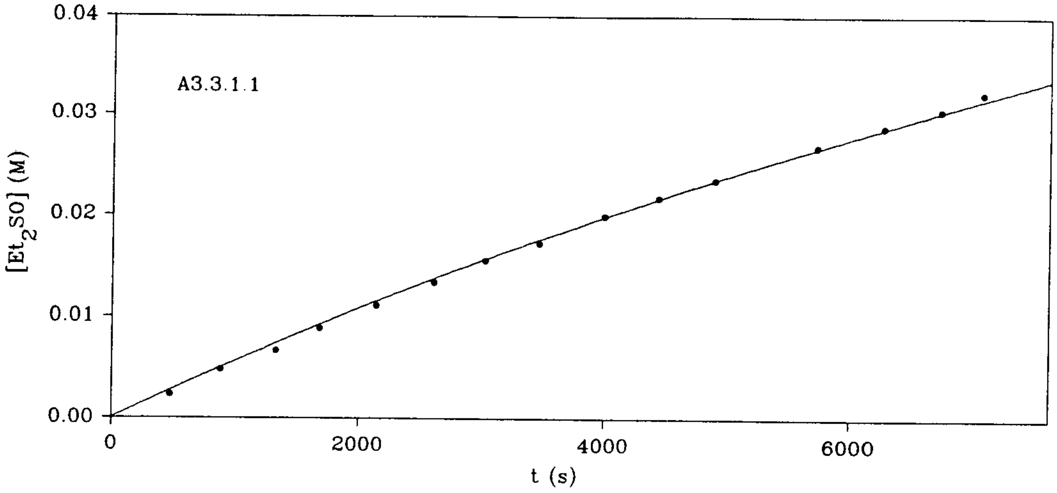
A3.3.1.1
[Et$_2$SO] (M)
0.00
0.01
0.02
0.03
0.04
t (s)
0
2000
4000
6000

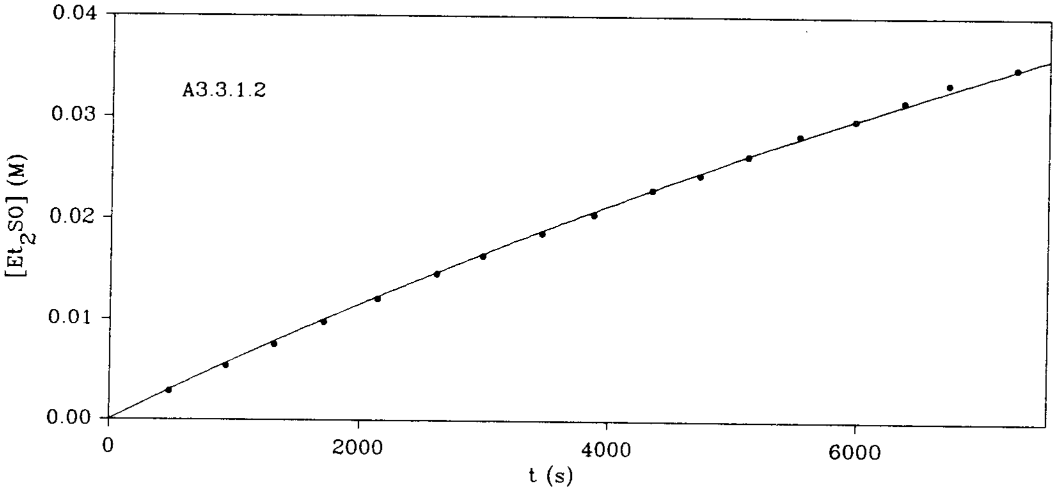
A3.3.1.2
[Et$_2$SO] (M)
0.00
0.01
0.02
0.03
0.04
t (s)
0
2000
4000
6000

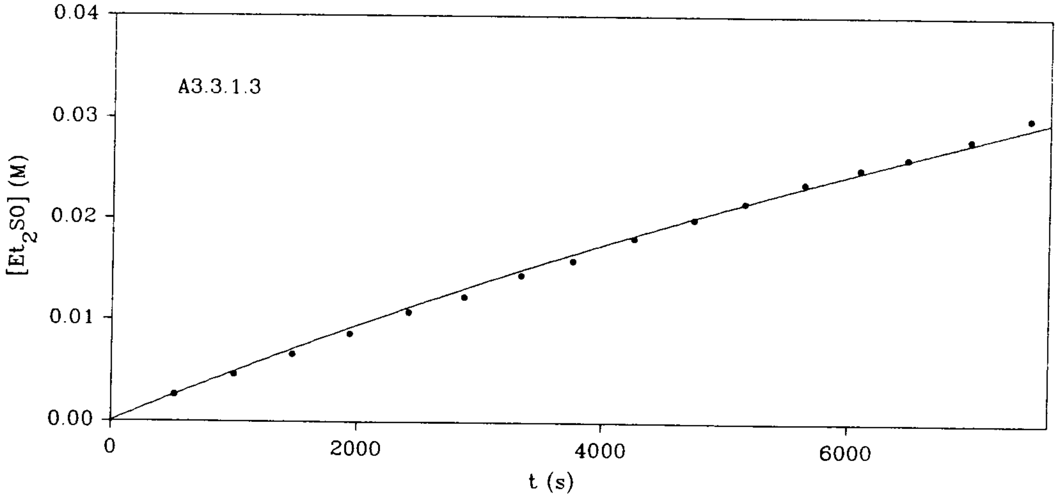
A3.3.1.3
[Et$_2$SO] (M)
0.00
0.01
0.02
0.03
0.04
t (s)
0
2000
4000
6000

## A3.3.2 Dependence of the Reaction Rates on the Volume of the Reaction Mixture

$[Ru]_o = 0.408 \pm 0.004$ mM

$[O_2] = 7.63 \pm 0.07$ mM

$[PhCOOH] = 24.4 \pm 0.1$ mM

$[Et_2S] = 0.742 \pm 0.006$ M

Shaking rate = 164 ± 10 cycles/min

Relative uncertainty in the solution volume ≈ 0.5-2%

| Graph # | Solution Volume (mL) | $k_{obs}x10^6$ | $\chi^2$ | Q |
|---|---|---|---|---|
| A3.3.2.1 | 10.0 | 8.14 | 34 | $3.5x10^{-4}$ |
| A3.3.2.2 | 5.00 | 8.64 | 3.8 | 0.97 |
| A3.3.2.3 | 2.00 | 13.3 | 14 | 0.33 |

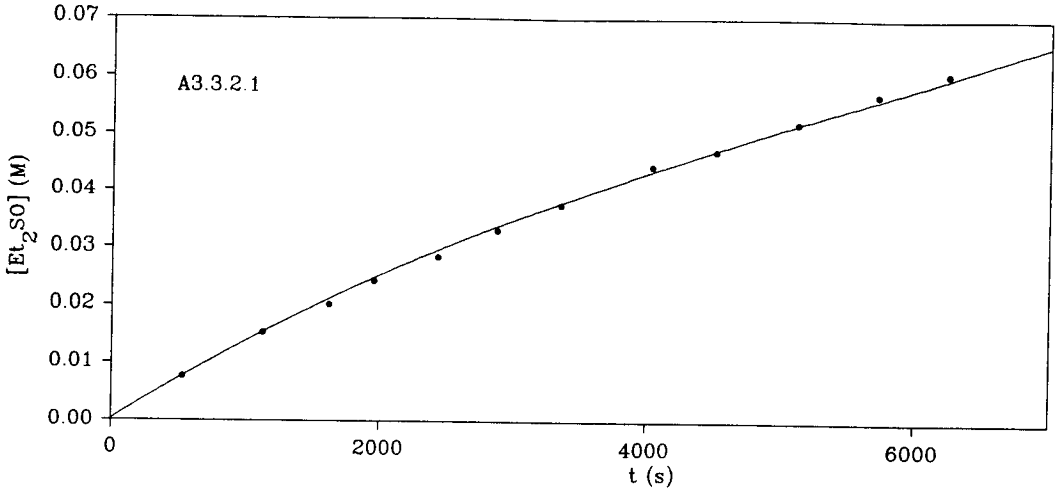
A3.3.2.1
[Et$_2$SO] (M)
0.00
0.01
0.02
0.03
0.04
0.05
0.06
0.07
t (s)
0
2000
4000
6000

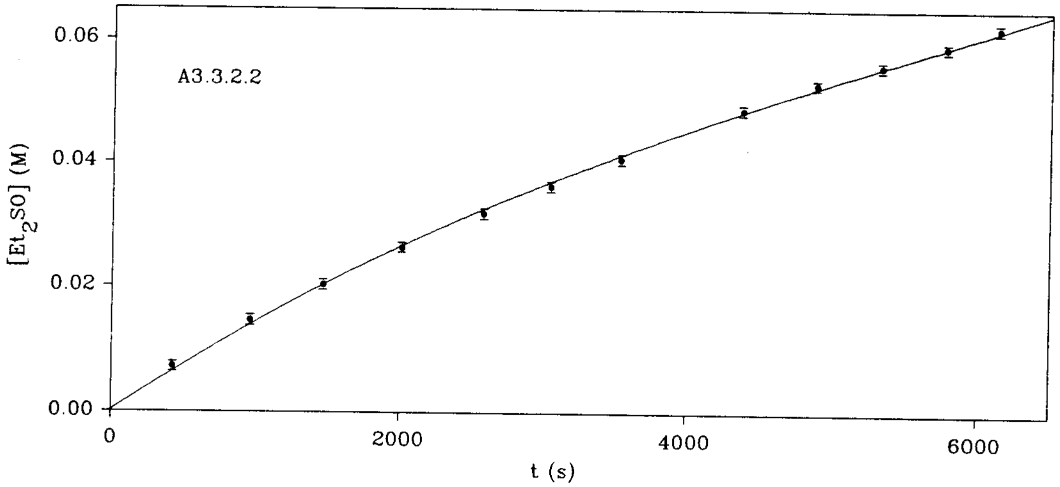
A3.3.2.2
[Et$_2$SO] (M)
0.00
0.02
0.04
0.06
t (s)
0
2000
4000
6000

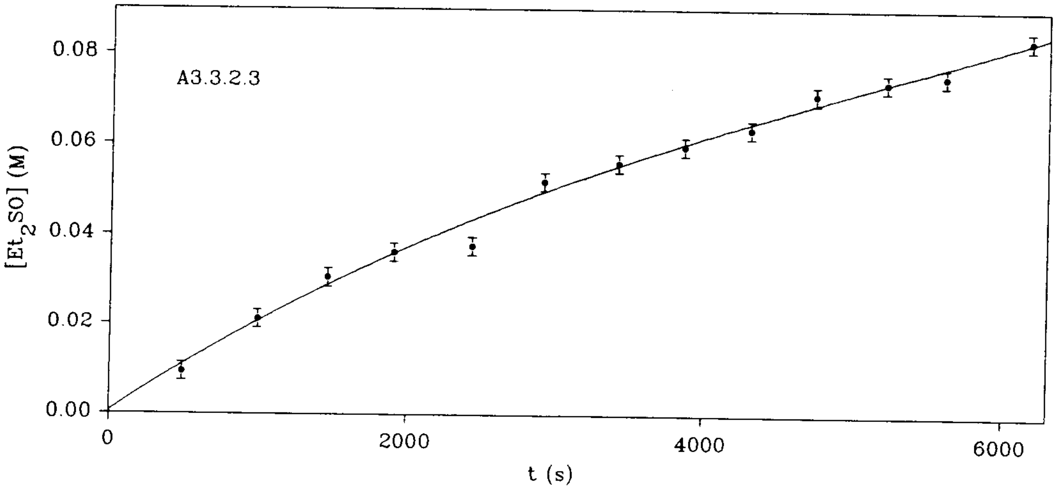
A3.3.2.3
[Et$_2$SO] (M)
0.00
0.02
0.04
0.06
0.08
t (s)
0
2000
4000
6000